UNIVERSITAT POLITÈCNICA DE VALÈNCIA

Instituto Interuniversitario de Investigación de Reconocimiento Molecular y Desarrollo Tecnológico (IDM)
Departamento de Química

Miquel Avella-Oliver

Towards label-free biosensing in compact disk technologies for point-of-need analysis

PhD. Supervisors

Ángel Maquieira Catalá

Rosa Puchades Pla

Valencia, July 2017

"We must not only be good,
we must be quick and cheap"

Royce W. Murray
Anal. Chem., 63 (**1991**), 379.

ACKNOWLEDGEMENTS

Thanks to the FPI program of the Spanish Ministry of Economy and Competitiveness for the doctoral grant.

Thanks to Ángel Maquieira and Rosa Puchades for their support, all their supervision work in this thesis, and for counting on me to join this research team.

Thanks to Sergi Morais for sharing his expertise along this project and for revising this manuscript.

Thanks to all the other people that I also worked with in the studies included in this thesis: Javier Carrascosa, David Gimenez, Vicente Ferrando, Juan A. Monsoriu, Sebastian Wachsmann, Richard McAloney, and M. Cynthia Goh.

Special thanks to all my family and to Reme for their unconditional support.

Thanks to all my friends inside and outside labs, particularly for their understanding during my "thesis mode".

Thanks to all the people that I also collaborated with in works involved in this project but not included in this thesis: Gabriel Sancho, Maria José Bañuls, Carlos A. Barrios, Natalia Sacco, Mauricio E. Calvo.

Many thanks to all the rest of the people with whom I also shared the everyday life in labs during this period: Luis Tortajada, Miguel A. González, Nuria Pastor, Eva M. Brun, Julia Atienza, M. Asunción Herrero, Pilar Aragón, Patricia Noguera, Enrique Guijarro, Jorge Escorihuela, Sara Santiago, Ernest Peris, Jesús Tamarit, Tania Arnandis, Diana Tamayo, Sergio Peransí, Francisco Ortega, Consuelo Chafer, Jose Luis Lopez, Patricia Navarro, Carlos Ribelles, Cristina Fuentes, Hugo García, Paulina Dobosz, Maria Adobes, Regina Niñoles, Salvador Mena, Elizabeth Hevia, Noelle do Nascimento, Raquel Montón, Cristina Ripollés, Ahmed Ali, Noelia Carbó, Eric Yamanaka, Daniel González, Pilar Jiménez, Victoria González, Ismael Guerrero, Beatriz Lucas, Stijn Van Cleuvenbergen, Tatu Rojalin, Changwon Lee, Zachary Smith, Kaiqin Chu, Tingjuan Gao, Augusto Juste, Maria José Juárez, Zeneida Díaz, Sara Martorell, Sofía Ingresa, Estrella Fernández, Adrián Poveda, Tabita Cenusa, Rafael Alonso, Ana Lázaro, Edurne Peña, and Salvador Mas.

ABSTRACT

The raise of instrumentation in analytical sciences has provided a wide range of sophisticated analytical equipment that plays a crucial role in countless key areas in the living standards of today's world, such as medical diagnosis, food safety, and environmental analysis among many others. However, these reference analytical equipment tend to be expensive, bulky, complex, and involve highly specialized and tedious analytical procedures. These facts strongly restricts the dissemination of analytical sciences in non-specialized environments as well as in resource-scarce settings, such as home diagnosis, remote areas, or developing countries.

The present thesis aims to exploit the great potential of consumer electronics to conceive inexpensive, portable, fast, simple, robust, sensitive, and high-throughput bioanalytical systems. Compact disk technologies are mature and massively produced consumer electronics that comprise very sophisticated optical, mechanical, and electronical systems at extremely low cost. Therefore, marrying these technologies with chemical analysis can offer user-friendly analytical devices to address the restrictions described above. On the other hand, the integration of biological materials in these systems expands their scope to the biosensing framework and entails important strengths to reach the premises that motivate this project. For instance, this fact favors the development of simple and highly selectivity systems for detecting clinically important biological targets, among many other strengths.

This thesis explores new analytical advances using compact disk biosensing technologies, and comprises six scientific publications distributed along four chapters. Special attention is herein payed to Thermochromic Etching Disks (TED) technology (Chapter 1), rational design of disk-based biorecognition assays (Chapter 2), and label-free detection systems for point-of-need analysis (Chapters 3 and 4).

This research begins by investigating the possibilities offered by TED systems for conceiving new disk-based biosensors. First, insights into a novel light-mediated signal developing system for biorecognition assays (based on TED disks and drives) are provided together with an overview of the state-of-the art and future trends in photo- and thermochromic biosensing. This signal developing approach exploits photo- and thermochromism for biosensing in an original manner and represents a potential strategy to simplify signaling processes in bioanalytical systems.

Then, how to transform TED technology into lab-on-a-disk systems is addressed. TED has proven to be a very versatile tool to perform sensitive analysis of biorecognition assays, using platforms and scanners easily obtained from regular disks and drives, respectively. Biologically relevant assays of different nature (microarray, cell culture, immunofiltration, turbidimetry, etc.) have been arrayed in a single disk and sensitively analyzed by imaging. This study highlights the

potential implementation of microfluidic elements and label-free detection strategies in these TED disk-based biosensors.

Regarding rational design, a theoretical-experimental method (INSEL) based on kinetics and mass-transport modelling for optimizing biorecognition assays and exploring their behavior is presented. INSEL has been implemented as an in silico tool that enables to characterize biointeractions with minimal experimentation, to perform optimizations directed towards custom objectives defined by the user, and to easily compute the effect of critical variables without further experiments. This study also demonstrates the capabilities of disk-based microarray immunoassays as routine technique to study biointeractions.

Label-free bioanalytical techniques allows binding events to be sensed without incorporating signaling elements. This fact involves many important advantages for biosensors, such as higher reliability of the results and simpler analytical procedures. However, label-free strategies typically require expensive and complex nanostructured materials and detection setups, and present rather low-throughput features. In view of all these facts, this project aims to face those limitations by exploiting the elements comprised in compact disk technologies to develop label-free biosensors. Along these lines, regular disks contain an embedded spiral-shaped grooved nanostructure whose adaptation to become an optically active transducer for label-free biosensing purposes have been addressed in the following studies.

Surface-enhanced Raman spectroscopy (SERS) is a technique that enables sensitive and selective analysis, and can reach label-free detection of biological targets. Herein, polycarbonate grooved structures obtained from standard recordable disks (CD-R and DVD-R) were coated with silver and tailored to become SERS-active. This strategy represents a cost-effective and industrially scalable alternative to the SERS substrates typically used for bioanalysis. These disk-based materials have presented tunable plasmonic responses, significant Raman enhancement, and have allowed complex biological targets (such as proteins and exosomes) to be analyzed by SERS without using labeled reagents as tracers. In addition to introduce inexpensive and large-scale SERS substrates for biosensing, this study also suggests the development of prospective Raman scanners based on disk drives.

Another approach herein presented addresses the implementation of diffraction-based sensing (DBS) in TED technology in order to conceive disk-based label-free biosensors based on standard disks and drives. DBS relies on monitoring the changes in the diffracted pattern of diffractive gratings constituted by biological probes (biogratings). At first, a comprehensive experimental assessment of the analytical possibilities offered by DBS is presented. This study describes how to tailor this technique to obtain many interesting features, such as label-free

detection, real-time and endpoint analysis, high materials compatibility, and sensitive determination of low molecular weight organic compounds (e.g., atrazine).

Then, from the knowledge about DBS provided in the previous study, the fabrication of arrays of protein biogratings on TED disks by a water-assisted variant of microcontact printing is investigated. Instead of expensive nanostructured materials, herein we have proposed the grooved nanostructures of regular disks as large-scale and low-cost masters to create biogratings. Sensitive analysis of antibodies in label-free conditions has been herein demonstrated by these arrays of protein biogratings on disks, scanned with adapted TED drives. This investigation has proved the concept for label-free detection based on regular TED technology, and provides important insights into cost-effective and industrially scalable functional materials and detection setups that exploit consumer electronics for label-free biosensing.

RESUMEN

El auge de la instrumentación en las ciencias analíticas ha dado lugar un amplio abanico de sistemas analíticos que juegan un papel crucial en multitud de áreas clave para los estándares de vida actuales, tales como el diagnóstico médico, la seguridad alimentaria y el control medioambiental, entre muchas otras. Sin embargo, estos sistemas de referencia tienden a ser caros, grandes, complejos y suelen involucrar procedimientos de análisis tediosos y altamente especializados. Este hecho restringe enormemente la difusión de las ciencias analíticas en entornos no especializados o con escasos recursos, como por ejemplo el diagnóstico en casa, áreas remotas y países en desarrollo.

Esta tesis persigue explotar el gran potencial de los productos electrónicos de consumo para concebir sistemas bioanalíticos baratos, portables, rápidos, simples, robustos, sensibles y con gran capacidad de trabajo. Los discos compactos son tecnologías de consumo maduras que se producen de forma masiva a nivel mundial y que están dotadas de elementos ópticos, mecánicos y electrónicos muy sofisticados, a coste extremadamente bajo. En esta línea, aunar el análisis químico con estas tecnologías plantea el desarrollo de dispositivos analíticos simples que afronten las restricciones comentadas anteriormente. Por otro lado, la integración de materiales biológicos amplía el alcance de estos sistemas y los sitúa dentro del marco del biosensado, lo que les proporciona un gran potencial para alcanzar las premisas que motivan este proyecto. Por ejemplo, esto hecho favorece el desarrollo de sistemas sencillos y altamente selectivos para detectar compuestos diana clínicamente importantes, entre otras capacidades.

Esta tesis explora nuevos avances en química analítica usando tecnologías de biosensado basadas en sistemas de disco compacto, y comprende seis publicaciones científicas distribuidas a lo largo de cuatro capítulos. Los estudios se han centrado en la tecnología *Thermochromic Etching Disks* (TED) (Capítulo 1), el diseño racional de ensayos de bioreconocimiento en discos compactos (Capítulo 2), y la detección sin marcaje para realizar análisis *in situ* (Capítulos 3 y 4).

Esta investigación comienza estudiando las posibilidades que ofrecen los sistemas TED para el desarrollo de nuevos biosensores basados en disco. Primero, enmarcado en una discusión del estado del arte y futuras tendencias en biosensado foto y termocrómico, se presenta un nuevo sistema (basado en discos y lectores TED) mediado por luz para el desarrollo de señales en ensayos de bioreconocimiento. Ésta constituye una estrategia novedosa para aprovechar el foto y termocromismo en biosensado, y presenta un gran potencial para simplificar los procesos de desarrollo de señal en sistemas bioanalíticos.

A continuación, se aborda cómo transformar la tecnología TED en sistemas analíticos integrados basados en discos compactos. TED ha demostrado ser una herramienta muy versátil para analizar, de forma sensible, ensayos de bioreconocimiento usando plataformas y escáneres

fácilmente obtenidos a partir de discos y lectores convencionales, respectivamente. Un único disco ha mostrado poder albergar varios ensayos biológicos importantes y de distinta naturaleza (micromatriz, cultivos celulares, inmunofiltración, turbidimetría, etc.), para ser analizados de forma sensible a través de imágenes. Este estudio remarca el potencial de los sistemas microfluídicos y la detección sin marcaje para ser implementados en los biosensores TED.

En cuanto al diseño racional, se presenta un método teórico-experimental (INSEL), basado en modelos cinéticos y de transporte de masa, para optimizar ensayos de bioreconocimiento y explorar su comportamiento. INSEL se ha implementado como una herramienta *in silico* que permite caracterizar biointeracciones mediante mínima experimentación, realizar optimizaciones dirigidas a objetivos particulares definidos por el usuario, y computar el efecto de variables críticas de forma sencilla y sin experimentos adicionales. También, este estudio demuestra las capacidades de los microinmunoensayos en disco compacto como técnica de rutina para estudiar biointeracciones.

Las técnicas bioanalíticas de detección sin marcaje permiten analizar eventos de bioreconocimiento sin incorporar elementos de señalización. Este tipo de detección presenta muchas ventajas para el desarrollo de biosensores, tales como protocolos de ensayo más simples y una mayor fiabilidad de los resultados. Sin embargo, estas técnicas tienden a requerir materiales nanoestructurados y equipos de medida caros y complejos, y suelen presentar capacidades de trabajo relativamente bajas. Así pues, este trabajo pretende afrontar esas limitaciones, mediante el aprovechamiento de los elementos integrados en las tecnologías de disco compacto, para desarrollar biosensores que permitan detección sin marcaje. En esta línea, los discos compactos convencionales contienen una nanoestructura en forma de surco en espiral, cuya adaptación como transductor ópticamente activo para biosensado sin marcaje ha sido abordada en los siguientes estudios.

Surface-enhanced Raman spectroscopy (SERS) es una técnica que permite análisis sensibles y selectivos, posibilitando en algunos casos la detección sin marcaje de analitos biológicos. En este trabajo, las nanoestructuras en forma de surco obtenidas a partir de discos regrabables convencionales (CD-R y DVD-R) fueron recubiertas con plata y adaptadas para ser activas en SERS. Esta estrategia supone una alternativa, económicamente efectiva e industrialmente escalable, a los sustratos SERS típicamente usados en bioanálisis. Estos materiales han mostrado respuestas plasmónicas sintonizables, una amplificación Raman significativa, y han permitido analizar muestras biológicas complejas (como proteínas y exosomas) mediante SERS sin usar marcadores. Además de introducir sustratos SERS grandes y baratos, este trabajo también sugiere el desarrollo de escáneres Raman basados en lectores de disco.

Otra aproximación presentada en esta tesis aborda la implementación de DBS (*diffraction-based sensing*) en tecnologías TED, con el fin de desarrollar biosensores para detección sin marcaje basados en discos y lectores convencionales. DBS se fundamenta en monitorizar cambios en los patrones difractados por redes constituidas por receptores biológicos (*biogratings*). Primero, se presenta una amplia evaluación experimental de las posibilidades analíticas ofrecidas por DBS. Este estudio describe cómo aprovechar esta técnica para desarrollar biosensores con capacidades interesantes, tales como detección sin marcaje, análisis en tiempo real, alta compatibilidad de materiales sustrato, y determinación sensible de compuestos orgánicos de bajo peso molecular (como por ejemplo atrazina).

Finalmente, a partir del conocimiento sobre DBS obtenido en los estudios previos, se investiga la fabricación de multitud de *biogratings* de proteínas sobre discos TED mediante impresión por microcontacto. En lugar de materiales nanoestructurados caros, en este estudio hemos propuesto utilizar las nanoestructuras tipo surco de discos convencionales como patrones para crear biogratings. Con estas matrices de biogratings de proteínas sobre discos compactos, se ha demostrado la determinación sensible y sin marcaje de anticuerpos, usando lectores TED adaptados como escáneres analíticos. Esta investigación ha probado el concepto para la detección sin marcaje en sistemas TED convencionales, e introduce avances importantes que apuntan al desarrollo de materiales funcionales y sistemas de detección, baratos e industrialmente escalables, que aprovechen las tecnologías de consumo para realizar biosensado sin marcaje.

RESUM

L'auge de la instrumentació en les ciències analítiques ha originat un ampli ventall de sistemes analítics que juguen un paper crucial en multitud d'àrees clau per als estàndards de vida actuals, com ara el diagnòstic clínic, la seguretat alimentària i el control mediambiental, d'entre moltes altres. No obstant això, aquests sistemes de referència tendeixen a ser cars, grans, complexos, i solen involucrar procediments d'anàlisi tediosos i altament especialitzats. Aquest fet restringeix enormement la difusió de les ciències analítiques en entorns no especialitzats o amb recursos escassos, com per exemple el diagnòstic en casa, àrees remotes, i països en desenvolupament.

Aquesta tesi pretén explotar el gran potencial dels productes electrònics de consum per tal de concebre sistemes bioanalítics barats, portables, ràpids, simples, robusts, sensibles i amb una gran capacitat de treball. Els discos compactes són tecnologies de consum madures que es produeixen mundialment de forma massiva i que estan equipades amb elements òptics, mecànics i electrònics molt sofisticats, a un cost extremadament baix. Així doncs, posar en comú l'anàlisi químic amb aquestes tecnologies apunta cap al desenvolupament de dispositius analítics que afronten les restriccions comentades anteriorment. D'altra banda, la integració de materials biològics amplia les capacitats d'aquests sistemes i els situa dins del marc del biosensat, la qual cosa els confereix un gran potencial per assolir les premisses que motiven aquest projecte. Per exemple, aquest fet afavoreix el desenvolupament de sistemes analítics senzills i altament específics per detectar compostos diana clínicament importants, d'entre altres capacitats.

Aquesta tesi explora nous avanços en la química analítica usant tecnologies de biosensat basades en sistemes de disc compacte, i comprèn sis publicacions científiques distribuïdes en quatre capítols. Els estudis s'han centrat en la tecnologia *Thermochromic Etching Disks* (TED) (Capítol 1), el disseny racional d'assajos de bioreconeixement en discos compactes (Capítol 2), i la detecció sense marcatge per realitzar anàlisi *in situ* (Capítols 3 i 4).

Aquesta investigació comença amb l'estudi de les possibilitats que ofereixen els sistemes TED per al desenvolupament de nous biosensors basats en discs. Primer, dins del marc d'una discussió de l'estat de l'art i tendències futures en biosensat foto i termocròmic, es presenta un nou sistema (basat en discos i lectors TED) per al desenvolupament de senyals mitjançant llum, en assajos de bioreconeixement. Aquesta constitueix una nova estratègia per aprofitar el foto i termocromisme en biosensat, mentre que també presenta una gran potencial per simplificar els processos de desenvolupament de senyal en sistemes bioanalítics.

Tot seguit, s'aborda com transformar la tecnologia TED en sistemes analítics integrats basats en discos compactes. TED ha demostrat ser una eina molt versàtil per analitzar, de forma sensible, assajos de bioreconeixement usant plataformes i escàners fàcilment obtinguts a partir de discos i lectors convencionals, respectivament. Un únic disc ha mostrat poder albergar diversos assajos

biològicament importants i de distinta naturalesa (micromatrius, cultius cel·lulars, immunofiltració, turbidimetria, etc.), per a ser analitzats de forma sensible a través d'imatges. Aquest estudi remarca el potencial dels sistemes microfluídics i la detecció sense marcatge per a ser implementats en els biosensors TED.

Pel que fa al disseny racional, es presenta un mètode teòric-experimental (INSEL), basat en models cinètics i de transport de massa, per optimitzar assajos de bioreconeixement i explorar el seu comportament. INSEL s'ha implementat com a una eina *in silico* que permet caracteritzar biointeraccions amb mínima experimentació, realitzar optimitzacions dirigides cap a objectius particulars definits per l'usuari, i computar l'efecte de variables crítiques de forma senzilla i sense experiments addicionals. També, aquest estudi demostra les capacitats dels microimmunoassajos en disc compacte com a tècnica de rutina per estudiar biointeraccions.

Les tècniques bioanalítiques de detecció sense marcatge permiteixen analitzar processos de bioreconeixement sense incorporar elements de senyalització. Aquest tipus de detecció presenta molts avantatges per al desenvolupament de biosensors, com ara protocols d'assaig més simples i resultats més fiables. No obstant això, aquestes tècniques tendeixen a requerir materials nanoestructurats i equips de mesura cars i complexos, i solen presentar capacitats de treball relativament baixes. Així doncs, aquest treball pretén fer front a aquestes limitacions, mitjançant l'aprofitament dels elements integrats en les tecnologies de disc compacte, per desenvolupar biosensors que permeten detecció sense marcatge. En aquesta línia, els discos compactes convencionals contenen una nanoestructura en forma de solc en espiral, l'adaptació de la qual com a transductor òpticament actiu per a biosensat sense marcatge s'ha abordat en els següents estudis.

Surface-enhanced Raman spectroscopy (SERS) és una tècnica que permet anàlisis sensibles i selectius, i possibilita en alguns casos la detecció sense marcatge d'analits biològics. En aquest treball, les nanoestructures en forma de solc obtingudes a partir de discos compactes regravables convencionals (CD-R i DVD-R) van ser recobertes amb plata i adaptades per a ser actives en SERS. Aquesta estratègia suposa una alternativa, econòmicament efectiva i industrialment escalable, als substrats SERS típicament usats en bioanàlisi. Aquests materials han mostrat respostes plasmòniques sintonitzables, una amplificació Raman significativa, i han permès analitzar mostres biològiques complexes (com proteïnes i exosomes) mitjançant SERS sense usar marcadors. A més d'introduir substrats SERS grans i barats, aquest treball també suggereix el desenvolupament d'escàners Raman basats en lectors de disc.

Una altra aproximació presentada en aquesta tesi aborda la implementació de DBS (*diffraction-based sensing*) en tecnologies TED, per tal de desenvolupar biosensors basats en discos i lectors convencionals que permeten detecció sense marcatge. DBS es fonamenta en monitoritzar canvis

en els patrons difractats per xarxes constituïdes per receptors biològics (*biogratings*). Primer, es presenta una amplia avaluació experimental de les possibilitats analítiques que ofereix aquesta tècnica. Aquest estudi descriu com aprofitar DBS per desenvolupar biosensors amb capacitats interessants, com ara la detecció sense marcatge, l'anàlisi en temps real, l'alta compatibilitat pel que fa als materials dels substrats, i la determinació sensible de compostos orgànics de baix pes molecular (com ara atrazina).

Finalment, a partir del coneixement sobre DBS obtingut en els estudis previs, s'investiga la fabricació de multitud de biogratings de proteïnes sobre discos TED mitjançant impressió per microcontacte. En lloc de materials nanoestructurats cars, en aquest estudi hem proposat utilitzar les estructures tipus solc de discos convencionals com a patrons per crear biogratings. Amb aquestes matrius de biogratings de proteïnes sobre discos compactes, s'ha demostrat la determinació sensible i sense marcatge d'anticossos, usant lectors TED adaptats com a escàners analítics. Aquesta investigació ha provat el concepte de detecció sense marcatge en sistemes TED convencionals, i introdueix avanços importants que apunten cap al desenvolupament de materials funcionals i sistemes de detecció, barats i industrialment escalables, que aprofiten les tecnologies de consum per dur a terme bioanàlisi sense marcatge.

DISSEMINATION OF RESULTS

The studies included in this thesis have lead to the scientific documents listed below.

Articles in indexed scientific journals:

1. M. Avella-Oliver, D. Gimenez-Romero, S. Morais, M.A. González-Martínez, P.R. Bueno, R. Puchades, A. Maquieira, "INSEL: an *in silico* method for optimizing and exploring biorecognition assays"
   Chemical Communications, 49 (**2013**), 10868-10870.
   Impact Factor (2017): 6.319

2. M. Avella-Oliver, S. Morais, J. Carrascosa, R. Puchades, A. Maquieira, "Total analysis systems with thermochromic etching discs technology".
   Analytical Chemistry, 86 (**2014**), 12037-12046.
   Impact Factor (2017): 6.320

3. M. Avella-Oliver, S. Morais, R. Puchades, A. Maquieira, "Towards photochromic and thermochromic biosensing".
   Trends in Analytical Chemistry, 79 (**2016**), 37-45.
   Impact Factor (2017): 8.442

4. M. Avella-Oliver, R. Puchades, S. Wachsmann-Hogiu, A. Maquieira, "Label-free SERS analysis of proteins and exosomes with large-scale substrates from recordable compact disks".
   Sensors and Actuators B: Chemical, 252 (**2017**), 657-662.
   Impact Factor (2017): 5.401

5. M. Avella-Oliver, V. Ferrando, J.A. Monsoriu, R. Puchades, A. Maquieira, "Diffraction-based sensing with biogratings for qualitative and quantitative analytical applications".
   Analytica Chimica Acta, In revision (**2017**).
   Impact Factor (2017): 4.950

6. M. Avella-Oliver, J. Carrascosa, R. Puchades, A. Maquieira, "Diffractive protein gratings as optically active transducers for high-throughput label-free immunosensing".
   Analytical Chemistry, In revision (**2017**).
   Impact Factor (2017): 6.320

Patents:

1. J.M. Avella Oliver, S.B. Morais Ezquerro, J. Carrascosa Rubio, A. Maquieira Catala, R. Puchades Pla, "Analytical sensor and method for the production thereof".
   National publication number: 2 524 744
   International publication number: WO 2015/118199 A1
2. J.M. Avella Oliver, S.B. Morais Ezquerro, J. Carrascosa Rubio, A. Maquieira Catala, R. Puchades Pla, "System and method for analysing samples".
   National publication number: 2 525 267
   International publication number: WO 2015/118200 A1

Communications in conferences:

1. M. Avella, D. Giménez-Romero, S. Morais, R. Puchades, A. Maquieira, "Aplicación de la modelización cinética a la optimización de inmunoensayos".
   VI Workshop on Sensors and and Molecular Recognition, Burjassot (Spain), 2012.
2. M. Avella, D. Giménez-Romero, S. Morais, J. Carrascosa, R. Puchades, A. Maquieira, "Tratamiento de señal en registros de ensayos heterogeneos".
   VI Workshop on Sensors and Molecular Recognition, Burjassot (Spain), 2012.
3. M. Avella-Oliver, D. Gimenez-Romero, S. Morais, R. Puchades, A. Maquieira, "Un método computacional para la exploración virtual de inmunoensayos".
   VI Workshop on Sensors and Molecular Recognition, Valencia (Spain), 2013.
4. M. Avella-Oliver, D. Gimenez-Romero, S. Morais, P.R. Bueno, R. Puchades, A. Maquieira, "Desarrollo de una metodología in silico para la optimización de inmunoensayos".
   XXXIV Reunión RSEQ, Santander (Spain), 2013.
5. M. Avella-Oliver, S. Morais, J. Carrascosa, R. Puchades, A. Maquieira, "Desarrollo de sistemas totales de análisis en Termochoromic Etching Discs".
   VIII International Workshop on Sensors and Molecular Recognition, Burjassot (Spain), 2014.
6. N.J. Sacco, E. Cortón, M. Avella-Oliver, S. Morais, R. Puchades, A. Maquieira, "Detection of pathogenic bacteria using immunofiltration and LightScribe technology".
   IEEE 9th Ibero-American Congress on Sensors, Bogotá (Colombia), 2014.
7. M. Avella-Oliver, S. Morais, R. Puchades, A. Maquieira, "Sistemas analíticos totales en superficies termocrómicas".
   XX Reunión SEQA, Santiago de Compastela (Spain), 2015.

8. M. Avella-Oliver, V. Ferrando, J.A. Monsoriu, R. Puchades, A. Maquieira, "Redes de diffracción de bioreceptores para monitorizar eventos de reconocimiento molecular". *IX International Workshop on Sensors and Molecular Recognition*, Valencia (Spain), 2015.

9. M. Avella-Oliver, C.S. Robertson, S. Wachsmann-Hogiu, R. Puchades, A. Maquieira, "Low-cost materials for SERS label-free biosensing". *Europt(r)ode XIII*, Graz (Austria), 2016.

10. M. Avella-Oliver, G. Sancho-Fornes, R. Puchades, S. Wachsmann-Hogiu, A. Maquieira, "Protein and exosome analysis with SERS-active substrates from consumer electronics". *X International Workshop on Sensors and Molecular Recognition*, Burjassot (Spain), 2016.

11. M. Avella-Oliver, J. Carrascosa, R. Puchades, A. Maquieira, "Analysing unlabelled biointeractions by diffractive networks of bioreceptors". *XXXVI Reunión RSEQ*, Sitges (Spain), 2017.

12. M. Avella-Oliver, J. Carracosa, R. Puchades, A. Maquieira, "Biogratings as optical transducers for point-of-care biosensing". *XI International Workshop on Sensors and Molecular Recognition*, Valencia (Spain), 2017.

ACRONYMS AND ABBREVIATIONS

4-ATP	4-aminothiophenol
Ab	Antibody
AFM	Atomic force microscopy
AOF	Aggregate objective function
BSA	Bovine serum albumin
CD	Compact disk
CFZ	Control feature zone
DBS	Diffraction-based sensing
DNA	Deoxyribonucleic acid
DVD	Digital versatile disk
ELIFA	Enzyme-linked immunofiltration assay
ELISA	Enzyme-linked immunosorbent assay
FESEM	Field emission scanning electron microscopy
FIB	Focused ion beam
GAR	Goat anti-rabbit ab
HPM	Hollow polymeric microspheres
HRP	Horseradish peroxisdase
IC_{50}	Half maximal inhibitory concentration
Ig	Immunoglobulin
IgG	Immunoglubulin G
IR	Infrared
LOD	Limit of detection
LOQ	Limit of quantification
pAb	Polyclonal antibody
PBS	Phosphate buffered saline
PC	Polycarbonate
PCR	Polymerase chain reaction
PDMS	Polydimethylsiloxane
PE	Polyester
PMMA	Polymethyl methacrylate
PS	Polystirene
PVDF	Polyvinylidene fluoride
R	Recordable
RNA	Ribonucleic acid
ROM	Read-only memory
RW	Rewritable
SD	Standard deviation

SEM	Scanning electron microscopy
SERS	Surface-enhanced Raman scattering
SNR	Signal-to-noise ratio
SPR	Surface plasmon resonance
TED	Thermochromic Etching Disks
TIR	Total internal reflection
TLC	Thermochromic liquid crystal
TMB	3,3',5,5'-tetramethylbenzidine
UV	Ultraviolet
Vis	Visible
μCP	Microcontact printing

CONTENTS

1. Introduction

1.1 The rise of bioanalysis

In its initial stages, analytical chemistry typically involved laborious manual procedures to separate and sense target analytes by means of their chemical reactivity. Qualitative and quantitative analysis of elements, functional groups, and molecules were performed by these methodologies, currently known as "classical analysis".[1] In contrast, the term "instrumental analysis" englobes analytical techniques that exploit technological instruments. Rather than chemical reactivity, these systems typically deal with physical properties of the analytes (light absorption or emission, conductivity, mass/charge ratio, etc.).[2] Dated in 1860, the flame emissive spectroscopy developed by Bunsen and Kirchhoff is considered the first instrumental method of analysis.[3] Instrumental analysis experimented a rising trend and constitutes the main playground of analytical chemistry since roughly the second half of the nineteenth century.[4]

Bioanalysis and bioanalytical chemistry are more recent fields that emerged from the driving forces of multidisciplinarity in analytical chemistry. From a broad viewpoint, this sub-discipline deals with measuring parameters involved in biochemicals (drugs, metabolites, proteins, nucleic acids, cells, etc.) and/or biological systems (blood, serum, saliva, tissues, microorganisms, cells, etc.). The first bioanalytical attempts sought the determination of drugs in biological fluids for forensic purposes.[5] From then on, the complexity of living systems became somehow an stimulating challenge that motivated the evolution of measurement sciences.[6] Nowadays, bioanalytical chemistry is an active scientific area that plays an important role in chemistry, biochemistry, pharmaceutics, and clinics, among other fields.

1.2 Sensors, biosensors, and biosensing

Chemical sensors (or chemosensors) are systems that transforms chemical information into analytically useful signals,[7] and are usually devoted to provide alternative solutions to regular analytical instrumental techniques. Therefore, these sensors aim to be simple, robust, compact, fast, and inexpensive, and enable accurate, sensitive, and selective analysis of samples.

Chemical sensors comprise a receptor component that transforms chemical parameters of interest into forms of energy that can be measured by a transducer.[7] Receptors typically entail materials that selectively interact with the analyte, and transducers are systems that transform stimuli from the receptor into an output useful analytical signal.[7] In addition to these parts, chemical sensors can also integrate components to perform other stages of the analytical process (sampling, sample preparation, signal processing, etc.).

Chemical sensors can be classified in different groups depending on the nature of the signal managed by the transducer. Optical chemosensors deal with modifications of optical magnitudes (absorption, fluorescence, scattering, refractive index, etc.) as a response of changes on the

chemical parameter of interest.[8] Analogously, electrochemical sensors typically involve electrodes to sense chemical parameters by means of their particular properties (potential, current, etc.).[9] Also, other physical phenomena can be involved in the transduction, for instance in mass-sensitive, magnetic, or thermometric chemical sensors.[7]

Biosensors are a particular sort of chemical sensors that incorporate receptors constituted by biological systems (enzymes, proteins, antibodies, nucleic acids, cells, biomimetics, etc.). Biosensors fall within the general framework of biosensing, and the term biosensing refers to the bioanalytical discipline that deal with biomolecular interactions, as an object of study or as a tool to sense other chemical parameters. Along these lines, it must be noted that analytical systems involving biomolecular interactions but not meeting the concept behind sensors also fall within biosensing.

Among the main strengths of biosensing, the use of biological materials as receptors enable to conceive extremely selective analytical systems. In addition to classical chemical analytes (organic molecules, metal ions, etc.), biosensing approaches are also a powerful tool to sense complex biological species (proteins, nucleic acids, cells, etc.). Therefore, biosensing also represents an important strategy to study chemical processes involved in living organisms.

A raising knowledge on enzymes and electrochemistry culminated in 1962 in the first description of a modern quantitative and instrumental biosensor.[10,11] From this point, biosensing experimented a continuous growth and nowadays entails an intense scientific and industrial activity.[12] To illustrate this rising trend, the global market for biosensors was estimated in 8.500 million USD in 2012 and is predicted to reach 16.8 billion USD by 2018.[13]

1.3 Biorecognition systems

Biorecognition is the main phenomenon involved in biosensing and biosensors. Many macromolecules from living organisms are capable of selectively binding (or recognizing) particular species. This docking phenomena is involved in a huge number of biological functions, and the expression “biorecognition systems” refers to the conjunction of these binding partners designed to interact each other. Using those biorecognition elements as receptor enables to selectively analyze its matching couple in complex samples. In these systems, the biochemical used as receptor and the compound to be analyzed are typically called probe and target, respectively. Also, the term receptor (or bioreceptor) is commonly employed to indistinctly denote any of these two elements.

Biorecognition systems are also often referred to as biorecognition assays, when applied to bioanalytical settings. Biorecognition assays are an important tool to study, *in vitro* and *in vivo*, the biochemical parameters of regulatory processes in biological systems. This fact entails major

relevance in fields like biology, health (medicine, pharmacology, etc.), environmental sciences, and agriculture, among others. Beyond this framework, the benefits of biorecognition assays also enable to conceive biosensors to perform chemical measurements in a range of classical analytical scenarios, such as clinical diagnosis, quality control in factories, or environmental analysis.[10]

Biorecognition assays are classified as homogeneous when probes and targets are in the same phase (commonly liquid, i.e. aqueous solutions), or heterogeneous when more than one phase is involved. In heterogeneous assays, probes are typically attached on the surface of a solid substrate (that acts as transducer) to analyze targets in solutions.[14]

ELISA multi-well plates (commonly made of polystyrene) are popular platforms to perform heterogeneous assays. Also, flat surfaces of different materials are commonly used to support heterogeneous biorecognition assays through microarray systems. In this format, small spots (typically micrometric) are densely arrayed on the surface of a chip, where each dot corresponds to a single assay. Microarrays enable multiplexed and high throughput analysis with small volumes of sample. Pioneered by commercial embodiments like the one of Affymetrix,[15] microarrays play an important role in massive screening for genomics and proteomics.[16] Fibers and membranes also entail particular benefits for heterogeneous assays, where lateral flow and ELIFA are some of the most representative approaches.[17] Metal electrodes are important platforms in these regards too. In fact, the electroanalytical systems for determining glucose levels in human blood are nowadays the most employed biosensors in the world.[18] Moreover, functional structures involving particular phenomena are also useful substrates for heterogeneous immunoassays. For instance, thin gold films, quartz crystals, and three-dimensional nanostructures enable to study biorecognition events by means of plasmon and acoustic resonances and light interference, respectively.[19,20]

Considering the biochemical nature of probes and targets, biorecognition assays can be classified in different groups, where the main ones are described below.

1.3.1 Biorecognition assays based on proteins

Immunoassays are one of the most representative biorecognition assays applied for bioanalytical purposes. In their heterogeneous format, immunoassays are based on immobilizing immunoreagents (antibodies or antigens) on solid substrates and incubating liquid samples on them, as shown in Figure 1A. The immobilized probes bind their matching targets, which enables to measure parameters (classically concentration) of targets present in samples.

Antibodies are extremely selective reagents, entail well-known production procedures, and can be designed to recognize targets of different nature, from small molecular weight compounds

(contaminants, metabolites, drugs, toxins, warfare agents, etc.) to macromolecular species (biomarkers, proteomic studies, etc.), particular proteins as antibodies (allergy diagnosis, immunology studies, etc.), and microorganisms (bacteria, virus, etc.). As a result, immunoassays are widely used and provide analytical solutions in an extremely broad range of applications.[21,22]

Enzymes are also very interesting receptors for biosensing (Figure 1B). The enzymatic assays enable to specifically sense target substrates, inhibitors, and activators by means of the enzymatic response,[23] measured by thermodynamic or kinetic methods.

In addition to antibodies and enzymes, other proteins are capable of recognizing and binding target biochemicals. These proteins can come from either natural or bioengineered origins and represent a valuable arsenal of bioreceptors for biorecognition assays. Among them, some proteins are typically used as versatile tools for many biosensing purposes. For instance, avidin and streptavidin selectively recognize biotin, and the (strept)avidin-biotin couple is commonly employed as a generic strategy to link bioreagents for bioanalytical purposes (Figure 1C). As another example, proteins A, G, and L selectively bind antibodies, and these binding partners are usually employed for probe anchoring and for antibodies purification.

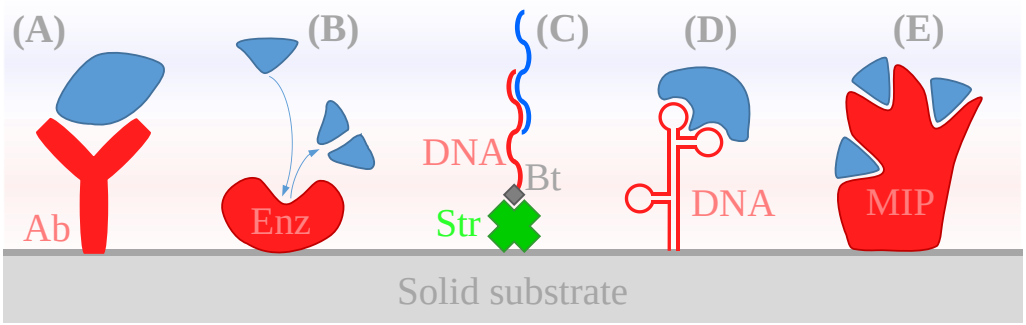

Figure 1. Illustration of different biorecognition assays in heterogeneous format, where probes are in red color and targets in blue. (A) Immunoassay. (B) Enzymatic assay. (C) DNA hybridization assay, using immobilized streptavidin (Str) and biotin (Bt) conjugation to attach oligonucleotide probes on the solid surface. (D) Biorecognition assay with nucleic acid aptamers. (E) Biorecognition based on MIPs.

1.3.2 Biorecognition assays based on nucleic acids

Single DNA and RNA probes selectively bind (hybridize) their complementary strands to form double-stranded structures, and this recognition principle is widely exploited for biosensing (Figure 1C). Target nucleotide sequences are commonly found at very low concentrations, so these assays typically analyze polymerase chain reaction (PCR) products instead of raw samples.

In addition to its amplification role for the subsequent hybridization assays, PCR can also be tailored to be a detection technique by itself.[24]

DNA hybridization assays are routinely employed for genomics through massive screening microarrays and for genotyping clinically important polymorphisms in patients. This strategy also enables to analyze particular organisms of interest (pathogens, allergens, GMOs, etc.) in samples. Besides DNA, hybridization assays can also by applied to RNA, for instance to study relevant species like microRNAs.[25]

Nucleic acids are labile polymers capable of adopting particular conformations depending on their nucleotides sequence. Aptamers are oligonucleotides with specific monomer sequences that generate three-dimensional conformations comprising selective binding sites for particular targets (Figure 1D). As a result, aptamers can be synthetized and used as receptors for analytes of different nature (small molecules, nucleic acids, proteins, etc.).[26]

1.3.3 Biomimetics for biorecognition assays

Within the bioanalytical scope, biomimetic systems are artificial materials designed to mimic biological properties applicable in sensing. The most paradigmatic example in these regards are molecular imprinted polymers (MIPs), giving their capability to mimic specific receptor-target interactions of biomacromolecules like antibodies (Figure 1E).[27] Among their main strengths, MIPs represents an artificial alternative to antibodies that can be produced by chemical synthetic methods and fashioned in functional structures.[28]

1.3.4 Other biorecognition assays

Thought the systems described above are the most representative ones, probes and targets of different nature can also be used to design biorecognition assays. For instance, some carbohydrates displayed on cell surfaces are tailored to specifically bind a particular group of proteins (the lectins), which is exploited to design carbohydrates-based biorecognition assays.[29] Also, more complex biological entities like phages (or bacteriophages) can also be employed for biosensing. Phages are viruses that selectively recognize and infect specific types of bacteria. For that, proteins contained in the membranes of phages bind biochemicals (proteins, carbohydrates, lipids, etc.) present in the bacterial cell walls. This fact enables to develop assays based on phages as bioreceptors for detecting bacterial pathogens as well as molecular and biomacromolecular targets.[30,31] Another example in these regards is the use of whole cells as receptors in biorecognition assays, which favors the direct analysis of physiologically relevant parameters and enable to assess the bioavailability of particular targets.[32]

1.4 Detection techniques

The main goal of biorecognition assays is to provide analytically useful signals to measure important parameters of (bio)chemical systems, such as concentrations, affinity constants, and conformational states, among others. In many instances, the binding events of biorecognition assays can not generate by themselves measureable stimulus by the transducer. In these cases, signaling elements known as "labels" (also tracers or tags) are introduced in the biorecognition systems. In contrast, some biosensing approaches enable biorecognition events to provide measurable phenomena without using labels. Considering this fact, bioanalytical systems can be classified as labeled and label-free.

The key aspects of the most significant detection techniques used for biosensing are described below and summarized in Table 1. Given the scope of this thesis, only optical biosensing systems are considered beyond this point, and approaches involving other measurement principles, such as electrochemical or acoustic transduction,[33-35] are not discussed.

1.4.1 Labeled systems

Labels are typically linked (also known as conjugated) to the species involved in the biorecognition events. Secondary antibodies in indirect immunoassays, target analogues in competitive formats, and polynucleotide sequences from PCR products, are some examples of compounds commonly labeled.[36]

One of the first labels employed in biorecognition assays were radioisotopes, such as ^{125}I. Measuring binding events by means of radioactive emission lead to sensitive immunoassays, among other strenghts.[37,38] However, the use of radioactive labeling was restricted mainly because of its potential risks.

These limitations with radioisotopes stimulated the development of enzymatic labels.[37] In this approach, biorecognition assays are performed using enzymes conjugated to biochemicals, and enzymatic substrates are added in order to develop a signal.[36,39] These developers are designed to exhibit changes in a measurable magnitude after their enzymatic modification. Horseradish peroxidase (HRP) together with substrates as 3,3',5,5'-tetramethylbenzidine (TMB) or o-phenylenediamine (OPD) are partner species typically used in enzymatic labeling. Alkaline phosphatase and 5-bromo-4-chloro-3-indolyl-phosphate (BCIP) is also a very useful enzymatic couple in these regards. With these systems, the binding event can be assessed spectrophotometrically. Moreover, TMB substrates yield blue precipitates that attenuate incident light by absorption and scattering.

Fluorophores are molecules suitable to be bioconjugated and their use as labels enable sensitive measurements of binding events.[36,40] Also, this strategy do not require additional signal

developing steps and can be monitored by reasonably simple setups. Some phenomena, like photobleaching and quenching, limits the performance of fluorescent labeling. However, the broad range of available fluorophores constitutes a significant advantage.[36]

Labels based on colored micro and nanoparticles can be naked-eye detectable and have been commonly used in qualitative assays, such as lateral flow tests. Latex nanobeads, carbon nanoparticles, and gold nanoparticles are some exemplary labels used in this framework.[41]

Table 1. Summary of the main features of representative detection techniques typically used in biorecognition assays.

System	Principle	Strengths	Limitations[a]	Ref[b]
Radioisotopes	Radioactivity	Sensitivity	Radiation hazards Labeled	37,38
Enzymes	Absorbance Luminescence	Sensitivity Great commercial offer	Labeled Signal developing	36,39
Organic fluorophores	Luminescence	Sensitivity Simplicity Great commercial offer	Labeled Quenching Photobleaching	36,40
Quantum dots	Luminescence	Enhanced luminescent properties	Labeled Complex synthesis Scarce commercial reagents	42,43
SPR	Plasmon resonance	Label-free Maturity Great commercial offer	Expensive equipment and materinals	44,45
Mach-Zehnder	Light interference	Label-free	Expensive nanofabrication Low multiplexing	46,47
Photonic crystals	Multiple	Label-free	Expensive nanofabrication Moderate multiplexing	47,48
SERS	Raman scattering	Label-free Selectivity	Expensive substrates Moderate multiplexing	49,50
Diffraction-based sensing	Light diffraction	Label-free Simplicity Inexpensive materials	Scarce commercial products	51,52

[a] Main representative limitations considering the current state-of-the-art.

[b] Illustrative references in biosensing.

Gold nanoparticles are also widely employed for signal development purposes. To this end, bioreagents are labeled with colloidal gold nanoparticles and a solution containing Ag^+ and a reducing agent (e.g., hydroquinone) is added. Gold nanoparticles trigger an autocatalytic Ag^+ reduction into insoluble metallic silver.[53] As a result, a precipitate whose magnitude is directly proportional on the amount of gold nanoparticles is obtained. These silver precipitates absorb, scatter and reflect light, thus enhancing the sensitivity of the assays several orders of magnitude compared to the raw colorimetric detection of gold nanoparticles.

Nanoscience and nanotechnology introduced new phenomena that can also be exploited to conceive labels with sophisticated functionalities. For instance, quantum dots offers an attractive alternative to regular fluorophores, given their improved fluorescent features.[42,43] Moreover, metallic nanoparticles can be used as labels to measure binding events by means of plasmonic systems, such as surface plasmon resonance (SPR) and surface-enhanced Raman scattering (SERS).[54,55]

1.4.2 Label-free

Optical label-free strategies typically deal with nanoscale phenomena that take place on the surface of functional materials, where biorecognition assays are placed. Thus, together with the raise of nanoscience and nanotechnology, a number of new label-free techniques emerged. Compared to labeled and signal enhanced systems, improving sensitivity is typically the main challenge of label-free techniques. However, these strategies involve many characteristic features that offset this limitation and offer appealing analytical strengths.

Omitting labels avoid signal artifacts caused by labels in the measurement of biorecognition events. Labels can interfere with the biointeraction being measured, for instance by steric hindrance or by occlusion of the binding sites. Also, different phenomena that affect the performance of labels, such as quenching and bleaching for fluorescent labels, are also potential artifact sources.[46] Moreover, label-free sensing deal with species in their native state, which allows for studying biointeractions in similar conditions to those taking place in living organisms.

Label-free systems simplify the analytical process by omitting stages, for instance incubations of labeled bioreagents and signal development steps. The bioconjugation of labels, which requires previous knowledge of the species to be labeled,[56] are also eluded. In addition, these facts favor the development of miniaturized and portable sensors.[57]

Regarding economical considerations, label-free detection usually requires functional materials that involve costly manufacturing processes, whose scope is typically restricted beyond the lab-scale. Also, the detection setups for label-free tend to be complex and expensive. In contrast, the

simplification of the analytical protocol enabled by label-free systems (i.e., less stages) entails an inherent higher cost-effectiveness, for instance in terms of the sample handling setups. Furthermore, expensive species such as labels (e.g., ready to bioconjugate fluorophores or noble metal nanoparticles), signal developers (such as silver), and additional labeled bioreagents (e.g., secondary antibodies in indirect immunoassays) are avoided.

Besides, most of labeled biosensing approaches employ labels and signal developers as a final step (after the biorecognition), thus only measuring the endpoint of the biointeraction. In contrast, real-time measurements provide dynamic data of binding events and enable monitoring their evolution along time. Whereas certain labeled strategies also allows real-time measurements, this is common feature in label-free systems since omitting labels strongly favors it. Appealing parameters, such as the evolution of the conformational states of probes and targets during their biorecognition, can be studied by label-free and real-time measurements.[58]

Optical label-free approaches can be classified according to the nature of the physicochemical phenomena exploited to sense binding events, and the most relevant groups are described below.

1.4.2.1 Surface plasmon resonance (SPR)

Electrons in the surface of metals are susceptible to undergo collective oscillations (plasmons) induced by an incident light. Plasmons resonate when they interact with specific light frequencies and can be detected as spectrophotometric absorptions. The frequency of these plasmon resonances depends on the nature of the metal-dielectric interfaces. Since binding events of biorecognition systems placed on this interface modify the amount of biological matter on it, they can be sensed by means of a shift in the resonance frequency.[44]

SPR biosensensors are probably the optical label-free systems that have reached the highest impact. Biacore launched in 1990 a commercial equipment to run SPR-based assays that is still nowadays a reference technique. The success of SPR relies, in part, on its simple measurement setup and its minimal nanofabrication requirements.[45]

1.4.2.2 Interferometry

Propagating waves interfere in a constructive or destructive manner when they overlap in different phases, and interferometry lies in measuring this phenomena. Interferometry englobes a number of label-free biosensing techniques,[46] where the Mach-Zehnder interferometer is one of the most paradigmatic examples. In this approach, a laser beam is conducted throughout a waveguide that splits into two arms to finally converge in one unique guide, which sends the light to a detector. Light propagating through these waveguides involves evanescent waves, i.e. electromagnetic oscillations on the surface of the material that penetrate in the adjacent medium

following an exponential decay. A biorecognition systems is placed on the surface of an arm, while the other one remains unaltered. As a result, binding events can be sensed by means of the light interference when both arms merge (i.e., the intensity measured in the detector).[46,47]

In addition to this approach, there are many other interferometric label-free biosensing systems, some ones based on similar strategies (e.g., Young and Hartman interferometry) and others that exploit interferometry through different approximations.[46,47,59]

1.4.2.3 Photonic crystals

Photonic crystals are materials periodically nanostructured that interact with electromagnetic radiation and lead to particular spectral bands (by transmission and/or reflection). Depending on the directions in which periodicity extends, these materials are known as one-, two-, or three-dimensional photonic crystals. For instance, layers of materials with different refractive index are alternately superposed in one-dimensional systems. These photonic crystals act as dielectric mirrors, in which interferences between the incident and reflected beams generate spectral bands.[60]

Photonic crystals can be tailored to exhibit spectral responses dependent on the refraction into or onto the material. Therefore, given that biological matter have a particular refraction index, binding events can be sensed by implementing biorecognition systems in photonic crystals.[47,48]

1.4.2.4 Surface-enhanced Raman Scattering (SERS)

Raman spectroscopy is an optical technique based on light scattering, which is used to analyze chemical compositions. When light interacts with matter part of the incident radiation becomes scattered. Light scattering can be explained by collisions between incident photons and matter particles (molecules, atoms, electrons, etc.) that originate light propagations in trajectories that do not meet the transmission and reflection conditions. Most of the scattered photons lead to elastic collisions that do not modify their energy (Rayleigh scattering), so this scattered light keeps its original wavelength. In contrast, around 1 of every 10^7 scattered photons undergo inelastic collisions (Raman scattering), in which incident and scattered photons have different wavelengths.

From a chemical point of view, the features of matter that yield Raman scattering can be correlated to particular molecular structures (moieties, functional groups, etc.). Therefore the scattered spectra reveals qualitative information about the chemical composition. In a typical Raman setup, a visible or near-IR laser beam is focused on a sample through an optical system, which also collects the polychromatic scattered light in order to address its spectroscopic analysis.

Raman spectra offers characteristic fingerprint data for particular compounds, which enables highly selective analysis. However, the low population of inelastically scattered photons restricts the sensitivity of regular Raman spectroscopy. Along these lines, SERS systems exploit the benefits of Raman spectroscopy and boost its sensitivity many orders of magnitude.[49]

SERS is based on measuring the Raman scattering of samples placed on particular substrates, which comprise metallic structures (typically silver and gold nanostructures) designed to undergo plasmon resonances at the laser wavelength.[49] As illustrated in Figure 2, SERS-active structures restrict the free propagation of surface plasmons, thus localizing surface plasmons in certain areas of the structure (called hotspots). The enhanced electric field confined in hotspots magnifies light-matter interaction, which originates the SERS enhancement. Moreover, scattered light can also couple with the structure to induce additional enhancement.

By placing biological matter and biorecognition assays on suitable nanostructured materials, SERS entails great biosensing potential thanks to its label-free capabilities, enhanced sensitivity, extraordinary selectivity, and the rich compositional information that this technique offers (compared to most of biosensing approaches).[50]

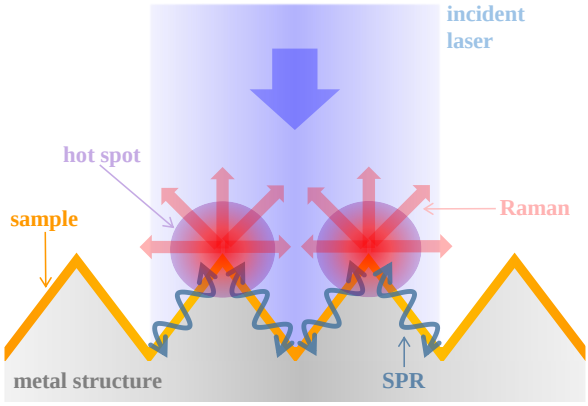

Figure 2. General scheme of SERS.

1.4.2.5 Diffraction-based sensing

Light diffraction describes the changes in the phase distribution of propagating waves when they hit structures comprising sizes in the wavelength range. As depicted in Figure 3A, planar waves propagate as circular wavefronts after interacting with a single slit. For several slits, the circular waves that emerge from them overlap in different phases and exhibit constructive and destructive interferences (Figure 3B). As a result, diffraction patterns constituted by brighter and darker motifs are projected in the planes along the propagation direction, whose features are directly related with the characteristics of the diffractive element.

In addition to slits, any object or structure that comprise variations (roughly sized in the wavelength range) of parameters that affect light propagation (absorption, refraction index, etc.) generate diffraction. Along these lines, diffractive gratings are periodic structures that can be designed to exhibit particular diffraction patterns. For instance, gratings are typically tailored to split an incident laser into many beams that emerge from the grating in different angles. These split beams, as well as their corresponding spots in the diffraction pattern, are called diffraction orders and numbered from -N to +N (natural numbers), where the 0^{th} order keeps the original direction (Figure 3C).

Diffraction-based sensing is an analytical technique that relies on patterning biological probes as diffraction gratings on solid substrates. The amount of matter constituting the grating increase when the immobilized probes bind their target, which enhance the diffraction efficiency of the grating (i.e., intensities ratio between incident beam and the 0^{th} order). As a result, molecular scale process can be measured by means of the intensity of a diffraction order. This is a simple and versatile analytical technique that entails close to background-free analysis and minimal nanofabrication requirements, and enables label-free and real-time measurements of molecular-scale events of different nature.[51,52]

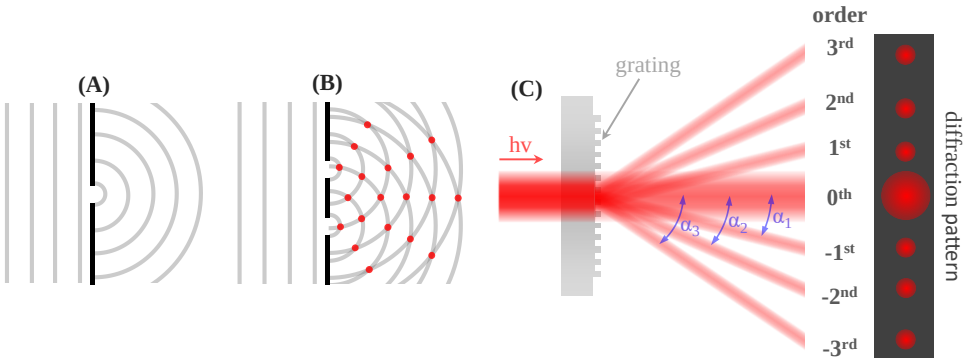

Figure 3. (A) Single slit diffraction. (B) Double slit diffraction, where red dots indicate spots of constructive interference. (C) General scheme of diffraction using a grating.

1.5 Point-of-need

Reference instrumental analysis techniques have established a model based on central laboratories, in which samples must travel from their sampling spot to these facilities. Also, the results of the analyses often have to be sent back to the sampling place, where decisions are made.

This situation involves important implications in terms of sample stability along time and under transporting conditions. Moreover, these time delays between sampling and the obtaining the

final results is a dramatic drawback in many situations, where clinical analysis represents one of the most paradigmatic examples. For instance, early detection of acute diseases and fast decision-making in emergency medicine strongly influences the success of the medical intervention.

This centralized model is particularly inefficient in remote areas, far away from urban centers, where the distance between sampling and the analysis is maximal. In addition to restrict the access of remote communities to analytical services (i.e., clinical analysis), these facts also involve a negative impact on other issues, such as environmental analysis.

Moreover, communities with scarce resources have a restricted access to these analytical instrumentation, because of their prohibitive costs. In addition to neglect the transversal benefits of analytical sciences in the present, these facts contribute to perpetuate precarious live conditions in these areas and strongly difficult their progress.

All these facts motivate the development of sensing systems applicable in point-of-need scenarios. Point-of-need means to perform the analysis and obtain the corresponding results in the same place and time in which the analysis is required. The term point-of-care refers to particular point-of-need systems applied for healthcare purposes.[61] Along these lines, the concept behind chemical sensors (i.e. sensitive, selective, inexpensive, portable, compact, fast, and simple analytical devices) strongly marry the point-of-need scope.

Science is currently focused on total analysis system, i.e. chemical sensors that integrate the whole analytical process (from sampling to results interpretation) to be preferably handled by non-trained personnel.[62] The development of chemical sensors and total analysis systems are thus partner areas. When they involve miniaturization, the terms micro total analysis systems or lab-on-a-chip are typically employed to denote these approaches.

Total analysis systems entail both aspects, sample handling and sensing. For the first one, microfluidics plays a central role since it allows for automatizing unit operations comprised in the analytical process (filtration, mixing, incubation, etc.). Regarding sensing, the benefits of label-free detection (in terms of simplicity and cost-effectiveness) strongly favors the goals inherent to chemical sensors, total analysis systems, and point-of-need.

Among the main challenges that chemistry have to address from today, Whitesides envisioned the development of new analytical techniques to enable relevant chemical measurements, as well as inexpensive and robust systems to distribute the benefits of technology across societies.[63] Indeed, the development of biosensors and total analysis systems for point-of-need enable to bring (bio)chemical measurements to new scenarios, introduces alternative perspectives for analytical sciences, and favors to transversally disseminate them across societies. These approaches provide new solutions in a number of fields, such as clinics, quality control, food safety, and environmental control, among others. Besides, the possibilities offered by point-of-

need systems generate new needs that society demands to be addressed. For instance in epidemic control and safeguarding biodiversity (invasive species), among other facts related with the massive movement of people and goods. In addition, the fact of bringing the result of the assay to the time and place that motivated the analysis, also provides new knowledge to better understand the systems under study.

1.6 Compact disk-based biosensors

Consumer electronics are technological systems conceived to be used for daily purposes (e.g., television screens, laptops, tablets, cell phones, printers, scanners, disk players, digital cameras, etc.). These devices are characterized by incorporating highly sophisticated mechanical and electronic elements that, thanks to their worldwide massive production, are commercially available at very low cost. In addition, consumer electronics are designed to be simple, compact, robust, fast, portable, and user-friendly in order to meet the concept behind consumer products. Therefore, by implementing analytical systems in these devices, the benefits of both parts are synergistically exploited to offer solutions towards the point-of-need goal.

Several consumer electronics have been employed for developing chemical sensors and biosensors, such as inkjet printers,[64] flatbed scanners,[65] digital cameras,[66] 3D printers,[67] and cell phones (recently involving major interest).[68] Along these lines, the compact disk technology is one of the first consumer devices applied for sensing purposes and probably the most paradigmatic example.[69,70]

1.6.1 Principles of CD technology

Compact disk are digital data storage optical systems, developed by Sony and Phillips.[71] The term compact disk is commonly used for indistinctly referring to all the embodiments within optical disk recording technologies (CD, Super Audio CD, DVD, High Density DVD, M-Disk, Blu-ray, etc.) and also for specifically denoting CD systems. Since its commercial launch in 1982, this consumer electronic have experimented a great social acceptance and a growing worldwide presence. Nowadays, about 400 million of disk drives are fabricated every year in the world, and the disks production in 2025 is predicted to be more than 4.000 million.[69]

This technology comprises two complementary elements: disks (also known as optical disks or compact disks) and disk drives (also known as players, readers, or recorders). The disks are circular platforms that support the digital data and are constituted by an ensemble of superposed layers of different materials. One of them is a polycarbonate plate comprising the track, a spiral-shaped groove microstructure that extends along the disk and holds the data (Figure 4).[72]

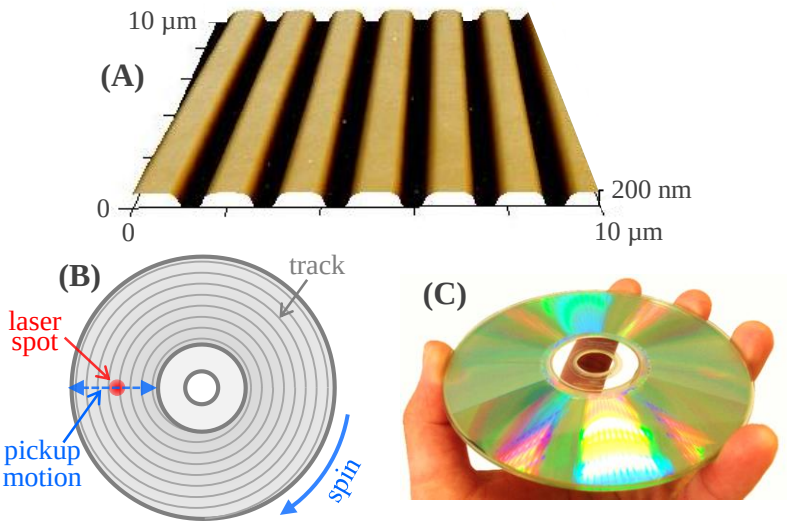

Figure 4. Images of the track embedded in compact disks. (A) AFM three-dimensional data of the track topography in a CD-R. (B) Schematized top view of a disk. (C) Image of a regular in CD-R diffracting white light because of the grooved structure.

The drives are employed to read and record data in disks. These devices are designed to sequentially analyze the whole track by irradiating it (with a pickup unit that moves along the radial direction) and simultaneously spinning the disks (with a spindle motor) (Figures 4B and 5A). As schematized in Figure 5B, the pickup unit basically comprises a laser diode and a photodiode to monitor the reflected light. An integrated autofocusing lens system is used, together with the bottom layers of the disk, to focus the laser on the track.

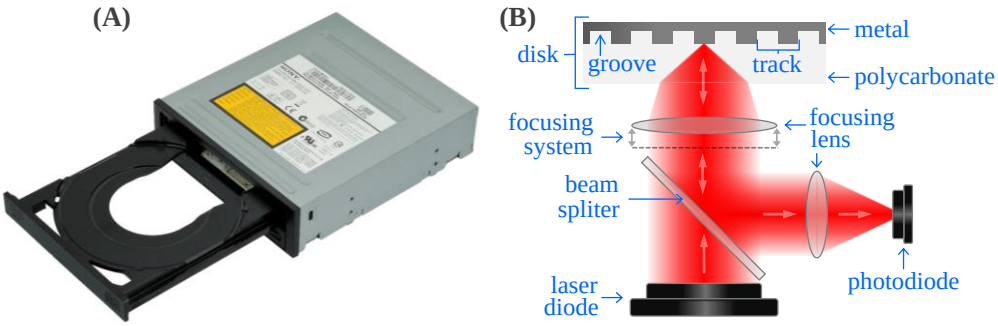

Figure 5. (A) Image of an optical disk drive. (B) Schematic diagram of the pickup unit.

In CD-DA (digital audio) and CD-ROM (read-only memory), the track is not a continuous groove and the binary data is encoded by means of stepped features, as illustrated in Figure 6. The steps that comprise closer planes to the pickup are called “pits”, whereas the ones with farther planes “lands”. The height difference between pits and lands coincides with a quarter of the laser wavelength in this medium. Since a reflective metallic layer (typically aluminum) is placed onto the track, a destructive interference caused by a $\lambda/2$ phase difference cancels the reflected beam when the laser scans pit-land interfaces (“0” in the binary code), whereas maximal laser intensity is reflected when pit-pit and land-land transitions are irradiated (“1” in the binary code). The pit/land sequence in these systems is embedded in the polycarbonate layer during the fabrication of the disks and cannot be modified.

For CD-R (recordable), the tracks are constituted by continuous grooves (Figure 6) and an organic dye recording layer (typically cyanines and phtalocyanines) is placed between the track and the metal layer. The laser diode works at different intensities, higher for recording and lower for reading. When the focused beam hits the recording dye at high intensity, this compound undergo a structural modification that attenuate the back-reflected beam. Therefore, binary data are encoded as “burned” dye (pit) sequences.

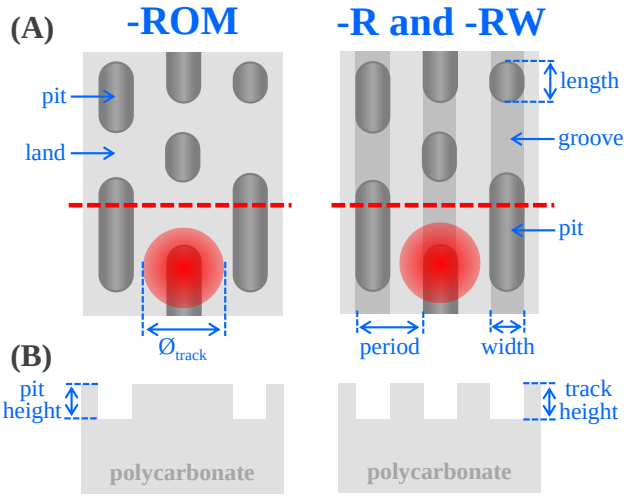

Figure 6. Features of the track microstructure: (A) Schematized top view of the track at microscopic scale and (B) the corresponding cross section profiles in the dashed red lines.

An analogous principle is used for CD-RW (rewritable), whereas the recording layer of these disks comprises crystalline alloys (Ag, In, Sb, and Te) that turns into amorphous when irradiated at high intensity (pit). Amorphous pits scatter light, which decreases the intensity of the back-reflected beam. This strategy is employed to encode binary data in the track and can be erased

by irradiating at intermediate intensity, thus returning the disk at its original crystalline state (blank disk).

Other optical disk technologies also rely on the above mentioned basis for CD. These technologies evolve towards higher track densities to achieve larger data-storage capacities, thus comprising smaller track features and shorter wavelength lasers. Each system entails particular disk structures and different laser wavelength to enable reading and recording data in their corresponding microstructures. The characteristic features of CD, DVD, and Blu-ray are listed in Table 2.

Other systems (such as Super Audio CD, M-Disk, and the forthcoming Holographic Versatile Disk) are based on matching principles, whereas they comprise some variations to enable different functionalities. For instance, LightScribe is a technology designed to laser-etch the label side of compact disks. LightScribe disks contains a photochromic layer on their label side that becomes darker when irradiated by the laser of the drive. Therefore, custom motifs designed by the user are easily etched on the label side in grayscale.[73]

1.6.2 State-of-the-art

The compact disk technology is a great mass-produced candidate for developing point-of-need biosensors. In addition to fulfill the particular characteristics of consumer electronics (robustness, compactness, inexpensiveness, ubiquity, etc.), this technology comprises two elements (disk and drive) and integrates appealing optical and mechanical features to be exploited for analytical purposes.

In an ideal situation, disks are tailored to become assay platforms that handle the full analytical process with no additional resources than regular drives. Current drives either comprise a USB connection or are already integrated in computers, so laptops or other compact computing systems can be used to manage the drive, record the output data, and compute the result of the analysis.

The advances in the analytical implementation of the compact disk technology can be classified in two main groups. One of them relies on the development of centrifugal microfluidic systems, often also known as lab-on-a-disk.[70] Among the main strengths of this approach, centrifugal microfluidics do not involve external pumps, but a single spinning motor is employed for managing the fluids. This pump-free strategy offers simpler and cheaper devices suitable for point-of-need. Microfluidic features (channels, chambers, valves, etc.) are created in circular platforms and designed to carry out sample handling operations using centrifugal force. Most of the developments are based on polymeric custom disk-like platforms, whereas some ones use standard compact disks. Specialized (expensive and bulky) instrumentation are typically

required to manage the pumping (e.g. stroboscopic cams, specialized workstations, etc.) and the sensing stage (e.g. fluorescence scanners, confocal microscopes, etc.), whereas some approaches have exploited the features of disk drives for microfluidic purposes.[70]

The other main direction towards the development of disk-based analytical systems is focused on the sensing part of the assay.[74,75] Many strategies have been addressed in these regards, where using disks as analytical platforms and drives as photometric scanners, is an important one.

Table 2. Characteristic features of representative optical disk recording technologies.

	CD	**DVD**	**Blu-ray**
Layered structure [a]	Label Reflective Layer Recording Layer (Track) Polycarbonate (1.2 mm)	Label Polycarbonate (0.6 mm) Reflective Layer Recording Dye (Track) Polycarbonate (0.6 mm)	Label Polycarbonate (1.1 mm) Reflective Layer Recording Dye (Track) Durabis Layer (0.1 mm)
Period [b]	1600 nm	740 nm	320 nm
Width [b]	600 nm	320 nm	130 nm
Length [b]	800 nm	400 nm	150 nm
$Ø_{track}$ [b]	1600 nm	1100 nm	480 nm
$Ø_{bottom}$ [c]	728 µm	504 µm	131 µm
Pit height [b]	126 nm	105 nm	65 nm
Track height [b]	200 nm	175 nm	20 nm
laser λ	780 nm	650 nm	405 nm
Intensity [d]	1 / 45-65 mW	0.7 / 12 mW	0.5 / 5-8 mW
Data capacity	0.7 GB	4.7 GB	25 GB
Price [e]	0.19 / 25 €	0.22 / 25 €	0.56 / 75 €

[a] Structure of disks by layers (laser incidence from the bottom). Recording layer must be omitted for -ROM disks. Thicknesses not specified are negligible at millimetric scale. Total disk thickness = 1.2 mm for all the systems.

[b] Parameters depicted in Figure 6. Pit height estimated by λ/(1.55 x 4). Track height experimentally measured by atomic force microscopy.

[c] Diameter of the laser spot on the bottom surface of the disk.

[d] Light intensity for reading / recording.

[e] Rough prices, disk (-R) / drive (reader + recorder).

Good results have been obtained by employing the disks as substrates to perform biorecognition assays in microarray format. To this end, arrays of small volumes of probe solutions are spotted on the surface of compact disks. Bioreceptors (mainly proteins and nucleic acids) can be attached by passive adsorption thanks to the good probe immobilization properties of polycarbonate, whereas surface functionalization for covalent probe attachment can also be accomplished on the disks.[76] Labels and signal developers are linked to the biorecognition systems in order to enable colorimetric detection. For instance, gold nanoparticles labeling with silver enhancement and HRP labeling with TMB signal developer, both lead to insoluble precipitates (that absorb and scatter light) whose intensity depends on the magnitude of the biointeraction of interest. This strategy have been applied to immunoassays and DNA hybridization assays, among other biorecognition systems, to analyze a wide range of analytes, such as biomarkers, pesticides, toxins, herbicides, pathogens, allergens, polymorphisms, or heavy metals. Microarray analysis boost the potential of disk-based systems and point towards massive multiplexed assays for point-of-need settings.[74]

Other strategies have been addressed to implement colorimetric assays on disks. Instead of microarrays, bioreceptors can be structured as strips to favor the detection of binding events in some approaches.[75] Moreover, thin layers of films constituted by molecular colorimetric sensors incorporated into hydrogels, can be placed on disks to analyze inorganic ions.[77]

Regarding disk drives as photometric scanners for disk-based analytical platforms, the laser beam goes through the colorimetric assay twice: when is focused towards the track and when is back-reflected to the pickup unit. Thus, if the colorimetric response is tailored to display absorption and/or scattering for the laser wavelength, the result of the assay generates a laser attenuation that can be measured by the photodiode included in the pickup unit.

In these developments, it must be took into account that the polycarbonate layer also acts as a focusing element for the laser. Optical disk systems are designed to tolerate certain level of physical modifications (scratches, dust, etc.), whereas higher alterations disrupt the laser. In this situations, the system can not follow the track and the scanning process aborts. These disk-based analytical developments are restricted by the track dependency, and the assays on the disks must keep a balanced situation between their size and the optical modifications that they introduce. Only mild physicochemical modifications and the integration of small elements are compatible with using standard disk drives as analytical scanners.

Laser disruptions below the abortion threshold lead to minor errors in the reading process that can be corrected by the system. The magnitude and position of these errors during the disk reading can be recorded using a free software (e.g., PlexTools Professional). This strategy enables to use regular unmodified drives to scan assays on compact disks, where the amount of errors is directly proportional to the magnitude of the colorimetric response.[75] The main strength

of this approach relies on the great ubiquity of the drives, which strongly favors the dissemination of these disk-based technology.

Other important approach is based on adapting the disk drives to become scanners for analogue optical signals. Basically, the output analogue signal from the photodiode of the pickup is digitalized by an acquisition board and sent to a computer through a USB connection. Then, the data string acquired from monitoring the track can be arranged to build an image that corresponds to the disk surface. As a result, grayscale scans of the assays placed on the disks are obtained and used to quantify the result of the analysis.[69] Unlike software-based analysis, these drive modifications restrict their ubiquity. However, minimal modifications enable to fully exploit the analytical potential of the compact disk technology. For instance, analogue acquisition entails better sensitivity than error analysis,[78] enable microscopic imaging,[79] and permits to add further detectors,[80] among other potential capabilities. Introducing minimal modifications that boost the analytical potential of consumer electronics, whilst also keeping their characteristic features (cheap, robust, compact, etc.), represents an attractive option for developing biosensors applicable in the point-of-need framework.

Specialized drives (with further capabilities than the standard ones) and regular players with significant hardware modifications have also been used in analytical systems.[81] Though not directly suitable for ready-to-disseminate sensors, these approaches can be useful for proof-of-concept studies and lab-scale developments. Along these lines, some companies have launched commercial disk-based sensor systems that include centrifugal microfluidics and sensing, such as Spinit (Biosurfit), Gyrolab (Gyros), and LabDisk platform (Hahn-Schickard). Those ones consist on custom instrumentation, whose miniaturized and automatic systems can offer interesting solutions. However, these commercial approaches keep many characteristic features of the typical benchtop equipment (e.g., price, size, etc.) that restrict their dissemination in non-specialized environments.

The compact disk technology offers great potential to reach the ambitious goal of developing disks with microfluidics for full sample handling and a sensing part to measure the analytes, together with using standard drives as unique instrumentation required to manage these disks. Some promising attempts have been performed in this direction.[82,83] However, these studies are based on track-dependent technologies, which introduce important restrictions to the microfluidic and sensing systems compatible with standard disks and drives. Only mild modifications and small microfluidic elements that do not disrupt the monitoring of the track can be implemented in these systems. These facts strongly motivates the development of alternative compact disk-based biosensors that enable to fully exploit sensing and sample handling, whereas also keep the advantages of standard disk and drives.

A few studies deal with label-free detection of biorecognition assays with compact disks. This is an appealing approach to conceive point-of-need systems that marry the inherent benefits of biosensors based on consumer electronics and the analytical performance of label-free detection in terms of assay simplification, costs, and reliability. Moreover, as commented in previous sections, one of the main limitations commonly found in label-free (versus labeled systems) is the higher complexity and expensiveness of the detection setups and the micro/nanostructured substrates required. Therefore, exploiting consumer electronics for label-free detection points towards beating those limitations, thus offering potential alternatives for point-of-need analysis.

Along these lines, some attempts using interferometry and SPR have been reported.[59,84] However these studies does not use actual consumer electronics, but they are based on disk-like platforms and custom optical detection systems instead of compact disks and drives, respectively. In a more promising approach, multilayered structures (similar to the recording layers of DVD-RW) were fabricated on polycarbonate plates containing the track and used to detect biomolecular interactions in label-free conditions by interferometry.[85] However, an expensive and specialized benchtop reader (optical disk drive tester) conceived to be used in manufacturing settings of the compact disk industry is required for the measurement, instead of standard drives.

Therefore, the implementation of label-free biosensors in actual mass-produced compact disk technologies is an important matter to be addressed. This approach entails great point-of-need potential and can offer more cost-efficient alternatives to the complex detection setups and nanofabricated materials typically required for analyzing biorecognition assays in label-free conditions.

1.7 References

(1) W.F. Pickering, *Modern analytical chemistry*, M. Dekker, Inc., New York, **1971**.
(2) D.A. Skoog, J.J. Leary, *Principles of Instrumental Analysis (4th Edltion)*, Saunders College Publishing, Philadelphia, **1992**.
(3) Y. Arikawa, *Anal. Sci.*, 17 (**2002**), 571.
(4) R.W. Murray, *Annu. Rev. Anal. Chem.*, 3 (**2010**), 1.
(5) H. Hill, *Bioanalysis*, 1 (**2009**), 3.
(6) R. Murray, *Anal. Chem.*, 63 (**1991**), 379.
(7) A. Hulanicki, S. Geab, F. Ingman, *Pure Appl. Chem.*, 63 (**1991**), 1247.
(8) H.H. Qazi, A.B. bin Mohammad, M. Akram, *Sensors*, 12 (**2012**), 16522.
(9) E. Katz, I. Willner, J. Wang, *Electroanalysis*, 16 (**2004**), 19.
(10) A.P.F. Turner, I. Karube, G.S. Wilson, *Biosensors Fundamentals and Applications*, Oxford University Press, New York, **1989**.
(11) L.C. Clark, C. Lyons, *Ann. N.Y. Acad. Sci.*, 102 (**1962**), 29.

(12) R.F. Taylor, J.S. Schultz, *Handbook of Chemical and Biological Sensors*, Institute of Physics Publishing, Bristol, **1996**.
(13) *Biosensors - A Global Overview*, Industry Experts, **2012**.
(14) M.-J. Bañuls, R. Puchades, A. Maquieira, *Anal. Chim. Acta*, 777 (**2013**), 1.
(15) T. Lenoir, E. Giannella, *J. Biomed. Discov. Collab.*, 1 (**2006**), 1.
(16) M. Hartmann, J. Roeraade, D. Stoll, M.F. Templin, T.O. Joos, *Anal. Bioanal. Chem.*, 393 (**2009**), 1407.
(17) S. Morais, A. Maquieira, R. Puchades, *Anal. Chem.*, 71 (**1999**), 1905.
(18) J. Wang, *Chem. Rev.*, 108 (**2008**), 814.
(19) M.L. Ermini, S. Mariani, S. Scarano, M. Minunni, *Biosens. Bioelectron.*, 61 (**2014**), 28.
(20) S. Sheikh, C. Blaszykowski, M. Thompson, *Anal. Lett.*, 41 (**2008**), 2525.
(21) J. Wu, Z. Fu, F. Yan, H. Ju, *Trends Anal. Chem.*, 26 (**2007**), 679.
(22) D. Wild, *The Immunoassay Handbook (Fourth Edition)*, Elsevier, Oxford, **2013**.
(23) T.N. Shekhovtsova, S.V. Muginova, I.A. Veselova, *Russ. Chem. Bull.*, 56 (**2007**), 606.
(24) M. Botes, M. de Kwaadsteniet, T.E. Cloete, *Anal. Bioanal. Chem.*, 405 (**2013**), 91.
(25) R.M. Graybill, R.C. Bailey, *Anal. Chem.*, 88 (**2016**), 431.
(26) M. Citartan, S.C.B. Gopinath, J. Tominaga, S.-C. Tan, T.-H. Tang, *Biosens. Bioelectron.*, 34 (**2012**), 1.
(27) T.S. Bedwell, M.J. Whitcombe, *Anal. Bioanal. Chem.*, 408 (**2016**), 1735.
(28) C.A. Barrios, C. Zhenhe, F. Navarro-Villoslada, D. López-Romero, M.C. Moreno-Bondi, *Biosens. Bioelectron.*, 26 (**2011**), 2801.
(29) X. Zeng, C.A.S. Andrade, M.D.L. Oliveira, X.-L. Sun, *Anal. Bioanal. Chem.*, 402 (**2012**), 3161.
(30) A.E. Smartt, T. Xu, P. Jegier, J.J. Carswell, S.A. Blount, G.S. Sayler, S. Ripp, *Anal. Bioanal. Chem.*, 402 (**2012**), 3127.
(31) A. Gonzalez-Techera, M.A. Zon, P.G. Molina, H. Fernandez, G. Gonzalez-Sapienza, F.J. Arevalo, *Biosens. Bioelectron.*, 64 (**2015**), 650.
(32) N. Raut, G. O'Connor, P. Pasini, S. Daunert, *Anal. Bioanal. Chem.*, 402 (**2012**), 3147.
(33) X. Luo, J.J. Davis, *Chem. Soc. Rev.*, 42 (**2013**), 5944.
(34) B. Rezaei, M. Ghani, A.M. Shoushtari, M. Rabiee, *Biosens. Bioelectron.*, 78 (**2016**), 513.
(35) C.I. Cheng, Y.-P. Chang, Y.-H. Chu, *Chem. Soc. Rev.*, 41 (**2012**), 1947.
(36) G.T. Hermanson, *Bioconjugate Techniques (Third Edition)*, Academic Press, London, **2013**.
(37) J.P. Sherry, *Crit. Rev. Anal. Chem.*, 23 (**1992**), 217.
(38) R.S. Yalow, *Trends Anal. Chem.*, 1 (**1982**), 128.
(39) M.R. Walker, R.A. Stott, G.H.G. Thorpe, *Methods Biochem. Anal.*, 36 (**1992**), 179.

(40) A.P. Demchenko, *Introduction to Fluorescence Sensing (Second Edition)*, Springer International Publishing, Cham, **2015**.
(41) D. Quesada-González, A. Merkoçi, *Biosens. Bioelectron.*, 73 (**2015**), 47.
(42) K.D. Wegner, N. Hildebrandt, *Chem. Soc. Rev.*, 44 (**2015**), 4792.
(43) Y.C. Wang, R. Hu, G.M. Lin, I. Roy, K.T. Yong, *ACS App. Mat. Interfaces*, 5 (**2013**), 2786.
(44) P. Singh, *Sens. Actuators B*, 229 (**2016**), 110.
(45) R.B.M. Schasfoort, A.J. Tudos, *Handbook of Surface Plasmon Resonance*, Royal Society of Chemistry, Cambridge, **2008**.
(46) A. Kussrow, C.S. Enders, D.J. Bornhop, *Anal. Chem.*, 84 (**2012**), 779.
(47) X. Fan, I.M. White, S.I. Shopova, H. Zhu, J.D. Suter, Y. Sun, *Anal. Chim. Acta*, 620 (**2008**), 8.
(48) C. Fenzl, T. Hirsch, O.S. Wolfbeis, *Angew. Chem. Int. Ed.*, 53 (**2014**), 3318.
(49) S. Schlücker, *Angew. Chem. Int. Ed.*, 53 (**2014**), 4756.
(50) S.-C. Luo, K. Sivashanmugan, J.-D. Liao, C.-K. Yao, H.-C. Peng, *Biosens. Bioelectron.*, 61 (**2014**), 232.
(51) J.B. Goh, R.W. Loo, R.A. McAloney, M.C. Goh, *Anal. Bioanal. Chem.*, 374 (**2002**), 54.
(52) X. Wang, X. Liu, X. Wang, *Sens. Actuators B*, 220 (**2015**), 873.
(53) R. Wilson, *Chem. Soc. Rev.*, 37 (**2008**), 2028.
(54) J. Cao, T. Sun, K.T.V. Grattan, *Sens. Actuators B*, 195 (**2014**), 332.
(55) Y. Wang, B. Yan, L. Chen, *Chem. Rev.*, 113 (**2013**), 1391.
(56) A.M. Armani, R.P. Kulkarni, S.E. Fraser, R.C. Flagan, K.J. Vahala, *Science*, 317 (**2007**), 783.
(57) R. Ince, R. Narayanaswamy, *Anal. Chim. Acta*, 569 (**2006**), 1.
(58) D. Giménez-Romero, M.A. González-Martínez, M.-J. Bañuls, I.S. Monzó, R. Puchades, Á. Maquieira, *J. Phys. Chem. B*, 116 (**2012**), 5679.
(59) K. O'Brien, M. Zhao, D. Nolte, *Micromachines*, 7 (**2016**), 31.
(60) H. Shen, Z. Wang, Y. Wu, B. Yang, *RSC Adv.*, 6 (**2016**), 4505.
(61) E. Petryayeva, W.R. Algar, *RSC Adv.*, 5 (**2015**), 22256.
(62) Á. Ríos, M. Zougagh, M. Avila, *Anal. Chim. Acta*, 740 (**2012**), 1.
(63) G.M. Whitesides, *Angew. Chem. Int. Ed.*, 54 (**2015**), 3196.
(64) H. Kido, A. Maquieira, B.D. Hammock, *Anal. Chim. Acta*, 411 (**2000**), 1.
(65) Z. Gorocs, A. Ozcan, *Lab Chip*, 14 (**2014**), 3248.
(66) K. Grudpan, S.D. Kolev, S. Lapanantnopakhun, I.D. McKelvie, W. Wongwilai, *Talanta*, 136 (**2015**), 84.
(67) B.C. Gross, J.L. Erkal, S.Y. Lockwood, C. Chen, D.M. Spence, *Anal. Chem.*, 86 (**2014**), 3240.
(68) D. Zhang, Q. Liu, *Biosens. Bioelectron.*, 75 (**2016**), 273.

(69) S. Morais, R. Puchades, Á. Maquieira, *Anal. Bioanal. Chem.*, 408 (**2016**), 1.
(70) S. Smith, D. Mager, A. Perebikovsky, E. Shamloo, D. Kinahan, R. Mishra, S.M.T. Delgado, H. Kido, S. Saha, J. Ducree, M. Madou, K. Land, J.G. Korvink, *Micromachines*, 7 (**2016**), 22.
(71) H. Wenninger, *Europhys. News*, 44 (**2013**), 22.
(72) A. Maquieira, *Compact Discs Technology for Clinical Analysis of Drugs* In *Biosensors and Molecular Technologies for Cancer Diagnostics*, K. E. Herold, A. Rasooly, CRC Press, Boca Ratón, **2012**.
(73) K.Y. Young, Patent US2006/0227680, **2006**.
(74) S. Morais, R. Puchades, Á. Maquieira, *Anal. Bioanal. Chem.*, (**2016**), 1.
(75) H.-Z. Yu, Y. Li, L.M.L. Ou, *Acc. Chem. Res.*, 46 (**2013**), 258.
(76) E. Peris, M.J. Banuls, R. Puchades, A. Maquieira, *J. Mater. Chem. B*, 1 (**2013**), 6245.
(77) R.A. Potyrailo, W.G. Morris, R. Wroczynski, L. Hassib, P. Miller, B. Dworken, A.M. Leach, S. Boyette, C. Xiao, *Sens. Actuators B*, 136 (**2009**), 203.
(78) S. Morais, L.A. Tortajada-Genaro, T. Arnandis-Chover, R. Puchades, A. Maquieira, *Anal. Chem.*, 81 (**2009**), 5646.
(79) H. Ramachandraiah, M. Amasia, J. Cole, P. Sheard, S. Pickhaver, C. Walker, V. Wirta, P. Lexow, R. Lione, A. Russom, *Lab Chip*, 13 (**2013**), 1578.
(80) E.M. Brun, R. Puchades, A. Maquieira, *Anal. Chem.*, 85 (**2013**), 4178.
(81) S.C.B. Gopinath, K. Awazu, J. Tominaga, P.K.R. Kumar, *ACS Nano*, 2 (**2008**), 1885.
(82) R. Burger, L. Amato, A. Boisen, *Biosens. Bioelectron.*, 76 (**2016**), 54.
(83) S. Santiago-Felipe, L.A. Tortajada-Genaro, J. Carrascosa, R. Puchades, Á. Maquieira, *Biosens. Bioelectron.*, 79 (**2016**), 300.
(84) A. Hemmi, T. Usui, A. Moto, T. Tobita, N. Soh, K. Nakano, H. Zeng, K. Uchiyama, T. Imato, H. Nakajima, *J. Sep. Sci.*, 34 (**2011**), 2913.
(85) M. Citartan, S.C.B. Gopinath, J. Tominaga, T.-H. Tang, *Analyst*, 138 (**2013**), 3576.

2. Objectives

This Ph.D. project aims the development of biosensor systems based on the compact disk technology, with special interest in conceiving label-free approaches that enable multiplexed analytical systems applicable in the point-of-need framework.

This general goal is pursued through the following particular objectives:

- To assess the biosensing potential of unexplored compact disk features and embodiments, especially in thermochromic etching disk (TED) systems (chapter 1).
- To design and apply a practical optimization method for biorecognition assays that enable the rational design of biosensors (chapter 2).
- To explore the performance of SERS and diffraction-based sensing (DBS) for developing high-throughput label-free biosensors based on compact disks systems (chapters 3 and 4).

3. Results and discussion

The results and discussions presented in this thesis have been structured in chapters that are related each other according to the flowchart below:

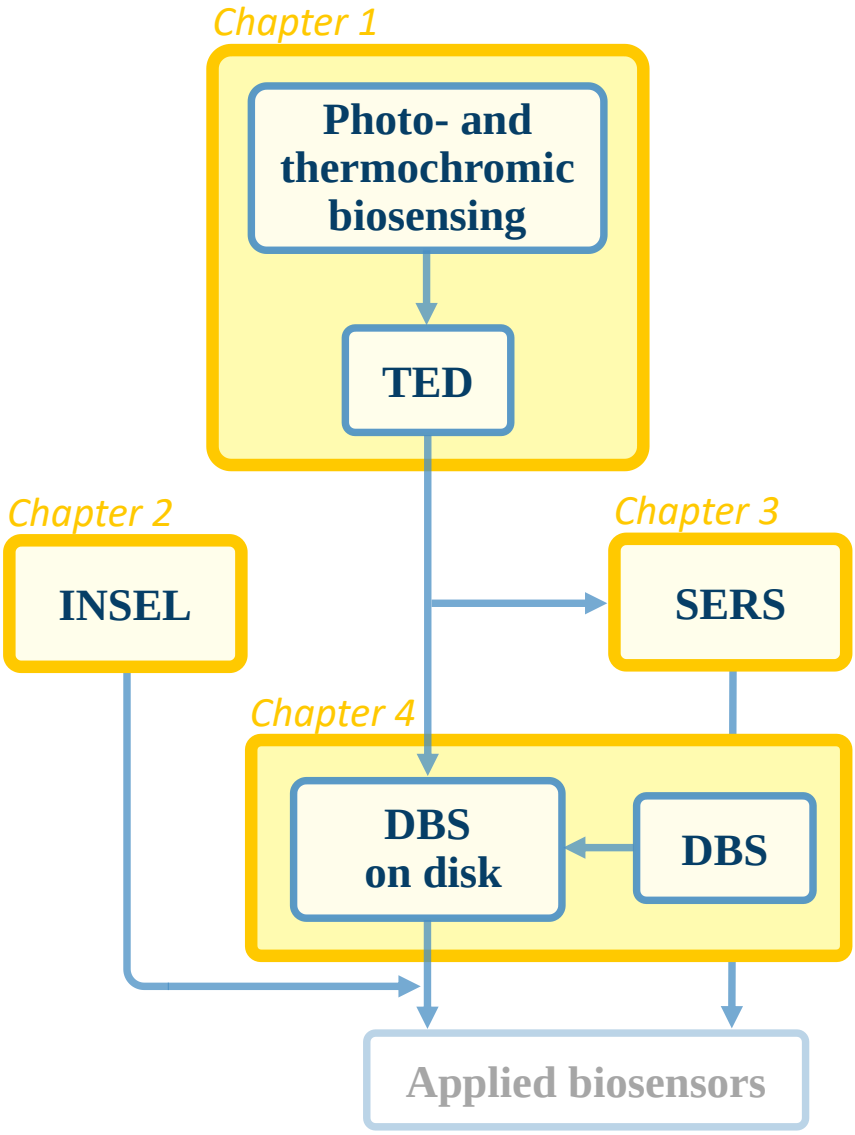

Each chapter entails one (chapters 2 and 3) or two (chapters 1 and 4) scientific publications, and also includes specific introduction and conclusions sections that highlight their role within the general framework of this thesis.

Chapter 1

3.1 Thermochromic/photochromic etching disk technologies for biosensing

3.1.1 Introduction

This chapter addresses the introduction of thermochromic etching disks (TED) into the bioanalytical field. TED systems are consumer electronics that entail both, disks containing photochromic/thermochromic coatings and disk drives. It must be noted that the term TED is herein employed to generically denote these disk technologies designed for etching the label side of compact disks, whereas the term LightScribe corresponds to a registered trademark that comprises particular commercial embodiments (disks and drives).

The first part of this chapter (section 3.1.2) is focused on the photo- and thermochromism aspect. Insights into the possibilities of a novel strategy that exploit photo- and thermochromic materials for light- and heat-mediated signal development in biorecognition assays, are provided. Moreover, a general discussion of the potential of this phenomena for biosensing is introduced. Within this framework, the state-of-the-art of LightScribe systems for scientific applications, is also revised.

The second part of this chapter (section 3.1.3) addresses the bioanalytical implementation of TED technology, rather from a lab-on-a-disk point of view. This study explores the features of this technology (such as its track-independency) to provide new advances in biosensing.

3.1.2 Towards photochromic and thermochromic biosensing

Trends Anal. Chem., 79 (**2016**) 37.

ABSTRACT

Photochromism and thermochromism are interesting physicochemical phenomena applied in the chemistry, health and biology fields and others. Nonetheless, exploiting these chromo-switchable properties in biosensing remains unexplored, and very few results have been reported in the scientific literature. Along these lines, the rich mature knowledge of these phenomena supports the challenge of facing the development of photo- and thermochromic bioanalytical systems. This work discusses potential approaches to exploit photochromism and thermochromism for biosensing, and it reviews the state-of-the-art of these phenomena in the surrounding areas of biosensing in order to plot a stimulating scenario for innovation.

Keywords: Photochromism; Thermochromism; Biosensing; Biorecognition assay; Molecular recognition; Point-of-care; Technology; LightScribe; Thermochromic liquid crystal; Antenna

1. Introduction

Photochromism and thermochromism are phenomena by which matter switches its colour as a response to electromagnetic radiation and thermal stimuli, respectively. These processes are driven by compounds that lead to light- and heat-induced changes between two states with different absorption spectra [1]. Photochromism and thermochromism can be found in nature. For instance, chameleon diamonds (high nitrogen content natural diamonds) undergo a thermally induced colour switch that reverses under darkness conditions [2]. Besides, in living organisms, visible light absorption of retinal bound to opsin proteins gives rise to a photochromic isomerisation that triggers the enzymatic pathway of the vision cycle [3].

Intense research has focused on the design and synthesis of photo- and thermochromic systems, which have provided broad knowledge in this field [4]. Moreover, the development of smart functional materials by integrating these switchable compounds into different environments has had a significant impact on industry. Thus many commercial products based on these technologies can be found in applications that range from ornamentation to data storage [5].

From the analytical chemistry point of view, many studies have addressed the development of chemical sensors based on photochromism, mostly for sensing inorganic ions [6]. However, photo and thermochromism in biosensing remain unexplored. Some works that used these phenomena in biological systems and medical applications are found in the bibliography, but they rarely point to biosensing or claim specific potential in this field. Indeed very few studies that directly deal with photo- and/or thermochromic biosensing systems have been reported.

The physicochemical phenomena involved in transduction strongly determine the application

field of a sensor system and the nature of the analytical information that can be obtained from the sample under study. From this perspective, exploring biosensing capabilities of photo- and thermochromism is an interesting challenge, whose potential is supported by the scientific and industrial relevance of these chromo-switchable systems.

This paper focuses on thermo- and photochromism for biosensing. In addition to reviewing works that have directly dealt with these phenomena for bioanalysis, an overview of the studies that report chemical sensors (non-biosensors), biological systems, medical applications and technological developments is presented. Moreover, new strategies are proposed and discussed throughout, including experimental results and significant bibliographic references that support the potential of these approaches. The criteria followed in this review seek to include relevant studies and strategies from different scientific areas in order to plot a scenario from which to outline a trend towards the development of photochromic and thermochromic biosensors.

The manuscript contains two sections: molecular and supramolecular systems; photochromic and thermochromic technologies. The first part offers a brief introduction to the main chemical and biochemical approaches of photochromism chemistry, and surveys on studies into biosensing surroundings. The second part reviews different thermo- and photochromic technological approaches, and highlights their bioanalytical capabilities.

2. Molecular and supramolecular systems

The design of photochromic molecules is an active scientific area that typically involves several families of compounds, such as azobenzenes, spiropyrans and diarylethenes [7]. These molecules switch between two isomeric forms with a different absorption spectrum under UV and visible light exposure (Fig. 1A). Moreover, assembling photochromes and fluorescent structures in the same molecule leads to photochromic compounds in which the light activated isomerisation of the photochrome modulates the fluorescent behaviour of the fluorophore [9,10].

By linking specific receptors that modify photochromic behaviour after analyte binding, these photochromes have applications in chemical sensing. Table 1 lists representative examples of photochromic chemical sensors for different kinds of analytes. Along these lines, several papers address the review of molecular photochromic compounds for chemical sensing, including a in-depth description of the mechanisms involved in these systems [1,6,7]. From the analytical point of view, it is worth highlighting a recent review by Song and coworkers, which comprises an interesting section about multianalyte discrimination [20].

Photochromic sensors have been widely studied to determine metal ions by modifying photochromes with moieties for selective recognitions [11,12], typically electron-rich groups (containing N, O or S atoms), crown ethers and calixarenes [6,20]. Moreover, many studies have

addressed photochromic molecular sensors for inorganic anions. Structural changes in spiropyran derivatives after CN^- nucleophilic addition [14] or after pyrophosphate (PPi) cooperative ligation interactions [15] are some examples of the chemical mechanisms that take place in these systems.

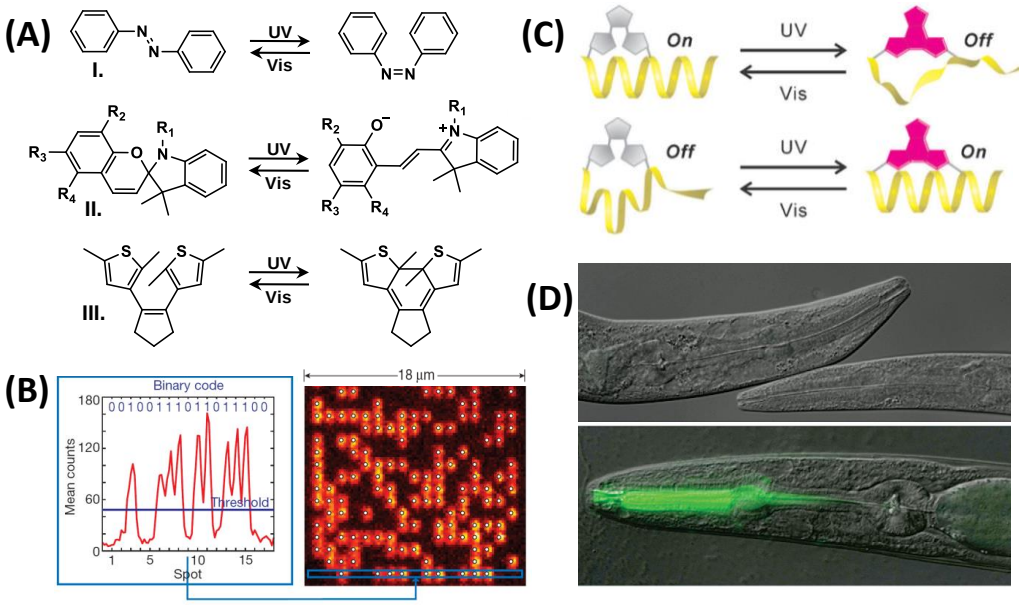

Fig. 1. (A) Chemical structures and photochromic switches of azobenzenes (I), spyropirans (II) and diarylethenes (III). (B) Data storage system based on the photoswitching properties of the photochromic green fluorescent protein. Reprinted by permission from Macmillan Publishers Ltd: [Nature] [8], copyright (2011). (C) Scheme of the photochromic control of the conformational state of a peptide. Reprinted by permission from Wiley-VCH Verlag GmbH&CO (*Chem. Eur. J.* 2012, 18, 9834–9840), copyright (2012). (D) Images of Caenorhabditis elegans biological control by photochromism. Adapted with permission from (*J. Am . Chem. Soc.* 2009, 131, 15966–15967). Copyright (2009) American Chemical Society

Regarding biosensing, some works have dealt with the modification of photochromes for sensing molecules involved in biological processes. For instance, Yang and coworkers reported a spiropyran that was modified with nitro groups for glutathione (GSH) sensing [17]. The thiol group of the peptide undergoes nucleophilic substitution and induces the isomerisation of the photochrome, which generates a spectral change from slightly yellow to orange-yellow. As an example of biomacromolecules detection, Tao et al. designed an electrochemical sensor for β-galactosidase (β-gal) by including a galactose molecule in the spiropyran structure [18]. This

enzyme hydrolyses the galactose moiety, which leads to a redox-active hydroquinone derivative after UV irradiation.

Table 1. Representative spiropyran-based photochromic molecular sensors for different analytes.

Structure*	Analyte	Limit of detection	Linear range	Selectivity**	Ref.
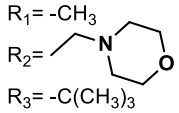	Cu^{2+}	0.106 µM	0.513–381 µM	Li^+, K^+, $Mg2^+$, Cd^{2+}, Co^{2+}, Hg^{2+}, Zn^{2+}, Ni^{2+}, Pb^{2+}, Fe^{3+}, Gly, Cys, His, Glu, Asp, BSA	[11]
	Co^{2+}	1 µM	1.0–10 µM	Na^+, Li^+, K^+, Mn^{2+}, Cd^{2+}, Pb^{2+}, Ni^{2+}, Hg^{2+}, Zn^{2+}, Fe^{2+}, Mg^{2+}, Cr^{3+}, Fe^{3+}	[12]
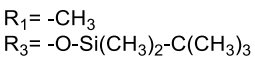	F^-	0.86 µM	5.0–100 µM	Cl^-, Br^-, I^-, HSO_4^-, NO_3^-, ClO_4^-, AcO^-, HCO_3^-, $H_2PO_4^-$	[18]
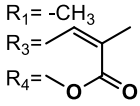	CN^-	0.5 µM	0.3–5 µM	F^-, Cl^-, Br^-, I^-, AcO^-, $H_2PO_4^-$, HSO_4^-, ClO_4^-, NO_3^-, SCN^-	[13]
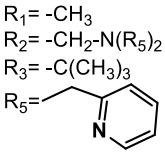	PPi	0.40 µM	1.0–500 µM	$H_2PO_4^-$, AMP, ADP, ATP, citrate, tartrate, succinic, oxalate, Na^+, K^+, Ca^{2+}, Cl^-	[14]
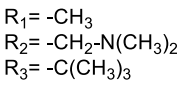	Cys Hcy	40 nM 40 nM	0.025–1 mM 0.1–1 mM	Gly, Leu, His, Glu, Asp, Met, Succinate, SCN^-, Li^+, K^+, Ca^{2+}, Zn^{2+}	[19]
	GSH	10 nM	0.05–0.8 µM	Tyr, Gly, Phe, Met, Leu, Arg, Pro, Lys, Glu, Gln, Asp, Iso, Ile, Val, His, Ser, Ala, Thr, Try, Asp	[15]
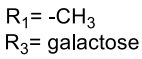	β-gal	0.06 U/mL***	0.21–1.64 U/mL***	BSA, thrombin, β-D glucosidase, phosphatase, acetylcholinesterase	[16]
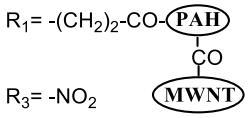	lysozyme	30 nM	Not reported	Cyclin A2, BSA, HSA, IgG	[20]

* The spiropyran R groups referred to in Figure 1A (II).

** Reported selectivity versus the listed species.

*** 1 U/mL corresponds to the amount of enzyme required for releasing 1 µM/min of galactose (pH 7.4).

Some studies have dealt with linking photochromic compounds to biomacromolecules, which directly points to biosensing in terms of labelling bioreceptors. For instance, Irie and coworkers labelled extracellular signal-regulated kinase with a photochrome-fluorophore dyad based on diarylethene and fluorescein [21]. Protein conjugation was performed through a succinimidyl ester unit in the dyad structure, and the authors claimed its easy transformation into nitrilotriacetic acid-Ni^{2+} to selectively bind to polyhistidine sequences. Medintz et al. labelled maltose binding protein with a spiropyran derivative at controlled dye/protein ratios (1 and 5), and successfully used it as a Förster resonance energy transfer system to control the light emission properties of quantum dots [22]. Regarding the importance of nanoparticles in biosensing labelling, it is worth mentioning a comprehensive review that summarises the synthesis and applications of nanoparticles labelled with photochromic compounds [9].

Along these lines, an interesting study has reported the synthesis of photochromic green fluorescent protein and its application for high-resolution microscopy imaging of living bacteria and mammalian cells [8]. Also, a thin layer of this photochromic protein was placed on glass, and binary information was recorded through switching the photochromic state of the protein at specific spots (~500 nm diameter bits) through irradiating with a confocal set-up (Fig. 1B). This strategy suggests further interesting prospective approaches. For instance, smart biosensors that compute or encode the information obtained from the assay could be designed by matching biorecognition systems with the photochromic properties of these data bits.

Supramolecular photochromic systems have also been extensively studied in biological control [23,24]. In this direction, Inouye and coworkers described a method to modulate the recognition affinity between a peptide and a DNA sequence by irradiating a diarylethene compound linked to the peptide [25]. The photochromic molecule was bound to two distant positions of the peptide, and the structural change of the photochrome after the UV irradiation induced a peptide conformation that modified its affinity for the target DNA (Fig. 1C). Dissociation constant values of 1 and 4 μM (before and after UV exposure, respectively) were experimentally obtained by quartz crystal microbalance. Babii et al. reported the spatial and temporal control of antimicrobial peptide gramicidin S by incorporating a diarylethene-based amino acid analogue into the protein structure [26]. This study has shown that the activity of this protein analogue against different gram-positive bacteria can be modulated by the isomeric conformation of the photochrome. In these strategies, using photochromes that contain specific receptors for other analytes is a potential approach for providing dual-response sensors that could be applicable in logic gates systems or in multiplexing. In addition to biomacromolecules, living cells and even organisms have been labelled with photochromic compounds [27]. In line with this, Branda et al. have reported a light-induced paralysis control of *Caenorhabditis elegans* by administrating a diarylethene compound that interfered with the energy production metabolic pathway in one of

the isomeric forms (Fig. 1D) [28].

The challenge of fully exploiting molecular photochromes for biosensing is supported by the state-of-the-art of this field. Using bioreceptors as recognition moieties in these molecules is an intuitive way to address this matter. Yet given the structural complexity of biomacromolecules, the high synthetic control required to specifically attach photochromes to precise positions of the biomacromolecule in order to yield the changes expected after recognition is a limitation to overcome. Several studies have reached this level of control in nucleic acids [23,24], which suggests direct application in DNA hybridisation and aptamer-based assays. Regarding proteins, apart from the works revised in this section, the controlled attachment of photochromes in complex protein systems, such as biological nanochannels, can also be attained [29]. Besides exploring the scientific possibilities of photochromism for biosensing, the advances made in this direction will have to take advantage of these phenomena in order to release practical functionalities for biosensors. A good example is the approach reported by Song et al., in which the light-mediated activity enhancement of peroxidase was exploited using multi-walled carbon nanotubes (MWNT) linked to a spiropyran derivative via poly(allylamine hydrochloride) to build an assay to determine the lysozyme (see Table 1) [19].

3. Photochromic and thermochromic technologies

The scientific developments that involve photochromism and thermochromism are of much interest for industry, from which a number of commercial products have arisen. Photo- and thermochromic compounds are typically integrated into different matrices in order to meet requirements for specific applications. In this section, relevant technologies that fall within the scope of this work are described, and their biosensing capabilities are discussed. It is important to note that the mass production of most of these systems is an important advantage for developing biosensors since it may enable low-cost and user-friendly sophisticated systems with high point-of-care potential.

3.1. Thermochromic and photochromic fibres

Interesting functional materials are obtained by integrating thermochromic and photochromic compounds into fibres. For instance, smart photo- and thermosensitive textiles can be designed and used for clothing [30]. Thus biosensing developments based on these systems could exploit the permanent skin contact for continuous sampling and long-term biomarkers monitoring.

Shuiping and coworkers reported the fabrication of cellulose photochromic nanofibres by electrospinning a solution of cellulose acetate and a spiropyran derivative [31]. This approach introduced a light-mediated modulation system for material properties like hydrophobicity.

Dramatic contact angle variations (~70°) after 10–20 seconds of UV exposure were obtained with these photochromic fibres. In a subsequent study, the same authors modified the bacterial cellulose surface in order to attach the same photochromic spiropyran derivative by hydrogen bonding [32]. Great potential is claimed for biosensors and optical devices in both cases. It is worth highlighting the high industrial importance of cellulose fibres, which may find analytical applications such as membranes for biosensing setups.

3.2. Thermochromic and photochromic inks

Thermochromic and photochromic inks comprise chromoswitchable compounds that are integrated into suitable matrices to be printed or transferred to other materials. These systems offer huge applications in the design and industrial labelling fields. For instance, photochromic inks are typically employed for food safety as labels in refrigerated food packaging to monitor breaks in the cold chain.

An interesting development that has indicated thermochromic inks for biosensing has been reported by Whitesides and coworkers [33]. In this work, conductive wires were patterned on one side of paper, whereas thermochromic inks were printed on the other side. Thus the electric current through the wires induced a temperature increase which triggered the colour change of the thermochromic compound. The system acts as a two-state screen capable of displaying designs previously printed with thermochromic ink (Fig. 2A). This device suggests interesting potential applications for biosensing. For instance, it could be coupled to an electroanalytical biosensing system that correlates electric current variations with a target concentration in order to obtain a low-cost sensor with a simple readout system.

3.3. Thermochromic liquid crystals

Thermochromic liquid crystal (TLC) materials are constituted by organic compounds, such as cholesteryl esters and (2methylbuthyl)phenyl-4-alkyl(oxy)benzoates (Fig. 2B), that adopt an intermediate molecular order between crystalline and liquid [35,36]. In TLCs, molecules are structured as superposed planes whose separation distance depends on temperature. These materials act as Bragg reflectors in visible spectra, and reflect different wavelengths depending on temperature (Fig. 2C). For many applications, TLCs are encapsulated in polymeric microcapsules with diameters that can range from microns to millimetres.

Many commercial products based on this technology are found in industry, such as strip thermometers and industrial labels. In medicine, thermochromic liquid crystal thermography can be used as an imaging tool to be applied to different scenarios [37]. For instance, Gao et al. reported a thermal system based on TLC arrays in thin elastomeric films capable of mapping

skin temperatures with a sub-millimetre resolution and ±50 mK precision [38]. The performance of this system was proved by imaging the ulnar artery and by monitoring changes in blood flow through epidermis temperature.

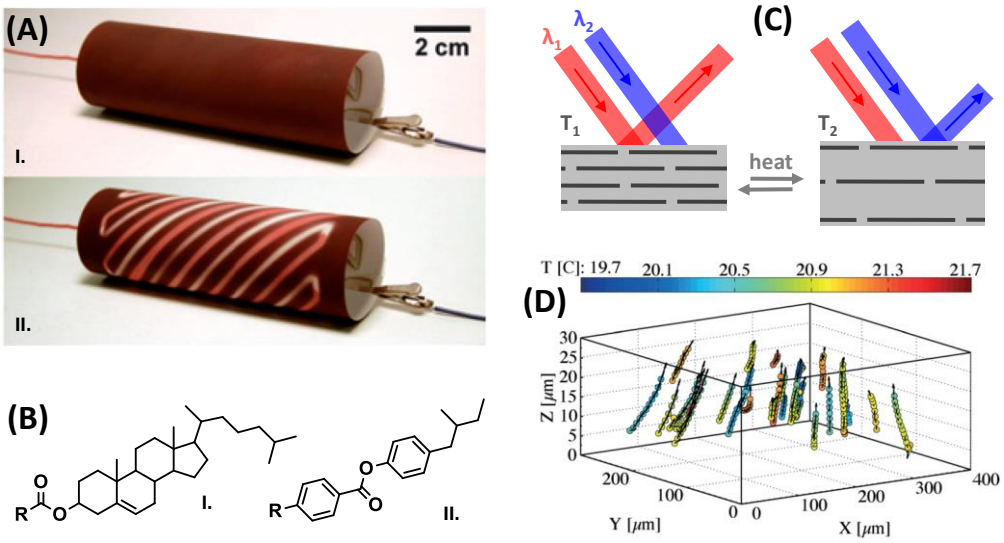

Fig. 2. (A) Paper display based on thermochromic ink in the inactivated (I) and activated (II) state. Reproduced from [33] with permission from The Royal Society of Chemistry. (B) Chemical structures of exemplary molecules used in TLCs: cholesteryl ester (I) and (2methylbuthyl)phenyl-4-alkyl(oxy)benzoates (II). (C) Scheme of thermochromic liquid crystals, where a reversible temperature change leads to different distances between molecules, which modify the reflection spectrum. (D) Real-time temperature and motion three-dimensional mapping of non-encapsulated TLC micro spheres in water emulsion. Reproduced from [34] with permission from The Royal Society of Chemistry

Regarding the bioanalytical field, thermochromic liquid crystals have been used to manage thermal issues in microfluidic systems. Controlling localized temperature is a major concern in biosensing, and the possibility of measuring temperature inside microfluidic features without perturbing thermal conditions is appealing to design lab-on-a-chip systems. This becomes crucial in highly temperature-dependant biorecognition systems, where PCR (polymerase chain reaction) is probably the most paradigmatic example.

In 1998 Chaudhari et al. reported a PCR temperature monitoring approach based on TLC technology [39]. Encapsulated TLCs were dispensed in microfabricated PCR vessels in order to monitor the actual temperature in the solution during amplification. From this work, several

approaches emerged to control temperatures in more sophisticated microfluidic systems. Slurries of encapsulated TLCs have been used to perform heating system calibrations in different PCR lab-on-a-chip devices [40–42]. In these studies, and prior to the amplification reaction, TLCs were allowed to flow through the system and colour changes were used to determine the correspondence between the power of heaters and the actual temperature inside channels and chambers. Controlling temperature distributions on a microscale with a calibration accuracy of 1°C has been accomplished by this approach [42].

De Mello and coworkers reported a TLC-based system for the real-time monitoring and controlling temperatures in microfluidics via the Reimer-Tiemann reaction as a model system [43]. In this study, a specific channel for TLCs slurry was introduced near the sample channel and colour changes were continuously measured by a miniaturized spectrometer that provided feedback for thermal control. Resolution of 0.4 °C was attained. In an attempt to meet an analogous goal, Hoang et al. used TLCs to track temperature changes throughout the PCR process in a microfluidic system [44]. A more recent work has improved TLCs-based temperature control in microfluidics by measuring three-dimensional thermal gradients in real time (Fig. 2D) [34].

In line with this, it is worth mentioning the revision work reported by Dabiri [36]. This review presents a comprehensive theoretical description and experimental data on thermometry and velocimetry using thermochromic liquid crystal particles. This may be a useful information source when planning to develop a new lab-on-a-chip microfluidic biosensor using TLCs for temperature management.

Thermochromic liquid crystals are highly sophisticated materials in terms of structure and three-dimensional conformation. Therefore, in addition to being used merely as temperature reporters in microfluidic systems, it would be interesting to fully exploit this characteristic chemical features for biosensing purposes. It is worth noting that the Bragg reflector behaviour of TLCs, originated by their aggregation structure, actually provides one-dimensional photonic crystal properties to this material [45]. This concept opens up interesting possibilities for developing new label-free biosensing systems. For instance, by chemically modifying TLC molecules to introduce selective receptors, the recognition of an analyte may change the distance between planes in the liquid crystal structure to thus modify the material's thermochromic properties.

3.4. LightScribe

LightScribe technology was designed as a labelling system for compact discs, and is mass-produced and commercialised integrated into CD and DVD discs and drives. LightScribe discs are regular CDs and DVDs that contain a photochromic coating in the label side of the disc. To

create the label, discs are flipped and placed inside the disc drive, where an image previously designed by the user (using specific software) is irradiated onto the photochromic coating by a 780 nm focused laser source. Thus the irradiated area becomes darker and the image is transferred to the label side of the disc on a greyscale.

LightScribe photochromic coatings are multilayer materials that involve a light receptor compound and a colour former, contained in a solid-state matrix [46]. When the laser beam hits the material, the light receptor absorbs radiation and transforms it into heat. This process is led by the photothermal effect, a thermal relaxation of molecules in excited electronic states [47]. Then the heat transfer provokes a thermal increase in the solid matrix, which triggers an irreversible chemical change in the colour former compound. Thus using leuco dyes (colourless in the initial state), the irradiated area becomes darker [48]. It is interesting to note that this material involves both photo- and thermochromism since light absorption induces a thermal process that triggers colour change.

In this section, different LightScribe approaches that indicate biosensing features are discussed and structured according to their scope.

3.4.1. Graphene patterning

LightScribe found an interesting scientific application for creating graphene structures on graphite oxide films by direct laser reduction. For this purpose, graphite oxide films are deposited on the label side of LightScribe discs and irradiated using the disc drive, where the power (~30 mW) and the focusing system (15 μm spot diameter on the coating) of the laser enables this reduction process. Graphene structures can be easily designed with the same procedure as regular LightScribe labels. Once fabricated, structures are peeled off to be used for different purposes.

This idea was exploited to create graphene microelectronic devices. El-Kady et al. fabricated flexible graphene-based elechtrochemical capacitors by sandwiching a polymer electrolyte layer between two films of laser-scribed graphene [49]. Then the same authors also exploited the resolution of LightScribe to design graphene super-microcapacitors [50]. Similarly, Tian et al. fabricated a resistive random access memory by coating a patterned LightScribe laser-reduced graphene oxide structure with hafnium oxide and silver [51].

Some studies have taken advantage of this approach for developing graphene-based physical sensors. Laser-scribed graphene foam-like structures sandwiched between graphene oxide undergo conductance changes as a response to a wide range of pressure (0~50 kPa) [52]. Also, a strain sensor based on laser-scribed graphene micro-ribbons has been reported, which shows a linear electric resistance response with the applied strain [53]. In both papers the authors claim the potential of these materials for biosensing, and also for medical applications, such as

electronic skin.

A couple of papers have addressed this graphene reduction approach to develop chemical sensors. Kaner and coworkers created laser-scribed graphene circuits which undergo reversible resistance changes as a response to NO_2 exposure in air (Fig. 3A) [54]. The performance of this system has been proved for many analysis cycles, and each cycle comprised 10 minutes of NO_2 exposure (20 ppm in dry air samples), followed by 10 minutes of purging. Besides, Griffiths et al. reported a study that proved the potential of LightScribe laser-reduced graphene electrodes for electrochemical sensing. In this work, laser-scribed graphene electrodes were characterised and electrochemically compared with a range of other carbon-based electrodes [55]. This study also highlighted the features of these graphene electrodes that support their potential for electrochemical biosensing.

In the biosensing direction, this bibliographic revision suggests promising LightScribe laser-reduced graphene biosensors that exploit the intrinsic graphene capabilities for electrochemical biosensing [56]. In this way, the simple fabrication system involved in this approach matches the do-it-yourself concept, which leads to interesting point-of-care implications. Besides, using laser-scribed graphene structures as a scaffold to electrochemically grow metal nanoparticles is also seen as an interesting research avenue to create optically active metallic structures for biosensing

3.4.2. Lab-on-a-disc systems

LightScribe can be exploited as a versatile bioanalytical tool, as reported by our group [57], where this technology was designated as Thermochromic Etching Discs (TED). The above-cited work describes how to turn LightScribe into a practical analytical system to develop integrated optical biosensors. This study experimentally demonstrates the sensing capabilities of this technology by means of different approaches, such as microarraying, immunofiltration, cell culture and turbidimetry [57]. In a subsequent work, an immunofiltration system implemented in LightScribe to analyze Escherichia coli in food samples was also reported by our group [58].

Many works have proven the biosensing potential of compact disc data-storage technologies (CD, DVD, Blu-ray) [59]. LightScribe implementation in this field opens up a whole range of physicochemical modification possibilities for developing lab-on-a-disc systems whilst keeping standard discs as assay platforms and disc drives as analytical instrumentation. These studies point to integrating into one disc centrifugal microfluidics for sample handling and bioassays for the sensing step.

These facts, together with using the regular disc player as a spinning and detection device, provide high suitability for point-of-care systems. Along these lines, computing the analysis

result to be directly written on the photochromic LightScribe material means a simple readout system, which would be useful for non-specialised environments (Fig. 3B, V).

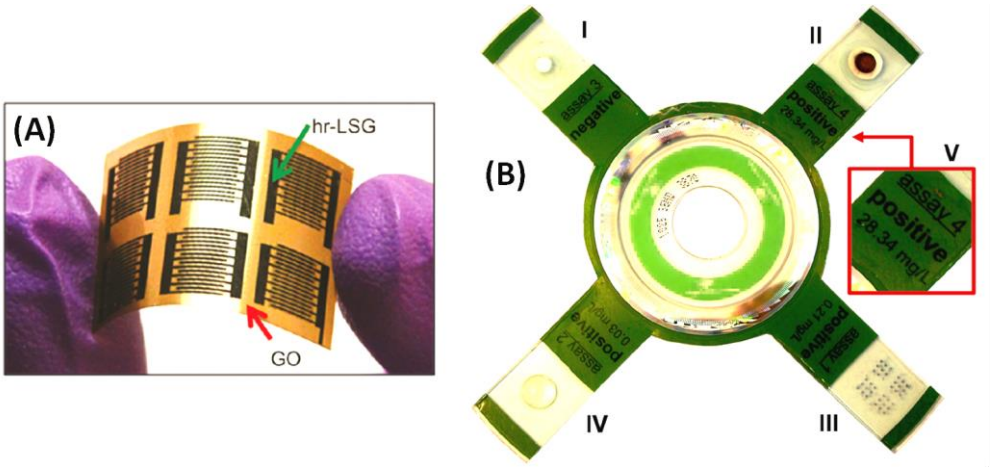

Fig. 3. (A) Highly reduced laser-scribed graphene (hr-LSG) electrode for NO2 sensing, patterned on graphite oxide (GO) by LightScribe. Adapted with permission from (*ACS Nano* 2012, 6, 1395–1403). Copyright (2012) American Chemical Society. (B) Exemplary LightScribe lab-on-a-disc system that includes turbidimetry (I), immunofiltration assay (II), microimmunoassay (III), cell culture (IV), and the analysis readout recorded on the photo/thermochromic material (V). Adapted with permission from (*Anal. Chem.* 2014, 86, 12037–12046). Copyright (2014) American Chemical Society

3.4.3. Photochromic/thermochromic substrates

The photochromic materials designed for laser etching surfaces suggest new biosensing solutions, where LightScribe photochromic coatings are probably the most paradigmatic example. Motivated by these materials, this section presents a new concept for exploiting thermochromic and photochromic surfaces for biosensing purposes, provides experimental results to support it, and discusses the trend towards its development.

The approach is based on using these materials to immobilise selective receptors and employing labels capable of interacting with the laser source and the photochromic substrate. So this system leads to two different kinds of labels: antenna compounds and scattering labels. As illustrated in Fig. 4A, antenna compounds absorb light and transform it into heat. Hence for a positive assay, the temperature of the area that contains the antenna will become higher than the background and a darker spot will be obtained. In contrast, scattering labels scatter the laser beam and reduce the amount of radiation received by the surface, which yields a lighter spot for a positive assay.

Therefore, this strategy introduces a signal development by just applying light, where the greyscale colour intensity of the spot after irradiating can correlate with the target concentration. In contrast, most signal development systems for biosensing are based on chemical or biochemical procedures which, even if they offer good performance for many applications, expensive chemical (Au, Ag, etc.) and biochemical (proteins, enzymatic substrates, etc.) reagents are still required [60]. Unlike these strategies, light-based signal development is a simpler, greener, safer and cheaper approach.

This approach comprises immobilising protein probes on the photochromic material and using bioreceptors or targets conjugated to the above-mentioned labels (Fig. 4B). Regarding probe immobilisation, the experimental adsorption isotherm by passive physisorption, and using bovine serum albumin (BSA) as a protein model system, offers a maximal immobilised protein surface density of 2.2 pmol/cm^2 (Fig. 4C). So this substrate attains comparable performance to other materials, such as polystyrene (~1.7 pmol/cm^2 for IgG)[1] and polycarbonate (1.1 pmol/cm^2 for BSA) [61].

The functionality and sensitivity of different labels on this photochromic material were evaluated. Indocyanine green and IR783 as antenna compounds, as well as 0.38 μm diameter hollow polymeric microspheres (HPM)[2] as scattering labels (Fig. 4D), were placed onto photochromic material at different surface concentrations.

Once irradiated, the employed compounds were active and showed the expected interaction between the laser and photochromic material in positive assays (Fig. 4E). Considering the lowest eye-detectable label surface density and the protein adsorption isotherm, minimal bioreceptor/label ratios of 7–13 and 0.001–0.003 for IR783 and HPM were calculated, respectively. These data ensure affordable bioreceptor-label conjugation ratios. However, lower minimal ratios would be desirable for highly sensitive assays since the whole biorecognition process may involve parameters that can potentially affect the performance of labels. These results correspond to standard photochromic coatings of LightScribe discs as substrates, which include antenna compounds in their original composition. Although the mass production of these materials is a major advantage, their configuration triggers a background colour change, even for negative assays, which reduces sensitivity. Therefore, omitting the antenna compounds in the composition of these materials is an interesting approach to enhance sensitivity.

Another strategy, which is compatible with the original coatings, relies on using a laser source and an antenna label tuned to a different wavelength from that of the antenna compound contained in the photochromic substrate. This option involves a selective colour change within the assay area for a positive assay (but not in the background), thus improving sensitivity. Also, using photochromic materials that involve colour development based on polymeric nanoparticle melting may be an interesting alternative option [62].

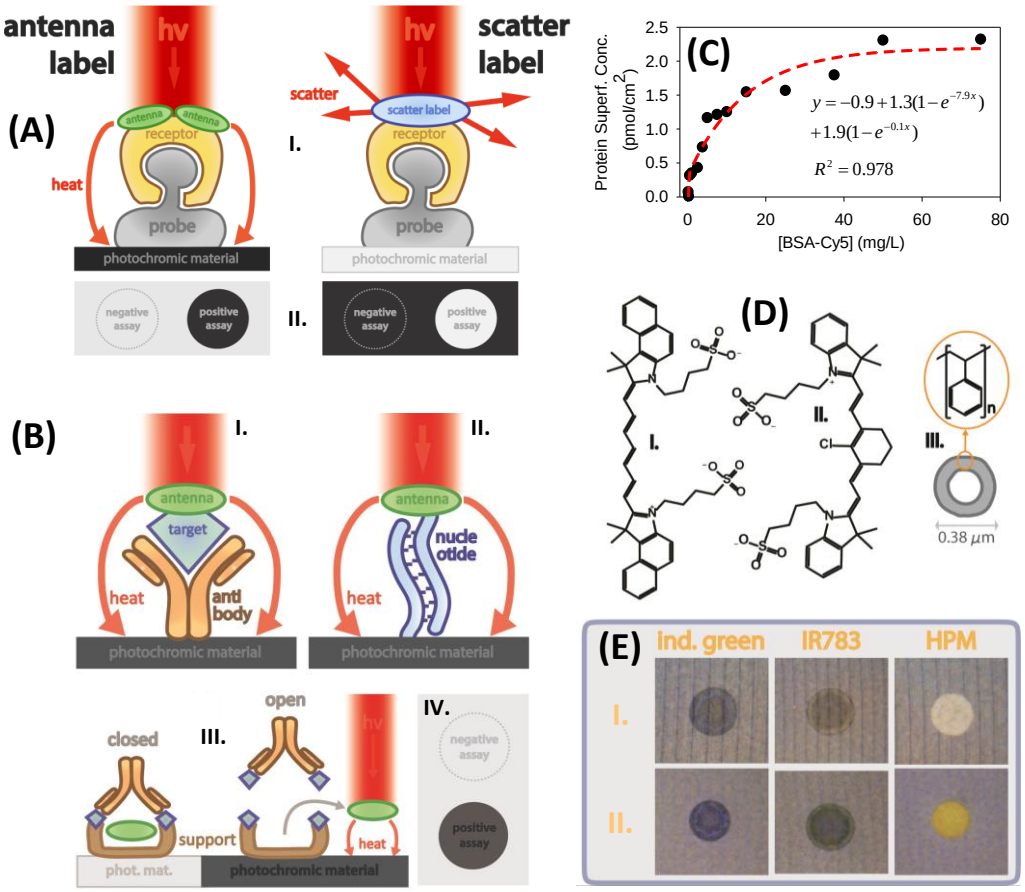

Fig. 4. (A) Assay scheme with antenna compounds and scatter labels (I), and the corresponding result in negative and positive assays (II). (B) Assay scheme using antenna labels in immunoassays (I), DNA hybridisation assays (II), controlled release sensing systems with (open) and without (closed) an analyte (III), and the corresponding negative and positive assay results (IV). (C) Protein adsorption isotherm using fluorescent-labelled BSA on a CD LightScribe photochromic coating. The experimental results were fitted to an exponential rise to maximum (5 parameters) equation. (D) Structure of the studied labels: Indocyanine green (I), IR783 (II), and HPM (III). (E) Images of irradiated spots with the studied labels on the photochromic material of CD LightScribe (I) and yellow-coloured DVD LightScribe discs (II).

Key processes for future research are the conjugation of labels and the bioreceptor and its influence on the antenna or scattering effect, as well as the probe homogeneity along the spot [63]. Also, number of different molecular antennas, which often present suitable moieties for bioconjugation, offer interesting options which may increase the energy transfer effect [48].

Along these lines, using ordered nanostructured systems indicates potential future research avenues to enhance label performance [64]. The photothermal effect of functional nanoparticle-based materials is also an appealing alternative to be implemented as antennas in this system [65,66].

In addition to immunoassays, other biorecognition approaches that use nucleic acids (aptamers, DNA probes, etc.) and other molecular docking systems (phages, MIPS, etc.) can be implemented, as schematised in Fig. 4B (II). Besides, controlled release systems designed for releasing encapsulated antennas in the presence of an analyte is an interesting strategy that is compatible with this approach (Fig. 4B, III).

3.5. Thermal paper

The scope of the approach described in Section 3.4.3 can be extended by means of other thermochromic and photochromic materials and energy source, and thermal paper technology is an attractive option.

Thermal paper holds a coating that contains a solid mixture of chemicals (colour developers, sensitisers, etc.) which generate permanent colour change in areas exposed to heat [67]. To exploit thermal paper technology for the described approach, colour developers, heat receptors, or preferably heat-isolating elements, should be used as labels. The low cost of this material, together with its mass production for many applications (receipts, tickets, labels, etc.), is an interesting point for it to be implemented into biosensing. There are many inexpensive and commercially available thermal printing devices (cash registers, faxes, portable printers, credit card payment terminals, etc.) that could be used as signal-developing instrumentation (Fig. 5).

4. Conclusions and future trends

Photochromism and thermochromism have a significant repercussion in academia and industry, but very few developments that exploit these phenomena for biorecognition assays have been reported. Nonetheless, the photo- and thermochromism advances in chemical sensing, biology, medical applications and technological systems provide a fertile scenario for raising new bioanalytical systems.

Regarding photochromic molecules and photochrome-fluorophore dyads, their modification by introducing bioreceptors that trigger a photochromic change after recognising a target is an intuitive option to extend these molecular systems to biosensing. The reported developments on photochromic biological control sets the basis for conjugating photo-switchable compounds to biomacromolecules which, in fact, strongly suggests the photochromic labelling of bioreceptors for biorecognition assays.

Fig. 5. Exemplary application of a point-of-care bioanalytical system that exploits thermochromic paper and commercial thermal printers.

A number of scientific studies based on commercially available photo- and thermochromic technologies have reported interesting advances towards biosensing. Thermochromic and photochromic fibres and inks, and thermochromic liquid crystals, are some examples that indicate new approaches, such as thermochromic displays for electrochemical biosensor analysis readouts, or nonsolid active structures for label-free bioanalysis.

LightScribe technology comprises very interesting features to address new biosensing systems. The underlying sensing capabilities of graphene, together with its easy patterning by direct laser reduction, are an appealing option to produce sophisticated graphene-based biosensing devices. Besides, LightScribe allows integrated lab-on-a-disc systems to be developed, where the whole analytical process could be run using LightScribe discs and drive units.

Photo- and thermochromic materials are promising substrates for immobilising bioreceptors, and to be used together with labels that simultaneously interact with these materials and the energy source. This strategy provides signal development that improves costs and safety, simplifies the analytical process, and yields simple qualitative and quantitative results. Achieving the full

performance of this approach implies scientific challenges from different chemistry areas, from which we envision exciting future advances

Acknowledgements

This work has been supported by the Spanish Ministry of Economy and Competitiveness (CTQ2013-45875-R), FEDER, and the Generalitat Valenciana (PROMETEO II/2014/040). M.A.-O. acknowledges the Spanish Ministry of Economy and Competitiveness for an FPI program grant.

The authors recognise the rich scientific heritage in the biosensing field of Prof. Marco Mascini.

Notes

[1] Costar 96-well medium binding polystyrene microplates (considering 150 kDa for IgGs).

[2] Ropaque Ultra E (Dow Chemical Company).

References

[1] J. Zhang, Q. Zou, H. Tian, Adv. Mater. 25 (2013) 378.

[2] E. Fritsch, L. Massi, G.R. Rossman, T. Hainschwang, S. Jobic, R. Dessapt, Diam. Relat. Mater. 16 (2007) 401.

[3] M.N. Mozgovaya, O.A. Smitienko, I.V. Shelaev, F.E. Gostev, T.B. Feldman, V.A. Nadtochenko, et al., Dokl. Biochem. Biophys. 435 (2010) 302.

[4] A. Perrier, F. Maurel, D. Jacquemin, Acc. Chem. Res. 45 (2012) 1173.

[5] S. Kawata, Y. Kawata, Chem. Rev. 100 (2000) 1777.

[6] M. Natali, S. Giordani, Chem. Soc. Rev. 41 (2012) 4010.

[7] M. Irie, T. Fukaminato, K. Matsuda, Chem. Rev. 114 (2014) 12174.

[8] T. Grotjohann, I. Testa, M. Leutenegger, H. Bock, N.T. Urban, F. Lavoie-Cardinal, et al., Nature 478 (2011) 204.

[9] T. Feczko, B. Voncina, Curr. Org. Chem. 17 (2013) 1771.

[10] J. Cusido, E. Deniz, F.M. Raymo, Eur. J. Org. Chem. (2009) 2031.

[11] N. Shao, Y.J. Jian, H. Wang, Y. Zhang, H.Y. Rong, H.C. Wing, Anal. Chem. 80 (2008) 3466.

[12] Y. Shiraishi, Y. Matsunaga, T. Hirai, Chem. Commun. 48 (2012) 5485.

[13] Y. Li, Y. Duan, J. Zheng, J. Li, W. Zhao, S. Yang, et al., Anal. Chem. 85 (2013) 11456.

[14] Y. Shiraishi, S. Sumiya, T. Hirai, Chem. Commun. 47 (2011) 4953.

[15] N. Shao, H. Wang, X. Gao, R. Yang, W. Chan, Anal. Chem. 82 (2010) 4628.

[16] N. Shao, J.Y. Jin, S.M. Cheung, R.H. Yang, W.H. Chan, T. Mo, Angew. Chem. Int. Ed Engl. 45 (2006) 4944.

[17] Y. Li, Y. Duan, J. Li, J. Zheng, H. Yu, R. Yang, Anal. Chem. 84 (2012) 4732.

[18] J. Tao, Y. Li, P. Zhao, J. Li, Y. Duan, W. Zhao, et al., Biosens. Bioelectron. 62 (2014) 151.

[19] Y. Song, C. Xu, W. Wei, J. Ren, X. Qu, Chem. Commun. 47 (2011) 9083.

[20] M. Qin, Y. Huang, F. Li, Y. Song, J. Mater. Chem. C (3) (2015) 9265.

[21] N. Soh, K. Yoshida, H. Nakajima, K. Nakano, T. Imato, T. Fukaminato, et al., Chem. Commun. 1 (2007) 5206.

[22] I.L. Medintz, S.A. Trammell, H. Mattoussi, J.M. Mauro, J. Am. Chem. Soc. 126 (2004) 30.

[23] W. Szymanski, J.M. Beierle, H.A.V. Kistemaker, W.A. Velema, B.L. Feringa, Chem. Rev. 113 (2013) 6114.

[24] J. Zhang, J. Wang, H. Tian, Mater. Horiz. 1 (2014) 169.

[25] K. Fujimoto, M. Kajino, I. Sakaguchi, M. Inouye, Chem. Eur. J. 18 (2012) 9834.

[26] O. Babii, S. Afonin, M. Berditsch, S. Reier, P.K. Mykhailiuk, V.S. Kubyshkin, et al.,

Angew. Chem. Int. Ed Engl. 53 (2014) 3392.

[27] H. Jung, S. You, C. Lee, S. You, Y. Kim, Chem. Commun. 49 (2013) 7528.

[28] U. Al-Atar, R. Fernandes, B. Johnsen, D. Baillie, A. Branda, J. Am. Chem. Soc. 131 (2009) 15966.

[29] Y.-L. Ying, J. Zhang, F.-N. Meng, C. Cao, X. Yao, I. Willner, et al., Sci. Rep. 3 (2013) 1.

[30] M.A. Chowdhury, M. Joshi, B.S. Butola, J. Eng. Fiber. Fabr. 9 (2014) 107.

[31] L. Shuiping, T. Lianjiang, H. Weili, L. Xiaoqiang, C. Yanmo, Mater. Lett. 64 (2010) 2427.

[32] W. Hu, S. Liu, S. Chen, H. Wang, Cellulose 18 (2011) 655.

[33] A.C. Siegel, S.T. Phillips, B.J. Wiley, G.M. Whitesides, Lab Chip 9 (2009) 2775.

[34] R. Segura, M. Rossi, C. Cierpka, C.J. Kähler, Lab Chip 15 (2015) 660.

[35] M. Parsley, Handbook of Thermochromic Liquid Crystal Technology, Hallcrest, Glenview, IL, 1991.

[36] D. Dabiri, Exp. Fluids 46 (2009) 191.

[37] T.W. Davison, K.L. Ewing, J. Fergason, M. Chapman, A. Can, C.C. Voorhis, Cancer 29 (1972) 1123.

[38] L. Gao, Y. Zhang, V. Malyarchuk, L. Jia, K.-I. Jang, R. Chad Webb, et al., Nat. Commun. 5 (2014) 4938.

[39] A.M. Chaudhari, T.M. Woudenberg, M. Allin, K.E. Goodson, J. Microelectromech. Syst. 7 (1998) 345.

[40] J. Liu, M. Enzelberger, S. Quake, Electrophoresis 23 (2002) 1531.

[41] J.-Y. Cheng, C.-J. Hsieh, Y.-C. Chuang, J.-R. Hsieh, Analyst 130 (2005) 931.

[42] V.J. Sieben, C.S. Debes-Marun, L.M. Pilarski, C.J. Backhouse, Lab Chip 8 (2008) 2151.

[43] A. Iles, R. Fortt, A.J. de Mello, Lab Chip 5 (2005) 540.

[44] V.N. Hoang, G.V. Kaigala, C.J. Backhouse, Lab Chip 8 (2008) 484.

[45] C. Fenzl, T. Hirsch, O.S. Wolfbeis, Angew. Chem. Int. Ed Engl. 53 (2014) 3318.

[46] V. Kasperchik, C.L. Dorsh, M.P. Gore, Patent US2007/0037088 A1, 2007.

[47] M. Tokeshi, M. Uchida, A. Hibara, T. Sawada, T. Kitamori, Anal. Chem. 73 (2001) 2112.

[48] R. Muthyala, Chemistry and Applications of Leuco Dyes, Kluwer Academic Publishers, New York, 2002.

[49] M.F. El-Kady, V. Strong, S. Dubin, R.B. Kaner, Science 335 (2012) 1326.

[50] M.F. El-Kady, R.B. Kaner, Nat. Commun. 4 (2013) 1475.

[51] H. Tian, H.Y. Chen, T.L. Ren, C. Li, Q.T. Xue, M.A. Mohammad, et al., Nano Lett. 14 (2014) 3214.

[52] H. Tian, Y. Shu, X.-F. Wang, M.A. Mohammad, Z. Bie, Q.-Y. Xie, et al., Sci. Rep. 5 (2015) 8603.

[53] H. Tian, Y. Shu, Y.-L. Cui, W.-T. Mi, Y. Yang, D. Xie, et al., Nanoscale 6 (2014) 699.

[54] V. Strong, S. Dubin, M.F. El-Kady, A. Lech, Y. Wang, B.H. Weiller, et al., ACS Nano 6 (2012) 1395.

[55] K. Griffiths, C. Dale, J. Hedley, M.D. Kowal, R.B. Kaner, N. Keegan, Nanoscale 6 (2014) 13613.

[56] M. Pumera, A. Ambrosi, A. Bonanni, E.L.K. Chng, H.L. Poh, Trends Anal. Chem. 29 (2010) 954.

[57] M. Avella-Oliver, S. Morais, J. Carrascosa, R. Puchades, A. Maquieira, Anal. Chem. 86 (2014) 12037.

[58] N.J. Sacco, E. Cortón, M. Avella-Oliver, S. Morais, R. Puchades, A. Maquieira, 2014 IEEE 9th Ibero-American Congress on Sensors (IBERSENSOR), IEEE, Bogotá, Colombia, 2014.

[59] P. Dobosz, S. Morais, E. Bonet, R. Puchades, A. Maquieira, Anal. Chem. 87 (2015) 9817.

[60] E. Peris, M.J. Bañuls, Á. Maquieira, R. Puchades, Trends Anal. Chem. 41 (2012) 86.

[61] M. Avella-Oliver, D. Gimenez-Romero, S. Morais, M.Á. González-Martínez, P.R. Bueno, R. Puchades, et al., Chem. Commun. 49 (2013) 10868.

[62] V. Kasperchik, J.C. Bhatt, M.P. Gore, Patent US2007/0065749, 2007.

[63] P.J. Yunker, T. Still, M.A. Lohr, A.G. Yodh, Nature 476 (2011) 308.

[64] V. Martínez-Martínez, R. García, L. Gõmez-Hortigüela, J. Pérez-Pariente, I.

Lõpez-Arbeloa, Chem. Eur. J. 19 (2013) 9859.

[65] S.E. Lee, D.Y. Sasaki, Y. Park, R. Xu, J.S. Brennan, M.J. Bissell, et al., ACS Nano 6 (2012) 7770.

[66] H.K. Moon, S.H. Lee, H.C. Choi, ACS Nano 3 (2009) 3707.

[67] J. Rajasärkkä, J. Koponen, R. Airaksinen, H. Kiviranta, M. Virta, Anal. Bioanal. Chem. 406 (2014) 5695.

3.1.3 Total analysis systems with thermochromic etching discs technology

Anal. Chem., 86 (**2014**) 12037.

ABSTRACT

A new analytical system based on Thermochromic Etching Discs (TED) technology is presented. TED comprises a number of attractive features such as track independency, selective irradiation, a high power laser, and the capability to create useful assay platforms. The analytical versatility of this tool opens up a wide range of possibilities to design new compact disc-based total analysis systems applicable in chemistry and life sciences. In this paper, TED analytical implementation is described and discussed, and their analytical potential is supported by several applications. Microarray immunoassay, immunofiltration assay, solution measurement, and cell culture approaches are herein addressed in order to demonstrate the practical capacity of this system. The analytical usefulness of TED technology is herein demonstrated, describing how to exploit this tool for developing truly integrated analytical systems that provide solutions within the point of care framework.

1. Introduction

The development of chemical biosensors is an active area in the scientific community and industry.[1] Overcoming the limitations of the established standard analytical techniques in order to directly improve the global public health constitutes one of the main motivations. The aim of biosensor development is the design of inexpensive, easy-to-use, robust, rapid, and portable systems to provide solutions in fields such as point-of-care, home diagnostics, and environmental analysis.[2,3] A fruitful way to address biosensors development consists of focusing chemical and engineering ingenuity on bonding analytical purposes with worldwide mass-produced technologies.[4,5] In this framework, since its early introduction in the analytical scenario,[6] compact disc technology represents one of the most paradigmatic approaches in academic and industrial research.[5,7]

Compact disc platforms and drives constitute a highly sophisticated low-cost technology in terms of optics, mechanics, and electronics. This fact, together with their robustness, portability, and ubiquity has resulted in a new biosensing approach which is key for really inferring on the current bench-based and central laboratories analysis concept. Since over 15 years ago up to now, an increasing number of scientific developments and commercial applications are found involving the implementation of analytical systems in optical disc recording technologies. Nowadays, many of these applications have been performed on compact disc (CD), super audio CD (SACD), digital versatile disc (DVD),[8] and Blu-ray.[9] Numerous smart approaches have been successfully developed for detecting and determining a wide range of analytes such as organic[9,10] and inorganic compounds,[11,12] proteins,[13,14] and nucleic acids.[15,16]

In this context, commercial discs are used as assay platforms and standard disc drives are employed as detectors, by performing analog acquisition or error rate analysis.[17] These analytical developments must take into account that the scanning process is highly dependent on the physical properties of the disc. Optical disc recording technologies (CD, DVD, SACD, Blu-ray, etc.) rely on supporting binary data on a spiral- shaped groove (track) contained in the disc. Thus, to recognize and scan the disc, the drive sequentially irradiates the track through an integrated orthogonal laser source, while controlling the disc rotation. Therefore, optical and mechanical disc modifications and the introduction of optical restricting elements disrupt the track irradiation and potentially abort the scanning process. This fact constitutes a hard drawback for developing analytical applications using disc drives as detectors. Along these lines, some reported approaches based on strong disc modifications employ noncommercial disc drives and custom instrumentation to perform the analysis.[18–21]

The design of truly integrated total analysis systems where sample handling and sensing stages are performed using standard disc drives as unique analytical instrumentation constitutes a crucial point for exploiting the maximal performance of these lab-on-a-disc systems. However, considering the current state-of-the-art, this objective is highly restricted by the track dependency of the optical disc recording technologies. Only limited materials, assay formats, detection methods, and mild physicochemical modifications that keep the optical and mechanical properties of the disc are allowed for the sensing step.[15] Regarding sample handling, the introduction of microfluidic features disrupt the track irradiation and abort the process using discs and drives for reflection measurements. In this context, smart strategies for cell counting have been reported,[22] which constitute an interesting approach toward this objective.

In support of the aforementioned endeavors, herein, we introduce Thermochromic Etching Discs (TED) technology in the analytical field. TED was developed by Hewlett-Packard and LiteOn as a labeling system for laser etching the label side of optical recording discs.[23] This technology is mass-produced being integrated on the standard disc drives and commercialized as LightScribe. Platforms compatible with TED technology are optical data recording discs (CD or DVD) containing a photochromic coating on the label side, that becomes darker when irradiated by the 780 nm integrated laser source. For creating the labels, TED discs are flipped in the drive and a motif previously designed by the user is etched on the label side in gray scale.

The main analytical capability of TED technology relies on its track independency in the scanning process using standard disc drives. Despite disc data storage systems, TED controls recognition and rotation by continuously irradiating a circular coordinate code contained in the inner part of the disc, called control feature zone (Supporting Information, Figure S1).[24] Thus, as long as the control feature zone is maintained, TED drive manages the platform regardless of the optical, mechanical, and chemical properties of the disc. Additionally, TED systems

present many attractive features such as the photochromic material contained in the discs, the high potency of the TED laser source, and the selective irradiation of the assay surface.

This manuscript presents TED and illustrates how to transform this technology into a versatile analytical tool. Rather than just developing a specific application, this paper seeks to provide insights into the wide range of analytical capabilities that this technology presents. For this purpose, TED features are disclosed, their optimization and setup procedures are described, and their practical perspective is demonstrated through different systems such as microarray immunoassay, immunofiltration test, solution measurements, and cell culture analysis. In order to pave the way for future approaches, key parameters to be considered for addressing TED analytical designs are also introduced and discussed. Herein, we aim to establish the basis to exploit this versatile tool for new analytical developments focused on truly integrated lab-on-a-disc systems.

2. Experimental section

2.1. Materials

Sodium phosphate buffers (PBS, 8 mM Na_2HPO_4, 2 mM KH_2PO_4, 137 mM NaCl, 2.7 mM KCl, pH 7.4), PBS-T (PBS containing 0.05% (v/v) Tween 20), and carbonate buffer (50 mM sodium, pH 9.6) were filtered through 0.22 μm pore size nitrocellulose membranes from Whatman GmbH (Dassel, Germany) before use. Tween 20, 5 nm colloidal gold-labeled goat antirabbit antibodies (GAR-Au), silver enhancer solutions, goat antirabbit peroxidase labeled antibodies (GAR-HRP), and tetramethylbenzidine liquid substrate (TMB) were supplied by Sigma-Aldrich (Madrid, Spain). Polyvinylidene fluoride (PVDF) and polycarbonate (PC) immunofiltration membranes were kindly supplied by Millipore Iberica (Madrid, Spain). Agar and LB Broth for solid cell culture media were from Fisher Scientific (Fair Lawn, NJ, USA). Hybriwell polymeric adhesive chambers were provided by Grace Biolabs (Bend, OR, USA). Commercial CD, DVD, and TED discs (CD LightScribe and DVD LightScribe) were purchased from MediaRange (MPO Ibeŕica, Madrid, Spain).

2.2 Instrumentation

CD and DVD disc scanning measurements were performed using a commercial disc drive (GSA-H42N, from LG Electronics Inc., Englewood Clifs, USA) as described elsewhere.[17] A noncontact microprinter (AD 1500 BioDot, Irvine, USA) was employed for microarray printing. For immunofiltration assays, an Easy-Titer ELIFA System (Pierce, Rockford, USA) and a Minipuls 3 peristaltic pump (Gilson, Villiers le Bel, France) were used. Surface fluorescence measurements

were carried out by an Axon Genepix 400B microarray scanner (Molecular Devices, Sunnyvale, CA, USA).

2.3 TED drive setup

A commercial disc drive (GSA-H55L, from LG Electronics Inc., Englewood Cliffs, USA) was used as an analog signal detector for the TED platforms. The drive contains a servo focus/tracking system (pickup) that simultaneously irradiates the disc surface with a 780 nm orthogonal laser source and collects the reflected beam. The pickup, disc rotor, and CFZ scanner are managed by a servo control system integrated in the standard drive. A 25.4 × 5.04 mm photodiode (SLSD-71N6 from Silonex, Montreal, Canada) was incorporated above the disc and the laser beam for the transmission measurements. Scanning areas were labeled with trigger footprints (black adhesive tape strips) in the outer rim of the disc to be measured with an incorporated photosensor (EE-SY125 from Omron, Schaumburg, IL, U.S.A.). All light sensors (pickup, photodiode, and trigger photosensor) were connected to a data acquisition board (DAB, DT9832A-02-OEM from Data Translation Inc., Menlo Park, CA, U.S.A.) that collects analog signal, digitalizes it, and transfers data to a computer through a USB2.0 connection. A similar setup was previously addressed in a CD drive for analog signal acquisition.[25] A scheme of the TED drive analytical setup is provided in Figure 1A.

2.4 TED analytical platforms

Five different platforms obtained from standard TED discs were studied: TED1 (regular thermochromic etching disc CD), TED2 (regular thermochromic etching disc DVD), TED3 (reflexive thermochromic etching disc CD), TED4 (reflexive thermochromic etching disc DVD), and TED5 (high transmission thermo- chromic etching disc CD). A scheme summarizing the notation, structure, assays prospects, and reading possibilities of the studied platform is depicted in Figure 2 and Table 1.

TED1 and TED2 are original unmodified thermochromic etching disc CD and DVD, respectively. TED3 and TED4 are reflective platforms obtained from TED1 and TED2, respectively, by dissolving the photochromic coating layer in an ethanol bath for 10 min at room temperature. Paper wipe rubbings were applied to trigger the coating solution process and to remove the remaining coating. TED5 is a high transmission disc obtained by eliminating the photochromic material, the protective layer, the metallic layer, and the recording dye of TED1, keeping the original layered structure in the central control feature zone part. For this, two circular grooves (4.7 and 11 cm diameter) on the label side of TED1 were cut using a blade, the photochromic and metallic layers were peeled off together from the cut groove, and the recording dye layer was dissolved in an ethanol bath for 10 s at room temperature. A scheme that describes

the procedure for making TED5 platforms from standard CD-TED is provided in the Supporting Information (Figure S1).

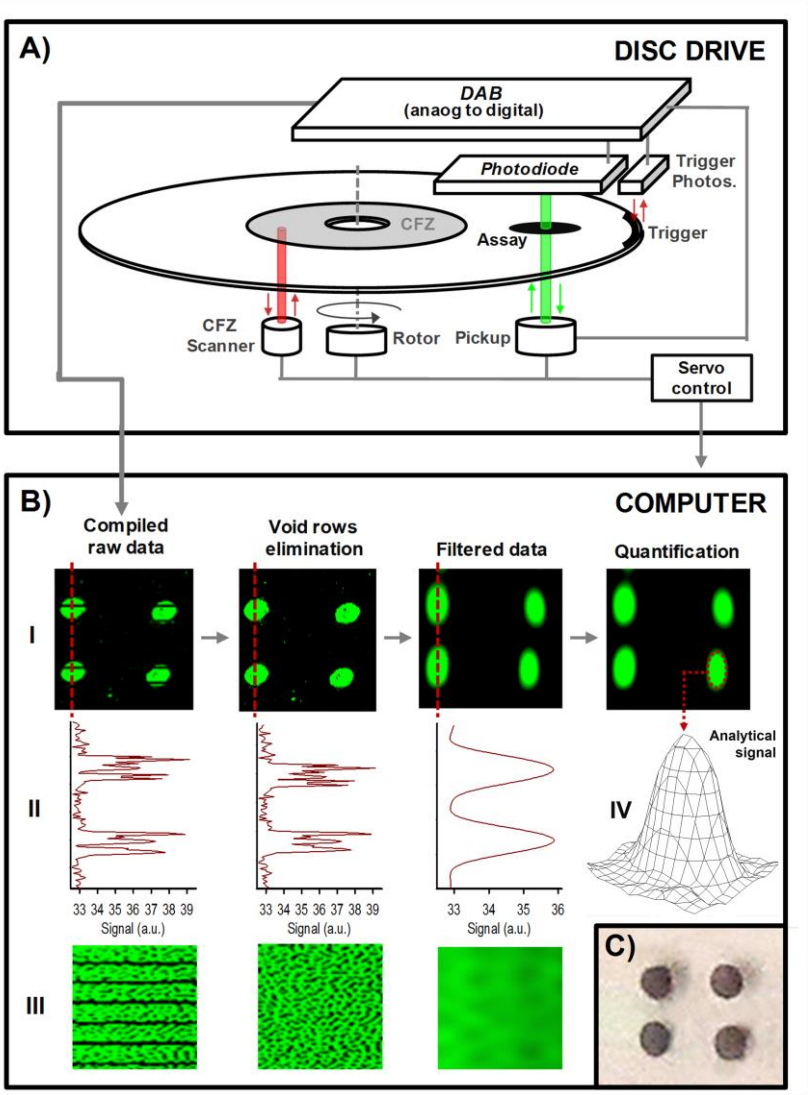

Figure 1. Scheme of the TED analytical implementation methodology. (A) TED disc drive setup. (B) Imaging and data processing procedure. Experimental imaging data (I), the corresponding bidimensional cross sections (II), and data zooms in the sample area (III) are presented for a scan of a microarray carried out with the TED system. Tridimensional representation of a microarray spot from the processed data (IV). (C) Image of a silver enhanced microarray in a TED5 platform surface.

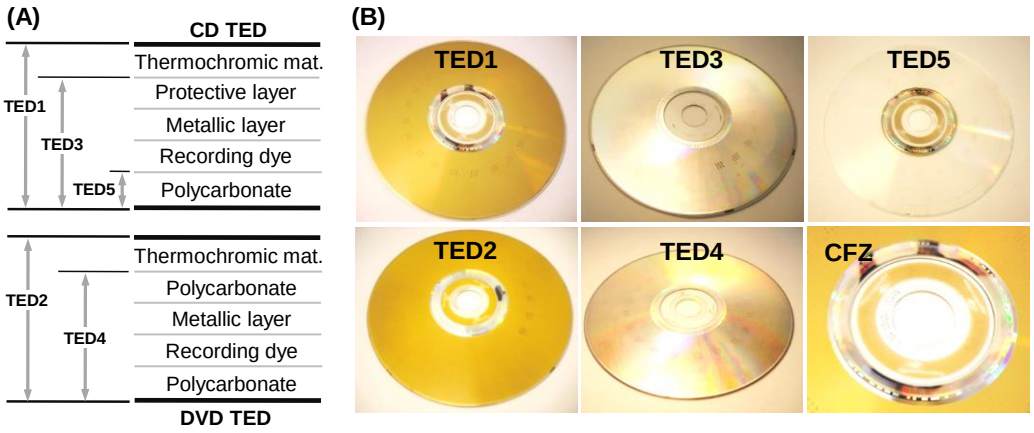

Figure 2. Description of the thermochromic etching disc analytical platforms. (A) TED discs layers structure. (B) Images of the TED platforms, used in a microarray assay, and the control feature zone (CFZ) of a TED2.

Table 1. Platforms characteristics and the corresponding notation used in this work.

Notation	Disc	Assay side*	Scanning mode	Assay surface
DVD	DVD	Down	Reflection	Polycarbonate
CD	CD	Down	Reflection	Polycarbonate
TED1	Thermochromic etching disc CD	Down	Reflection	Thermochromic material
TED2	Thermochromic etching disc DVD	Down	Reflection	Thermochromic material
TED3	Reflexive thermochromic etching disc CD	Down	Reflection	Protective layer
TED4	Reflexive thermochromic etching disc DVD	Down	Reflection	Polycarbonate
TED5	High transmission thermochromic etching disc CD	Down	Reflection Transmission	Polycarbonate
		Up	Transmission	Polycarbonate

* Down refers to the laser incidence surface during the disc scan, while up the opposite side.

Assays were performed on the outer surface of the laser incidence side during TED disc scan. Therefore, as described in Table 1, TED platforms provide different materials for sensing substrates. An interesting aspect to comment on is the new chemical immobilization and bioconjugation challenge that the sophisticated photochromic material of TED1 and TED2 introduces, beyond the typical substrates employed for biosensing.

Regarding scanning mode, this system was designed to measure events on the disc surface that attenuate the intensity of the disc drive laser beam. In the platforms keeping the metallic layer (TED1, TED2, TED3, and TED4), the incident laser hits this layer and reflects back to the pickup, thus allowing reflection measurements. On the other hand, TED5 is constituted by a transparent 1.2 mm polycarbonate layer, allowing reflection and transmission measurements. Light reflection was detected using the pickup because of the laser beam partial reflection in the air−polycarbonate interface, while the transmitted laser light was measured using an additional photodiode integrated in the DAB. Therefore, in addition to the down side, TED5 allows one to perform assays on the up side of the disc when carrying on transmission measurements. A scheme that graphically describes the scanning mode and assay side of every disc system is provided in the Supporting Information (Figure S2).

2.5 Imaging and data analysis

TED platforms were introduced in TED drives, and disc irradiations were managed by Nero CoverDesigner software. When scanned data is transferred from drive to computer, custom C++ based software (Biodisk) collects the signals from the pickup and photodiode and computes them, together with the photosensor signal, for arranging this data into an image. Thus, Biodisk provides a 16-bit gray scale tiff image that matches with the surface of the scanned disc, where intensity corresponds to light attenuations generated by the assay. Then, empty data rows were removed from the image by applying a custom Matlab function that calculates the standard deviation of each row, applies a Laplacian edge detection operator to automatically identify these data rows, deletes these rows, and builds a new file without them. These empty data rows (around 2 of every 12 pixel rows) come from TED disc drives intermittent irradiation stops during the disc scanning while acquisition continues. Next, signal was digitally processed using a Matlab function that transforms the image into a frequency domain through the Fourier transform, removes the signal contributions above an input frequency threshold, and transforms the processed data back into the spatial domain. Finally, Genepix software (Axon Instruments, Union City, CA, U.S.A.) was employed to quantify signal from the images. For this process, neat signals were obtained by subtracting the measured background value to the sample intensity. Grubbs' test (confidence level of 95%) was applied to discriminate outliers. This imaging and data analysis process was common for every different TED platform, while pickup data was

employed for reflection measurements (TED1, TED2, TED3, TED4, and TED5) and photodiode data was used for transmission scans (TED5 transmission). A scheme of the imaging and data processing procedure is provided in Figure 1B.

2.6 Microarray assay

To evaluate the performance of the developed platform, a simple assay was carried out as a model system. For this, gold labeled antibody solutions in carbonate buffer were dispensed on the analytical platform surface in microarray format (3 × 3) by a noncontact nanoprinter and incubated for 16 h at 4 °C. Then, surfaces were rinsed with PBS-T and deionized water and dried by centrifugation. After that, 1 mL of silver enhancer solution was applied and distributed along the whole disc surface using a polycarbonate dummy disc. After 8 min, the disc surface was rinsed with water and dried by centrifugation. The resulting silver dots precipitated on the disc surface (Figure 1C) were measured by disc drive on transmission and reflection modes.

2.7 Immunofiltration.

For the immunofiltration assays, PVDF and PC membranes where placed on the ELIFA (enzyme linked immunofiltration assay) system. Previously, the PVDF membranes were conditioned by immersion in methanol for 10 min. Volumes of 0.2 mL/well were used in each step and filtered at a flow rate of 40 μL/min per well. In all steps, PBS-T was used as working and washing buffer. Probe immobilization was carried out by filtering GAR-Au and GAR-HRP dilutions followed by washing with PBS-T five times. After that, signal developing solutions (silver enhancer and TMB, respectively) were dispensed (0.2 mL/well). After 8 min of incubation, the solutions were filtered as above. Finally, membranes were cut and fixed on the down side of a TED5 platform with adhesive film. The disc was scanned, and the signal was obtained by transmission measurements.

2.8 Cell culture

For culture media preparation, 0.375 g of agar was mixed with 0.5 g of LB broth and dissolved in 25 mL of milli-Q water. The solution was heated in a microwave until completely melted and homogenized. Then, 400 μL of melt media was directly dispensed on the down side of a TED5. Once solidified, this procedure provided circular films suitable for cell culture. The cell counting was performed by scanning the disc under the transmission principle.

2.9 Chamber measurements

Adhesive polymeric chambers were placed on the planar surface of a TED5. The chamber was filled by pipetting 90 μL of the solution and was sealed with seal tabs before scanning the disc by transmission.

3. Results and discussion

3.1 Analytical platforms and microarray assay

One of the key points that support the success of the compact disc technology implementation in the analytical field is its capability to provide practical and inexpensive analytical platforms. In this regard, Thermochromic Etching Discs technology provides a rich source of interesting and versatile discs for performing assays. As described in Experimental Section, five new analytical platforms with different properties were created from standard TED discs. Herein, the analytical performance of these new platforms was evaluated by means of their protein immobilization capabilities and sensitivity for microarray assays, being also compared with the reference platforms CD and DVD. For this, a simple microarray model system based on the passive immobilization of gold labeled antibodies and silver enhancement was selected.

First of all, optical resolution features for microarray assays were optimized for every disc. Resolution is a key point that characterizes assay platforms and detection systems. In comparison with CD and DVD, the optical resolution of TED platforms is higher in the track direction but lower in the radial direction (Supporting Information, Table S1). Assay sensitivity in microarray systems is highly influenced by the probe dot diameter and the detector resolution.[26] For a given resolution value, there is a critical dot diameter below which signal and sensitivity decrease. Considering these facts, the dependency between signal and dot diameter was experimentally studied for each analytical platform, and the minimal dot diameter that ensures maximal sensitivity was selected (Supporting Information, Figure S3). In most of the systems, microarray dot diameters around 600 μm were found to be enough for attaining over 95% of the total signal. Higher optimal diameter values were selected for the platforms TED1, TED3, and TED4. For TED1, this higher value presumably relies on the low protein passive adsorption capabilities of the thermochromic etching CD disc coating, while the reason for TED3 and TED4 may be related to a resolution loss associated with the slight surface heterogeneities generated in the platforms preparation.

The signal processing issue was also addressed in the optimization study. TED laser emission discontinuities generate high frequency noisy data, which cause low signal-to-noise ratios (SNR) thus reducing the assay sensitivity. To overcome this limitation, the analytical data were digitally processed using a low-pass Fourier filter in order to discriminate the high frequency signal

contributions (Figure 1B). For this reason, an experimental study to determine the SNR dependence with the filter cutoff was performed for each disc approach and optimal cutoff values were selected (Supporting Information, Figure S4). Once optimized, antibody adsorption isotherm curves using the immunoassay model system and the corresponding SNR evolutions were evaluated and compared (Figure 3). The results demonstrate high sensitivity for analytical applications after signal processing in most of the approaches.

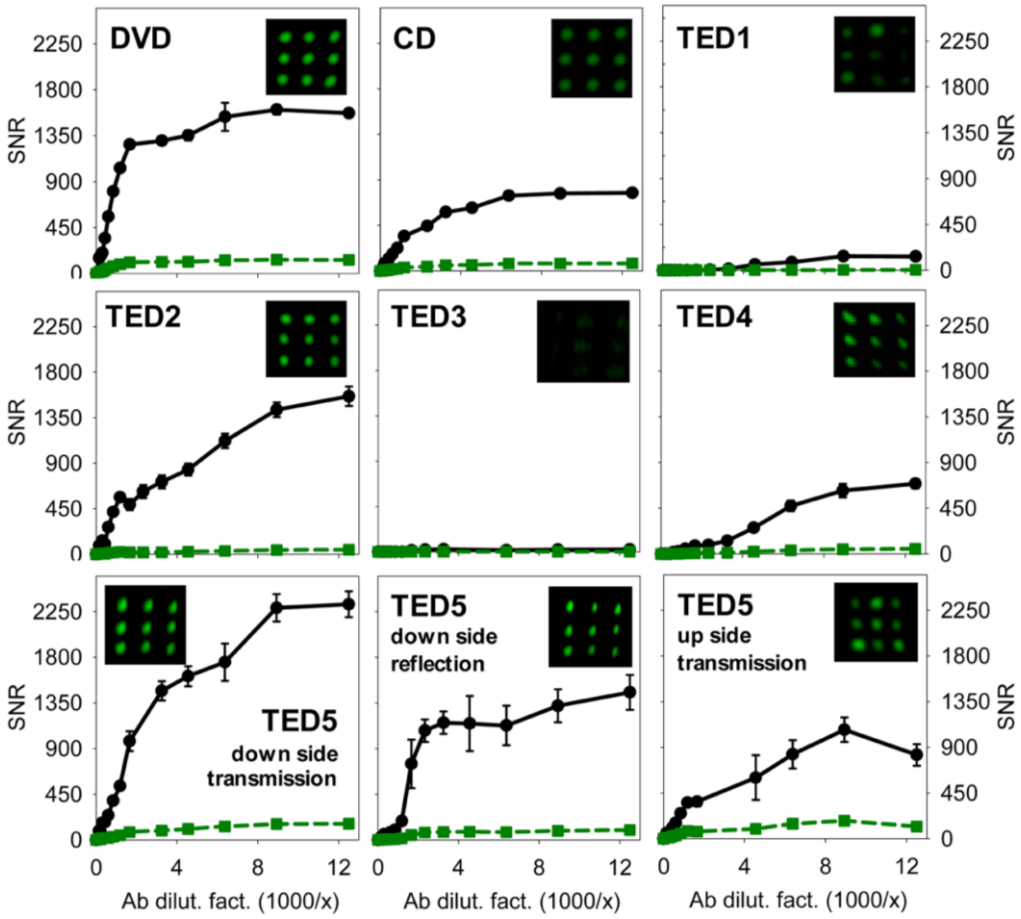

Figure 3. Antibody adsorption isotherms with (black ●) and without (green ■) signal processing. The insets are processed microarray data performed in each system.

The proposed signal processing methodology dramatically increases the sensitivity of every disc system, in particular up to 15-fold in TED2 and in down side TED5 measured by transmission. Both systems, TED2 and down side TED5 (reflection and transmission reading modes), have

equivalent analytical performance to DVD, reaching SNR levels above 1500 in the top of the isotherm curves, with down side TED5 measured by transmission being the best. Then, TED4 and up side TED5 show lower sensitivity, comparable to CD, while the SNR values for the second one are slightly higher (around 920 in the top of the curve).

Finally, the low maximal SNR values obtained in TED1 and TED3 (around 140 and 20, respectively) exhibit poor performance for the addressed assay. TED1 behavior suggests low protein immobilization yield by passive physisorption on the photochromic coating of this platform, while TED3 results fit with the low surface hydrophobicity observed in contact angle measurements (Supporting Information, Figure S5). Also, an additional interesting result of this study to highlight is the good protein immobilization performance showed by the TED2 photochromic coating.

In summary, after the optimization of high transmission thermochromic etching disc CD (TED5), this system becomes a high performance analytical platform with great versatility for developing new applications. The transparency of this disc allows one to perform transmission measurements in both sides of the disc, using the platforms easily created from standard TEDs.

3.2 Analytical features

The track independency of TED discs constitutes an important advantage that opens a new window for physical and chemical modifications as well as the introduction of features in these platforms. Track independency was graphically demonstrated by applying different optical restricting elements (Figure 4). This serves as a proof of concept for optical limiting components such as photonic structures, microfluidic features and devices, different materials, and strong chemical modifications. First, four star-shaped black opaque films were equidistantly disposed on the down side surface of a TED5 and a DVD. This shape allows one to monitor an optical restriction progressive increase in the track direction. As shown, the TED system scans the whole element without interruption, while the DVD aborts the scanning process when the optical restriction becomes around two millimeters large. Then, different diameter holes in the disc were also created and scanned as an example of a disc strong modification. In this case, TED5 was compared with the CD, since the DVD layer structure becomes disassembled during the mechanical process of holes creation. Data shows that CD track dependency makes the scan get into an error loop when measuring the smallest hole (0.5 mm in diameter) that ends up aborting the process. However, the TED system irradiates the holes array without disruption. Also, it is shown that the 0.15 μm resolution in the track direction for the TED systems (Supporting Information, Table S1) well enables the scanning of 500 μm features, which is good enough for many applications as the ones addressed below in this work.

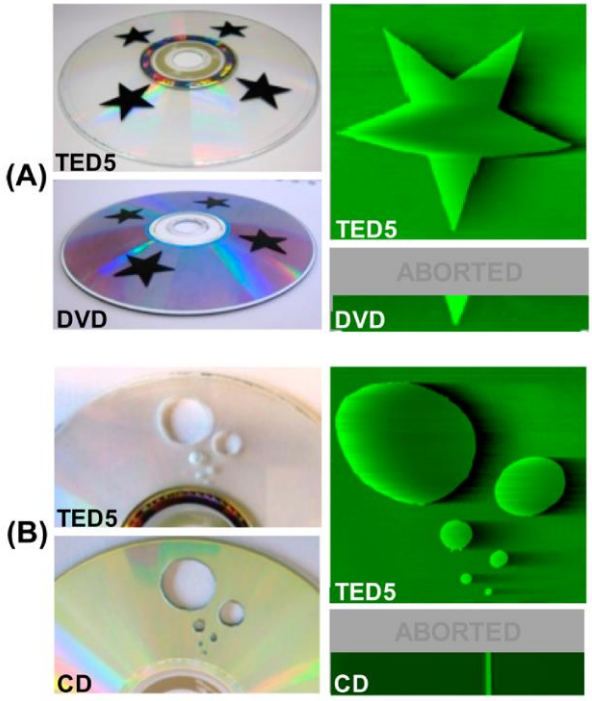

Figure 4. Demonstration of TED track independency, compared with the DVD and CD. (A) Disc images and scanned results of star-shaped opaque films on TED5 (down side, reflection) and DVD. (B) Disc images and scanned data of an array of different diameter holes (0.5, 1, 2, 4, 8, and 16 mm, from bottom to top) in TED5 (down side, reflection) and CD.

To deal with the track dependency of optical discs recording technologies, the development of bioanalytical applications typically involves immobilization of bioreceptors in small areas on the disc surface by mild procedures, together with assay formats that generate an insoluble precipitate as a biorecognition reaction product. TED exposes new assay strategies compatible with the disc drive measurement.

To demonstrate this potential, the capability of TED technology for performing immunofiltration assays was studied. The high opacity of the immunofiltration membranes makes these assays a good proof of concept. Also, immunopreconcentration capability constitutes a good option for developing future applications in which the sensitivity is a key factor. Thus, using an ELIFA (enzyme linked immunofiltration assay) configuration,[27] this study presents a membrane-based concept in which bioreceptors and biorecognition reaction products are retained in the immunofiltration membrane.[28]

Two different kinds of membranes were studied, polyvinylidene fluoride (PVDF) typically employed for protein capture and polycarbonate (PC) membranes. The low opacity of PC compared to PVDF membranes (65% and 53% of transmission in the TED system, respectively) may constitute a good option for performing transmittance measurements (Supporting Information, Figure S6).

This study was addressed using an assay in which GAR-Au and GAR-HRP were immobilized on the membranes, and then, silver enhancement solution and TMB were used to develop the signal, respectively. As shown in Figure 5A, disc immunofiltration transmission measurements provide good correspondence between signal and concentration in both assay systems (GAR-Au/Silver and GAR-HRP/TMB) using PVDF membranes and just in the GAR-Au/Silver approach when working with PC membranes.

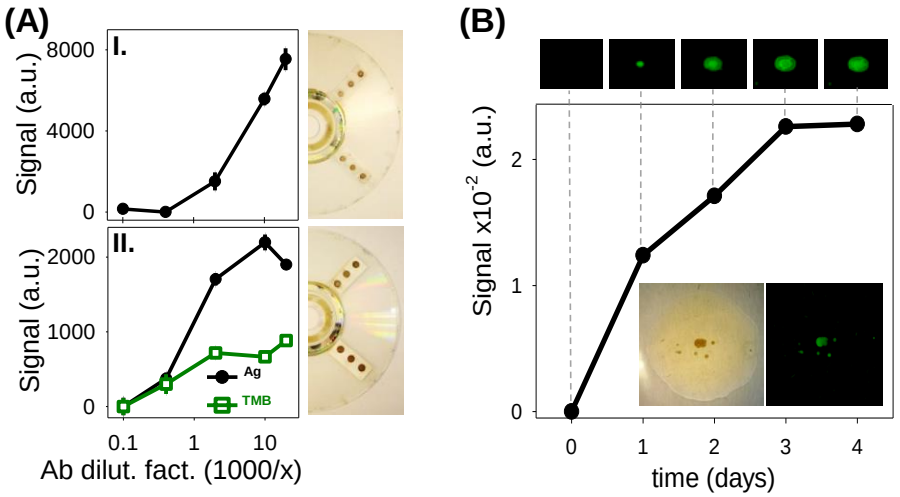

Figure 5. Disc-based analytical approaches with TED systems. (A) Response curves for the disc immunofiltration assay system, using PC (I) and PVDF (II) membranes. Images on the right side are the corresponding immunofiltration disc systems. (B) Cell colony growth monitoring on the cell culture TED system. Top images are the scanned colony at the corresponding times, and graph inset is an image of a culture media on the disc and the related scanned data.

The greater transparency of PC membranes generated higher signals (7500 au) than PVDF (2200 au). However, PVDF membranes illustrate signal response at lower antibody concentration than PC (dilution factors 1/2500 and 1/500, respectively), presumably due to its higher protein capture performance. These results fully demonstrate the TED capability for performing real assays with high optical restricting elements such as opaque membranes and, in particular, the potential for carrying out disc filtration-based assays.

Membrane integration in the disc, together with microfluidic structures for automating the filtration process, constitutes an interesting option for future analytical developments. This approach would allow one to improve the limits of detection by in situ sample preconcentration in the disc. Also, disc immunofiltration configuration suggests more analytical possibilities based on similar designs. Thus, the introduction of different membranes becomes viable and

promising for including the sampling stage in the disc. For instance, filtration membranes for particulate matter and solid phase micro- extraction materials would yield attractive results for disc in situ sampling and measurement.

For a further demonstration of the analytical prospects of this technology, TED platforms application for cell culture analysis was addressed. Cell culture media introduction constitutes a step toward the design of more complex biochemical analysis. For this, nonselective agar solid culture media was spun in the down side of the disc surface to reach better optical resolution (Supporting Information, Figure S7). For this study, eight independent cell culture areas were created on a TED5 and the colonies evolution was monitored by transmission measurements. According to the simulations data (Supporting Information, Figure S7), culture media were disposed in the down side of the disc to obtain better resolution. As shown in Figure 5B, spontaneous colonies growth took place on the culture media and their growth process was monitored and quantified by using the TED approach. Thus, a single colony growth was successfully analyzed and detected after 1 day of culture. These results represent a starting point for future cell analysis developments, for instance, total cells number or colony former unities determinations, considering the inherent limitations of these analytical systems.[29]

Thermochromic Etching Disc can also be employed for measuring the optical properties of solutions, as an example of a new assay to be performed in these systems. TED enables lab-on-a-disc analytical measurements of solutions through the creation of chambers in the disc. This approach allows a simple implementation of many analytical procedures for providing solutions in different fields. For instance, in this work, polycarbonate adhesive chambers on the disc are used to carry out light absorption and scattering measurements of analytical reaction products (Figure 6A).

First, black dye aqueous solution measurements were performed as a proof of concept for molecular absorption systems. Also, different concentrations of colloidal carbon nanoparticles in aqueous suspensions were measured. Carbon nanoparticles are used as a label for biorecognition assays, so this serves as an interesting model in this study. In both systems, the good signal-response curve obtained and low concentrations detected (0.02% and 0.01% w/v for dye and carbon nanoparticles, respectively) provide insights into the potential of the approach (Figure 6A, I and II). Also, turbidimetric assays on the disc were performed using this chamber configuration. The relevance of this approach relies on the significant solutions that turbidimetry provides in chemistry and clinical fields. Classical sulfate determination was studied to assess turbidimetry performance, by adding $BaCl_2$ for the creation of the insoluble $BaSO_4$ salt. The good signal to concentration correspondence obtained (Figure 6A, III) and the low $BaSO_4$ concentration detected (3 mM) corroborate the potential of the turbidimetric system. It must be noted that 250 μm tall chambers were employed, so higher sensitivity could easily be attained by

just using longer optical path length chambers. This approach means a simple strategy to perform turbidimetry and other related assays on lab-on-a-disc systems, which is often a hard matter to carry out by biosensing approaches.

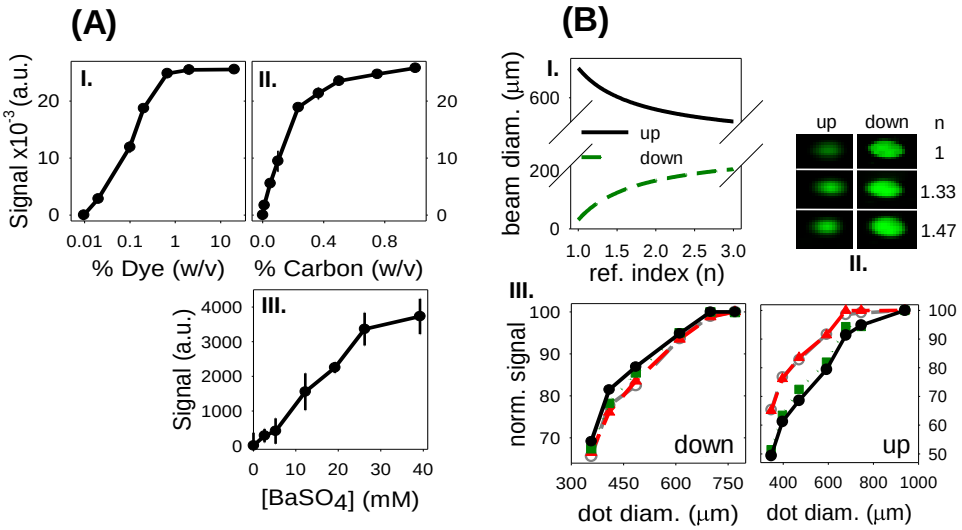

Figure 6. Results of TED solution chamber systems. (A) Response curves for the measurement of the optical properties of compounds in solution: molecular absorption dye (I), colloidal carbon nanoparticles (II), and $BaSO_4$ (III). (B) Results of chamber-based light focusing system on the disc. (I) Simulation of the resolution dependence with the refraction index of the solution in the chamber, in both sides of a TED5 disc. In this study, optical resolution is addressed in terms of the diameter of the laser beam hitting the assay surface. It must be noted that optical resolution is inversely proportional to beam diameter in the assay surface. (II) Experimental data of a scanned microarray with different refraction index solutions in the chamber. As predicted, optical resolution is directly proportional to the refraction index in the up side and inversely proportional in the down side. (III) Signal vs microarray dot diameter experimental curves in both sides of TED5, without the chamber (black ●) and filling the chamber with air (green ■, n = 1), water (red ▲, n = 1.33), and glycerol (gray ○, n = 1.47).

Besides sample solutions measurements, this chamber configuration can also be employed for creating optical elements that modulate the resolution on the assay surface. Chamber position, its path length, and the refraction index of the liquid inside affect the laser beam shape along the platform, modulating thus the resolution. To study the effect of this light focusing system, 250 μm tall polycarbonate chambers were disposed in the down side of TED5 and filled with different refraction index solutions. First, microarray dots on both sides of the disc were measured by

transmission and the results showed a good correlation between simulated data (Figure 6B, I) and experimental tendency (Figure 6B, II). Then, experimental data that describe the relationship between the measured signal and the microarray dot diameter were obtained for different refraction index solutions, in order to quantify the beam focusing effect of the chambers system. Considering the relationship between microarray dot diameter and signal intensity, the calibration curve must rise to a maximum at lower microarray dot diameter when the resolution of the system becomes higher.[26] As shown in Figure 6B, III, experimental results agree with the simulations and demonstrate that this chamber-based light focusing element can be employed to modulate the performance of the analytical system.

The selective irradiation of the disc surface constitutes an additional TED feature that can be exploited for analytical purposes. Instead of the track continuous irradiation with optical disc recording technologies, TED allows one to set the irradiation area shape on the disc and the corresponding laser averaged intensity. This capability can be employed to selectively scan the sensing area, thus making the reading process faster and reducing the data volume. As an experimental example of a TED selective irradiation, Figure S8 (Supporting Information) shows the data acquisition of a motif selectively irradiated on a TED5 assay surface. Also, an application that automatically computes the analytical data from the scanning process and employs selective irradiation to etch the assay result on the photochromic material is an attractive approach for disseminating these systems in nonspecialized environments, since it provides user-friendly analysis readout.

Another TED characteristic is its capability to create analytical disc-based platforms with singular shapes, for instance, different diameter circular discs or even noncircular configurations. This feature could be useful for different purposes, as fitting the platform in specific instrumentation for running analytical stages (pumps, centrifuges, heaters, etc.), facilitating the introduction of devices in the platform, or just providing a good isolation between the different assay areas. As an example of selective irradiation and singular shaping, Figure 7 shows a cross-shaped TED platform containing four isolated different assays (microarray, cell culture, turbidimetry, and immunofiltration). It comprises a TED5 area in the blade edges where assays are performed and a thermochromic material part for labeling and etching the analytical results.

An additional attractive TED feature to be analytically exploited is the laser potency. Compared to other disc systems, the potency of the TED laser during the irradiation becomes up to 54 times higher (Supporting Information, Table S1). This characteristic can be employed for introducing preparative stages, for instance, sample heating, sample desorption, or inducing protein nucleation.[30,31] Also, this feature together with the selective irradiation suggests interesting future investigations concerning laser irradiated ferrowax microvalving[21] or even involving the do-it-yourself microfluidics concept.[32]

Moreover, TED5 is a 1.2 mm thick transparent polycarbonate disc containing the track structure in the down side. Thus, it is interesting to note that the direct access to the track microstructure in this platform also suggests new sensing approaches involving the digital structures in the molecular analysis concept introduced by Burkart and co-workers.[33]

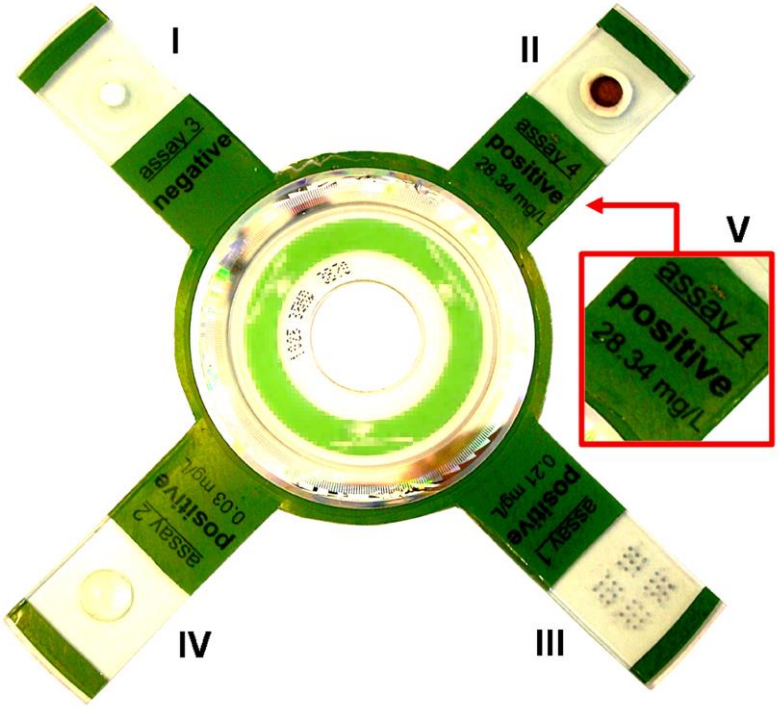

Figure 7. TED cross-shaped analytical platform containing different sensing systems isolated in each blade: turbidimetry chamber (I), immunofiltration membrane (II), microarray (III), and cell culture (IV). This approach also includes exemplary assay readouts etched on the photochromic coating part of the disc (V).

4. Conclusions

The results of this work show that Thermochromic Etching Discs technology has great potential for developing new disc- based total analysis systems beyond the limitations of other optical recording disc technologies, by employing assay platforms obtained from standard discs and drives as analyzers. Several assay platforms with different analytical characteristics can be easily created from commercial TED discs. The application of the proposed data processing method, mainly based on low-pass Fourier filtering, dramatically improves the SNR levels for every disc system (including CD and DVD). Once optimized, the high transparency thermochromic etching

disc CD (TED5) offers the best performance among all TED platforms and attains even higher sensitivity than the DVD. Also, TED5 is a useful platform that maintains the distinctive TED characteristics, while additionally widening the capabilities of this technology by performing transmission and reflection measurements and by carrying out assays on both sides of the disc.

TED technology (disc and driver) offers many characteristic features (track independency, selective irradiation, laser potency, etc.) with great analytical capabilities. Several exemplary applications such as the microarray assay, immunofiltration, cell culture, and turbidimetry demonstrate its practical perspective.

Herein, we demonstrate how to transform TED technology into a powerful and versatile analytical tool and open the way for future compact disc-based developments. The results prove Thermochromic Etching Discs potential to expand lab-on-a- disc prospects toward a new generation of truly integrated disc- based sensor systems.

Acknowledgments

This work has been supported by the Spanish Ministry of Economy and Competitiveness (project CTQ2013-45875-R) and Generalitat Valenciana (PROMETEO II/2014/040). M.A.-O acknowledges the Spanish Ministry of Economy and Competitiveness for a FPI program grant.

References

(1) Arora, A.; Simone, G.; Salieb-Beugelaar, G. B.; Kim, J. T.; Manz, A. *Anal. Chem.* 2010, *82*, 4830−4847.

(2) Gubala, V.; Harris, L. F.; Ricco, A. J.; Tan, M. X.; Williams, D. E. *Anal. Chem.* 2012, *84*, 487−515.

(3) Borisov, S. M.; Wolfbeis, O. S. *Chem. Rev.* 2008, *108*, 423−461.

(4) Delaney, J. L.; Hogan, C. F.; Tian, J.; Shen, W. *Anal Chem.* 2011, *83*, 1300−1306.

(5) Erickson, J. S.; Ligler, F. S. *Nature* 2008, *456*, 178−179.

(6) Kido, H.; Maquieira, A.; Hammock, B. D. *Anal. Chim. Acta* 2000, *411*, 1−11.

(7) Mark, D.; Haeberle, S.; Roth, G.; von Stetten, F.; Zengerle, R. *Chem. Soc. Rev.* 2010, *39*, 1153−1182.

(8) Yu, H.-Z.; Li, Y.; Ou, L. *Acc. Chem. Res.* 2013, *46*, 258−268.

(9) Arnandis-Chover, T.; Morais, S.; Gonzaĺez-Martínez, M. A.; Puchades, R. Maquieira, A. *Biosens. Bioelectron.* 2014, *51*, 109−114.

(10) Avella-Oliver, M.; Gimenez-Romero, D.; Morais, S.; Gonzalez- Martinez, M. A.;

Maquieira, A. *Chem. Commun.* 2013, *49*, 10868−10870.

(11) Potyrailo, R. A.; Morris, G. M.; Leach, A. M.; Sivavec, T. M.; Wisnudel, M. B.; Boyette, S. *Anal. Chem.* 2006, *78*, 5893−5899.

(12) Wang, H.; Ou, L. M. L.; Suo, Y.; Yu, H.-Z. *Anal. Chem.* 2011, *83*, 1557−1563.

(13) Lange, S. A.; Roth, R.; Wittemann, S.; Lacoste, T.; Vetter, A.; Graössle, J.; Kopta, S.; Kolleck, M.; Breitinger, B.; Wick, M.; Hörber, J. K. H.; Dübel, S.; Bernard, A. *Angew. Chem., Int. Ed.* 2006, *45*, 270−273.

(14) Li, Y.; Ou, L. M. L.; Yu, H.-Z. *Anal. Chem.* 2008, *80*, 8216−8223.

(15) Bañuls, M.-J.; García-Piñón, F.; Puchades, R.; Maquieira, A. *Bioconjugate Chem.* 2008, *19*, 665−672.

(16) Gopinath, S. C. S.; Awazu, K.; Tominaga, J.; Kumar, P. K. R. *ACS Nano* 2008, *2*, 1885−1895.

(17) Morais, S.; Tortajada-Genaro, L. A.; Arnandis-Chover, T.; Puchades, R. Maquieira, A. *Anal. Chem.* 2009, *81*, 5346−5654.

(18) Wang, X.; Zhao, M.; Nolte, D.; Ratliff, T. L. *Biosens. Bioelectron.* 2011, *26*, 1871−1875.

(19) Barrios, C. A.; Canalejas-Tejero, V.; Herranz, S.; Moreno-Bondi, M. C.; Avella-Oliver, M.; Puchades, R.; Maquieira, A. *Plasmonics* 2014, *9*, 645−649.

(20) Gopinath, S. C. S.; Fons, P.; Tominaga, J.; Kumar, P. K. R. *Anal. Chem.* 2009, *81*, 4963−4970.

(21) Gorkin, R.; Park, J.; Siegrist, J.; Amasia, M.; Lee, B. S.; Park, J. M.; Kim, J.; Kim, H.; Madou, M.; Cho, Y. K. *Lab Chip* 2010, *10*, 1758−1773.

(22) Ramachandraiah, H.; Amasia, M.; Cole, J.; Sheard, P.; Pickhaver, S.; Walker, C.; Wirta, V.; Lexow, P.; Lione, R.; Russom, A. *Lab Chip* 2013, *13*, 1578−1585.

(23) Anderson, D. E.; Gore, M. P.; McClellan, P. J. Integrated CD/ DVD recording and labeling. US 7172991 B2, Feb 6, 2007.

(24) Huang, W.; Lai, C.; Kuo, C.; Huang, S. Method and apparatus for capturing encoded signals on label surface. US 0260017, Oct 14, 2010.

(25) Brun, E. M.; Puchades, R.; Maquieira, A. *Anal. Chem*. 2013, 85, 4178−4186.

(26) Ekins, R. P.; Chu, F. W. *Clin. Chem.* 1991, *37*, 1995−1967.

(27) Morais, S.; Maquieira, A.; Puchades, R. *Anal. Chem.* 1999, *71*, 1905−1909.

(28) Szewczuk, A.; Kuropatwa, M.; Rapak, A. Arch. *Immunol. Ther. Exp*. 1992, *40*, 325−329.

(29) Han, J. W.; Breckon, T. P.; Randell, D. A.; Landini, G. Mach. *Vision Appl*. 2012, *23*, 15−24.

(30) Najam-ul-Haq, M.; Rainer, M.; Huck, C. W.; Hausberger, P.; Kraushaar, H.; Bonn, G. K. *Anal. Chem*. 2008, *80*, 7467−7472.

(31) Murai, R.; Yoshikawa, H. Y.; Hasenaka, H.; Takahashi, Y.; Maruyama, M.; Sugiyama, S.; Adachi, H.; Takano, K.; Matsumura, H.; Murakami, S.; Inoue, T.; Mori, Y. *Chem. Phys. Lett.* 2011, *510*, 139−142.

(32) Bruzewicz, D. A.; Reches, M.; Whitesides, G. M. *Anal. Chem.* 2008, *80*, 3387−3392.

(33) Najmabadi, P.; La Clair, J. J.; Burkart, M. D. Org. *Biomol. Chem.* 2007, *5*, 214−222.

SUPPORTING INFORMATION

Total analysis systems with thermochromic etching discs technology
Anal. Chem., 86 (**2014**) 12037.

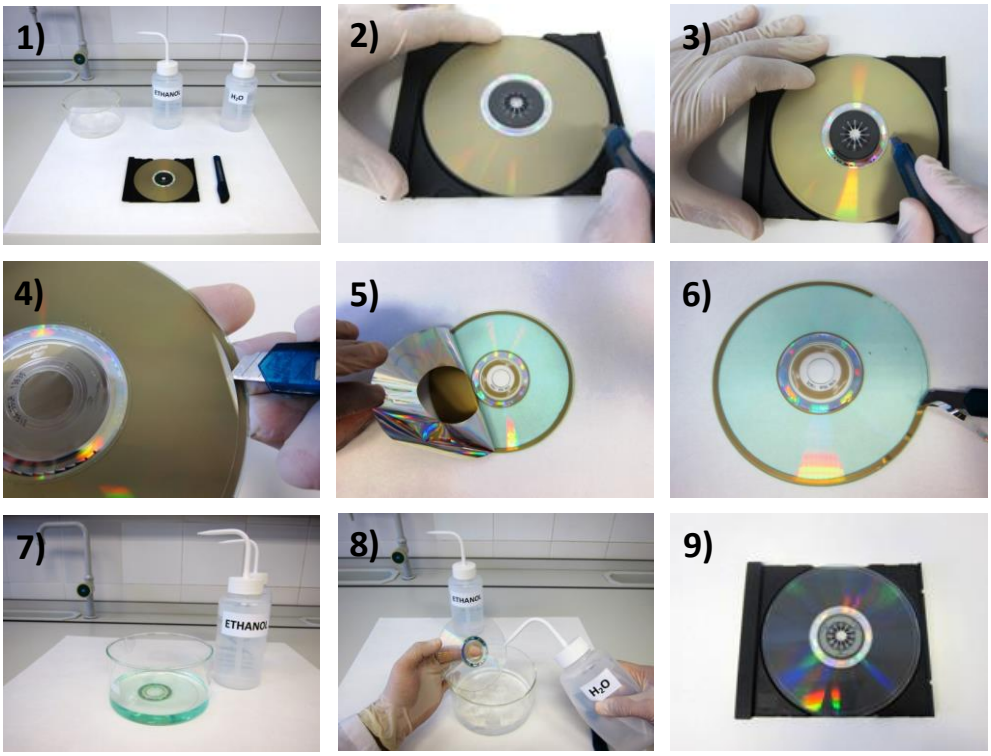

Figure S1. Procedure for creating TED5 platforms from standard CD-TED. 1) Materials. 2) Making 11 cm diameter grove on the label side with a blade. 3) Creating 4.7 cm diameter grove. 4) Taking photochromic and metallic layers from the 11 cm diameter groove. 5) Peeling off photochromic and metallic layers. 6) Peeling off outer part of the layers. 7) Solving the Recording dye in an ethanol bath. 8) Water rinsing. 9) Obtained TED5 platform.

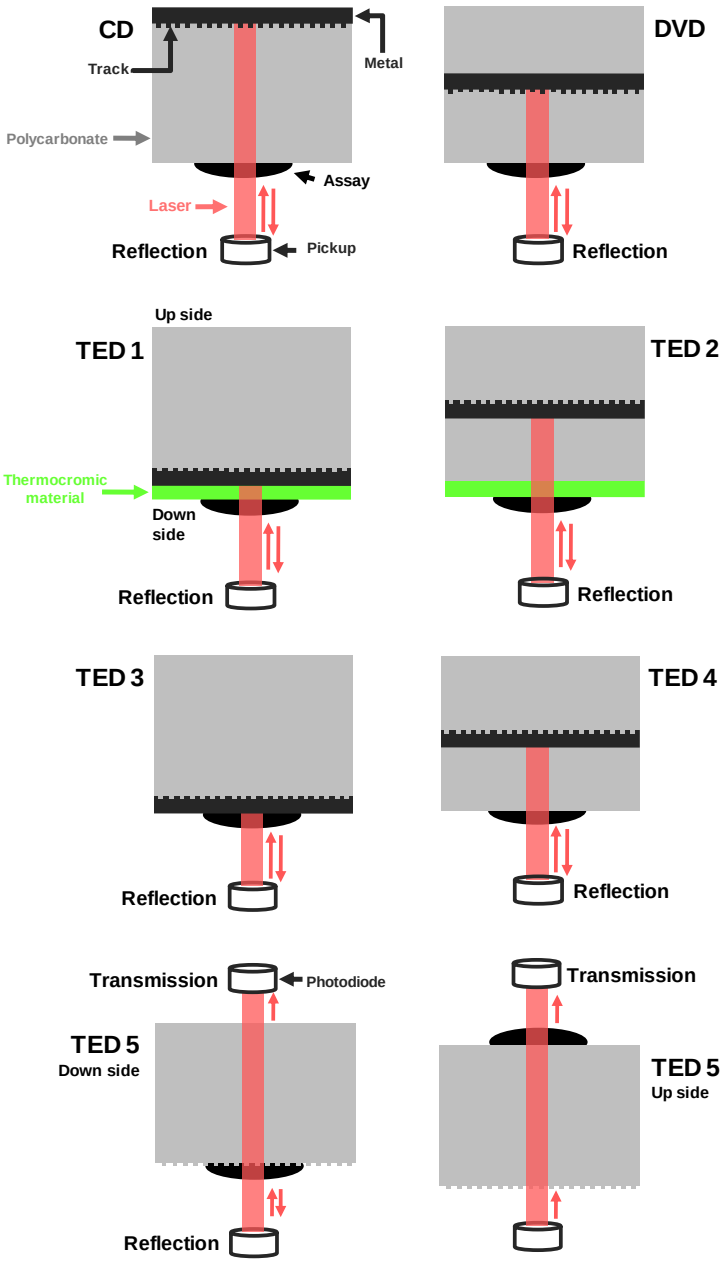

Figure S2. Representation of the scanning mode and assay side of every disc system. Serigraphy layer of CD and DVD, and protective layer of TED1 and TED2, are omitted in the scheme in order to simplify the plot.

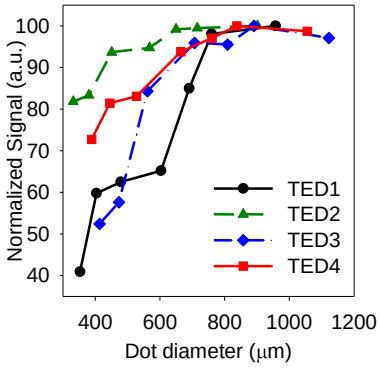

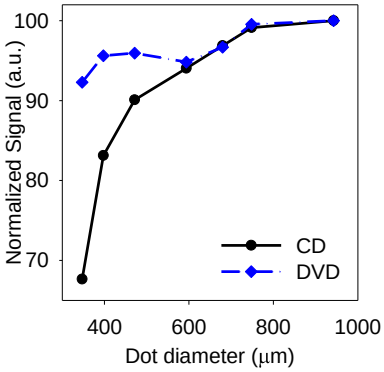

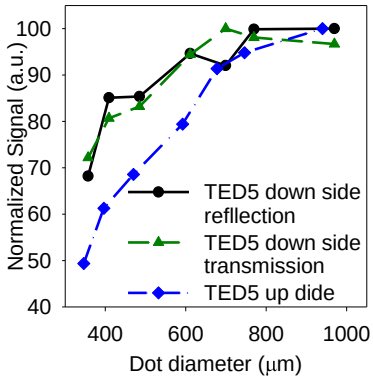

Platform	Optimal dot diameter (μm)	Optimal volume (nL)
CD	595	50
DVD	595	50
TED1	760	100
TED 2	570	50
TED 3	705	50
TED 4	665	50
TED 5 down side, ref.	610	50
TED 5 down side, trans.	610	50
TED 5 up side	595	100

Figure S3. Microarray dot diameter optimization for every disc system. Graphs describe the signal response for a range of microarray dot diameters, while keeping the microarray conditions. Dot diameter was experimentally modulated by setting probe solution drop volumes, and the correspondence between dot diameter and drop volume was calculated as described elsewhere (*Chem. Eng. Sci.* 2012, 69, 522–529). The table contains the selected dot diameter and volume optimal values.

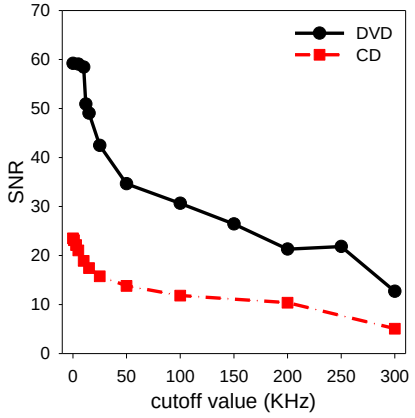

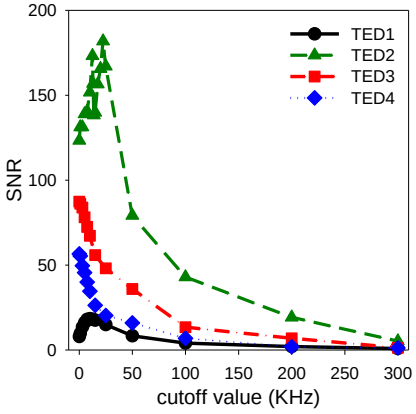

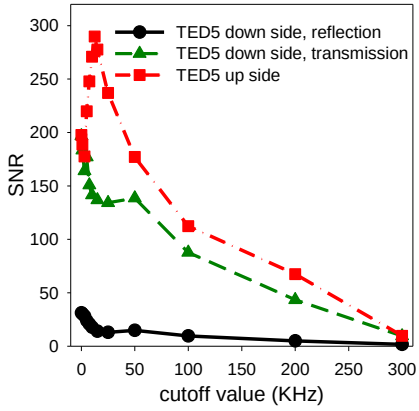

Platform	Selected cutoff value (KHz)
CD	5
DVD	10
TED1	10
TED 2	22.5
TED 3	50
TED 4	50
TED 5 down side, ref.	50
TED 5 down side, trans.	50
TED 5 up side	12.5

Figure S4. Signal processing optimization for every disc system. Graphs show the SNR dependence with the frequency cutoff value used in the signal processing. Optimal values were selected considering both, SNR enhancement and resolution losses at low cutoff values. Table contains the selected optimal frequency cutoff values.

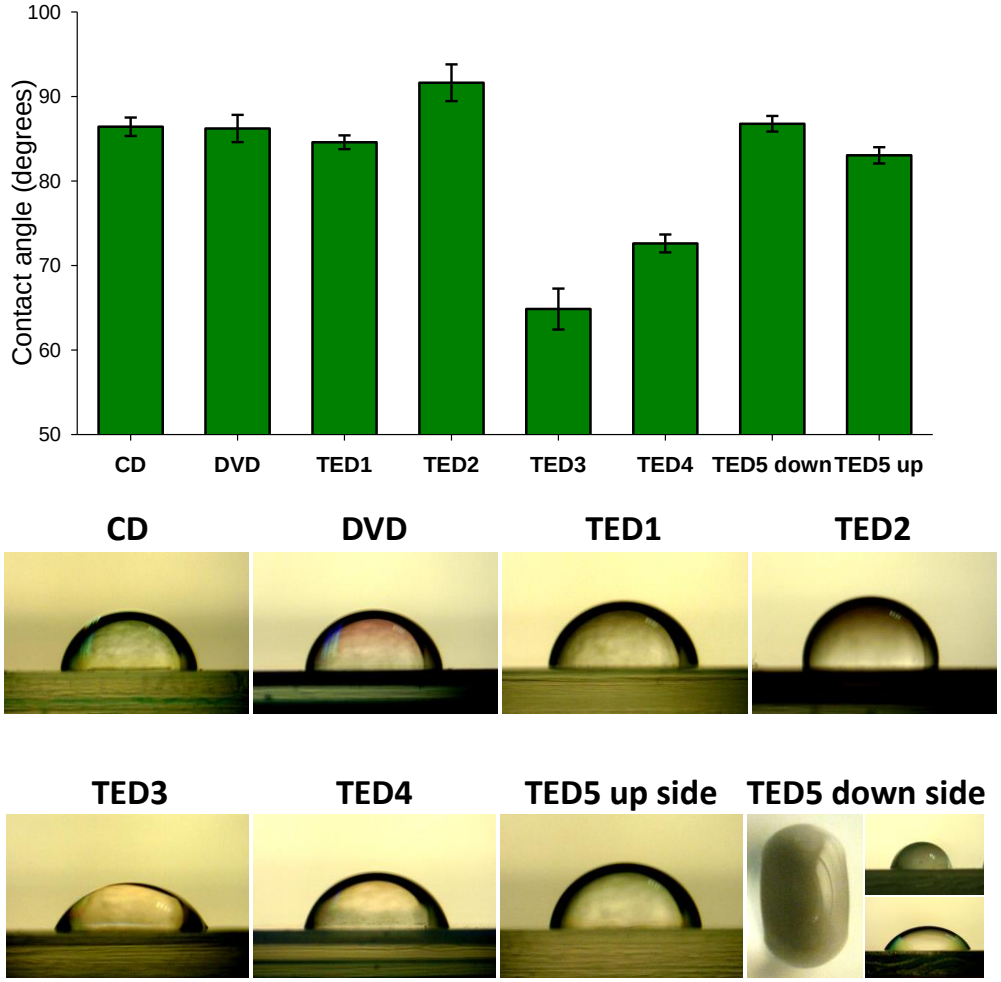

Figure S5. Contact angle results. Assay surface hydrophobicity is a key variable in passive physisorption process. The more hydrophobic the surface, the higher probe immobilization yield is achieved by passive protein adsorption. Measurements show equivalent hydrophobicity for most of the platforms. TED2 surface exhibits higher hydrophobicity and different value than TED1, which suggest differences in the photochromic material configuration. Also, the polymeric protective layer low hydrophobicity and the effect of the coating elimination, results on a low contact angle obtained for TED3 and TED4, respectively. Moreover, a longer drop obtained in the track direction compared to radial direction when dispensing big water drops volumes (≈ 5 µL) in the down side of TED5, macroscopically demonstrates the influence of the track microstructure in this platform.

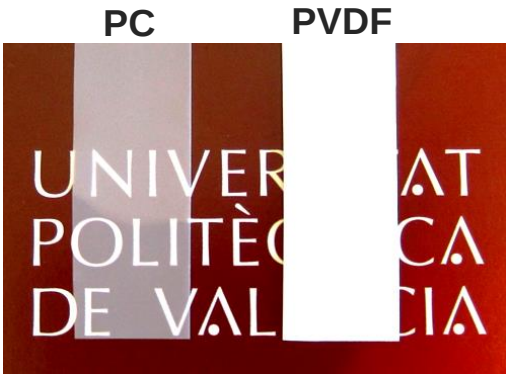

Figure S6. Strips of the polycarbonate (PC) and polyvinilidene fluoride (PVDF) membranes used in the immunofiltration study placed on a colourful background. This figure graphically shows the opacity differences of these membranes

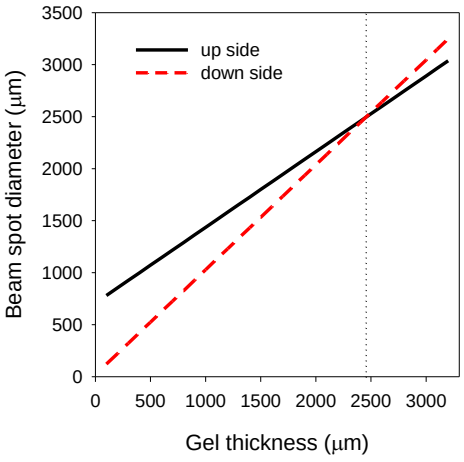

Figure S7. Simulation of the optical resolution dependence with the agar culture gel thickness in both sides of TED5, measuring by transmission. In this study, optical resolution is considered as the diameter of the laser beam when irradiating the assay surface. As seen in the graph, better resolution is obtained when performing the assay in the down side for gel thickness values below 2450 µm.

(A)

(B)

Figure S8. Experimental data acquisition of a motif selectively irradiated on the assay surface of a TED5 platform. For this experiment, transmission scan of a TED5 was performed while selectively irradiating the IDM logo (A), thus obtaining the corresponding scanned data (B) with the TED system.

Table S1. Technical features comparison of the different optical disc recording technologies addressed in this study.

Platform	Laser λ (nm)	Resolution (μm)*			Laser potency (mW)
		spot diam.	radial	track**	
CD	780	728	1.6	0.65	1
DVD	650	504	0.74	1.75	0.7
TED	780	15 / 713 ***	30	0.15	~ 30

* Spot diameter is referred to the diameter of the laser beam when irradiating the assay surface. Radial means the resolution in the direction perpendicular to the track (distance between tracks). Ttrack means the resolution along the track direction (depends on the rotation speed and the sampling frequency).

** Rotation speed = 1x and sampling frequency = 2 MHz.

*** Down side / up side.

3.1.4 Conclusions

TED technology, using LightScribe commercial disks and drives, introduces a new range of possibilities for developing biosensors and conceiving disk-based systems to overcome the inherent limitations of other compact disk technologies. First, it has been proved that these systems entail particular suitability to be used as substrate and as irradiation source for the light-mediated signal developing system presented in this chapter, which introduces many potential advantages to conceive point-of-need systems. On the one hand, standard LightScribe substrates have revealed high immobilization properties to attach bioreceptors by passive adsorption, comparable to polystyrene plates and polycarbonate disks. On the other, labels of different chemical nature (organic dyes as antennas and polymeric microspheres as scattering labels) interact with the laser source and the substrate in order to display the expected photochromic response for these assays. Affordable probe/label bioconjugation ratios have been inferred from experimental data, whereas future studies should address sensitivity issues, for instance by conjugating bioreagents to more efficient labels in terms of energy transfer. In addition to TED, this signal developing system could also be applied to other photo- and thermochromic materials, many of them commercialized at very low cost.

Besides, it has been shown that TED is an excellent platform to develop biosensor systems that face the restrictions of the track-based compact disk technologies. The signal processing strategy presented in this study introduces up to 15-fold sensitivity increases, which provides TED with comparable strengths to reference disk systems (CD and DVD) for analyzing colorimetric microarray immunoassays. Moreover, unlike other disk technologies, TED represents a versatile and high-throughput tool to implement multiple biological assays of different nature in a single platform to be sensitively scanned with the adapted drive. For instance, 1-day colonies growths and 3 mM of sulfates in solution can be detected by cell culture and turbidimetric TED designs, respectively. Among the range of materials and sensing configurations enabled by these disks, TED1 and TED2 should be highlighted given their suitability as platforms for the described light-mediated signal developing strategy. TED5 must be also remarked, since they enable biological assays to be sensed by reflection and transmission in both sides of the disk. Also, TED5 platforms comprise the track microstructure accessible on the external surface of one side, which presents appealing possibilities to be used as optically active materials for label-free biosensing.

Within the main framework of this thesis, the bioanalytical features of the TED systems herein developed will be further investigated in following chapters.

Chapter 2

3.2 In silico optimization and exploration

3.2.1 Introduction

The optimization of biorecognition assays is an essential step in order to achieve their maximal performance. In addition to purely analytical parameters, an efficient optimization system can also influence the final cost of the assay, for instance by minimizing the concentrations of the required bioreagents. Besides optimizations, a great part of the studies focused in biosensing (mainly in research environments) are dedicated to explore and understand biorecognition systems of interest.

Optimizing biorecognition assays and characterizing their behavior is hindered by the inherent complexity of biointeractions, and experimental methods typically employed in these regards (such as checkerboard titration) tend to be tedious and provide limited information about the system under study. In order to provide solutions in this direction, this chapter introduces a theoretical-experimental methodology (INSEL) for exploring and optimizing biorecognition assays. Unlike other strategies, this is a multi-parametrical approach grounded on kinetic laws and mass transport phenomena to enable multiobjective assessments of biorecognition assays INSEL is implemented as an *in silico* tool, which aims to involve minimal experimentation and provide maximal profit in terms of optimization performances and predicting/exploring capabilities.

Within the scope of this thesis, this approach is helpful to understand the behavior of the biorecognition systems under study. This work was conducted by immunoassay microarrays using DVDs as platforms and drives as scanners, what makes this article one of the first reports that prove the capabilities of disk-based analytical biosensors as routine technique to study biointeractions.

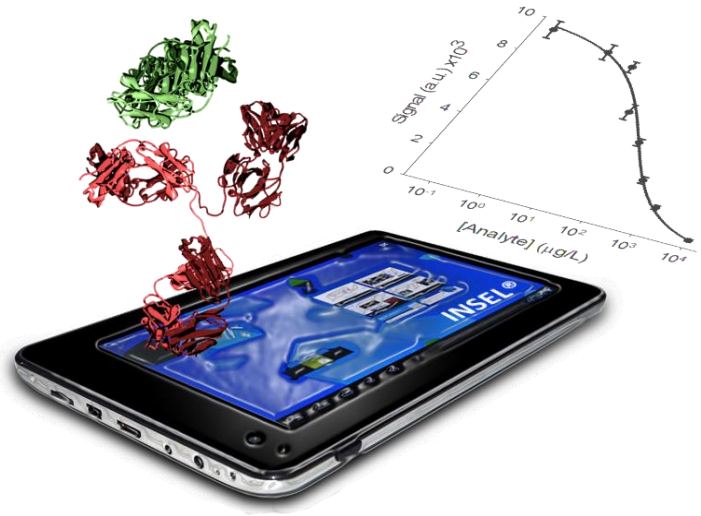

3.2.2 INSEL: an in silico method for optimizing and exploring biorecognition assays

Chem. Commun., 49 (**2013**) 10868.

ABSTRACT

A practical *in silico* method for optimizing and exploring biointeraction-based events is developed.

Introduction

Protein and nucleic acid screening techniques are of high interest in basic and applied science.[1] However, the complexity of the molecular biointeraction processes involved in these assays makes their optimization difficult. Classical assessment methodologies are based on either trial-and-error or mono- and bi-parametric studies.[2] Despite these approaches offering good performance for many applications, they are quite limited as they imply a huge volume of experimental work, and the interaction effects between variables are frequently omitted.[3a] In many approaches, statistical design of experiments is applied to optimize biorecognition systems, and improvements are accomplished mainly in terms of variable interactions.[3b] However, these procedures are also labour intensive.[3]

Nowadays a new concept, based on theoretical models, for developing *in silico* environments to deal with biomolecular systems is emerging in science.[4] The main strength of theoretical modelling relies on its potential for providing a comprehensive point of view, for reducing empirical requirements and for considering the overall interactions involved in the process. Herein, we aim to establish the basis for exploiting the benefits of theoretical models in order to develop an effective predictive method for biorecognition assays. To this end, this study presents a new method, named INSEL, aiming to be a powerful tool for performing multiobjective optimizations, predicting assay behaviour and the effect of the involved variables. This method requires minimal experimentation and carries out multi-parametrical assessment, thus solving the limitations of the aforementioned methodologies. Similar theoretical–experimental strategies are commonly applied to other fields such as engineering, economics, manufacturing, mathematics or physics.[5] However, despite the fruitful investigations involving biointeraction approaches,[6] no methodologies for employing theoretical modelling in the optimization of biorecognition assays are described in the scientific literature, as Yager and co-workers had suggested some time ago.[6a]

As a proof of concept of generic biorecognition assays we studied two different systems, a non-competitive sandwich and a competitive coating conjugate-based immunoassay for the determination of immunoglobulins and low molecular weight compounds, respectively (ESI,† Materials and methods).[7] The comprehensiveness of these model

systems, especially the second one, constitutes a powerful proof of concept for other biointeraction systems.

To apply our computational method, we start selecting a theoretical model to characterize each particular biorecognition process. Although sophisticated models are found in the literature,[6] a theoretical–experimental approach, based on the reaction scheme illustrated in Fig. 1, was designed. The corresponding differential equations system (ESI,† Materials and methods) allows us to compute the assay response by means of the amount of the measurable product (the superficial concentration of the probe–receptor complex, Θ^{RB}, in this case) for the given assay conditions.

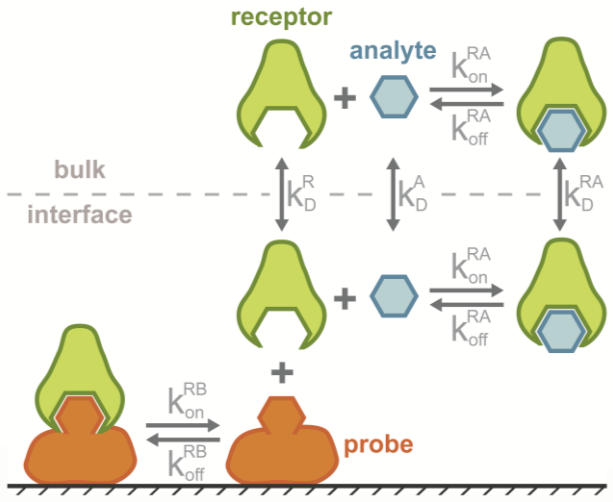

Fig. 1. Reaction scheme. The reaction is based on mass transport phenomena and kinetic laws. k_D, k_{on} and k_{off} are the phenomenological mass transport constant, formation constant and dissociation constant, respectively.

Using this model, three basic experiments to characterize the system are required when there is no prior knowledge. First, an immobilization isotherm must be obtained to find out the probe coating coverage (ESI,† Fig. S1). Then as the model is generic for any transducer, a response curve that links Θ^{RB} with the analytical signal is needed (ESI,† Fig. S2 and S3). Finally, the kinetic and diffusion constants to relate the system response and assay conditions must be obtained by kinetic studies.

The results show a good correlation in the simulations and constant values within the typical range for antibody-based biorecognition assays in both systems (Fig. 2A),[8] thus demonstrating the model capabilities to describe the biorecognition events under experimental working conditions.

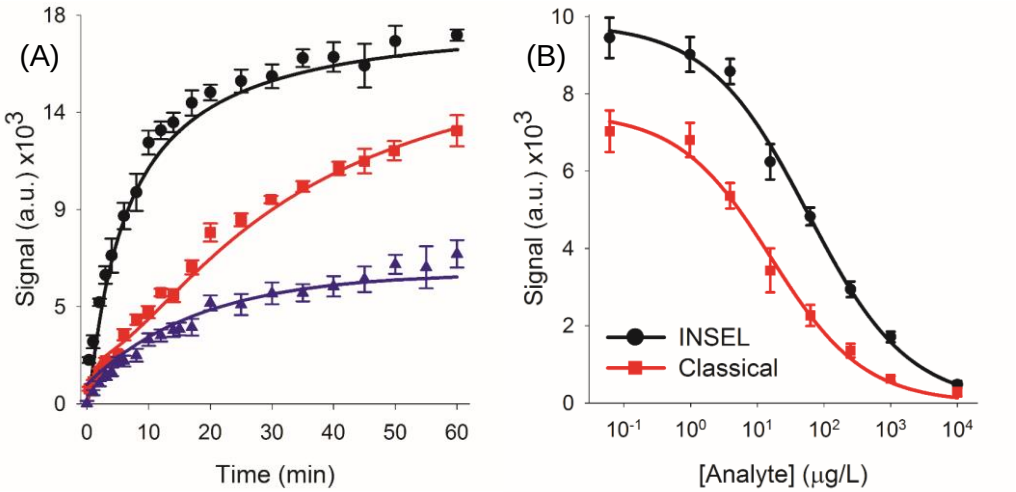

Fig. 2. Comparison of experimental and predicted results. (A) Kinetic curve simulations, where dots are the experimental data and solid lines are the predicted curves. The kinetic curve for the non-competitive model system (▲) at a receptor concentration of 0.119 mg L^{-1} (R^2 = 0.944). The corresponding constant values are k_{on}^{RB}= 2.98 x 10^7 s^{-1} M^{-1}, k_{off}^{RB} = 0.032 s^{-1} and $k_D^R >> k_{on}^{RB}$. Kinetic curves for the studied competitive assay at an analyte concentration of 62.5 mg L^{-1} (■) and without the analyte (●) (R^2 = 0.987 and R^2 = 0.974, respectively). For this system, the corresponding constant values are k_{on}^{RA} = 4.13 x 10^6 s^{-1} M^{-1}, k_{off}^{RA} = 0.06 s^{-1}, k_{on}^{RB} = 1.56 x 10^9 s^{-1} M^{-1}, k_{off}^{RB} = 0 s^{-1}, k_D^R = 0.011 s^{-1}, k_D^A = 0.01 s^{-1} and k_D^{RA} = 0.003 s^{-1} (B) comparison of experimental results of classical and INSEL optimization approaches.

Biorecognition assays are characterized by dose–response curves. To predict such curves, INSEL computes Θ^{RB} for different analyte concentrations under the established conditions (incubation time, probe and specific receptor concentrations). Then, the analytical signal is calculated as described above and the dose–response curve is obtained. Good agreement is achieved by comparing the experimental ELISA dose–response curves with those predicted by INSEL in both model systems (ESI,† Fig. S4 and S5). These results corroborate the potential of the computational methodology and reaffirm the predictive performance of the model.

Optimization is a critical issue involving laboratory practice in chemical and life science binding-based assays. In order to seek a new alternative, INSEL has been extended to the optimization process. For this purpose, we developed a strategy based on the aggregate objective function (AOF),[5a] a mathematical expression that defines optimality. This means

an opened optimum concept since users can design the AOF according to any desired assay prospects, such as sensitivity, precision, total assay time, *etc.* To this end, the AOF is systematically calculated to find out its minimum by providing the corresponding optimal condition values (ESI,† Fig. S6).

To apply INSEL for the optimization, we designed a useful multiobjective AOF to obtain the experimental conditions for best sensitivity and precision. This AOF comprises terms that consider assay sensitivity (half maximal inhibitory concentration, IC_{50}) and precision through the confidence interval for IC_{50},[9] as described by eqn (1):

$$AOF = \lambda \cdot IC_{50} + (1 - \lambda) \cdot \frac{SD_{bck}}{\frac{DS}{DA}}$$

where λ is the weight coefficient, *S* is the signal response, SD_{bck} is the background standard deviation (noise) and *A* is the analyte concentration. This AOF can be easily set by the user by selecting the λ value, thus modulating the relative contribution of sensitivity and precision according to the desired assay objective.

For the optimization of the studied coating conjugate-based model system, we used the above-described AOF and a λ value calculated by the Min–Max principle (λ= 0.1888). Moreover, an incubation time for response variation smaller than 15% in 2 minutes was introduced in order to set an upper limit that ensures high inter-assay precision. Having defined these inputs, the subsequent optimal values of the experimental variables (receptor concentration, probe concentration and incubation time) and the corresponding analytical parameters (IC_{50}, confidence interval, dynamic range and signal levels) are quickly computed and provided by INSEL.

To demonstrate the optimization capability of the method, we compared the experimental curve obtained from the INSEL optimal conditions (probe concentration = 12.36 mg L^{-1}; receptor concentration = 0.34 mg L^{-1}; incubation time = 13 min) with that obtained from the classical optimization procedure (probe concentration = 5.00 mg L^{-1}; receptor concentration = 0.25 mg L^{-1}; incubation time = 20 min) (ESI,† Fig. S7).[9] The predicted and experimental curves match well and similar analytical parameters are obtained with both optimization approaches (Fig. 2B). The classical optimization results are slightly more sensitive ($IC_{50}^{classical}$ = 16.2 mg L^{-1}, IC_{50}^{INSEL}= 57.3 mg L^{-1}). However, the INSEL approach has a comparable limit of detection ($LOD^{classical}$ = 2.2 mg L^{-1}, LOD^{INSEL} = 5.6 mg L^{-1}), but significantly improves the precision ($P^{classical}$ = 7%, P^{INSEL} = 2%) and dynamic range ($DR^{classical}$ = 2.2–140.6 mg L^{-1}, DR^{INSEL} = 5.6–629.4 mg L^{-1}) of the assay. These results agree with

the enhancement of the maximal signal-to-noise ratio ($SNR_{max}^{classical}$ = 49, SNR_{max}^{INSEL} = 65) according to the employed AOF.

The scope of the method herein described goes beyond assay optimization. The predictive performance of this tool offers great potential to explore biorecognition assays, apart from experimental patterns, by predicting unknown results from testing input conditions. This approach allows researchers to interpret binding assay properties and to generate hypotheses to enhance knowledge about the system under study.

Thus, INSEL is first applied to discover empirical relationships for describing the assay behaviour by exploring the influence of receptor and probe concentrations on assay sensitivity. For this purpose, the IC_{50} values are predicted for a wide range of receptor and probe concentrations. The results demonstrate the greatest influence of receptor concentration on assay sensitivity as compared to the superficial concentration of the probe (Fig. 3A).

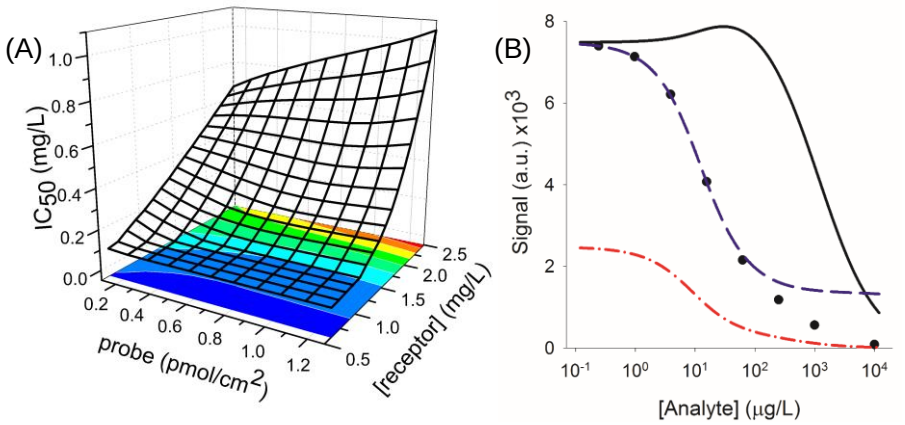

Fig. 3 *In silico* exploration results. (A) Predicted IC_{50} for a range of different receptor and probe concentrations. (B) Computational investigation of diffusion effects: simulated dose-response curves for high diffusion values of receptor-analyte complex (——), low diffusion values of analyte (– –), experimental diffusion values (●) and low receptor diffusion values (–·–·–). The plot describes the aforementioned dose-response curve deformations. The hook effect on the low analyte concentrations of the high diffusion of receptor-analyte complex curve is observed. The graph also shows a minimal asymptotic signal that differs from zero at high analyte concentrations in the low diffusion of receptor curve.

Another interesting point of INSEL exploration deals with the prediction of the effect of critical parameters on binding studies, such as the influence of diffusion of reactants. Diffusion is a key factor to be explored because optimization processes are often carried out in

the steady state or this variable is usually omitted. For this study, dose–response curves for a range of phenomenological mass transport constant values are predicted. The results show that diffusion greatly influences the assay response and is involved in typical dose–response curve deformations (Fig. 3B).[10] The data indicate that the signal reduces when receptor diffusion decreases as it hinders receptor–probe complex formation. Moreover, a different minimum asymptotic signal to zero is predicted by the free receptor excess in the interface, caused by low analyte diffusion. This study also suggests that the receptor accumulation in the interface, due to the high diffusion of the receptor–analyte complex, increases IC_{50} and generates the prozone phenomenon or hook effect.[1]

In conclusion, the evidence presented in this study demonstrates the capability of INSEL to exploit theoretical modelling for performing directed optimizations and *in silico* exploration of biorecognition assays by taking into account the synergic effects between variables and involving minimal experimentation. Furthermore, insights into the predictive performance of the developed theoretical–experimental model are provided.

The results presented in this communication constitute a starting point for expanding INSEL in a wide range of protein and DNA screening scenarios. For instance, the prospective of this *in silico* approach suggests interesting future investigations in genomic analysis, drug screening assays, preclinical studies and *in vivo* conditions as well.[11] INSEL is a development providing scientists with a practical interactive tool which maximizes the scope of experimentation in chemistry and life sciences.

This work has been supported by the Spanish Ministry of Economy and Competitiveness FEDER-CTQ2010-15943, Programa FPI and Programa Ramón y Cajal, Generalitat Valenciana (PROMETEO 2010/008) and Universitat Politècncia de València (PAID-06-12).

Notes and references

1 E. Mahon, Z. Mouline, M. Silion, A. Gilles, M. Pintealab and M. Barboiu, *Chem. Commun.*, 2013, 49, 3004; J. Tamayo, P. M. Kosaka, J. J. Ruz, A. San Paulo and M. Calleja, *Chem. Soc. Rev.*, 2013, 42, 1287; X. Chen, Y.-H. Lin, J. Li, L.-S. Lin, G.-N. Chen and H.-H. Yang, *Chem. Commun.*, 2011, 47, 12116; C. Katz, L. Levy- Beladev, S. Rotem-Bamberger, T. Rito, S. G. D. Rudiger and A. Friedler, *Chem. Soc. Rev.*, 2011, 40, 2131; K.-S. Song, S. B. Nimse, J. Kim, J. Kim, V.-T. Ta, V.-T. Nguyen and T. Kim, *Chem. Commun.*, 2011, 47, 7716.

2 N. Karoonuthaisiri, R. Charlermroj, U. Uawisetwathana, P. Luxananil, K. Kirtikara and O. Gajanandana, *Biosens. Bioelectron.*, 2009, 24, 1641.

3 (*a*) W. Luo, M. Pla-Roca and D. Juncker, *Anal. Chem.*, 2011, 83, 5767; (*b*) A. E. Rubin, S.

Tummala, D. A. Both, C. Wang and E. J. Delaney, *Chem. Rev.*, 2006, 106, 2794.

4 (*a*) Q. C. Zhang, D. Petrey, L. Deng, L. Qiang, Y. Shi, C. A. Thu, B. Bisikirska, C. Lefebvre, D. Accili, T. Hunter, T. Maniatis, A. Califano and B. Honig, *Nature*, 2012, 490, 556; (*b*) B. T. White, *Science*, 2012, 337, 424; (*c*) M. Bergland, K. Klyczek, C. Lin, M. Lundeberg, R. Tosado-Acevedo, A. Toro, D. White and B. Wolter, *Science*, 2012, 337, 426; (*d*) Y. Park and E. M. Marcotte, *Nat. Methods*, 2012, 9, 1134.

5 (*a*) S. S. Rao, *Engineering Optimization: Theory and Practice*, John Wiley & Sons, Hoboken, NJ, USA, 2009; (*b*) O. Shoval, H. Sheftel, G. Shinar, Y. Hart, O. Ramote, A. Mayo, E. Dekel, K. Kavanagh and U. Alon, *Science*, 2012, 336, 1157.

6 (*a*) J. O. Foley, K. E. Nelson, A. Mashadi-Hossein, B. A. Finlayson and P. Yager, *Anal. Chem.*, 2007, 79, 3549; (*b*) M. Khorshid, J. Hausser, M. Zavolan and E. Nimwegen, *Nat. Methods*, 2013, 10, 253; (*c*) D. Yin and X. S. Zhao, *Acc. Chem. Res.*, 2011, 44, 1172.

7 S. Morais, L. A. Tortajada-Genaro, T. Arnandis-Chover, R. Puchades and A. Maquieira, *Anal. Chem.*, 2009, 81, 5646; S. Morais, R. Marco- Moles, R. Puchades and A. Maquieira, *Chem. Commun.*, 2006, 2368.

8 D. Gimenez-Romero, M. A. Gonzalez-Martinez, M. Bañuls, I. S. Monzo, R. Puchades and A. Maquieira, *J. Phys. Chem. B*, 2012, 116, 5679.

9 P. Tijssen, *Laboratory Techniques in Biochemistry and Molecular Biology*, Elsevier Science Publishers B.D., Amsterdam, The Netherlands, 1993.

10 A. Hatch, A. E. Kamholz, K. R. Hawkins, M. S. Munson, E. A. Schilling, B. H. Weigl and P. Yager, *Nat. Biotechnol.*, 2001, 19, 461.

11 N. K. Tafreshi, A. Silva, V. C. Estrella, T. W. McCardle, T. Chen, Y. Jeune-Smith, M. C. Lloyd, S. A. Enkemann, K. S. M. Smalley, V. K. Sondak, J. Vagner and D. L. Morse, *Mol. Pharmaceutics*, 2013, 10, 3175.

ELECTRONIC SUPPLEMENTARY INFORMATION (ESI)

INSEL: an in silico method for optimizing and exploring biorecognition assays

Chem. Commun., 49 (**2013**) 10868.

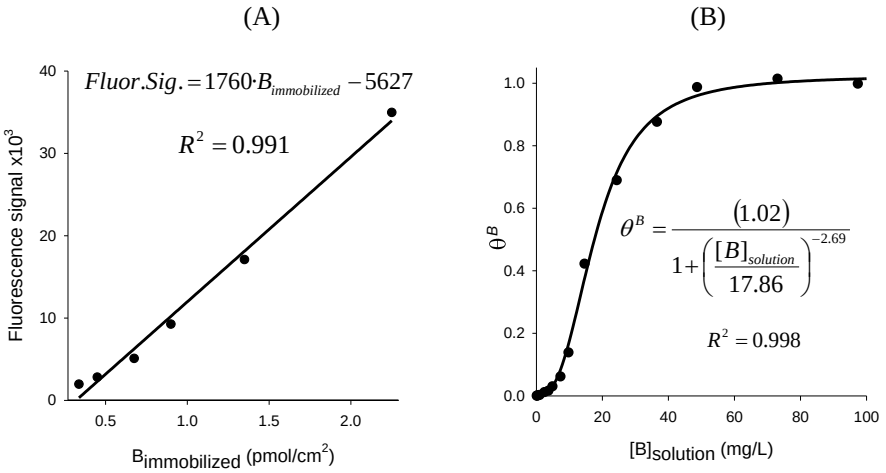

Fig. S1 Immobilization isotherm. (A) Calibration curve. (B) Immobilization isotherm. The regression equation allows to relate the probe solution concentration with the corresponding immobilized superficial concentration by means of its θ^B (ESI†, Materials and methods, Modelling). The experimental results fit the type V isotherm. From these data, an equation that relates θ^{RB} with the signal is established by adjusting the subsequent response curve (ESI†, Fig. S2-S3). Since probe molecules (BSA conjugate) are prolate ellipsoids, where the polar axis (140 Å) is larger than the equatorial axes (40 Å),[S1] the experimental superficial density obtained ($16 \cdot 10^{-15}$ mol/cm^2) and the values for the two limit orientations (equatorial $12 \cdot 10^{-15}$ mol/cm^2 and polar $43 \cdot 10^{-15}$ mol/cm^2) suggest that BSA is mainly physisorbed as an equatorially oriented monolayer.

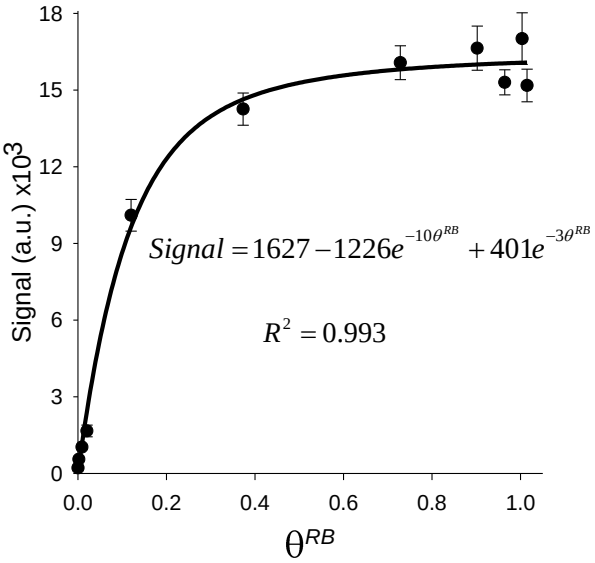

Fig. S2 Response curve for the competitive coating conjugate-based immunoassay model system. Experimental data fit to an exponential curve (rise to a maximum four parameters).

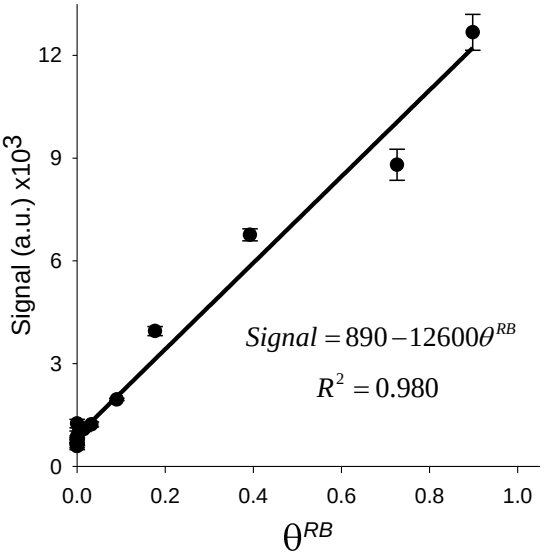

Fig. S3 Response curve for the non-competitive sandwich immunoassay model system. Experimental data fit to a linear equation.

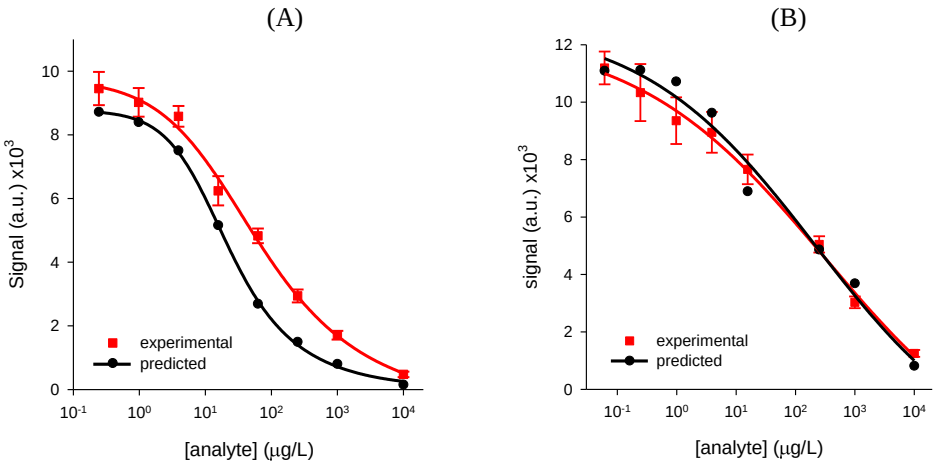

Fig. S4 Predicted and experimental dose-response curves for the competitive coating conjugate-based immunoassay model system. (A) The probe and receptor solution concentration are 11.90 mg/L and 0.34 mg/L, respectively, with an incubation time of 13 min (R^2 = 0.872). (B) The probe and receptor solution concentrations are 40.00 mg/L and 0.36 mg/L, respectively, with an incubation time of 26 min (R^2 = 0.952). It must be highlighted that predictive performance is enhanced by considering that the model is designed for only one epitope and that the biorecognition process is described by a first-order equation, whereas a polyclonal antibody is used as a receptor.

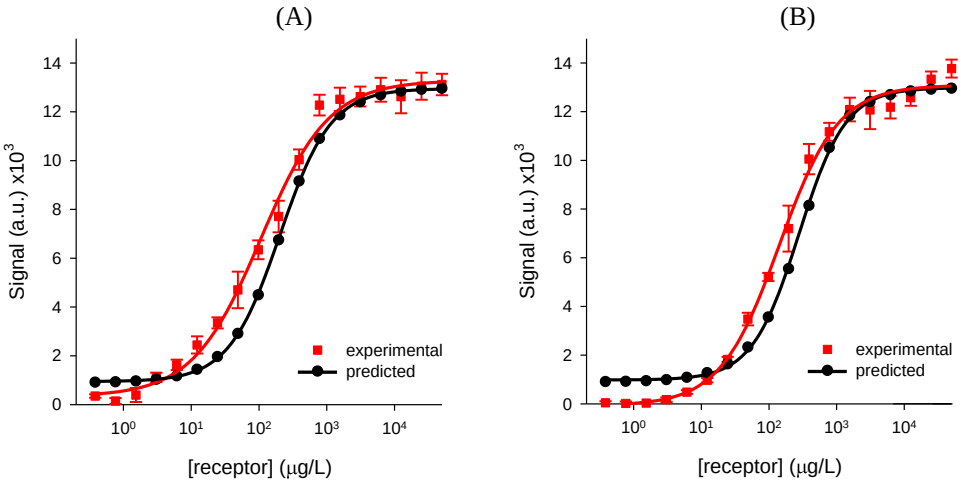

Fig. S5 Predicted and experimental dose-response curves for the non-competitive sandwich immunoassay model system. (A) Probe solution concentration 50 mg/L and incubation time 30 min (R^2 = 0.968). (B) Probe solution concentration 50. mg/L and 17 min incubation time (R^2 = 0.969).

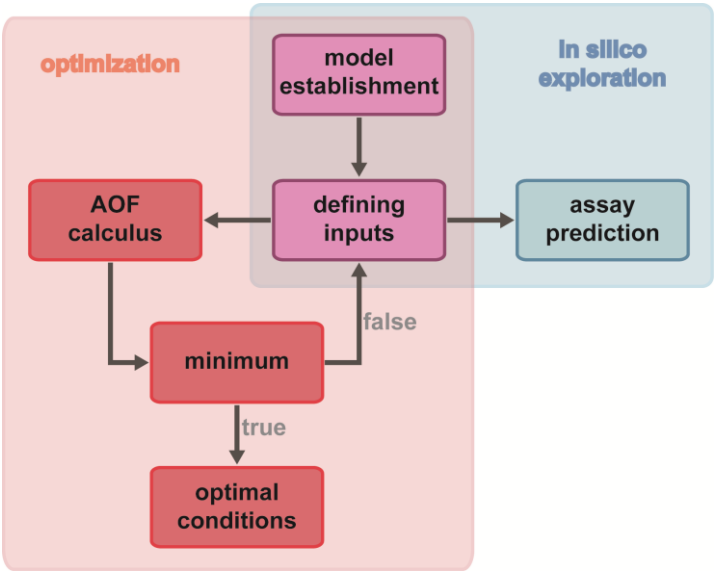

Fig. S6 Flux diagram of the proposed *in silico* approach.

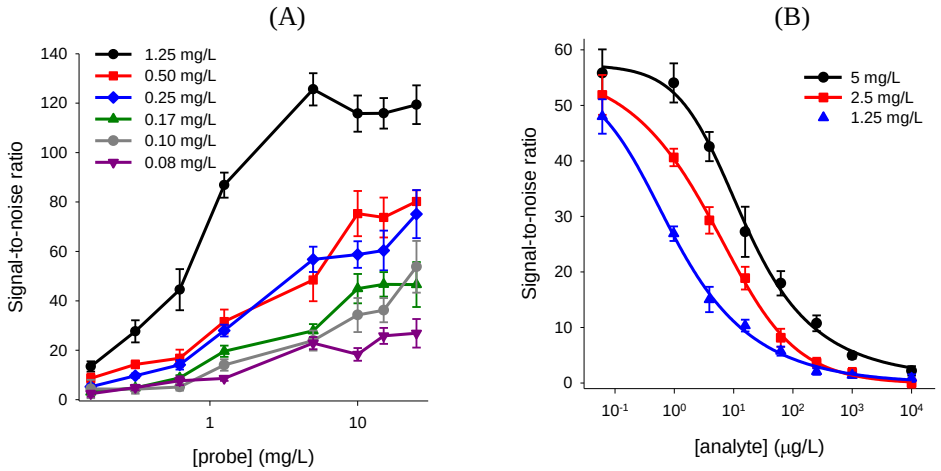

Fig. S7 Titration and dose-response curves from classical optimization. (A) Titration curves for different receptor concentrations. In this case, the receptor concentration of 0.25 mg/L and the probe concentration at around 2.5 mg/L were selected to be tested in the next step. (B) Dose-response curves at a fixed receptor concentration (0.25 mg/L) and three different probe concentrations (5, 2.5 and 1.25 mg/L). In this case, the receptor and probe concentrations of 0.25 and 5.0 mg/L, respectively, were selected as optimum. The incubation time in these experiments was 20 minutes.

Materials and methods

Modelling. Biointeraction assay modelling. The proposed biointeraction reaction scheme (Fig. 1 in manuscript) implies the ordinary differential equations system presented in Eq. (S1-S7). This system is numerically solved by the LSODA methodology and by considering the boundary conditions described in Eq. (S8) – (S11):

$$\frac{d[R_b(t)]}{dt} = -\,k_D^R\,([R_b(t)] - [R_i(t)]) - \,k_{on}^{RA}\cdot[A_b(t)]\cdot[R_b(t)] + \,k_{off}^{RA}\cdot\,[RA_b(t)] \quad \text{Eq. (S1)}$$

$$\frac{d[A_b(t)]}{dt} = -\,k_D^A\,([A_b(t)] - [A_i(t)]) - \,k_{on}^{RA}\cdot[A_b(t)]\cdot[R_b(t)] + \,k_{off}^{RA}\cdot[RA_b(t)] \quad \text{Eq. (S2)}$$

$$\frac{d[RA_b(t)]}{dt} = -\,k_D^{RA}\,([RA_b(t)] - [RA_i(t)]) + \,k_{on}^{RA}\cdot[A_b(t)]\cdot[R_b(t)] - k_{off}^{RA} \cdot[RA_b(t)] \quad \text{Eq. (S3)}$$

$$\frac{d[R_i(t)]}{dt} = \,k_D^R\,([R_b(t)] - [R_i(t)]) + \,k_{off}^{RB}\cdot\theta^{RB}(t) - \,k_{on}^{RB}\cdot[R_i(t)]\cdot\theta^B(t) - \\ - k_{on}^{RA}\cdot[R_i(t)]\cdot[A_i(t)] + \,k_{off}^{RA}\cdot[RA_i(t)] \quad \text{Eq. (S4)}$$

$$\frac{d[A_i(t)]}{dt} = k_D^A\,([A_b(t)] - [A_i(t)]) - \,k_{on}^{RA}\cdot[A_i(t)]\cdot[R_i(t)] + \,k_{off}^{RA}\cdot[RA_i(t)] \quad \text{Eq. (S5)}$$

$$\frac{d[RA_i(t)]}{dt} = \,k_D^{RA}\,([RA_b(t)] - [RA_i(t)]) + \,k_{on}^{RA}\cdot[A_i(t)]\cdot[R_i(t)] - k_{off}^{RA}\cdot[RA_i(t)] \quad \text{Eq. (S6)}$$

$$\frac{d\theta^{RB}(t)}{dt} = k_{on}^{RB}\cdot[R_i(t)]\cdot\theta^B(t) - \,k_{off}^{RB}\,\theta^{RB}(t) \quad \text{Eq. (S7)}$$

$$\theta^{RB}(0) = \,[R_i(0)] = [A_i(0)] = [RA_i(0)] = [RA_b(0)] = 0 \quad \text{Eq. (S8)}$$

$$\theta^B(0) = \theta_0^B \quad \text{Eq. (S9)}$$

$$[R_b(0)] = [R]_0 \quad \text{Eq. (S10)}$$

$$[A_b(0)] = [A]_0 \quad \text{Eq. (S11)}$$

where *R* is receptor, *A* is analyte, *B* is probe, subscripts *b* and *i* refer to the bulk and interface respectively, k_D^i is the phenomenological mass transport constant of compound *i*, k_{on}^i and k_{off}^i are the formation and dissociation constants of *i*, θ^i is the coverage degree of *i* on the transducer surface and subscript *0* refers to the initial point. In this analytical system, kinetics is based on first-order equations and the diffusion of the species between the bulk and the interface is

described by a phenomenological mass transport constant that accounts for diffusion, migration and convection.[S2]

Assay. Two different assays are employed as a model system for proving the concept in this study, a non-competitive sandwich immunoassay for immunoglobulins analysis and a competitive coating conjugate-based immunoassay for low molecular weight compounds determination. Given their comprehensiveness, these systems serve as a powerful proof-of-concept for the potential of the methodology here presented for generic biorecognition assays, specially the second one.

In this study, we used a microarray detection system based on the compact disc technology, as described elsewhere.[S3,S4]

The non-competitive model system studied is a sandwich immunoassay for rabbit antibodies determination. As this system does not involve competition, only the half reaction scheme (Fig. 1 in manuscript) concerning the processes between probe and receptor is required for the modelling. As noted in the scheme, in this system the probe is goat anti-rabbit polyclonal antibody and the receptor is polyclonal rabbit immunoglobulin. Although rabbit antibodies actually act as analyte in this assay, we denominate this element as receptor for keeping the generic notation of the presented reaction scheme.

The competitive model system studied is a coating conjugate-based immunoassay for atrazine (Atz) analysis. According to the reaction scheme (Fig. 1 in manuscript), in this system the analyte is Atz, the receptor is a polyclonal anti-atrazine antibody (pRAb-Atz) and the probe is a coating protein-hapten conjugate (BSA-2d)[S4]. The principle of the assay is based on competition between the free analyte and probe for the binding sites of the receptor.

For these assays, the probe solution in carbonate buffer (0.1 M sodium carbonate, pH 9.6) is arrayed on the transducer surface by a non contact microprinter (25 nL/spot) and is left for 16 h at 4ºC for immobilization. Afterward, sensing surfaces are rinsed with PBS-T (8 mM sodium phosphate dibasic, 2 mM sodium phosphate monobasic, 137 mM sodium chloride, 3 mM potassium chloride, 0.05% Tween 20, pH 7.5) and deionized water, and are dried by centrifugation. Then, receptor solutions in PBS-TT (PBS-T, 0.1 M taurine, pH 7.5) for the non-competitive system, or receptor and analyte mixture solutions in PBS-TT for the competitive system, are dispensed on the arrays. After the incubation time, sensing surfaces are rinsed again with PBS-T and deionized water, and are dried by centrifugation. Then, solutions of 5 nm colloidal gold-labelled goat anti-rabbit immunoglobulin in PBS-TT (1/30 dilution in the sandwich immunoassay and 1/100 dilution in the coating conjugate-based immunoassay) are dispensed on the arrays and allowed to react (20 min for the non-competitive system and 15 min

for the competitive assay). Next, sensing surfaces are rinsed as before and dried by centrifugation, and silver enhancer solution is dispensed and distributed (1 mL per disk). After 8 min, the platform is rinsed with deionized water and dried again. Finally, the assay signal is measured.

Kinetic curves. To obtain the kinetic curves, an assay is performed within a range of incubations times. To characterize the interaction of the receptor with the probe and the analyte in competitive systems, this experiment includes the kinetic curve without analyte and the one with analyte (preferably an analyte concentration that is around the IC_{50} value) for a fixed probe and receptor concentrations. In contrast, non-competitive systems as sandwich immunoassays require only one kinetic curve for characterization.

Immobilization isotherm. To perform the immobilization isotherm experiment, a sensing strategy that allows to directly measuring the dispensed probe solutions is required to establish the corresponding calibration curve. In this case, we carry out these experiments by fluorescence measurements on polycarbonate chips. For this purpose, serial dilutions of BSA-Cy5 in carbonate buffer are arrayed on the chips by a non contact microprinter (25 nL/spot). After 16 h at 4ºC in the darkness, the chips are scanned using a fluorescence scanner (635 nm) and the subsequent data are employed as a calibration curve. Then, chips are rinsed with deionized water, dried by air flow and measured again. From these results, the immobilization isotherm is obtained.

The immobilization of the probe in this model system is based on passive physisorption. For assays involving different probe immobilization strategies analogue experiments must be performed, according to the corresponding immobilization methodologies.

Different assays utilizing similar probes, as well as different probes using the same carrier protein, will presumably show the same immobilization behaviour for a given transducer surface. Therefore, the immobilization isotherm experiment for characterizing the model should be avoided when prior knowledge on the system is available.

Response curve. To obtain the response curve, an assay with serial probe dilutions applying an excess of receptor (and without analyte in the competitive systems) must be performed. After considering the immobilization isotherm experiments and the response curve experimental data, the relationship between the analytical signal and Θ^{RB} is obtained by adjusting the experimental results to an equation.

Classical optimization. The classical standard bi-parametrical optimization procedure is divided into two steps: titration and dose-response curve. To carry out titration experiments, the signal-to-noise ratio vs. probe concentration curves are performed for a range of receptor concentrations. From these data, the binary combinations that generate a signal-to-noise ratio of around 50 are selected in order to keep the whole linear range of the dose-response curve above the limit of quantification. The second step consists in building the dose-response curves of the binary conditions selected in the titration experiment. For this purpose, the signal-to-noise ratio vs. analyte concentration curves are carried out for each selected binary combination. From these results, the conditions that generate the lowest IC_{50} in the dose-response curves are selected as optimal conditions.

References

S1. J.L. Harris, E. Skaletsky and A. McPherson, J. *Mol. Biol*., 1998, **275**, 861.

S2. R.A. Vijayendran, F.S. Ligler and D.E. Leckband, *Anal. Chem*., 1999, **71**, 5405.

S3. S. Morais, L.A. Tortajada-Genaro, T. Arnandis-Chover, R. Puchades and A. Maquieira, *Anal. Chem*., 2009, **81**, 5646.

S4. J. Tamarit-Lopez, S. Morais, M. Bañuls, R. Puchades and A. Maquieira, *Anal. Chem*., 2010, **82**, 1954.

3.2.3 Conclusions

As demonstrated in this study, INSEL is a theoretical-experimental strategy that enable rational explorations and optimizations of biorecognition assays in order to reach their maximal performance. Unlike classical optimization methods for biorecognition assays, such as checkerboard titration, INSEL involves minimal experimentation and characterizes the affinity and mass transport parameters of the system. This strategy also permits to direct optimizations towards custom objectives designed by the users, such as a weighted ratio between sensitivity and precision as herein demonstrated. Once characterized, INSEL allows researchers to explore the behavior of biorecognition systems without further experimentation. For instance, critical variables like mass transport constants can be computationally assessed by this approach. On the other hand, this work is also one of the first approximations that demonstrates the performance of disk-based microarrays as routine technique to assess biointeractions. The success of INSEL have been demonstrated with competitive (coating conjugate-based) and non-competitive (sandwich) immunoassay formats. However, it must be highlighted that thanks to the generic reaction scheme employed to build the model, this *in silico* strategy can also be potentially expanded to other biorecognition assays.

Though it has been left as future work within the general context of this thesis, INSEL could be directly applied to the biosensor systems developed in the other chapters, aiming to achieve their maximal performance. Besides, the knowledge obtained in this work is also related with the subsequent studies, for instance in terms of characterization of the kinetic and adsorption behavior of the employed bioreagents and assays.

Chapter 3

3.3 SERS-on-a-disk

3.3.1 Introduction

SERS-active substrates are nanostructured functional materials that enable label-free detection and address the reproducibility limitations of nanoparticle-based SERS systems. However, these substrates are typically produced as very small chips by expensive and non-scalable methods, which strongly restricts their dissemination in real-world applications. Therefore, exploiting mass-produced technologies to conceive new SERS systems can offer important solutions in these regards.

Grounded on the knowledge obtained in the previous chapters, this work aims to tailor the track nanostructure of recordable compact disks to become SERS-active and enable label-free biosensing. Since regular recordable disks are worldwide produced in a massive and inexpensive fashion, and each disk comprises a large area of embedded nanostructure, this approach points towards really affordable materials to bring SERS and label-free biosensing to the point-of-need. Also, given that Raman systems and pickup units share many structural features, prospective Raman scanners based on TED drives and designed to analyze these SERS-active disks, can be envisioned from this approach.

Unlike other biosensing techniques, the main distinctive feature of SERS for biosensing relies on the specific fingerprint spectra of the target under study that this technique provides. From a general viewpoint, this work also aims to become the starting point for exploiting the enhanced specificity of SERS for analyzing biorecognition assays in label-free conditions, which is a challenging issue (mainly because of sensitivity limitations) and remains rather unexplored.

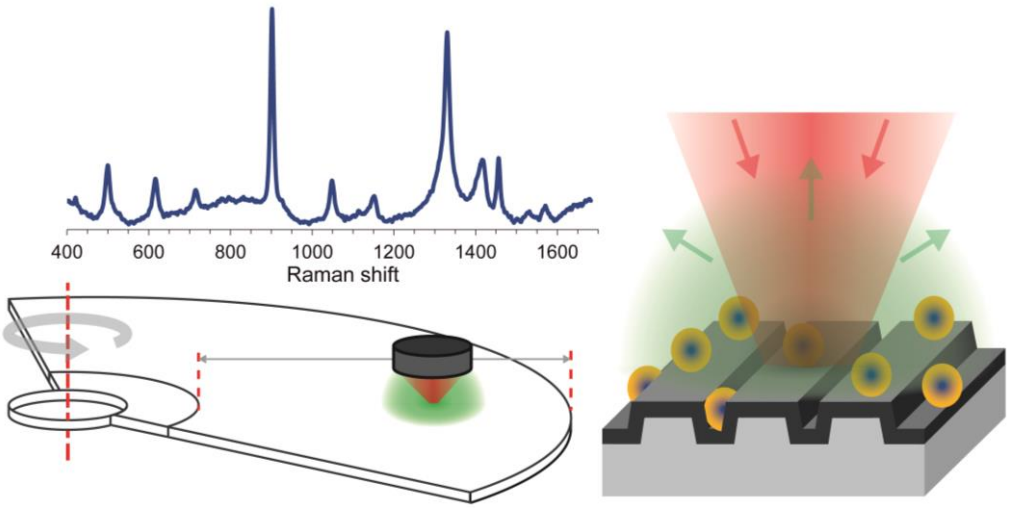

3.3.2 Label-free SERS analysis of proteins and exosomes with large-scale substrates from recordable compact disks

Sens. Actuators B, 252 (**2017**) 657.

ABSTRACT

A central aspect to fully reach the biosensing scope of plasmonics beyond the research environment is its implementation in inexpensive and homogeneous functional nanostructured materials that can be manufactured in a large-scale fashion. Herein, we study the capabilities of consumer-grade compact disk technology for label-free SERS analysis of complex biological targets. Substrates from regular recordable disks (CD-R and DVD-R) coated with silver exhibit significant Raman enhancement. The magnitude of this enhancement depends on the nanostructure on the polycarbonate substrate, the silver thickness, and the excitation wavelength. The Raman fingerprint of hemoglobin and exosome samples were experimentally obtained in label-free conditions, which demonstrates the biosensing potential of this approach and suggests prospective developments towards fully exploiting the bioanalytical capabilities of SERS in point-of-care settings.

Keywords: SERS, compact disk, label-free, exosome, point-of-care, low-cost.

1. Introduction

Over the past two decades, an intense research focus on the interaction and manipulation of light and matter at the nanoscale has advanced the frontiers of the knowledge in nanoscience and nanotechnology [1]. Out of laboratories, the implementation of these advances demands large-scale nanostructured functional materials capable to be industrially manufactured in an inexpensive and reproducible manner [2, 3]. Also, developing alternatives to the benchtop setups and specialized equipment typically employed in research settings will support their impact in non-specialized environments.

Within this framework, surface-enhanced Raman spectroscopy (SERS) uses the resonant interaction of light with plasmons in metallic nanostructures to produce large enhancement of Raman signals for analyzing chemical and biochemical species [4]. Among its main strengths over other sensing techniques, SERS provides a characteristic fingerprint spectra that is a rich source of information to identify and characterize the targets under study [5-7].

Transferring nanoscience and nanotechnology advances in (bio)chemical sensing from the lab to real-life applications requires scaling up the manufacturing process. One simple way to achieve this is by adapting existing consumer-grade technologies to perform tasks otherwise possible only in the lab [8, 9]. This strategy provides user-friendly approaches based on robust and cost-effective systems. Promising attempts reported towards joining SERS with consumer technologies (cell phones, pens, etc.) do not deal with biosensing, neglect SERS label-free detection, and remain dependent on specialized instrumentation [10-14].

Compact disk technologies are consumer electronics based on monitoring the reflected intensity of a laser beam focused on spiral-shaped nanogrooves embedded in polycarbonate disks, and their analytical implementation presents appealing features for point-of-care lab-on-a-disk biosensors [15, 16]. Interesting approaches using aluminum nanohole arrays [17] and interferometry in multilayered structures [18] have been reported for label-free biosensing with compact disks, but these works do not exploit the benefits of SERS since they deal with other detection techniques. Along these lines, two recent studies have successfully developed SERS substrates from standard Blu-ray and HD DVD structures coated with gold [19, 20]. These papers address the sensing of pure low-molecular weight organic molecules significantly active in Raman (melamine, vitamin A, and β-carotene) that, even thought involved in biological functions, do not comprise the complexity of biomacromolecular targets.

Herein we introduce the implementation of the compact disk technology for label-free SERS analysis of complex biomolecular targets by means of structured polycarbonate substrates obtained from standard recordable disks (CD-R and DVD-R) coated with silver. This is an inexpensive alternative to the classical nanofabrication methods of functional SERS nanostructured materials. Unlike previous studies using gold, silver coatings were herein selected given the much lower price of this metal than gold, which supports the point-of-care scope of this development. The influence of the silver thickness, the polycarbonate structure, and the excitation wavelength was experimentally studied, and the relationship of these variables with the plasmonic behavior and the Raman enhancement was assessed. Additionally, the optimal substrates were characterized by microscopy and their biosensing potential demonstrated by analyzing hemoglobin and exosomes in label-free format. This work aims to prove the concept for these materials and to become the first step towards a cost-effective lab-on-a-disk technology involving SERS-active disks to perform biorecognition assays and dedicated Raman scanners based on standard disk drives.

2. Materials and methods

2.1 Materials

4-aminothiophenol (4-ATP) and hemoglobin were purchased from Sigma-Aldrich. Recordable optical disks (CD-R and DVD-R LightScribe) were from MediaRange. Exosome solutions were from a lung cancer cell line (A549 UC) purified by ultracentrifugation. SERS measurements were performed with a Renishaw InVia Raman Microscope, using a 50X objective lens with a numerical aperture of 0.75 (spot diameter ~ 1.25 μm). An Agilent 8543 spectrophotometer was employed for the absorption spectra measurements. Silver sputtering was done with a Kurt J. Lesker sputterer. Field emission scanning electron microscopy (FESEM) and focused ion beam (FIB) characterization was performed using a focused ion beam scanning electron microscope

Zeiss Auriga compact. For the AFM scans, a Bruker Multimode 8 equipment and a Bruker SNL-10 probe were employed.

2.2 Fabrication

Standard polycarbonate structures from regular recordable optical disks (CD-R and DVD-R) were coated with silver in a range of metal thicknesses and employed as SERS substrates, as shown in Fig. 1. Polycarbonate CD-R structures were obtained by peeling off the label and metal layers from a circular cut created in the outer edge of the disk, as described elsewhere [21]. For DVD-R structures, both polycarbonate plates that compose these disks were disassembled, keeping the metal layer in the plate that contains the label. Then, the remaining dye layer on the CD-R and DVD-R structured plates was dissolved in an ethanol bath (1 minute, room temperature) and the resulting polycarbonate plates were rinsed with ethanol and dried under an air stream. All these polycarbonate structures were finally coated with different thicknesses of silver by sputtering. The corresponding flat analogues of the substrates were created by metallizing the outer side of the polycarbonate plates and used as unstructured controls. Sputtering conditions were set to deposit a range of thicknesses: 0, 50, 100, 150, and 200 nm.

2.3 4-ATP monolayers

To create self-assembled monolayers of 4-ATP on the silver surface, the substrates were cut in chips (~ 1x1 cm) and immersed in an ethanolic solution of this compound (1 mM, 1 mL, 2 h) in sealed vials. Then, substrates were rinsed with ethanol and dried under an air stream.

2.4 Raman measurements

Substrate chips were positioned structure-up under the optical setup of the Raman system and the images from optical microscopy were used to align the grooved structures with the laser polarization. Exposure times of 10 seconds and a resolution of 0.8 cm^{-1} were selected. Raman spectra from at least six spots randomly distributed (one spectrum per spot) and an internal laser power calibration from a silicon master were taken for every sample. In order to provide insights into prospective Raman scanners based on disk drives, 633 and 785 nm lasers were selected for the excitation, since these wavelengths are very close to the ones in the laser sources of regular DVD and CD drives (650 and 780 nm, respectively).

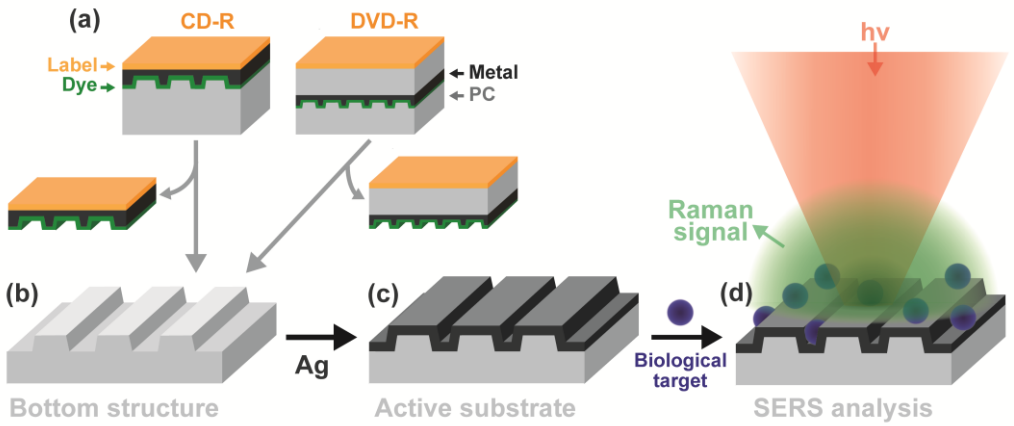

Fig. 1. Illustration of the fabrication of disk-based SERS-active substrates and the sample analysis. Recordable compact disks (a) were processed to obtain polycarbonate grooved structures (b) that once coated with silver (c) become SERS-active substrates (d).

2.5 Data processing

The intensities of the recorded raw spectra were normalized considering the maximal peak intensity from the corresponding silicon calibration. Then, background signals were subtracted (polynomial fitting) and the spectra smoothed by a denoising filter (low-pass Fourier filter), using a custom Matlab routine. Outliers were identified by Grubbs' test (90% confidence level). To this end, characteristic peaks for each system were determined (Table S1) and their intensities (averaged within ±2 cm^{-1}) were used as parameters to assess the variability within series of replicates. Measurements identified as outliers by the test in more than one characteristic peak were removed, and the rest of them were averaged.

2.6 Microscopy characterization

For the FIB-FESEM measurements, the areas to be analyzed were previously coated by a layer of platinum to improve the definition of the scans in the outer boundary of the silver layer. Ditches perpendicular to the groves were created by a focused gallium (Ga^+) beam and the height profiles were scanned by FESEM (54 degrees tilt). The sizes and shapes of the features in the polycarbonate structures and the silver layer were determined from these FIB-FESEM data using the ImageJ software.

20x20 µm and 2x2 µm AFM scans (1x1 and 2x2 kilopixels, respectively) were performed by contact mode in air. The data analysis was done by the Nanoscope software. A zeroth order polynomial flatten was applied to all the scans. For averaged cross sections, the height profiles

along the direction of the grooves for every row of pixels were averaged in a single profile. Roughnesses were determined by root mean squared values [22].

2.7 Biological analysis

A range of concentrations of hemoglobin and exosome solutions in deionized water were manually dispensed on the substrates (5 µL) and let to dry in an active fume hood. Raman signals on the spots were measured as described above.

3. Results and discussion

3.1 Spectrophotometric characterization

First, the plasmonic behavior of the substrates was investigated. As shown in Fig. 2, several absorption bands in the visible spectral range were observed with silver-coated structures, indicating plasmonic resonances. Both excitation wavelengths used in this study are located inside these resonances. No absorption peaks were found for uncoated substrates (Fig. 2, 0 nm) and in the corresponding unstructured analogues (Fig. S1). One interesting observation to highlight is the ability to tune the resonance by adjusting the silver thickness, since the absorption bands shifts towards shorter wavelengths when the silver thickness increases.

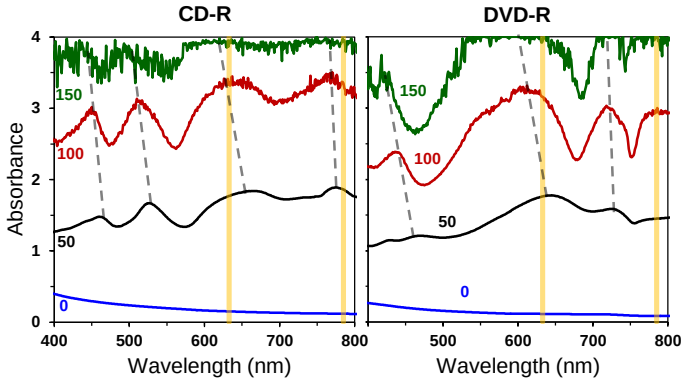

Fig. 2. Absorption spectra of the studied structures with different silver thicknesses, from 0 to 150 nm. Vertical lines indicate the employed excitation wavelengths, and dashed lines show the shift of the plasmonic bands. Saturated absorbance spectra were obtained for 200 nm thickness.

3.2 SERS performances

Then, the Raman response of the substrates was investigated. Flat spectra were observed in all of the raw substrates coated with silver, whereas uncoated structures (0 nm) presented a

characteristic polycarbonate spectrum that disappears with 50 nm metal coatings (Fig. S2). The SERS activity was assessed using self-assembled monolayers of 4-ATP on the silver surfaces as Raman reporters [23]. As shown in Fig. 3, the characteristic 4-ATP spectra were obtained at both excitation wavelengths with the structured substrates, while uncoated materials kept the polycarbonate spectrum as expected (Fig. S3) and no Raman responses were displayed by the analogous unstructured substrates (Fig. S4). These results reveal a Raman enhancement dependence on the polycarbonate structure (CD-R or DVD-R), the excitation wavelength (λ_{exc}), and the thickness of the metal coating. The silver thicknesses that lead to maximal enhancement, selected for the subsequent experiments, were 100 nm for CD-R and DVD-R at λ_{exc} = 633 nm, as well as 50 nm for CD-R and 150 nm for DVD-R at λ_{exc} = 785 nm.

Recordable compact disks contain a continuous grooved structure comprising ridges and valleys, whose spiral curvature can be neglected at the nanoscale. Maximal enhancement was obtained when the focal plane of the excitation beam coincided with the top of the ridge and the polarization of the laser was perpendicular to the groves (Fig. S5 and Fig. S6). In these conditions, enhancement factors about four and five orders of magnitude were estimated for these substrates (see Table S2).

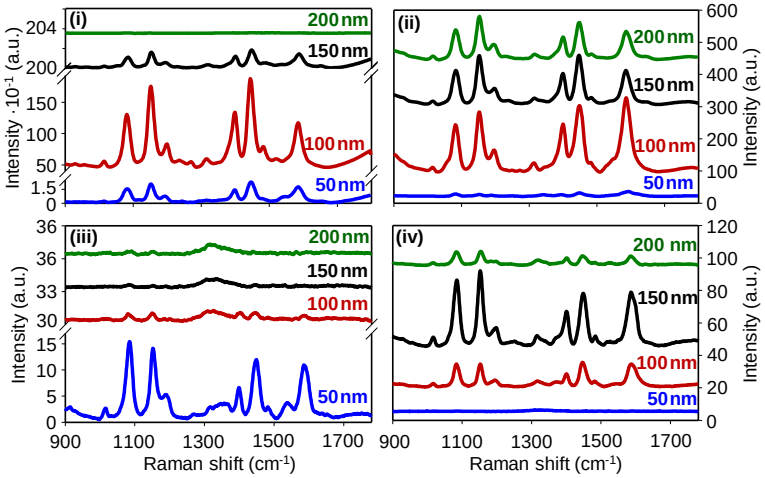

Fig. 3. Raman spectra of 4-ATP monolayers on (i) CD-R at λ_{exc} = 633 nm, (ii) DVD-R at λ_{exc} = 633 nm, (iii) CD-R at λ_{exc} = 785 nm, and (iv) DVD-R at λ_{exc} = 785 nm, with different silver thicknesses.

It is worth highlighting that all these results point out the crucial role of this structuration in the SERS activity of these materials. Unlike structured substrates, the corresponding flat analogues showed no plasmonic absorptions in the UV-Vis range and undetectable Raman signals from

4-ATP. Considering previous reports [24, 25], the differences in the SERS enhancements displayed by these materials must be caused by the complex interplay between three factors: (i) the structures of the disks that lead to localized surface plasmon resonances, (ii) the surface roughness that contributes to additional surface plasmon resonances, and (iii) the silver thickness that determines the penetration depth of plasmons and the potential leakage into the adjacent underlying layer. For larger structures (CD-Rs), the enhancement is mainly determined by the roughness and thickness of the metallic layer, with thinner layers yielding larger enhancements. For smaller structures (DVD-Rs), the localized surface plasmon resonances becomes also significant and pushes the maximum enhancements towards larger thicknesses. This trend is more accentuated for measurements at 785 nm, which is in agreement with simulations showing that the strongest electric fields of flat surfaces excited at this wavelength are achieved for thinner silver layers (compared with 633 nm) and decrease quickly with increasing thicknesses [24].

3.3 Microscopy characterization

FESEM data of the optimal substrates revealed that the characteristic grooves remain after coating the polycarbonate structure (Fig. 4a). Also, metal clusters were found along all the surfaces, whose sizes distribution depends on the coating thickness. For 50 nm coatings, predominant cluster sizes within the range of 20-30 nm and scarce clusters larger than 50 nm were observed. For the rest of the coatings, these dimensions increase about 5 nm for every additional 50 nm of silver thickness.

Micrometric ditches perpendicularly oriented to the grooves were created on the substrates by FIB and analyzed by FESEM in order to characterize the structuration across the height axis. Given the uniformity of these substrates along the longitudinal direction, this approach enabled to determine the shapes and sizes of both polycarbonate structures and metal thickness profiles. As shown in Fig. 4b, the polycarbonate grooves are constituted by sloped walls and rounded ridge edges. Rather than reproducing the bottom pattern, the metal coating process created new structures mainly constituted by rounded profiles whose features depend on the silver thickness and the polycarbonate structure (Fig. S9). Only the top of the ridges and certain parts of the valleys are coated with the metal thicknesses experimentally set for the metallization.

The topographic characterization performed by atomic force microscopy (AFM) revealed that the outer boundary of the silver layers coincide with the profiles observed by FIB-FESEM (Fig. 4c). The slight differences observed may be due to artifacts caused by the hindered access of the AFM tip to the sharp edges of the structures, especially in the valley rims of DVD-R substrates coated with 150 nm of silver. Clustered topographies were also observed in these data (Fig. S11). Regarding roughness, most of the substrates presented values between 2 and 4 nm. Similar results were observed in the grooved substrates (ridge and valley areas) and their corresponding

flat analogues, so this grooved structuration did not increase roughness on the outer boundary of the silver layer (Fig. S12).

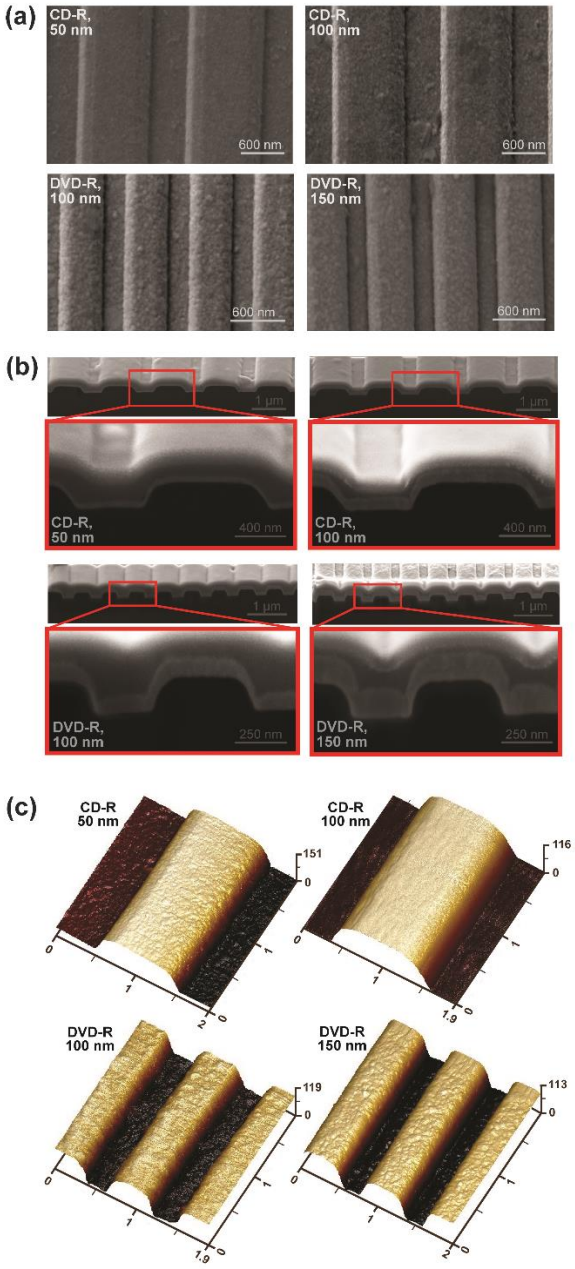

Fig. 4. Microscopy characterization. (a) FESEM images. See Fig. S7 and Fig. S8 for enlarged images and larger scan areas. (b) FIB-FESEM images at two magnifications. From bottom to top, black profile are the polycarbonate structures, whitish layers on it correspond to Ag coatings, and the following greyish layers are platinum deposited to improve quality of the scans. (c) Three-dimensional view of AFM data (height axis in nm, other axis in µm). See Fig. S10 and Fig. S11 for top views and cross sections of 20x20 µm and 2x2 µm scans, respectively.

3.4 Analysis of biological samples

To provide insights into the biosensing potential of this approach, hemoglobin samples with a range of concentrations were placed on the substrates and their SERS response was analyzed in label-free conditions. Hemoglobin is a representative model system for proteins, an important target in some clinical situations, and detecting its presence can also be important in real biological samples where this protein can be present as a blood residue. As shown in Fig. 5, an active response and the Raman fingerprint for this protein [26] were obtained for all the substrates.

Moreover, an array of exosome dilutions coming from a lung cancer cell line was also studied in order to assess these substrates in real biological samples. Active SERS responses were obtained with all the structures, especially intense for the DVD-R substrates (Fig. 5). Determining the specific vibrations of these Raman peaks becomes hindered by the complex biochemical composition of these vesicles, but some spectral features are shared with previous studies [27].

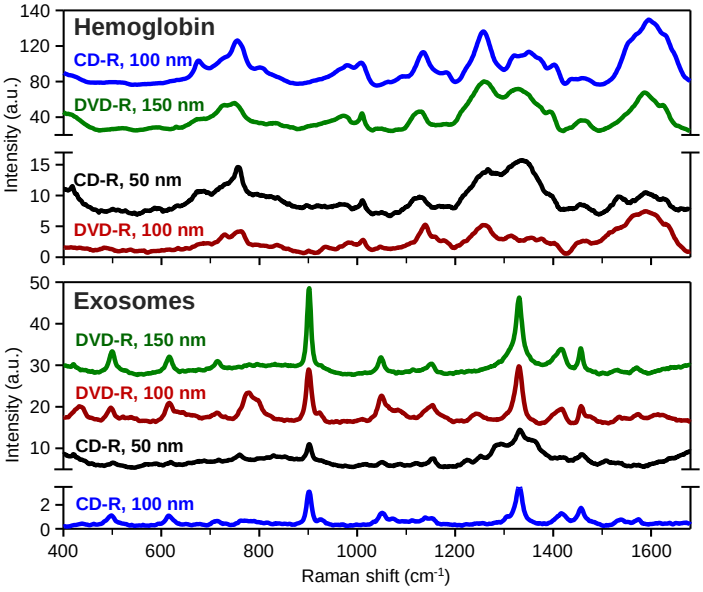

Fig. 5. Raman spectra obtained in the label-free analysis of hemoglobin (100 µg/mL) and exosome (1/100 dilution) samples using the optimal structures for λ_{exc} = 633 (CD-R, 100 nm; DVD-R, 100 nm) and λ_{exc}= 785 nm (CD-R, 50 nm; DVD-R, 150 nm).

3.5 Future perspectives

While presenting many other particular biosensing strengths, compared to previous reports these substrates displayed a slightly lower sensitivity for hemoglobin analysis (Table S2). Also, moderate correlations between signal intensity and sample concentration were obtained for both hemoglobin and exosomes (Fig. S13). All these facts point out the importance of surface functionalization and selective binding in future developments. Work is in progress towards the development of biorecognition assays on these functional materials in order to make the most of their bioanalytical potential. The greatest strength of SERS over other biosensing techniques relies on providing characteristic fingerprint data of the analyzed samples. Marrying biorecognition assays and SERS involve appealing prospects to selectively capture and preconcentrate multiple targets of interest from complex biological samples on the surface of SERS substrates, and then using the fingerprint output data to detect them in label-free and multiplex fashion.

Besides proving the concept for nanostructured mass-produced materials as plasmonic substrates for label-free SERS biosensing, this study also suggests future avenues of research towards the development of inexpensive, portable, and robust Raman scanners based on regular optical disk drives. These drives comprise orthogonal laser irradiation and a signal collection unit that is designed to autofocus in the grooved structures of the disks, which shares many features with the optical setups typically used in Raman microscopes. Standard drives also integrate three different lasers sources (405, 650, and 780 nm) whose intensity can be controlled. This approach offers appealing features to automatically scan disks with more than 85 cm^2 of the SERS-active substrates herein described, thus proposing a cost-effective alternative to the bulky and expensive standard Raman equipment. Moreover, optical disk drives can be modified to control the laser position and the disk spinning, which involve attractive possibilities for coupling centrifugal microfluidics in these prospective biosensor systems [21, 28-30]. Within this scope, the results presented in this work also suggest point-of-care systems that exploit the potential of Raman scattering to characterize exosome contents for non-invasive cancer diagnosis [27, 31].

4. Conclusions

This study introduces large-scale SERS substrates obtained in a simple and inexpensive manner from regular recordable optical disk structures coated with silver. These substrates exhibit tunable plasmonic resonances in the visible range, and the silver metallization generates surfaces with new features whose optimal Raman enhancement depends on the polycarbonate structure, the silver thickness, and the excitation wavelength. The biosensing capabilities of these SERS substrates to analyze complex biomolecular targets is demonstrated by experimentally obtaining the Raman fingerprint of hemoglobin and exosomes in label-free conditions. The results herein

presented also suggest prospective Raman microscope units based on optical disk drives, thus offering integral solutions towards the transference of SERS and its biosensing potential from laboratories to non-specialized environments.

Acknowledgments

This work was supported by the Spanish Ministry of Economy and Competitiveness (CTQ2013-45875-R), FEDER, and the Generalitat Valenciana (PROMETEO II/2014/040). S.W-H would like to acknowledge financial support from UCDavis Office of Research. M.A-O also acknowledges the FPI program of the Spanish Ministry of Economy and Competitiveness for a PhD and an EEBB grant. We would like to thank Dr. Randy P. Carney for the exosome samples.

References

[1] Focusing in on applications, Nat Nanotechnol, 10 (2015) 1.

[2] C.R. Kagan, At the Nexus of Food Security and Safety: Opportunities for Nanoscience and Nanotechnology, ACS Nano, 10 (2016) 2985-2986.

[3] M.Y. Lv, H.Y. Teng, Z.Y. Chen, Y.M. Zhao, X. Zhang, L. Liu, et al., Low-cost Au nanoparticle-decorated cicada wing as sensitive and recyclable substrates for surface enhanced Raman scattering, Sens Actuators B, 209 (2015) 820-827.

[4] S. Schlücker, Surface-Enhanced Raman Spectroscopy: Concepts and Chemical Applications, Angew Chem Int Ed, 53 (2014) 4756-4795.

[5] X.X. Han, Y. Ozaki, B. Zhao, Label-free detection in biological applications of surface-enhanced Raman scattering, Trends Anal Chem, 38 (2012) 67-78.

[6] S.-C. Luo, K. Sivashanmugan, J.-D. Liao, C.-K. Yao, H.-C. Peng, Nanofabricated SERS-active substrates for single-molecule to virus detection in vitro: A review, Biosens Bioelectron, 61 (2014) 232-240.

[7] W.A. El-Said, D.M. Fouad, S.A. El-Safty, Ultrasensitive label-free detection of cardiac biomarker myoglobin based on surface-enhanced Raman spectroscopy, Sens Actuators B, 228 (2016) 401-409.

[8] M. Avella-Oliver, S. Morais, R. Puchades, Á. Maquieira, Towards photochromic and thermochromic biosensing, Trends Anal Chem, 79 (2016) 37-45.

[9] G. Comina, A. Suska, D. Filippini, Towards autonomous lab-on-a-chip devices for cell phone biosensing, Biosens Bioelectron, 77 (2016) 1153-1167.

[10] S. Ayas, A. Cupallari, O.O. Ekiz, Y. Kaya, A. Dana, Counting Molecules with a Mobile Phone Camera Using Plasmonic Enhancement, ACS Photonics, 1 (2014) 17-26.

[11] L. Polavarapu, A.L. Porta, S.M. Novikov, M. Coronado-Puchau, L.M. Liz-Marzán, Pen-on-Paper Approach Toward the Design of Universal Surface Enhanced Raman Scattering Substrates, Small, 10 (2014) 3065-3071.

[12] W.W. Yu, I.M. White, Inkjet Printed Surface Enhanced Raman Spectroscopy Array on Cellulose Paper, Anal Chem, 82 (2010) 9626-9630.

[13] C. Leordean, B. Marta, A.-M. Gabudean, M. Focsan, I. Botiz, S. Astilean, Fabrication of highly active and cost effective SERS plasmonic substrates by electrophoretic deposition of gold nanoparticles on a DVD template, Appl Surf Sci, 349 (2015) 190-195.

[14] X. Dou, P.-Y. Chung, P. Jiang, J. Dai, Surface plasmon resonance and surface-enhanced Raman scattering sensing enabled by digital versatile discs, Appl Phys Lett, 100 (2012) 041116.

[15] S. Morais, R. Puchades, Á. Maquieira, Disc-based microarrays: principles and analytical applications, Anal Bioanal Chem, 408 (2016) 4523-4534.

[16] X.J. Zhao, X.C. Li, C.E. Cui, H.Z. Yu, DVD diagnostic software for reading disc-based bioassays, a comparative study, Sens Actuators B, 195 (2014) 116-122.

[17] C.A. Barrios, V. Canalejas-Tejero, S. Herranz, M.C. Moreno-Bondi, M. Avella-Oliver, R. Puchades, et al., Aluminum Nanohole Arrays Fabricated on Polycarbonate for Compact Disc-Based Label-Free Optical Biosensing, Plasmonics, 9 (2014) 645-649.

[18] S.C.S. Gopinath, K. Awazu, P. Fons, J. Tominaga, P.K.R. Kumar, A Sensitive Multilayered Structure Suitable for Biosensing on the BioDVD Platform, Anal Chem, 81 (2009) 4963-4970.

[19] M.K. Nieuwoudt, J.W. Martin, R.N. Oosterbeek, N.I. Novikova, X. Wang, J. Malmström, et al., Gold-sputtered Blu-ray discs: simple and inexpensive SERS substrates for sensitive detection of melamine, Anal Bioanal Chem, 408 (2016) 4403-4411.

[20] A.I. Radu, Y.Y. Ussembayev, M. Jahn, U.S. Schubert, K. Weber, D. Cialla-May, et al., HD DVD substrates for surface enhanced Raman spectroscopy analysis: fabrication, theoretical predictions and practical performance, RSC Adv, 6 (2016) 44163-44169.

[21] M. Avella-Oliver, S. Morais, J. Carrascosa, R. Puchades, Á. Maquieira, Total Analysis Systems with Thermochromic Etching Discs Technology, Anal Chem, 86 (2014) 12037-12046.

[22] E.S. Gadelmawla, M.M. Koura, T.M.A. Maksoud, I.M. Elewa, H.H. Soliman, Roughness parameters, J Mater Process Technol, 123 (2002) 133-145.

[23] Y.-F. Huang, D.-Y. Wu, H.-P. Zhu, L.-B. Zhao, G.-K. Liu, B. Ren, et al., Surface-enhanced Raman spectroscopic study of p-aminothiophenol, Phys Chem Chem Phys, 14 (2012) 8485-8497.

[24] C. Lee, C.S. Robertson, A.H. Nguyen, M. Kahraman, S. Wachsmann-Hogiu, Thickness of a metallic film, in addition to its roughness, plays a significant role in SERS activity, Sci Rep, 5 (2015) 11644.

[25] M. Kahraman, P. Daggumati, O. Kurtulus, E. Seker, S. Wachsmann-Hogiu, Fabrication and Characterization of Flexible and Tunable Plasmonic Nanostructures, Sci Rep, 3 (2013) 3396.

[26] M. Kahraman, S. Wachsmann-Hogiu, Label-free and direct protein detection on 3D plasmonic nanovoid structures using surface-enhanced Raman scattering, Anal Chim Acta, 856 (2015) 74-81.

[27] C. Lee, R.P. Carney, S. Hazari, Z.J. Smith, A. Knudson, C.S. Robertson, et al., 3D plasmonic nanobowl platform for the study of exosomes in solution, Nanoscale, 7 (2015) 9290-9297.

[28] D. Choi, T. Kang, H. Cho, Y. Choi, L.P. Lee, Additional amplifications of SERS via an optofluidic CD-based platform, Lab Chip, 9 (2009) 239-243.

[29] R. Burger, L. Amato, A. Boisen, Detection methods for centrifugal microfluidic platforms, Biosens Bioelectron, 76 (2016) 54-67.

[30] A.A. Sayad, F. Ibrahim, S.M. Uddin, K.X. Pei, M.S. Mohktar, M. Madou, et al., A microfluidic lab-on-a-disc integrated loop mediated isothermal amplification for foodborne pathogen detection, Sens Actuators B, 227 (2016) 600-609.

[31] T. Katsuda, N. Kosaka, T. Ochiya, The roles of extracellular vesicles in cancer biology: Toward the development of novel cancer biomarkers, Proteomics, 14 (2014) 412-425.

SUPPLEMENTARY MATERIAL

Label-free SERS analysis of proteins and exosomes with large-scale substrates from recordable compact disks

Sens. Actuators B, 252 (**2017**) 657.

Table S1. Characteristic peaks selected for the data processing.

λ_{exc}	Structure	Compound	Peak 1 (cm^{-1})	Peak 2 (cm^{-1})	Peak 3 (cm^{-1})	Peak 4 (cm^{-1})
633 nm	Uns. CD-R[a]	Polycarbonate[b]	1121	1189	1243	1611
		4-ATP	1080	1152	1446	1584
	CD-R	Polycarbonate[b]	1121	1243	1533	1611
		4-ATP	1078	1150	1444	1582
		Hemoglobin	753	1131	1254	1591
		Exosomes	495	614	901	1333
	Uns. DVD-R[a]	Polycarbonate[b]	1121	1189	1244	1611
		4-ATP	1080	1150	1444	1583
	DVD-R	Polycarbonate[b]	1121	1189	1244	1611
		4-ATP	1080	1150	1444	1583
		Hemoglobin	725	1138	-	-
		Exosomes	901	1330	1455	-
785 nm	Uns. CD-R[a]	Polycarbonate[b]	898	1120	1188	1610
		4-ATP	1086	1444	1379	1582
	CD-R	Polycarbonate[b]	898	1188	1525	1610
		4-ATP	1086	1444	1379	1582
		Hemoglobin	759	1331	1538	-
		Exosomes	682	758	1332	1532
	Uns. DVD-R[a]	Polycarbonate[b]	898	1120	1241	1610
		4-ATP	1082	1146	1444	1584
	DVD-R	Polycarbonate[b]	898	1120	1241	1610
		4-ATP	1082	1146	1444	1584
		Hemoglobin	748	1008	1323	1588
		Exosomes	498	616	900	1330

[a] Unstructured analogues for CD-R and DVD-R bottom structures.
[b] Uncoated structures (0 nm of silver)

Table S2. Comparison of the peaks intensity for the optimal CD-R and DVD-R, and nanobowl structures under the same conditions and exciting at 633 nm (A) and 785 nm (B).

(A) structure	Peak intensity 1140 cm^{-1}	1320 cm^{-1}	ratio[a]
CD-R	27.0	27.8	$4.8 \cdot 10^{-1}$
DVD-R	3.9	1.9	$4.7 \cdot 10^{-2}$
nanobowl	70.4	48.3	-

(B) structure	Peak intensity 1140 cm^{-1}	1320 cm^{-1}	ratio[a]
CD-R	13.7	7.3	$2.3 \cdot 10^{-2}$
DVD-R	27.9	24.2	$5.9 \cdot 10^{-2}$
nanobowl	578.1	339.7	-

[a] Averaged intensity ratios ($I_{disk}/I_{nanobowl}$) considering both Raman peaks.

The enhancement factor of the optimal structures were estimated by comparing their SERS response for hemoglobin (50 µg/mL) at two Raman peaks with the corresponding response of previously reported nanobowl structures (*Sci. Rep.*, 2015 (5), 11644; *Nanoscale*, 2015 (7), 9290). These are 800 nm in diameter and 400 nm in depth nanovoid structures in PDMS coated with 60 nm of Ag, that exhibit an enhancement factor of 6 orders of magnitude (*Sci. Rep.*, 2015 (5), 11644). As shown in this table, an enhancement factor about one order of magnitude lower can sbe estimated for the optimal CD-R structure at 633 nm, and two orders lower for the rest of structures.

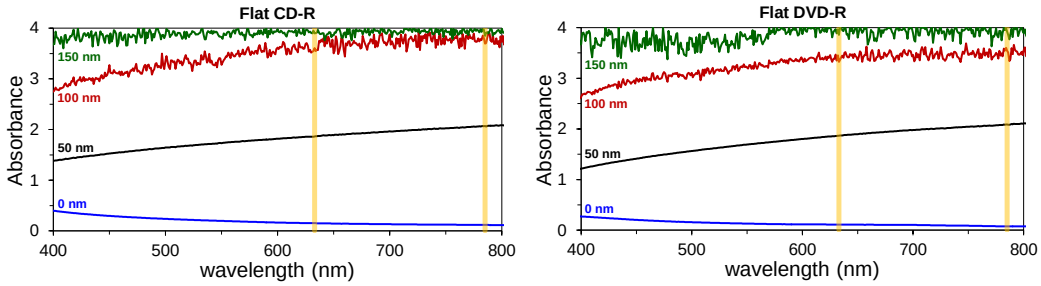

Fig. S1. UV-Vis absorption spectra of the unstructured substrates with different metal thickness.

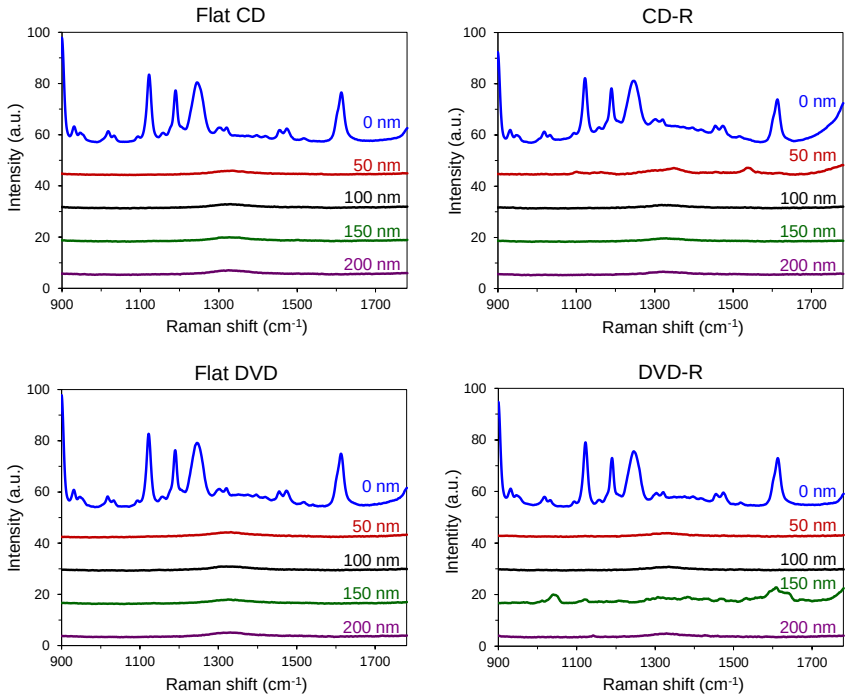

Fig. S2. Raman spectra of the studied structures and their corresponding flat (unstructured) analogues, without any Raman reporter or sample on the substrate (λ_{exc} = 785 nm).

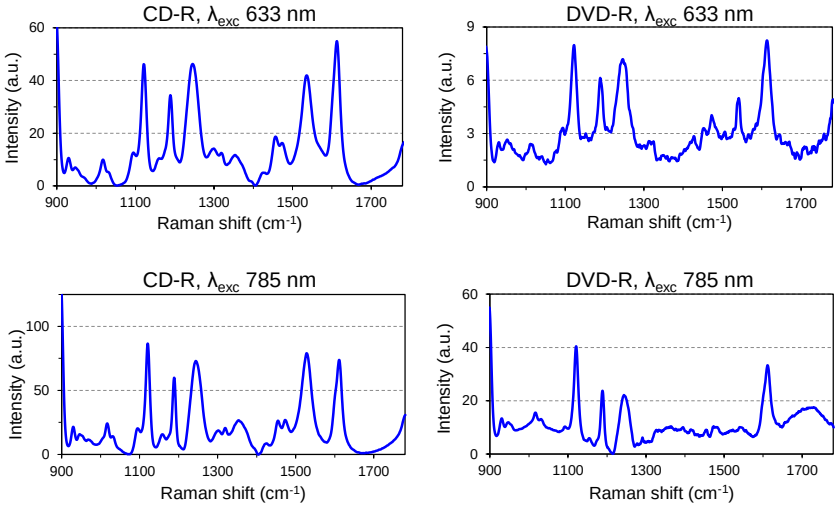

Fig. S3. Raman spectra of the uncoated structured substrates (0 nm) exposed to 4-ATP in the same conditions than the substrates coated with silver displayed in Fig. 3.

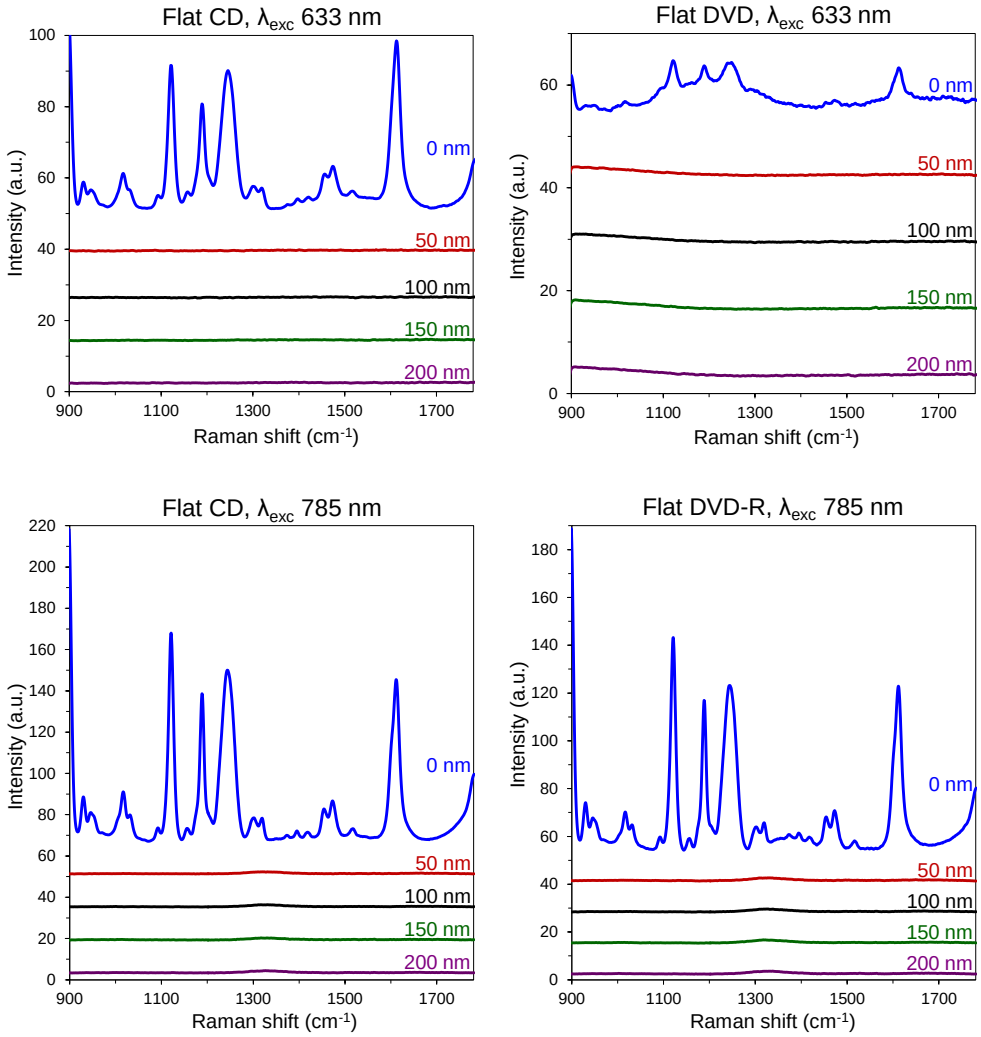

Fig. S4. Raman spectra of the corresponding non-structured substrates containing a 4-ATP monolayer.

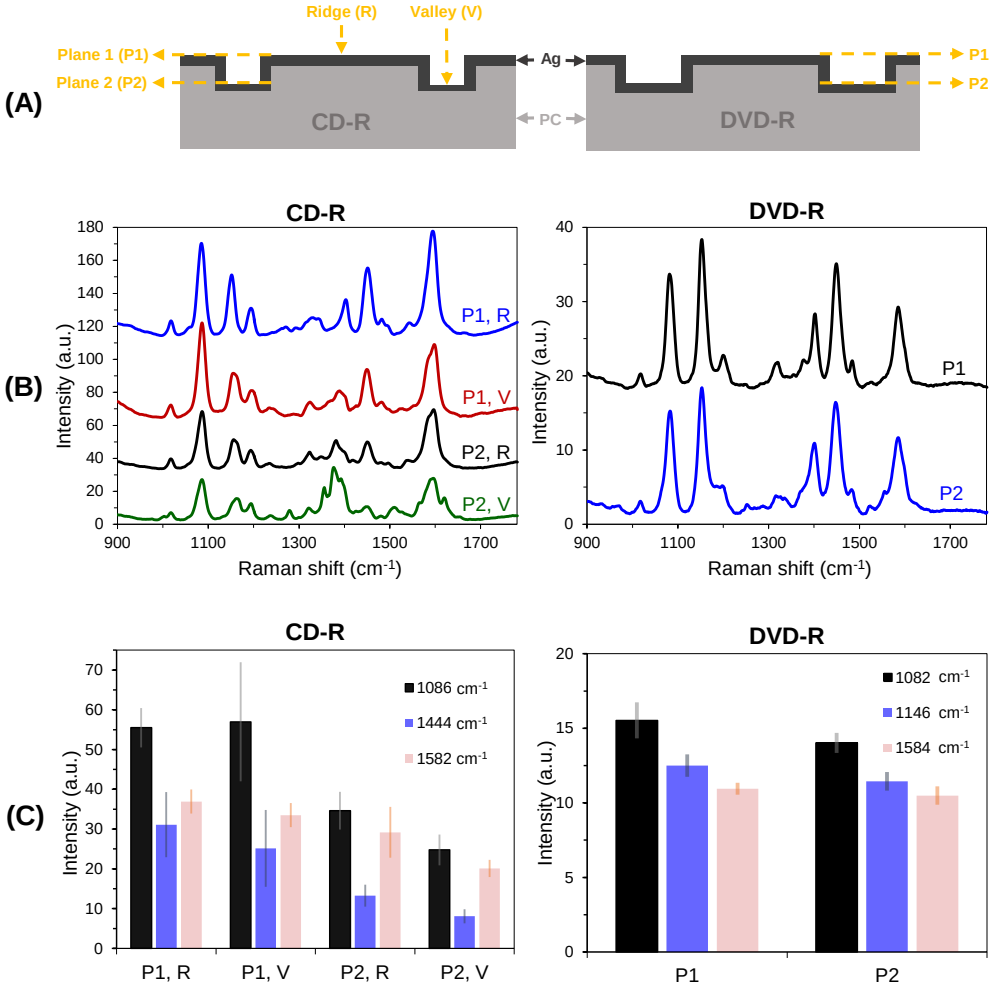

Fig. S5. SERS response of the optimal CD-R and DVD-R structures with 4-ATP under different laser focusing conditions (λ_{exc} = 785 nm). (A) Simplified illustration of the structures, where the main features of the groove and the focal planes are indicated. (B) Raman spectra and (C) the corresponding intensity of selected peaks using 4-ATP as reporter. Ridges and valleys cannot be discriminated when focusing on DVD-R structures given their smaller sizes.

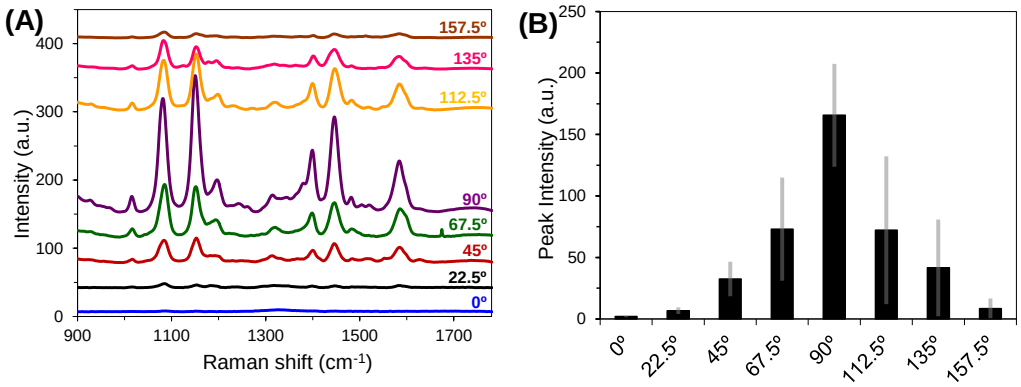

Fig. S6. (A) Raman spectra of the optimal DVD-R structure (λ_{exc} = 785 nm) functionalized with 4-ATP, for a range of angles between the polarization of the incident laser and direction of the grooves, and (B) the corresponding trend in the intensity of a Raman peak (1082 cm^{-1}).

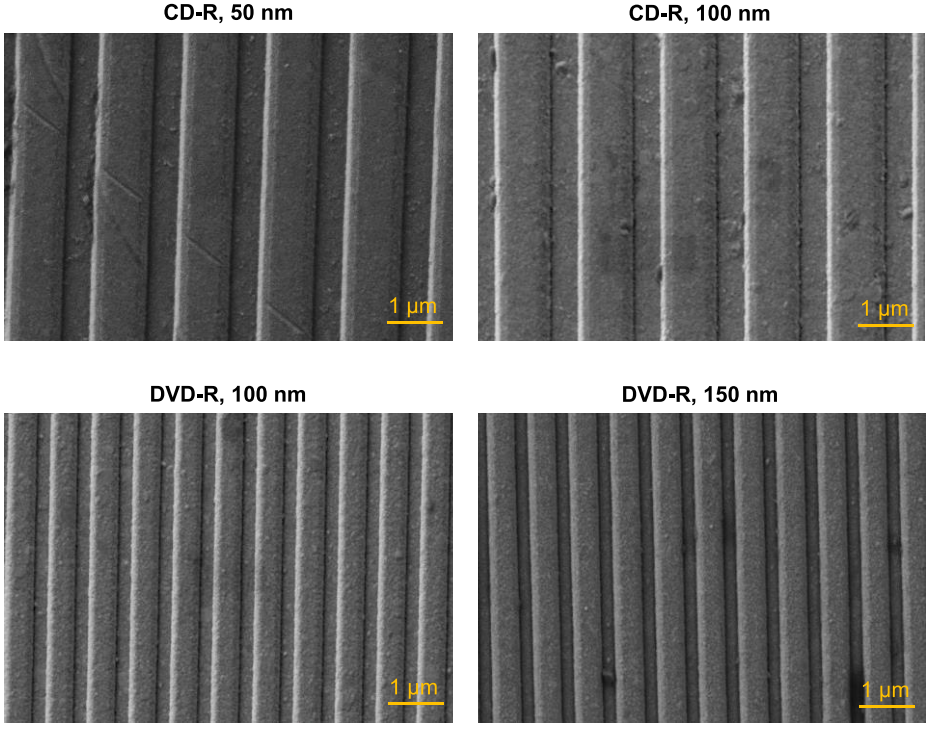

Fig. S7. FESEM images of larger scan areas.

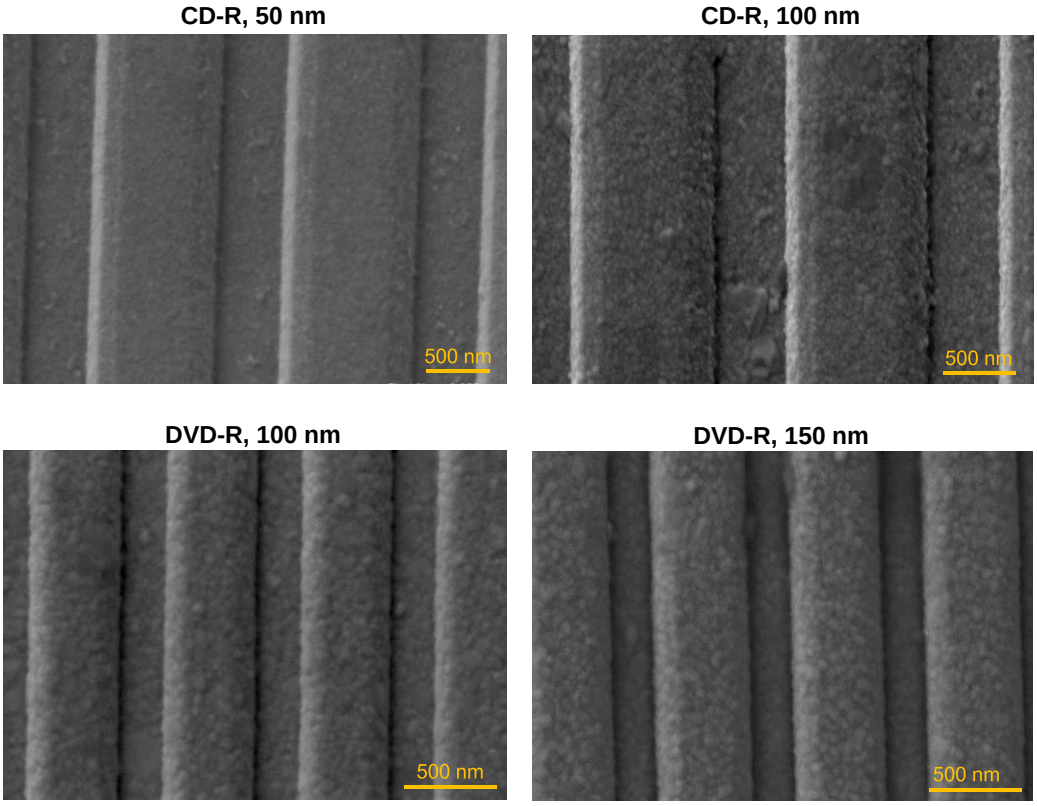

Fig. S8. Enlarged view of the FESEM images included in Fig. 4A.

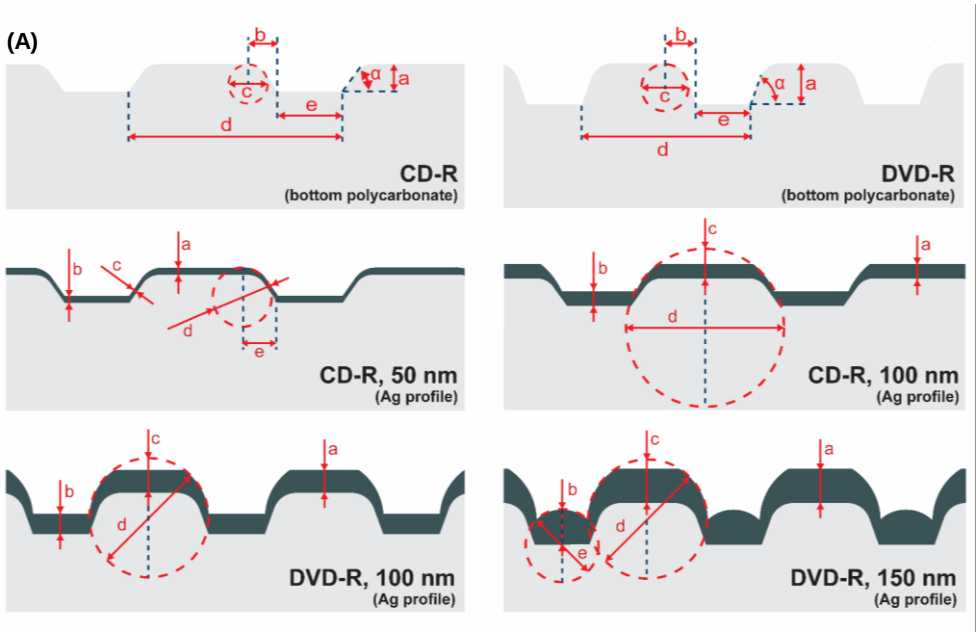

(B)

	bottom polycarbonate struct.		silver profile			
	CD-R	**DVD-R**	**CD-R, 50 nm**	**CD-R, 100 nm**	**DVD-R, 100 nm**	**DVD-R, 150 nm**
a (nm)	203 ± 7	175 ± 6	53 ± 5	110 ± 6	99 ± 5	145 ± 13
b (nm)	230 ± 20	107 ± 10	48 ± 7	108 ± 9	87 ± 9	147 ± 4
c (nm)	290 ± 20	199 ± 9	30 ± 5	235 ± 10	143 ± 9	182 ± 7
d (nm)	1600 [a]	740 [a]	260 ± 30	1130 ± 40	500 ± 17	517 ± 8
e (nm)	489 ± 6	240 ± 80	220 ± 20	-	-	330 ± 20
α (deg)	59 ± 3	76 ± 4	-	-	-	-

[a] Reference values.

Fig. S9. (A) Schemes of the bottom polycarbonate structures and the silver thickness profiles in the optimal substrates and (B) the corresponding sizes experimentally determined from FIB-FESEM scans. Light and darker gray shapes represent polycarbonate and silver, respectively. The resulting dimensions were determined by averaging six scans from different areas.

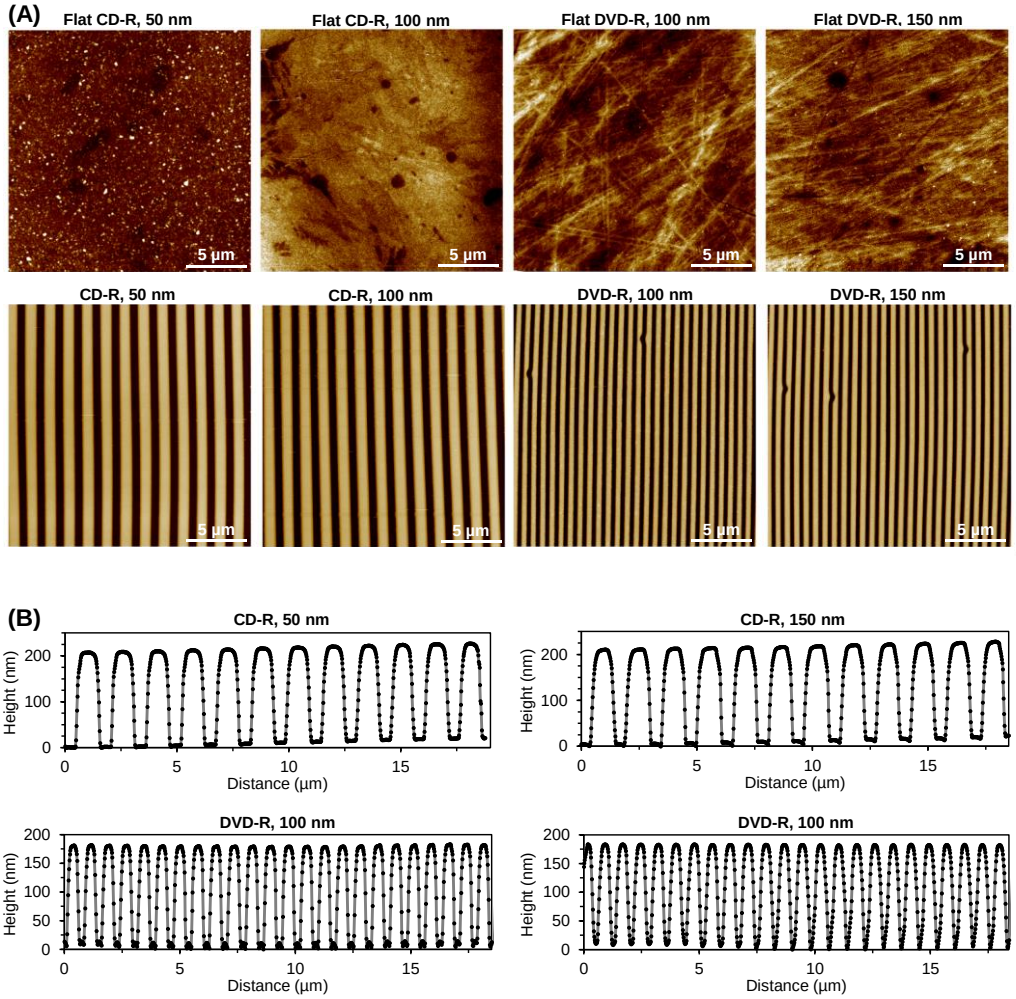

Fig. S10. AFM scans (20x20 µm) of the optimal structures and their flat analogues. (A) Images and (B) the corresponding averaged cross section profiles for the structured substrates.

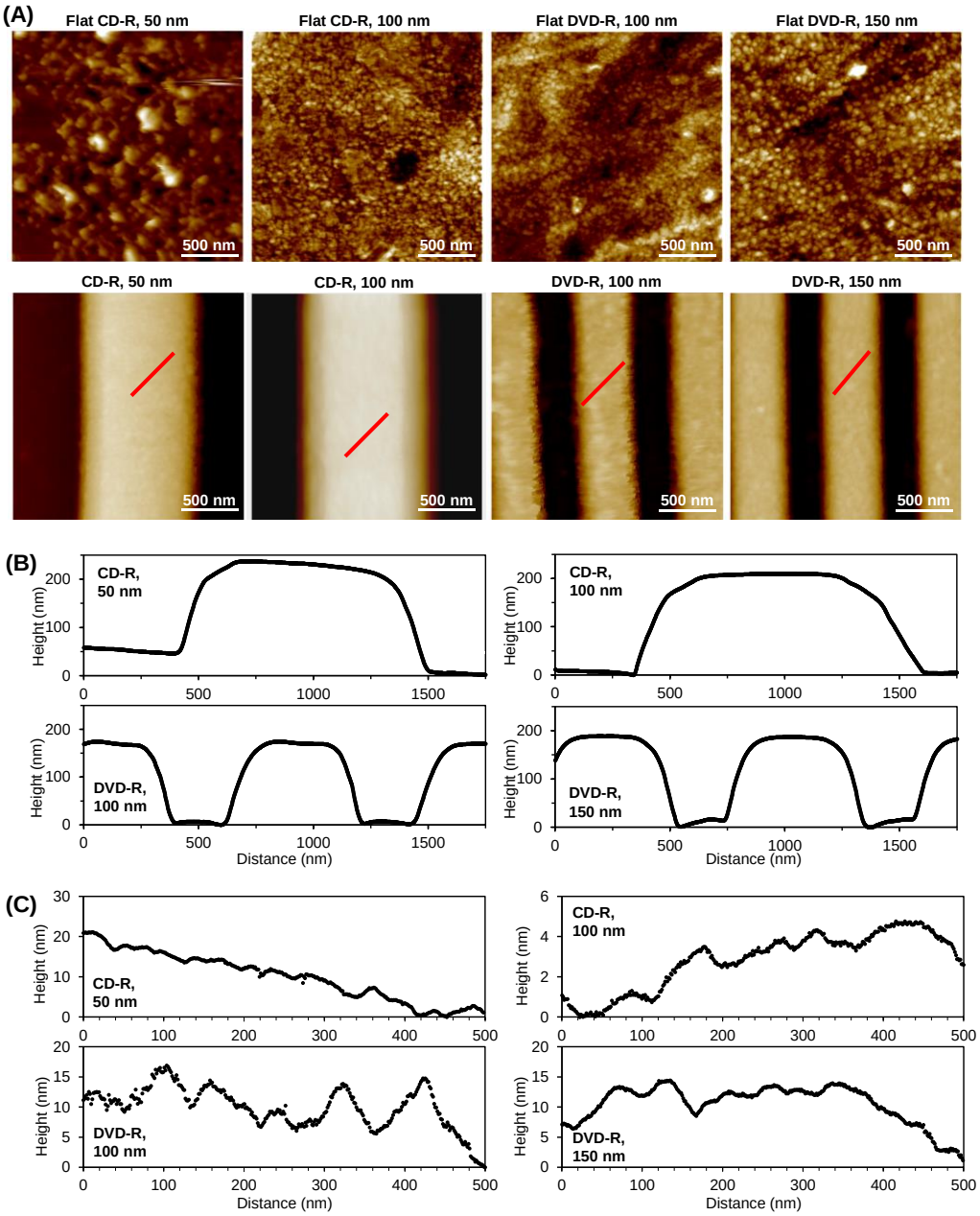

Fig. S11. AFM scans (2x2 µm) of the optimal structures and their flat analogues. (A) Images and (B) the corresponding averaged cross section profiles for the structured substrates. (C) Cross sections (red lines in Fig. S11A) to show the clustered topography.

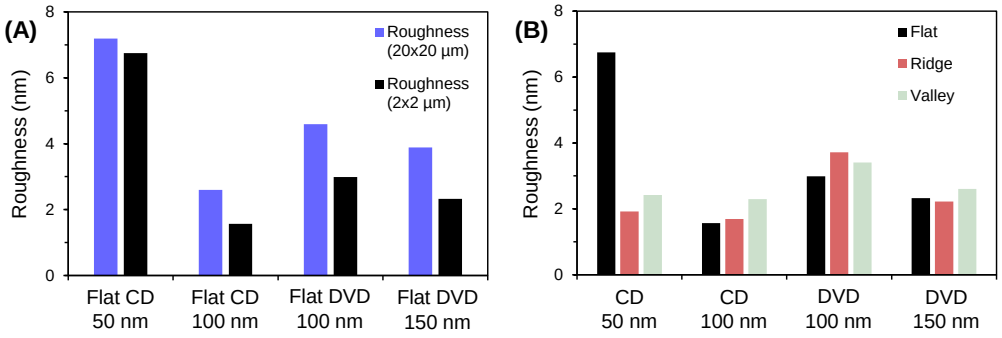

Fig. S12. Roughness results from AFM data. (A) Comparative roughness of different scan sizes in flat substrates. Higher values in larger scans must be generated by plane deformations artifacts. (B) Roughness results of the ridge and valley areas, and the corresponding flat analogue of the optimal structures (from 2x2 µm scans).

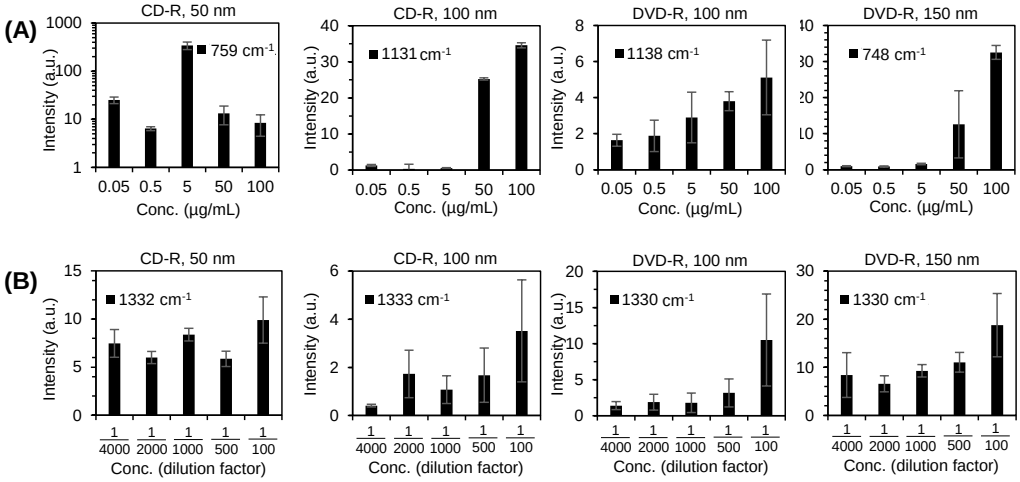

Fig. S13. Raman peak intensity versus concentration of (A) hemoglobin and (B) exosomes, using the optimal substrates for λ_{exc} = 633 (CD-R, 100 nm; DVD-R, 100 nm) and λ_{exc} = 785 nm (CD-R, 50 nm; DVD-R, 150 nm).

3.3.3 Conclusions

Active SERS substrates, with tunable plasmonic behavior and significant Raman enhancement, can be easily fabricated by metallizing with silver the track nanostructure contained in CD-R and DVD-R polycarbonate plates. The bioanalytical possibilities of these materials have been demonstrated by obtaining the Raman fingerprint of hemoglobin and exosomes in label-free conditions. This strategy introduces an inexpensive and large-scale alternative to the SERS substrates created by classical nanofabrication methods.

Besides SERS substrates, this study also provides insights into the development of Raman microscope units based on regular drives, specific for scanning these SERS-active disk platforms. Regular disk drives are designed to automatically focus on the disks and scan their whole surface, and pickup units share many features with the optical setups used in Raman microscopes. Given that the substrates herein introduced entail strong physicochemical modifications of the disk (i.e., modifying the original layered structure and coating with silver), TED technology entails particular suitability for this final goal. It must be noted that the CD-R disks used as structured plates in this study are TED5 platforms described in the first chapter. Regarding DVD-R structured plates, they could be obtained from TED2, keeping their native control feature zone or attaching another one in the center of the disk, in order to be scanned by TED drives.

It is also worth highlighting that the excitation wavelengths employed in this work (633 and 785 nm) are significantly close to the ones of the lasers integrated in regular disk drives (650 and 780 nm), which also supports the potential success of the suggested approach. Important hardware modifications, such as integrating additional spectrophotometer units for the detection, would be required to develop this device. Though challenging, this study can constitute the first step of a long-term project for conceiving inexpensive, robust, and compact systems that synergistically exploit, for the first time, the strengths of biosensors and consumer electronics to bring SERS to point-of-need scenarios.

Chapter 4

3.4 Diffraction-based sensing disk biosensors

3.4.1 Introduction

As commented in section 1.4, label-free strategies involve important strengths for biosensing, whereas also tend to present several restricting features that strongly limit their scope, especially for point-of-need developments. Motivated by this issue and grounded on the previous findings in this thesis, herein we aim to conceive label-free biosensors based on consumer electronics for high-throughput multiplexed analysis. For that, we propose the integration of diffractive bioreceptor gratings (biogratings) in compact disk systems in order to sense biointeraction by means of diffraction-based sensing (DBS).

The first part of this chapter (section 3.4.2) addresses a comprehensive experimental assessment of the DBS capabilities for measuring binding events. This study aims to provide the basis and the knowledge for the subsequent introduction, in disk-based sensor systems, of this detection technique together with microcontact printing (μCP) to fabricate biogratings. Also, from a general viewpoint, this work also seeks to establish DBS in the biosensing scenario by proving and discussing its potential through experimental results and particular applications.

In the second part (section 3.4.2), the development of compact disk DBS biosensors for measuring unlabeled immunoassays is addressed. For that, the transparency of TED5 platforms as well as the versatility of TED drives offers interesting possibilities to scan arrays of biogratings by transmission measurements. Furthermore, the track microstructures of CD-R disks act as diffraction gratings for visible light, and herein we also project to use the structured side of TED5 disks as a low-cost and large-scale starting material to create and replicate optically active protein biogratings on disks. Therefore, this approach aims to make the most of consumer electronics to conceive inexpensive and industrially scalable biosensors that bring the advantages of label-free biosensing to non-specialized settings.

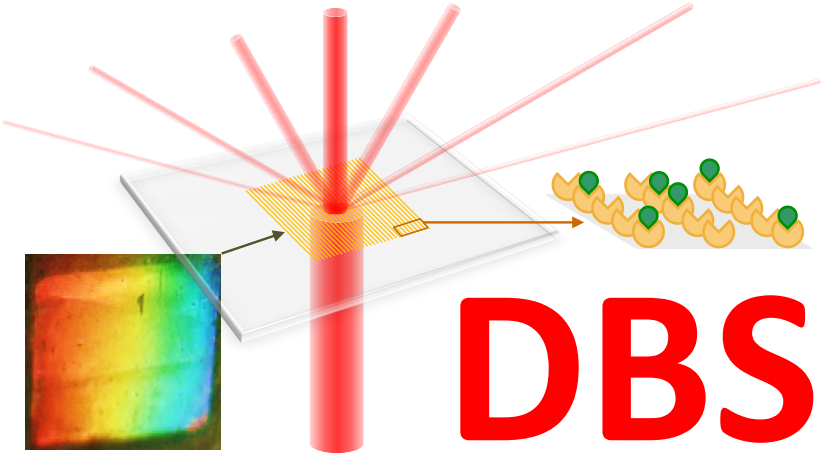

3.4.2 Diffraction-based sensing with biogratings for qualitative and quantitative analytical applications

Anal. Chim. Acta, In revision (**2017**).

ABSTRACT

Diffraction-based sensing (DBS) is a powerful technique for analyzing molecular-scale processes. Trough measuring the diffractive response of gratings constituted by biological materials, DBS allows monitoring biorecognition events in label-free and real-time conditions, among many other particular bioanalytical features. Herein we present a detailed description of this technique, address a comprehensive experimental assessment of its sensing possibilities, empirically demonstrate its performance in biorecognition systems, and discuss its scope. The keys for implementing diffraction-based sensing are provided in this work, to serve as a practical reference guide for stimulating new advances in biochemical sensing. In addition, this study also describes the development of a DBS immunosensor for low-molecular-weight organic compounds and discusses its bioanalytical capabilities. In particular, this approach have been arranged for the analysis of atrazine residues in water by implementing a protein-hapten conjugate-based displacement immunoassay in a DBS setup, reaching a detection limit of 1.1 ng mL^{-1} of atrazine in label-free conditions.

Keywords: biograting, diffraction-based sensing, atrazine, label-free microcontact printing, displacement immunoassay.

1. Introduction

The convergence of molecular sensing with nanoscience and nanotechnology has given rise to a range of measurement techniques that use different nanoscale phenomena for biosensing [1, 2]. These systems typically exhibit label-free capabilities that enhance their analytical scope, for instance by improving the reliability of the results and by simplifying the analytical procedure [3, 4].

Herein we focus on diffraction-based sensing (DBS), an optical technique that exploits light diffraction to monitor molecular recognition events. DBS is grounded on patterning onto solid supports materials sensitive to a variable of interest, according to a grating structure designed to diffract an incident beam (Fig. 1A). When this variable changes, the optical properties (refractive index, absorption, etc.) of the grating material change too, which affects the diffraction efficiency of the grating. Hence the variable of interest can be analyzed by means of the intensity of the diffracted orders.

DBS and its bioanalytical implementation were firstly introduced in the scientific literature by Tsay and coworkers [5], and then further explored mainly by the Goh's lab and more recently by Wang *et al* [6-9]. Along these lines, Axela Inc. has introduced important advances by

commercializing its dotLab™ System, an integrated benchtop device for automatically running routine binding assays in a particular DBS configuration [10, 11].

To analyze biorecognition events by DBS, biological probes (proteins, antibodies, nucleic acids, etc.) must be used as sensitive materials to build the diffractive gratings, as depicted in Fig. 1. Then, samples interact with these grating and target molecules bind the immobilized probes, thus modifying the amount of matter that constitutes the grating, which changes its diffraction efficiency. As a result, molecular-scale events can be sensed by measuring the intensity of the diffracted light.

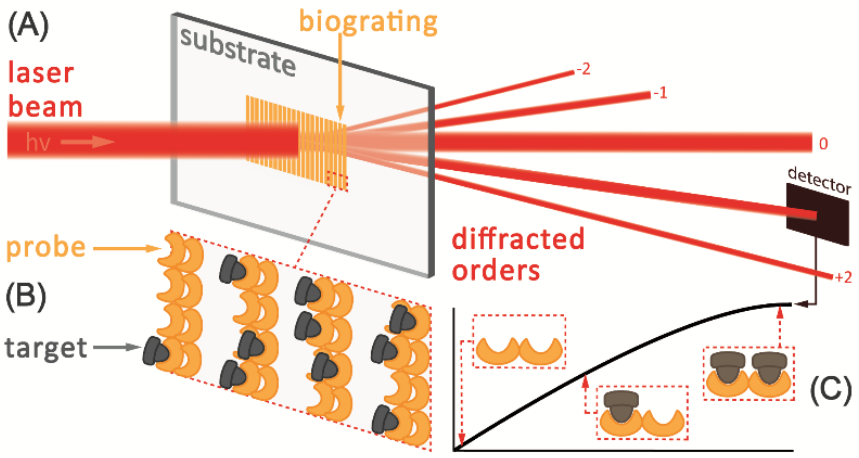

Fig. 1. Scheme of diffraction-based sensing at (A) macroscopic and (B) microscopic scale. (C) Exemplary real-time monitoring of a recognition event.

Unlike most nanostructured bioanalytical systems [1, 4, 12, 13], DBS entails diffractive gratings constituted by biomaterials patterned on plain solid substrate, without further pre-patterned supports (Fig. 1B). This kind of structures allow for conceiving particular transduction systems in which the analytical signal only depends on the state of the bioreceptor, but not on the structuration of the substrate. Herein we employ the term “biograting” to denote these biomolecular networks [14].

Microcontact printing (µCP) is an appealing technique to produce biogratings for DBS [15, 16]. The simplicity, inexpensiveness, and versatility of this approach offset its moderate reproducibility [17]. Furthermore, once obtained the masters, countless biogratings can be easily produced without requiring nanofabrication facilities.

This paper comprises two parts. First, a comprehensive experimental comparative assessment of the different bioanalytical possibilities offered by DBS is presented. This technique entails a range of setups and configurations, and their control lead to particular sensing strengths, such as real-time and label-free analysis. Note that this comparative assessment covers some particular configurations previously reported. However, a general study that explores, discusses, and experimentally demonstrates the biosensing features of DBS, as well as many particular items within this assessment, have never been reported. Herein we address central aspects of DBS in order to provide the keys for fully exploiting it and stimulate future advances.

Second, this study uses the knowledge presented in the previous part to introduce, for the first time, the development of effective DBS immunosensors for quantifying low-molecular-weight organic compounds. Promising attempts in this direction have been previously reported using diffractive gratings constituted by stimuli-responsive hydrogels (for glucose sensing) [18, 19] and molecularly imprinted polymers (for 2,4-D and enrofloxacin analysis) [9, 20]. These approaches provide good solutions for particular applications, but present rather moderate sensitivity (estimated detection limits from 14 to 60 µM) and selectivity (especially in hydrogels). Herein, we present a sensitive DBS label-free biosensor for atrazine based on a displacement immunoassay. Atrazine is one of the most used pesticides in the world, banned in Europe from 2004 and widely employed in many other areas nowadays, especially in the US [21-23]. This is a highly persistent contaminant in water, atmosphere, and soil [23, 24], and entails important human´s health and ecotoxicological implications [24, 25]. Moreover, besides atrazine, this approach also aims to prove the concept for exploiting DBS and displacement immunoassays in other scenarios.

2. Experimental section

2.1 Materials

Buffer solutions employed in this study, sodium phosphate buffer (PBS, 8 mM Na_2HPO_4, 2 mM KH_2PO_4, 137 mM NaCl, 2.7 mM KCl, pH 7.4), PBS-tau (PBS containing taurine 0.1 M), and PBS-TT (PBS-tau with polysorbate 20 0.05% v/v), were prepared with purified water (Milli-Q, Millipore Iberica, Madrid, Spain). Polydimethylsiloxane (PDMS) Sylgard 184 was from Dow Corning (Wiesbaden, Germany). Bovine serum albumin, gelatin, hemoglobin, polysorbate 20 (Tween 20), taurine, anti-BSA rabbit IgGs, goat anti-rabbit IgGs labelled with 5 nm colloidal gold nanoparticles, silver enhancer solutions, and allyl trimethoxysilane were supplied by Sigma-Aldrich (Madrid, Spain). Atrazine was from Riedel-de Haën (Seelze-Hannover, Germany) and Casein from Merck (Madrid, Spain). Polycarbonate substrates were created from regular LightScribe compact disks (MediaRange, MPO Iberica, Madrid, Spain) as described elsewhere [26]. Gold substrates were obtained by sputtering a 50 nm thick layer of metal on

polycarbonate chips. Glass slides were purchased from Labbox (Mataró, Spain), polystyrene slides were from Evergreen (Ted Pella Inc., Redding, CA, USA), and polymethyl methacrylate and polyester substrates were kindly supplied by Plexi (Valencia, Spain). Atrazine protein-hapten conjugates were synthetized and anti-atrazine antibodies obtained by immunization, as described elsewhere [27].

2.2 Setup

The diffraction measurements were experimentally performed with custom optomechanical setups (Fig. S1), using a collimated 650 nm diode laser as light source (LDM650/5LJ, Roithner Lasertechnik GmbH, Vienna, Austria) and a monochromatic CMOS camera as detector (Edmund eo-1312m, York, UK).

Normal (0 degrees) and tilted (80 degrees) irradiations, with respect to the substrate surface, were selected for transmission and external reflection measurements, respectively. For total internal reflection, glicerol was added between substrates and prism as index matching agent. The intensity of the fifth diffraction order was measured and used as analytical signal in all the configurations described in this work. Custom gaskets were attached on the substrates in order to incubate solutions on biogratings created on hydrophilic surfaces (Fig. S1 and S2).

Atomic force microscopy (AFM) scans were performed by noncontact mode in air using a Multimode 8 microscope (Bruker) and RFESPA probes (MPP-21120-10, Bruker). Nanoscope software was used for the analysis, and first order polynomial flatten was applied to the data.

2.3 Methods

Polymeric diffractive lenses containing a binary grating of parallel lines (Fig. S3A) were used as masters to create the stamps for μCP. PDMS was poured on the grating side of the master, degassed 30 min by vacuum, and polymerized overnight at 60 ºC. PDMS stamps were peeled off and cut in 4x4 mm squared pieces. Prior to their use, stamps and substrates were sonicated 5 min in ethanol (30% in water) and dried under a stream of air.

Probe solutions (50 μL) were placed on the grating side of the stamps for inking during a given time (inking time). Afterwards, stamps were rinsed with water and dried under a stream of air. Then, the grating side of the stamps was placed in contact with the substrate surface, slight pressure was initially applied on the opposite side to favour the contact, and probes were left to transfer during a given time (stamping time). Finally, stamps were removed and the resulting biogratings rinsed and dried as before. Stamps were washed 3 times by sonication (5 min, ethanol 30% in water) and stored in this ethanolic solution to be reused.

Solutions (50 µL) were incubated on the biogratings at room temperature (about 25 ºC) in a humidified environment (to prevent evaporation). For endpoint measurements, the biogratings were rinsed and dried as before after each incubation. In real-time analysis, solutions were dispensed on small and known volumes of pre-dispensed buffer on the biogratings, in order to keep the hydration state of the patterned biomaterials.

A molecular recognition model system based BSA as probe and rabbit anti-BSA IgG as target was employed in the comparative experimental assessment (sections 3.1-3.6). PBS-tau was used to improve the IgGs stability [28]. Concentrations of 1000 µg mL^{-1} for proteins and 0.05% (v/v) for polysorbate 20 in PBS-tau were used for blocking, and a dilution factor of 1/50 for incubations of labelled antibodies.

Glass functionalizations were carried out by immersing slides in allyltrimethoxysilane (2% v/v in toluene, 2 hours, orbital agitation). Then, the slides were rinsed with toluene, dried by air, cured (110 ºC, 30 min), and the silanization was monitored by contact angle measurements (Fig. S2).

For atrazine displacement immunoassay (section 3.7), biogratings of protein-hapten conjugates were created on glass, and atrazine and antibody (1/50 dilution factor) solutions in PBS-TT were dispensed on them. The detection limits of this system were calculated as the analyte concentration associated to a 10% displacement, inferred from the sigmoidal regression of experimental dose-response curves [29].

3. Results and discussion

3.1 Biogratings development and characterization

A biorecognition model system based on bovine serum albumin (BSA) as probe and anti-BSA rabbit IgGs as target was used for this experimental comparative assessment. Protein probes were patterned on solid substrates by µCP according to a grating structure that distribute diffraction efficiencies mainly in 3 orders (Fig. S3). In this section, the behavior of these biogratings on glass substrates was studied through protein adsorption isotherms. Three key variables were addressed: inking time, stamping time, and protein concentration in the inking solution.

First, the diffraction intensity of protein gratings obtained by different inking times was measured to investigate this variable (Fig. 2A). Considering preliminary results (Fig. S4), experimental conditions to ensure high protein transfer were selected. The kinetics of inking is hindered by the moderate affinity of the protein for the elastomer used for the stamps (PDMS). This intermediate affinity must be high enough to enable probe adsorption from solution during inking, and lower than the one of the substrate to ensure the subsequent protein transfer. Then, stamping was studied by the same strategy. The stamping kinetics is favored by the higher

protein affinity for the substrate and hindered by the solid-state nature of this process, but behaves much faster than inking (Fig. 2B). Finally, the probe concentration in the inking solution was also studied as before, which displayed the expected response for a protein adsorption isotherm (Fig. 2C). As shown in Fig. 2A-2C, all the curves presented an exponential behavior. From all these results, an inking time of 160 min, 20 min for stamping time, and a protein concentration in the inking solution of 250 µg mL^{-1} were selected as optimal biograting fabrication conditions for the subsequent experiments.

Surface mappings of biogratings from different protein concentrations were studied by AFM. Although flatter substrate surfaces at the nanoscale would favor the topographic characterization, consistent results were obtained by averaged cross section profiles (Fig. S6). As shown in Fig. 2D, the topographic measurements clearly reveal the biogratings' structure. The dependence between grating height and protein concentration fitted an exponential curve that reached a maximal height of 3.5 nm at 1000 µg mL^{-1} of BSA (Fig. S7).

Only a small proportion of the proteins in the inking solution becomes finally patterned by µCP [30]. In this study, we observed that optimal biograting fabrications consumed negligible BSA concentrations. Therefore, the practical efficiency of this approach can be easily improved by just reusing the inking solution.

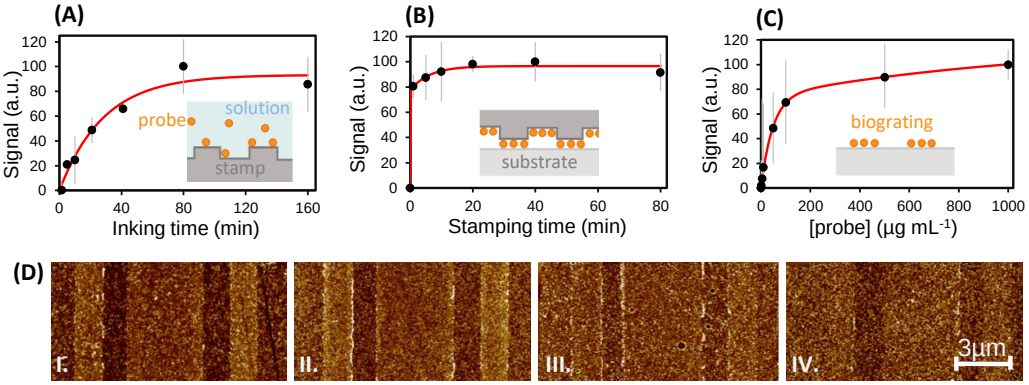

Fig. 2. Experimental assessment of the biograting fabrication variables: (A) inking time ([probe] = 100 µg mL^{-1}, $t_{stamping}$ = 60 min), (B) stamping time ([probe] = 100 µg mL^{-1}, t_{inking} = 160 min), and (C) probe concentration (t_{inking} = 160 min, $t_{stamping}$ = 25 min). Data recorded by transmission (see Fig. S5 for other configurations) and experimental curves fitted to an exponential (rise to maximum, 5 parameters) equation ($R^2_{ink.}$= 0.963, $R^2_{stamp.}$= 0.994, and $R^2_{[prot]}$= 0.999). Inset images are schematic illustrations of the corresponding µCP stages at microscopic scale. Normalized signal in the vertical axes. (D) AFM data of probe gratings using (I) 1000, (II) 100, (III) 10, and (IV) 1 µg mL^{-1} of probe protein in the inking solution.

3.2 Detection setups

The experimental setups for diffraction-based sensing must enable light to efficiently interact with the biogratings and to project an output diffraction pattern that favor the measurement of the diffracted orders. Different detection configurations are compatible: transmission, external reflection, and total internal reflection (TIR).

In the transmission arrangement, the substrate is positioned between the light source and the detector, the laser beam goes through the substrate and interacts with the biograting, and the outgoing diffracted pattern is monitored (Fig. 3A). For external reflection, the incident laser beam hits the substrate, interacts with the biograting, and the reflected diffracted pattern is measured (Fig. 3B). In TIR, the laser beam hits the substrate at an incident angle that meets the total internal reflection condition at the interface that contains the biograting. Then, light interacts with the grating by means of evanescent waves, the diffraction pattern is reflected, and its intensity is monitored (Fig. 3C). It must be noted that substrate materials compatible with transmission and TIR setups must be transparent at the employed light wavelength.

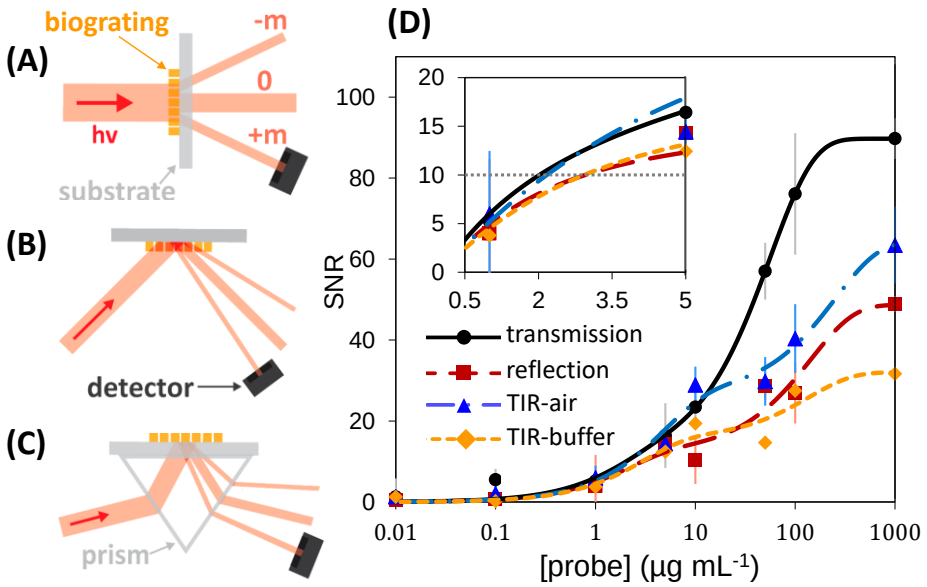

Fig. 3. Schemes of the detection setups: (A) transmission, (B) external reflection, and (C) TIR. (D) Experimental results of the protein adsorption isotherms measured by the different detection setups. The graph inset zooms in on the quantification limit area. The standard deviations of ten blank gratings (0 µg mL^{-1} of probe) were used as noise values to calculate SNR. Experimental data fit exponential equations (rise to maximum 4 parameter, $R^2_{trans.}$= 0.996, $R^2_{reflec.}$= 0.967, $R^2_{TIR-air}$= 0.982, and $R^2_{TIR-buffer}$= 0.947). Real images of the setups in Fig. S1.

According to experimental results and Fresnel conditions, the reflection/transmission intensities ratio in all these detection setups greatly depends on the incidence angle of the laser beam (Fig. S8). Maximal sensitivity is reached with an orthogonal laser incidence for transmission measurements, while high angles (close to 90 degrees) should be selected for external reflection. Besides, TIR requires angles that generate total internal reflection at the interface that contains the biograting. When considering Snell's law, experimentally impracticable angles (above 90 degrees) should be applied with air or aqueous solutions in this interface. Thus, coupling a prism to the substrate solves this problem and provides a simple TIR setup (Fig. 3C).

Transmission, external reflection, and TIR without (TIR-air) and with buffer (TIR-buffer) on the biograting were experimentally compared. Adsorption isotherms from an array of protein concentrations were obtained and their sensitivity determined by signal-to-noise ratios (SNR). As shown in Fig. 3D, similar quantification limits (SNR = 10) were accomplished for all the configurations, about 2.5 µg mL^{-1} for this model system. Besides, a greater signal variation vs. probe concentration was displayed with the transmission setup, TIR-buffer presented a lower curve slope, and the external reflection and TIR-air setups showed an intermediate behavior.

3.3 Signal acquisition strategy

DBS enables both the endpoint and real-time measurements. Endpoint measurements provide discrete results after the probe-target interaction, which is particularly handy for high-throughput systems designed to quantify target concentrations in samples. On the other hand, real-time measurements provide dynamic information about the interactions that take place between the immobilized probe and the target. The TIR configuration is particularly suitable for real-time measurements, since the exponential decay of the evanescent field confines light at the interface that contains the grating and restricts its interaction with the bulk of the sample [7]. So even if samples are kept on the biograting during the measurements, the effect of potential interferences from their interaction with the laser (absorption, scattering, etc.) is minimal.

Endpoint and real-time approaches were experimentally compared by measuring the probe-target recognition over time. As shown in Fig. 4, overlapped curves and comparable signal levels and standard deviations (SD) were obtained. Therefore, endpoint and real-time can be indistinctly valued in terms of analytical performance, while the nature of the information provided by each approach must be considered to select the most suitable working format.

Beyond target quantifications, DBS real-time measurements may provide new perspectives to investigate the molecular-scale reality of recognition events (interaction mechanisms, conformational changes, affinity parameters, etc.) [31]. For instance, kinetic data obtained from

DBS monitoring could be employed to explore and optimize biorecognition events for the rational design of biosensors [32].

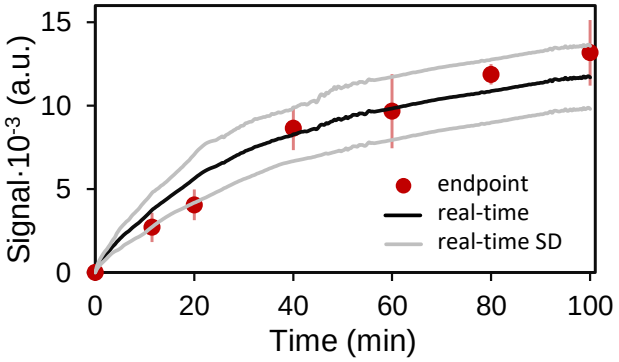

Fig. 4. Experimental assessment of endpoint and real-time measurements. In both cases, TIR-buffer assays were taken with 10 µg mL^{-1} of target.

3.4 Blocking and stabilization

The diffraction response strongly depends on the state of the interface that contains the biograting. Modifications (e.g., solution additions and blocking events) have major effects on the system. This section characterizes the nature of these processes in order to understand and control them.

Adding aqueous solutions to dry protein gratings causes an abrupt signal decay, followed by exponential stabilization (Fig. S9). This phenomenon can be explained by the greater refractive index (RI) difference between proteins and air, compared to proteins and water ($RI_{proteins} \approx 1.4$, $RI_{air} \approx 1$, $RI_{water} \approx 1.3$). Therefore, adding aqueous solutions reduce the RI contrast between protein and gap strips in the biogratings, which decreases diffraction efficiency. Besides, the substrate surface and the immobilized probes may be susceptible to solvation, which might lead to significant conformational changes and affect the diffracted efficiency too. In the model system under study, 10 min solvation ensures enough stability for subsequent steps (Fig. S9).

Once stabilized, biogratings must be blocked to prevent non-specific adsorptions. Blocking agents in DBS bind available active sites of the substrate surface, mainly in biograting gaps, but also in probe areas. Thus background-free responses can be obtained by using blocking agents with similar properties to probes.

Different proteins (hemoglobin, BSA, gelatin, and casein) and a surfactant (polysorbate 20) were studied as blocking agents. Firstly, it was experimentally demonstrated that blocking allows to achieve this system's maximal performance, as shown in Fig. 5A. More than 2- and 5-fold signal

increases were obtained when performing recognition after blocking with hemoglobin and polysorbate 20, respectively.

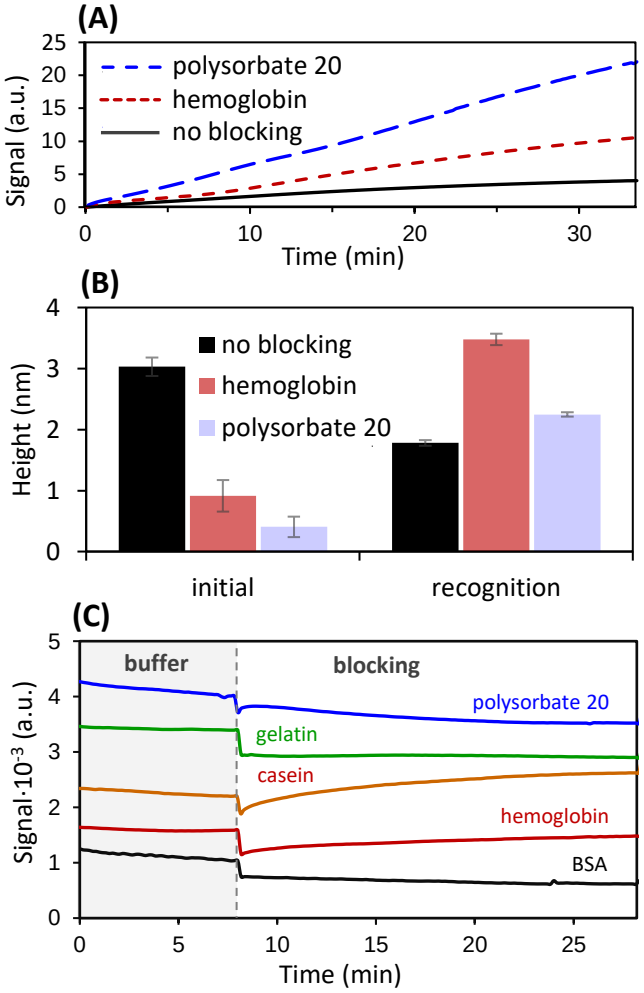

Fig. 5. Blocking and stabilization results. (A) Real-time recognition curves with and without blocking agents. (B) Grating height displayed by AFM (Fig. S10) for the studied blocking and target recognition. (C) Real-time curves for stabilization (buffer) and blocking stages, using different blocking agents.

At microscopic scale, it was observed that the relative height of the probe strips compared to gaps was much shorter for blocked biogratings (Fig. 5B), which indicates selective adsorption of blocking agents in the gaps. After target recognition, height increased in blocked biogratings but decreased in non-blocked conditions. This fact points out significant target adsorptions on unblocked gaps and selective target binding in the probe strips of blocked biogratings.

The behavior of the blocking agents in this system was also studied by real-time measurements. As shown in Fig. 5C, adding blocking solutions initially lead to sharpened diffraction efficiency

decreases. This effect could be related with the lower RI contrast when blocking agents adsorb in the biograting gaps, and also with the higher RI of the solutions that contain blocking agents compared with plain buffer.

Different trends were observed after this initial sharpened reduction (Fig. 5C). BSA and gelatin kept a stable signal level, while hemoglobin and casein initiated an exponential diffraction efficiency raise. Diverse processes related with the nature of the proteins in interfaces might be involved in this non-systematic phenomenon (adsorption kinetics, aggregation, solvation, conformational changes, etc.). Polysorbate 20 described a simple signal diminution, which we attribute to its rapid adsorption and stabilization at the interface.

From these results, polysorbate 20 was selected as the blocking agent for the following studies. Moreover, it was experimentally observed that individual blocking agent incubations can be skipped by including this surfactant in the target matrix (Fig. S11).

3.5 Biogratings on different materials

The substrate material that supports the grating is a key aspect when conceiving a DBS sensor system. Good substrates for µCP must be flat enough and have a suitable composition to favor maximal and homogeneous probe transference during stamping.

Different substrate material for DBS were experimentally studied and compared. Glass is the most representative substrate for µCP, and functionalized glass (with allyltrimethoxysilane) introduces interesting options for covalent probe attaching and surface properties modulation. Polystyrene is a well-known material for biosensing and polycarbonate is also interesting thanks to its good immobilization features and its compatibility with lab-on-a-disk biosensor [26]. Polymethyl methacrylate and polyester were selected as synthetic polymers for broadening the scope of this comparison.

Gold substrates were investigated too. This material comprises well-known probe immobilization capabilities and suggests appealing approaches for coupling DBS with other biosensing techniques using this substrate material (e.g., SPR and QCM) [33]. Obtaining real-time data simultaneously from different coupled sources could provide an interesting synergy to elucidate molecular-scale biointeraction processes.

Recognition curves with an array of target concentrations were studied for all these substrates. As Fig. 6 shows, target concentrations of at least 0.5 µg mL^{-1} were sensed with all of them. The studied polymers showed similar curve slopes to glass, while functionalized glass and gold presented slightly higher slopes. Greater precision was obtained with glass, since the optimized conditions for this material were used in this experiment. Specific optimization for each substrate

should be considered for a quantitative comparison, whereas this study provides a qualitative assessment and demonstrate the substrates' versatility of DBS.

3.6 Labelling and signal developing

In addition to label-free detection, DBS is also compatible with assays using labels and signal developers. Herein, secondary antibodies conjugated to gold nanoparticles (Ab-Au) as labels and silver precipitation (Ag) as signal developing were studied. As shown in Fig. 7A, the label-free target recognition curve presented the expected response, and the Ab-Au recognition displayed equivalent kinetic behavior, but doubled the maximal signal. Silver precipitation underwent a sudden diffraction efficiency rise that reached a 15-fold enhancement after 20 min of reaction. Along these lines, it is worth noting that other labels and signal-developing systems could lead to different behaviors (Fig. S12).

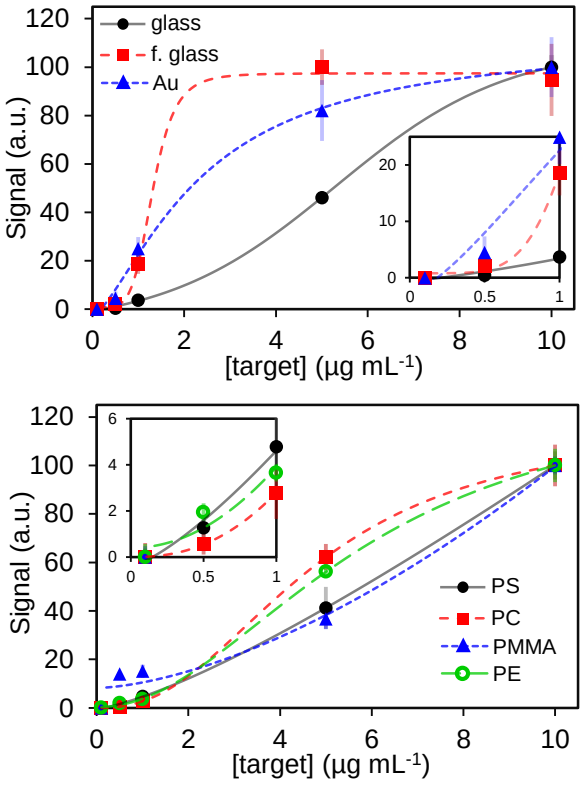

Fig. 6. Experimental endpoint data and sigmoidal regressions (logistic 4 parameters) for target recognition curves with biogratings fabricated on glass (R^2 = 0.9999), functionalized glass (f. glass, R^2 = 0.9984), gold (Au, R^2 = 0.9979), polystyrene (PS, R^2 = 1), polycarbonate (PC, R^2 = 1), polymethyl methacrylate (PMMA, R^2 = 0.9812), and polyester (PE, R^2 = 0.9999). Gold substrates were measured by external reflection, and the other materials by transmission. Vertical axes display normalized signals.

As an additional sensitivities assessment, dose-response curves for an array of target concentrations were compared. The results (Fig. 7B) showed that a target concentration of at

least 0.1 µg mL^{-1} was sensed in label-free conditions. Gold nanoparticles labelling and silver enhancement presented significantly higher sensitivities, reaching increases of three (0.1 ng mL^{-1}) and four (10 fg mL^{-1}) orders of magnitude, respectively.

Interesting results were also obtained from the topographic measurements. As shown in Fig. 7C (see also Fig. S13), the biograting height decreased after the recognition stages with targets (including blocking) and labelled antibodies, whereas diffraction efficiency increases were measured for these stages. Therefore, an intuitive explanatory model, involving ordered growth of biomacromolecules in the probe strips during the recognition stages, would presumably not accurately explain the molecular reality of this system. These results suggest a more complex model, in which recognition processes lead to conformational changes that reduce the biograting height while increase its diffraction efficiency (thus involving denser protein layers), but this hypothesis should be confirmed.

Regarding signal enhancement, chaotic or three-dimensional silver growth would modify the biograting structure and strongly affect diffraction efficiency. However, selective and ordered silver precipitation in the probe strips was achieved for short reaction times, which generated sharpened metallic structures (Fig. 7C and S13). A progressive diffraction efficiency decrease was observed for long reaction times (Fig. 7A and S14) and high concentrations (Fig. 7B), which suggests that strong signal developing conditions caused non-specific silver precipitation that modify the biograting structure.

As shown in Fig. 7D, silver precipitation turns biogratings into metallic structures that strongly diffract white light. This metallization enables to easily confirm the proper fabrication of biogratings and could also be used to spectroscopically characterize their features. Moreover, instead of collecting the intensity of diffracted monochromatic beams, this fact suggests DBS approaches based on measuring color variations.

3.7 Atrazine DBS immunosensor

This section part makes the most of the previous studies reported in this paper to address the development of a label-free DBS immunosensor for atrazine (Atz) sensing. The recognition of low-molecular-weight compounds (such as Atz) by immobilized antibodies leads to rather negligible changes in the amount of matter on the sensing surface. Also, small organic compounds can not simultaneously bind two antibodies, so sandwich immunoassays are not suitable and competitive formats must be implemented. Herein a displacement immunoassay, using protein-hapten conjugates as patterned probes, have been developed to sense Atz by DBS. For that, biogratings constituted by BSA-hapten conjugates were fabricated according to the optimal conditions previously reported in this work, since the probe adsorption is mediated by

BSA in both cases. Then, antibodies against Atz were incubated on the biogratings to bind the immobilized haptens until saturation. Once antibodies are loaded, free Atz in samples competes with immobilized haptens for the binding sites of the antibodies, thus displacing them from the biogratings to the solution. Therefore, Atz additions lead to significant changes in the matter constituting the biogratings, which is transduced as a diffraction efficiency decrease.

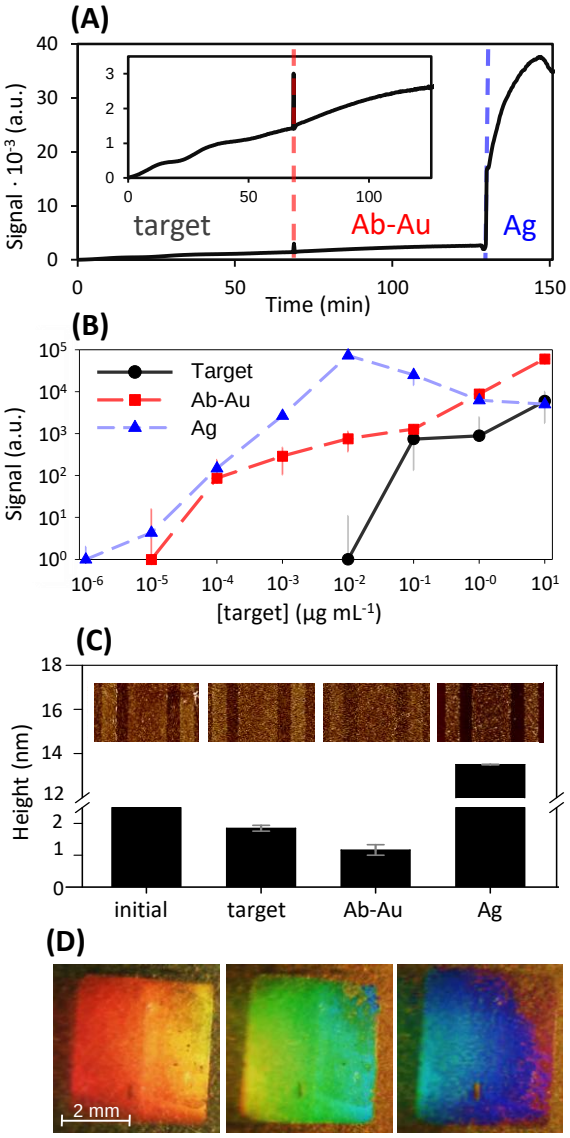

Fig. 7. Results for labelling and signal developing. (A) Real-time curve for target recognition (1 µg mL^{-1}), Ab-Au recognition, and silver precipitation enhancement. (B) Sensitivity comparison of label-free, gold labelling, and signal development (endpoint transmission measurements). (C) Biograting heights at the different assay stages, and the corresponding AFM scans. (D) Images of a BSA biograting on glass, with Ab-Au recognition and silver enhancement, diffracting white light at different angles.

First, a screening study for a set of Atz bioreagents was experimentally performed. In displacement immunoassays, the affinity of free antibodies against immobilized haptens must be good enough to enable high antibody loading, but lower than the one for the analyte in order to generate great displacements that favor sensitive analysis. Considering the results of this screening (Table S1), the conjugate BSA-2a and the antibody KLH-2d (IV) were selected, because this combination led to the highest displacement for Atz additions.

The kinetic behavior of the system was studied by real-time measurements in TIR-buffer configuration (Fig. S15). Since the antibody was selected to have a moderate affinity for the hapten (compared to the one for Atz), its loading on the biograting involves slow kinetics. Overnight incubations (16 hours) were selected to load the antibody on the biograting, which corresponds to a 91.4 % of its equilibrium state, according to the regression equation.

The antibody displacement by free Atz in solution also entails slow kinetics (Fig. S15). It must be took into account that diffusion is the unique mass transport phenomena comprised in this system, so these values represent upper limits for the kinetics. Obviously, faster responses would be achieved by just introducing convection in the incubations (stirring, flow, etc.). As an alternative, we selected a kinetic method to drastically improve the assay times by using the slope of real-time displacement curves as analytical signal. As shown in Fig. 8A, the experimental kinetic dose-response curve for Atz determination presents good results with one-minute incubations. A detection limit of 80.1 ng mL^{-1} (371 nM) was calculated from this curve, and longer incubation times did not improve this value.

Displacement dose-response curves were also performed by endpoint measurements, in a transmission setup. For that, Atz solutions were incubated for 90 min on loaded biogratings, which corresponds to a 64.4% of the total biointeraction (Fig. S15). Experimental data fits well to a sigmoidal curve (Fig. 8A) and reach a detection limit of 1.1 ng mL^{-1} (5.1 nM).

Then, the regeneration of biogratings, to be used in more than one analysis, was studied. Thought the approach herein presented meets the concept behind disposable chips for single assays, regenerating the biogratings could offer interesting options in terms of green and costs issues. Since the analysis procedure does not modify the protein-hapten biograting (but just displaces antibodies bound on it) this regeneration only needs for a subsequent antibody incubation in order to reload them on the biograting.

To study this issue, successive antibody loads and Atz incubations were performed and their endpoint response was analyzed by transmission. As shown in Fig. 8B, the sensing capabilities of these biogratings can be only partially regenerated through this approach. Two different trends are observed in these results. First, after the initial analysis cycle, the signal of loaded biogratings underwent a significant decrease and kept constant in successive cycles. This fact could be

related with different phenomena taking place during incubations and washing steps, such as desorption of the stamped probes, instability of the BSA-2a conjugation, and loss of activity by conformational changes of the immobilized probe. Future studies focused on the biograting regeneration should assess other protein-hapten conjugates and more effective probe attachment modes. On the other hand, it is also observed that the signal decrease caused by the displacement becomes smaller along the successive analysis cycles and tend to be null. This phenomena can be explained by the fact that polyclonal antibodies were used in this study, which contains a mixture of antibodies with different paratopes, some ones with higher affinity for free Atz and others for the immobilized hapten. Therefore, the displacement of this second kind of antibodies during Atz incubations is not favored, thus becoming their population on the biograting increased along successive analysis cycles and causing a loss of sensitivity. Therefore, better regeneration capabilities could be obtained, for instance, by using monoclonal antibodies.

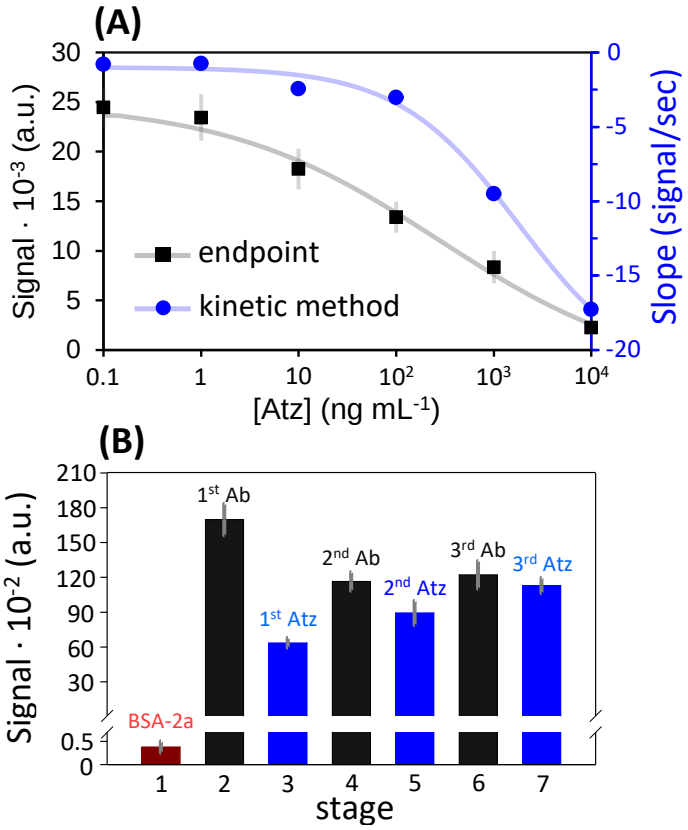

Fig. 8. Results for the Atz immunosensor. (A) Experimental data and sigmoidal regression (logistic 4 parameters) for dose-response curves obtained by kinetic methods and by endpoint measurement ($R^2_{kinetic}$ = 0.9944 and $R^2_{endpoint}$ = 0.9917). (B) Biograting regeneration results, including its original state (BSA-2a) and successive antibodies (Ab) and Atz incubations, performed with 6 replicates.

This label-free displacement immunosensor represents an appealing option for prospective in-field assays. Once fabricated and loaded with antibody, a chip containing the biograting could

be easily brought to the point of need, incubated with the sample, and analyzed using a simple optical setup. Along these lines, work is in progress towards the development of a compact and portable device for DBS measurements. Also, assays and biograting preparations could be easily speeded up by implementing simple convective setups for the incubations. Besides time issues, a sample flow system for the displacement stage would also potentially increase the sensitivity of the assay, since free analytes contained in large sample volumes could displace loaded antibodies in an additive fashion, thus presenting a preconcentration-like effect.

4. Conclusions

Diffraction-based sensing is an appealing technique for detecting and monitoring molecular recognition events. Good results are obtained with biogratings from optimized conditions in the studied model system (BSA/anti-BSA), and μCP allows functional biogratings to be built on a range of substrate materials, such as glass, polymers and metals.

DBS is compatible with different configurations, whose choice mainly depends on the substrate characteristics and on the nature of the information to be obtained. Transmission and external reflection setups are good options for endpoint measurements, while TIR confers advantages for real-time biosensing. Proteins and surfactants can be successfully employed as blocking agents to improve the performance of the system. In addition to label-free, DBS is compatible with labels and signal enhancers, which allows modulating the sensitivity of the assay.

Low-molecular-weight organic compounds (such as atrazine) can be analyzed by DBS in label-free conditions using a displacement immunoassay format, along with biogratings constituted by protein-hapten conjugates. Kinetic methods and endpoint measurements both enable well-correlated dose-response curves that reach detection limits of 80.1 and 1.1 ng mL^{-1} of atrazine, respectively. The results obtained in this work also point out prospective strategies to further improve the capabilities of this DBS immunosensor in terms of sensitivity, faster responses, and biograting regeneration.

Acknowledgements

This work was supported by the Spanish Ministry of Economy and Competitiveness (CTQ2013-45875-R and FIS2011-23175), FEDER, and the Generalitat Valenciana (PROMETEO II/2014/040 and PROMETEO II/2014/072). Special thanks go to Richard A. McAloney and M. Cynthia Goh for hosting M.A.-O. as visiting researcher, sharing their expertise, and offering their valuable support. M.A.-O. also acknowledges the FPI program of the Spanish Ministry of Economy and Competitiveness for a PhD and an EEBB mobility grant.

References

[1] Z. Cai, N.L. Smith, J.-T. Zhang, S.A. Asher, Two-Dimensional Photonic Crystal Chemical and Biomolecular Sensors, Anal. Chem., 87 (2015) 5013-5025.

[2] J. Escorihuela, M.A. Gonzalez-Martinez, J.L. Lopez-Paz, R. Puchades, A. Maquieira, D. Gimenez-Romero, Dual-Polarization Interferometry: A Novel Technique To Light up the Nanomolecular World, Chem. Rev., 115 (2015) 265-294.

[3] R. Méjard, H.J. Griesser, B. Thierry, Optical biosensing for label-free cellular studies, Trends Anal. Chem., 53 (2014) 178-186.

[4] A. Kussrow, C.S. Enders, D.J. Bornhop, Interferometric Methods for Label-Free Molecular Interaction Studies, Anal. Chem., 84 (2012) 779-792.

[5] Y.G. Tsay, C.I. Lin, J. Lee, E.K. Gustafson, R. Appelqvist, P. Magginetti, R. Norton, N. Teng, D. Charlton, Optical biosensor assay (OBA), Clin. Chem., 37 (1991) 1502-1505.

[6] J.B. Goh, R.W. Loo, R.A. McAloney, M.C. Goh, Diffraction-based assay for detecting multiple analytes, Anal. Bioanal. Chem., 374 (2002) 54-56.

[7] J.B. Goh, R.W. Loo, M.C. Goh, Label-free monitoring of multiple biomolecular binding interactions in real-time with diffraction-based sensing, Sens. Actuators B, 106 (2005) 243-248.

[8] X. Wang, X. Wang, Aptamer-functionalized hydrogel diffraction gratings for the human thrombin detection, Chem. Commun., 49 (2013) 5957-5959.

[9] X. Wang, X. Liu, X. Wang, Surface-relief-gratings based on molecularly imprinted polymer for 2,4-dichlorophenoxyacetic acid detection, Sens. Actuators B, 220 (2015) 873-879.

[10] B.J. Pak, F. Vasquez-Camargo, E. Kalinichenko, P.L. Chiodini, T.B. Nutman, H.B. Tanowitz, I. McAuliffe, P. Wilkins, P.T. Smith, B.J. Ward, M.D. Libman, M. Ndao, Development of a Rapid Serological Assay for the Diagnosis of Strongyloidiasis Using a Novel Diffraction-Based Biosensor Technology, Plos Negl. Trop. Dis., 8 (2014).

[11] T.J. Gnanaprakasa, O.A. Oyarzabal, E.V. Olsen, V.A. Pedrosa, A.L. Simonian, Tethered DNA scaffolds on optical sensor platforms for detection of hipO gene from Campylobacter jejuni, Sens. Actuators B, 156 (2011) 304-311.

[12] C.A. Barrios, V. Canalejas-Tejero, S. Herranz, M.C. Moreno-Bondi, M. Avella-Oliver, R. Puchades, A. Maquieira, Aluminum Nanohole Arrays Fabricated on Polycarbonate for Compact Disc-Based Label-Free Optical Biosensing, Plasmonics, 9 (2014) 645-649.

[13] S. Schlücker, Surface-Enhanced Raman Spectroscopy: Concepts and Chemical Applications, Angew. Chem. Int. Ed., 53 (2014) 4756-4795.

[14] E.K. Gustafson, J. Lee, E. Calenoff, R. Trebino, Y.-g. Tsay, Bio-grating for light diffraction immunoassay|having a poly:silicon or single crystalline silicon surface with a diffraction grating

design of binding reagent, Yellowstone Diagnos; Adeza Biomedical; Adeza Biomedical Corp, 1988.

[15] C. Wendeln, B.J. Ravoo, Surface Patterning by Microcontact Chemistry, Langmuir, 28 (2012) 5527-5538.

[16] J. Lee, K. Icoz, A. Roberts, A.D. Ellington, C.A. Savran, Diffractometric detection of proteins using microbead-based rolling circle amplification, Anal. Chem., 82 (2010) 197-202.

[17] V. Romanov, S.N. Davidoff, A.R. Miles, D.W. Grainger, B.K. Gale, B.D. Brooks, A critical comparison of protein microarray fabrication technologies, Analyst, 139 (2014) 1303-1326.

[18] G. Ye, X. Li, X. Wang, Diffraction grating of hydrogel functionalized with glucose oxidase for glucose detection, Chem. Commun., 46 (2010) 3872-3874.

[19] G. Ye, X. Wang, Glucose sensing through diffraction grating of hydrogel bearing phenylboronic acid groups, Biosens. Bioelectron., 26 (2010) 772-777.

[20] C.A. Barrios, C. Zhenhe, F. Navarro-Villoslada, D. López-Romero, M.C. Moreno-Bondi, Molecularly imprinted polymer diffraction grating as label-free optical bio(mimetic)sensor, Biosens. Bioelectron., 26 (2011) 2801-2804.

[21] Regulation (EU) NO 649/2012 of the European Parliament and of the council of 4 july 2012, Official Journal of the European Union, 27.7.2012.

[22] Edition of the Drinking Water Standards and Health Advisories, EPA, 2011.

[23] N.D. Jablonowski, A. Schäffer, P. Burauel, Still present after all these years: persistence plus potential toxicity raise questions about the use of atrazine, Environ. Sci. Pollut. Res., 18 (2011) 328-331.

[24] N.D. Jablonowski, G. Hamacher, R. Martinazzo, U. Langen, S. Köppchen, D. Hofmann, P. Burauel, Metabolism and Persistence of Atrazine in Several Field Soils with Different Atrazine Application Histories, J. Agric. Food. Chem., 58 (2010) 12869-12877.

[25] K.R. Solomon, J.A. Carr, L.H. Du Preez, J.P. Giesy, R.J. Kendall, E.E. Smith, G.J. Van Der Kraak, Effects of Atrazine on Fish, Amphibians, and Aquatic Reptiles: A Critical Review, Crit. Rev. Toxicol., 38 (2008) 721-772.

[26] M. Avella-Oliver, S. Morais, J. Carrascosa, R. Puchades, Á. Maquieira, Total Analysis Systems with Thermochromic Etching Discs Technology, Anal. Chem., 86 (2014) 12037-12046.

[27] D. Jornet, M.Á. González-Martínez, Á. Maquieira, R. Puchades, Advanced Homogeneous−Heterogeneous Immunosensing Format Employing Restricted Access Supports, Anal. Chem., 79 (2007) 9331-9339.

[28] S. Damodaran, On the molecular mechanism of stabilization of proteins by cosolvents: role of Lifshitz electrodynamic forces, Langmuir, 28 (2012) 9475-9486.

[29] Immunoassay, in: E.P. Diamandis, T.K. Christopoulos (Eds.) Immunoassay, Academic Press, San Diego, 1996, pp. 569-579.

[30] A. Bernard, E. Delamarche, H. Schmid, B. Michel, H.R. Bosshard, H. Biebuyck, Printing Patterns of Proteins, Langmuir, 14 (1998) 2225-2229.

[31] Y. Lin, Q. Fu, J. Zhu, J.M. Miller, J.E. Van Eyk, Development of a qualitative sequential immunoassay for characterizing the intrinsic properties of circulating cardiac troponin I, Clin. Chem., 56 (2010) 1307-1319.

[32] M. Avella-Oliver, D. Gimenez-Romero, S. Morais, M.A. Gonzalez-Martinez, P.R. Bueno, R. Puchades, A. Maquieira, INSEL: an in silico method for optimizing and exploring biorecognition assays, Chem. Commun., 49 (2013) 10868-10870.

[33] Y. Zong, F. Xu, X. Su, W. Knoll, Quartz Crystal Microbalance with Integrated Surface Plasmon Grating Coupler, Anal. Chem., 80 (2008) 5246-5250.

SUPPLEMENTARY MATERIAL

Diffraction-based sensing with biogratings for qualitative and quantitative analytical applications

Anal. Chim. Acta, In revision (**2017**).

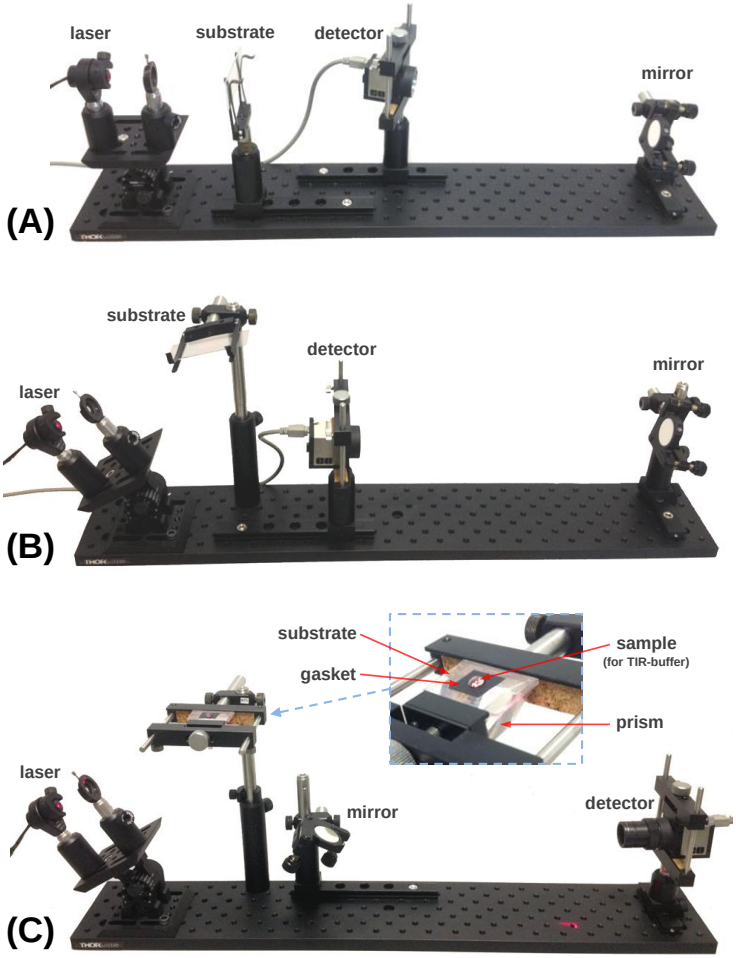

Fig. S1. Images of the optical setups for the different configurations: (A) transmission, (B) external reflection, and (C) total internal reflection. Custom gaskets to incubate samples on hydrophilic substrates were made with adhesive polymeric tape, and biogratings were positioned in the center of their inner circular hole (5 mm of diameter). To include the mirror in these setups facilitates the experimental alignment of the systems, whereas all the configurations could be further simplified by omitting this element and directly positioning the detector to be hit by the diffracted order of interest

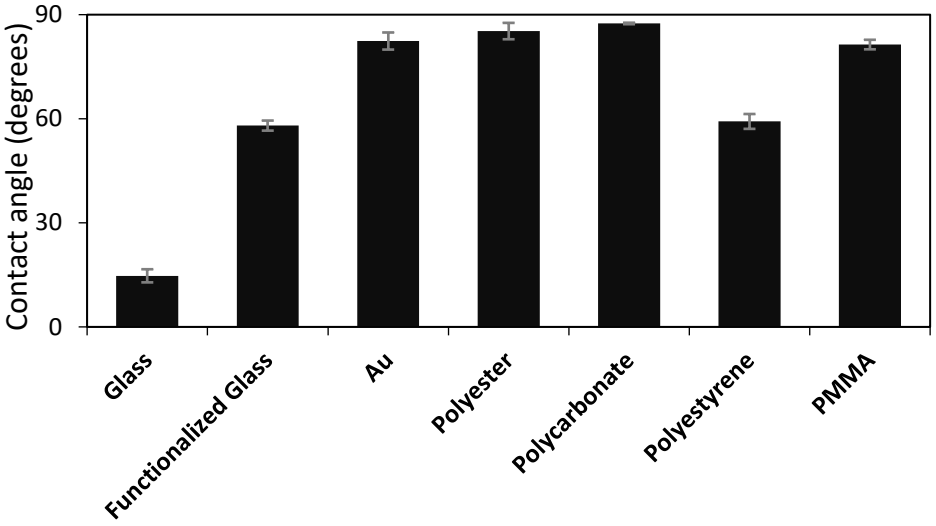

Fig. S2. Contact angles of the different substrate materials. Measured in water, 2 µL droplets.

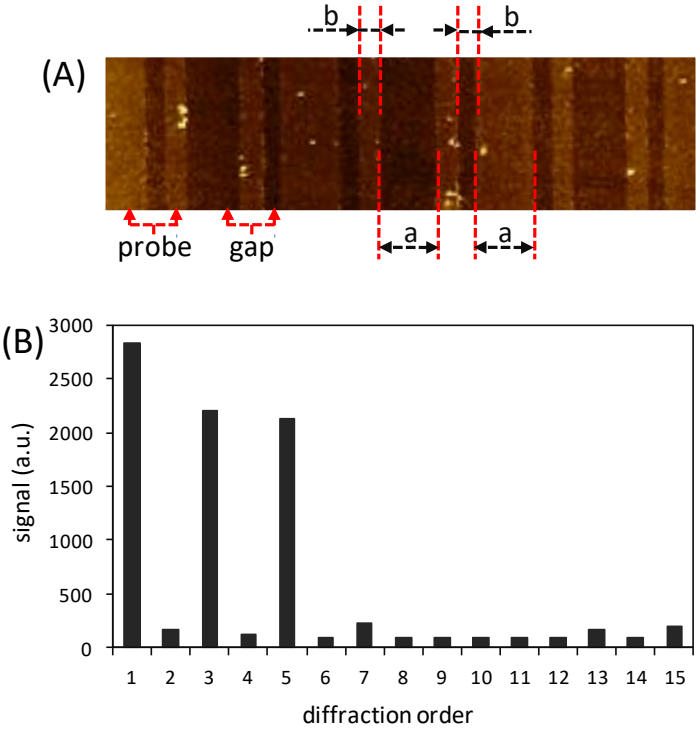

Fig. S3.
(A) Configuration of the grating used in this study, where a = 4.5 µm and b = 1.5 µm. AFM image of a BSA biograting on glass ([BSA] = 1000 µg mL^{-1}, t_{inking} = 180 min, $t_{stamping}$ = 25 min). (B) Relative distribution of the diffraction efficiency along the diffracted orders, experimentally measured with the grating employed in this study.

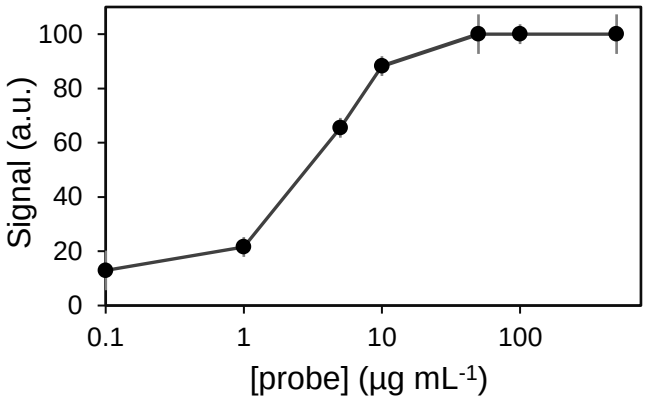

Fig. S4. Probe concentration curve by discrete transmission measurements (t_{inking} = 30 min, $t_{stamping}$ = 30 min). Normalized signal in the vertical axis.

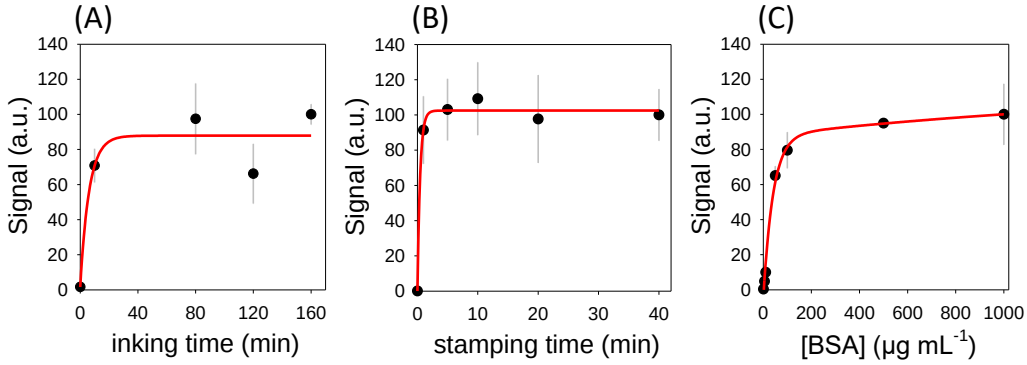

Fig. S5. Assessment of the µCP variables registered by total internal reflection with PBS on the biograting (TIR-buffer): (A) inking time ([probe] = 100 µg mL^{-1}, $t_{stamping}$ = 60 min), (B) stamping time ([probe] = 100 µg mL^{-1}, t_{inking}= 160 min), and (C) probe concentration (t_{inking}= 160 min, $t_{stamping}$= 25 min). Normalized signal in vertical axes.

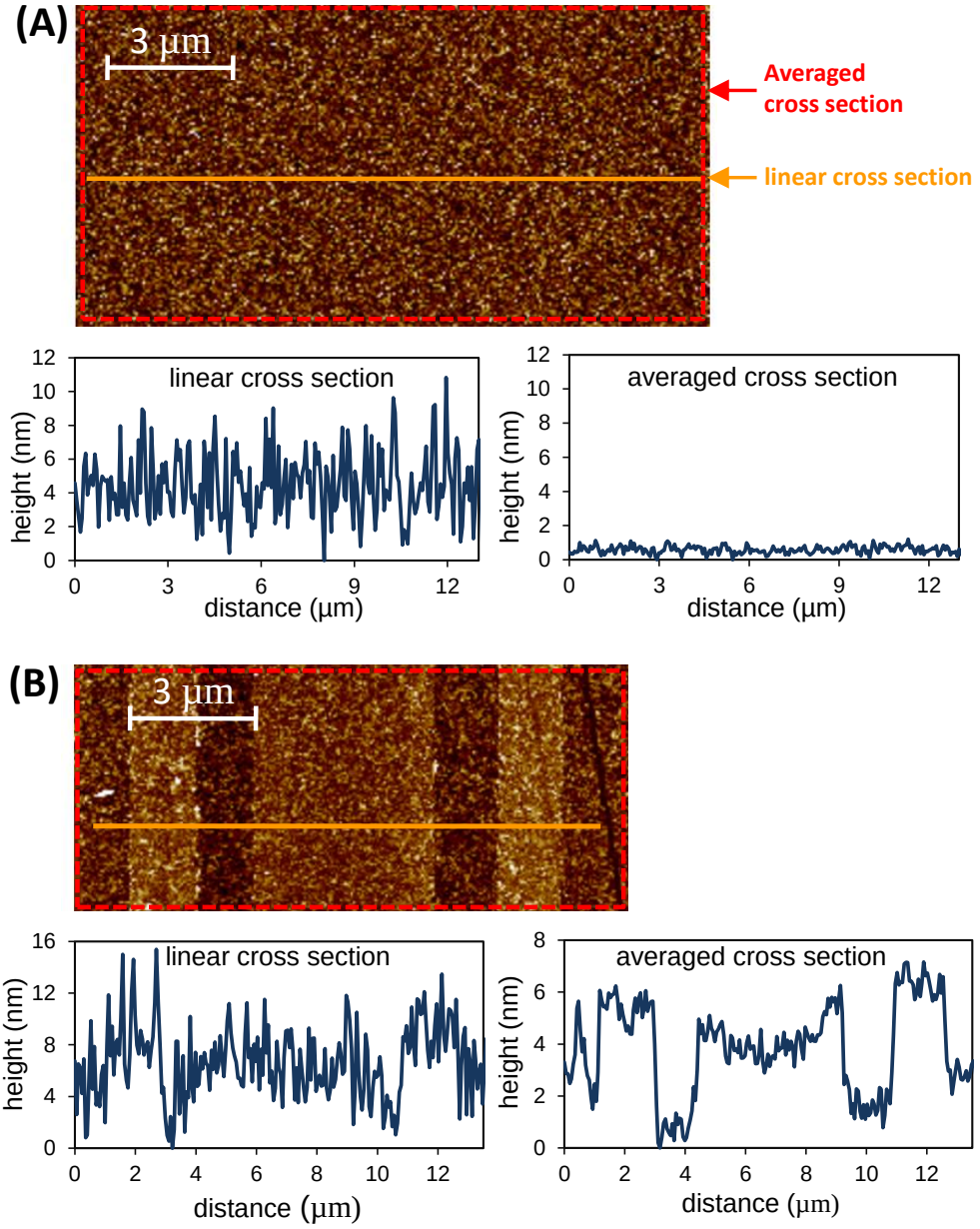

Fig. S6. Comparison between linear and averaged AFM cross section profiles of (A) bare glass and (B) probe grating. AFM measurements revealed a roughness of 2.213 ± 0.012 nm for bare glass substrates (root mean squared roughness, in 15 x 15 µm). This roughness introduces random noise that hinders height determinations by linear cross sections. However, to average every data row along the grating direction within a given area reduce this noise around one order of magnitude and enables these topographic characterizations.

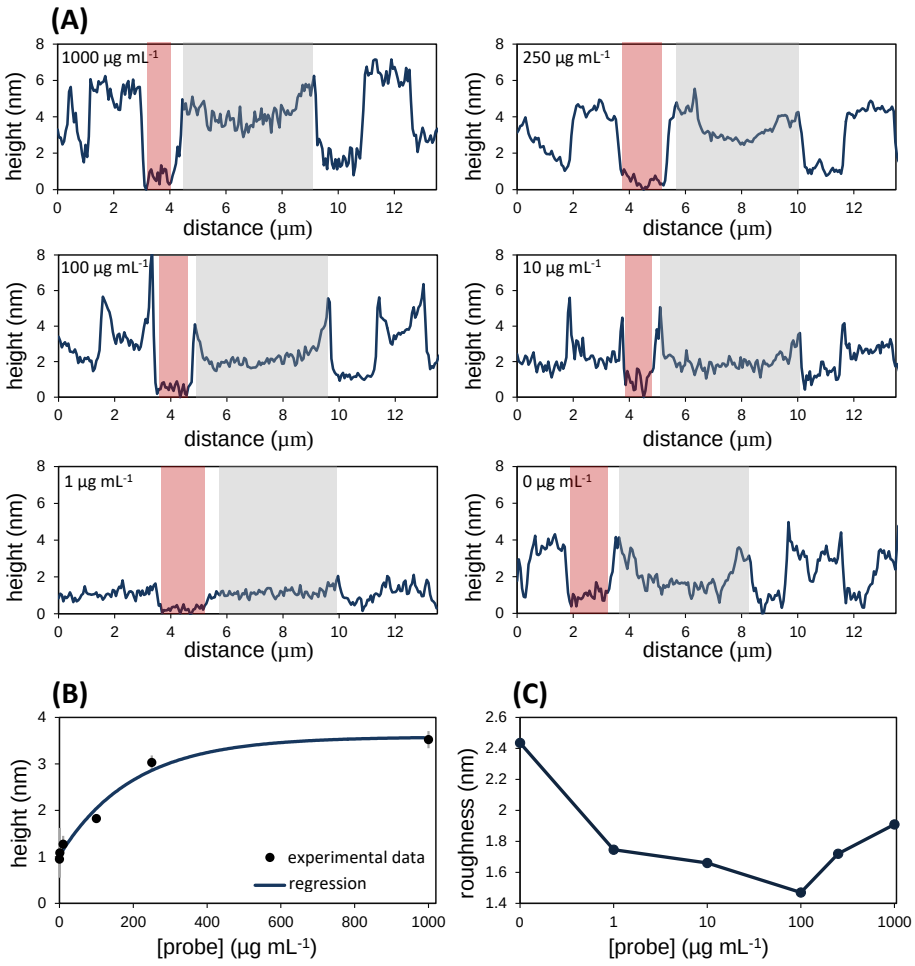

Fig. S7. AFM results of biogratings created from an array of protein concentrations. (A) Averaged cross sections, calculated as described in Fig. S6. (B) Correlation between biograting heights and protein concentrations. Height is calculated by subtracting the averaged value in the gap strip (red bands in Fig. S7A) to the averaged height in the protein strips (blue bands in Fig. S7A). A maximal value of 3.52 ± 0.19 nm is reached in the top of the curve. The non-zero height registered in the biogratings involving 0 µg mL^{-1} of probe in the inking solution, might be caused by remaining protein on the stamp surface or diffused in the PDMS bulk of reused stamps (*Langmuir*, 14, 1998, 2225; *J. Am. Chem. Soc.*, 119, 1997, 3017). This fact could also be originated by residual polymer from the stamps (*Analyst*, 135, 2010, 845). The potential effect of this issue in the resulting biogratings would be reduced when using high probe concentrations, as the one selected as optimal in this study (250 µg mL^{-1}). (C) Roughness (root mean squared) measurements in the protein strip within 15 x 15 µm scans containing a biograting.

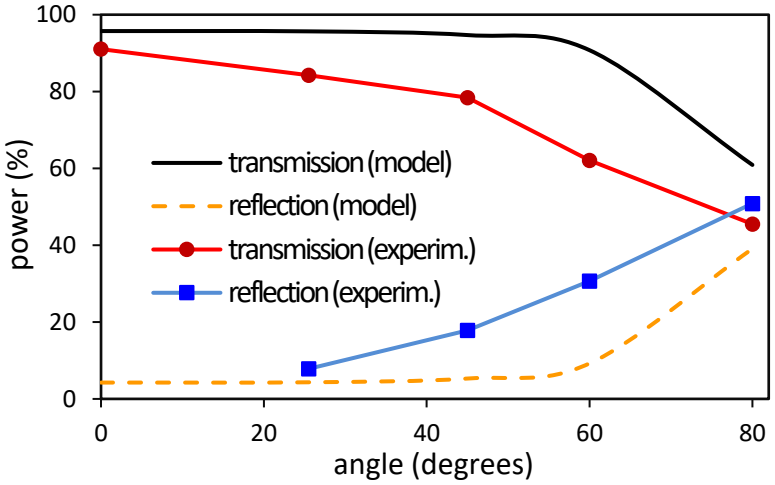

Fig. S8. Experimental and theoretical assessment of the relative reflection/transmission intensity dependence with the incidence angle of the laser beam. In this representation, 0 degrees means perpendicular to the substrate surface. Theoretical data were calculated considering Snell's law. Discrepancies between theoretical and experimental results must mainly be caused by light dispersion and multilayer reflections, not considered in the theoretical model.

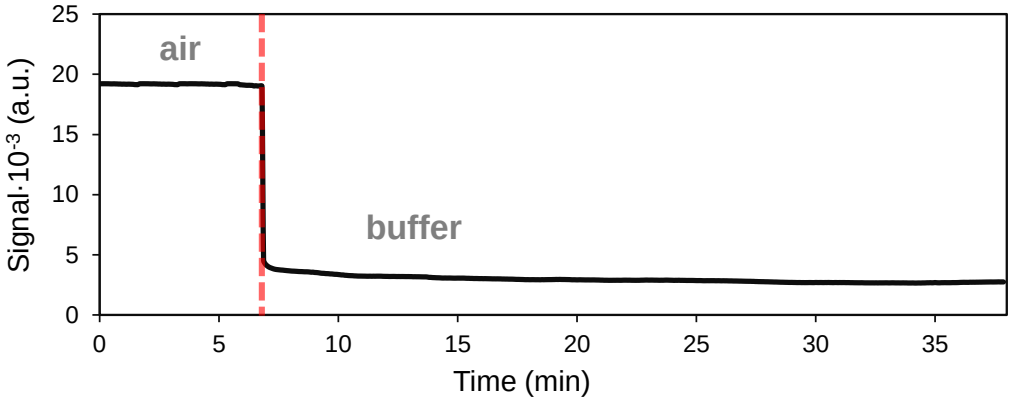

Fig. S9. Experimental results of an aqueous solution addition on a dry protein biograting, measured
by TIR.

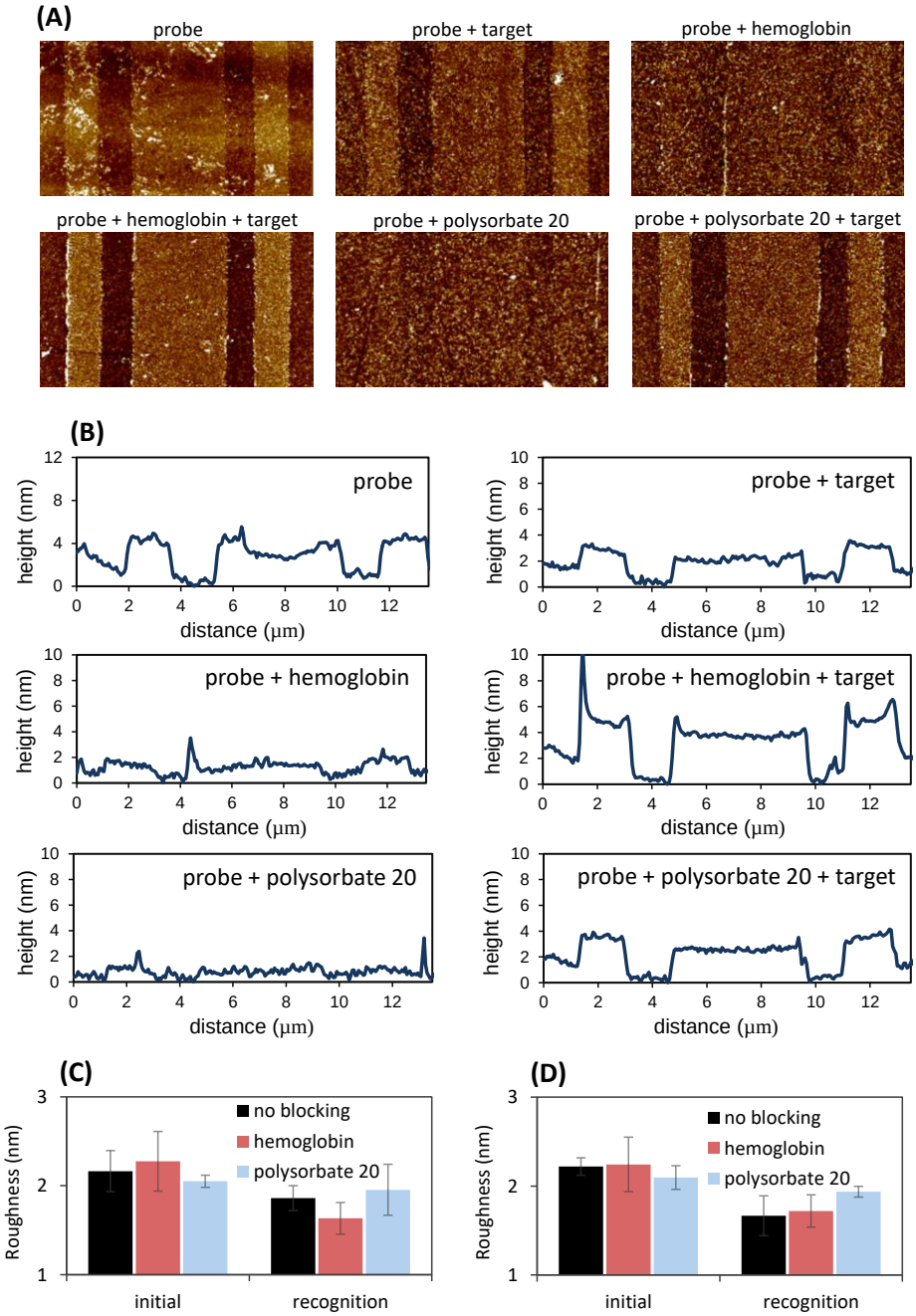

Fig. S10. AFM results of blocking (with hemoglobin and polysorbate 20) and recognition (with target, 10 μg mL^{-1}) stages for the studied model system: (A) AFM data, (B) averaged cross section profiles (calculated as described in Figure S6), roughness results (C) in the gaps and (D) in the probe strips (root mean squared values).

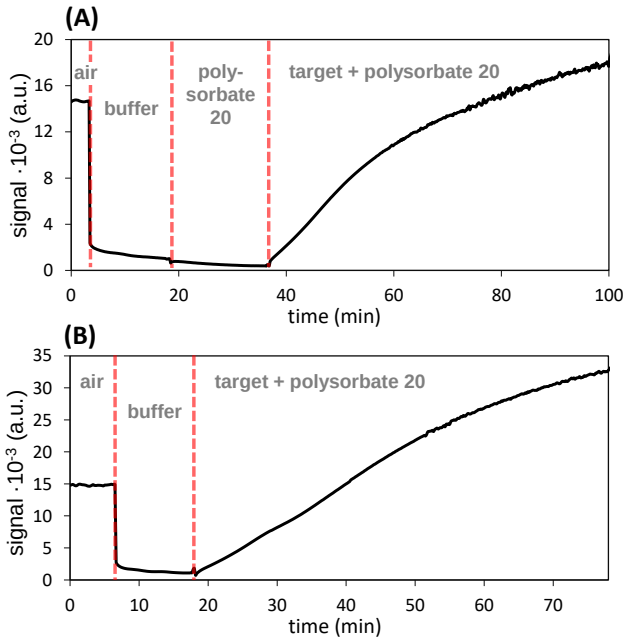

Fig. S11. Kinetic measurements of stabilization, blocking, and recognition (10 µg mL^{-1} of target) using polysorbate 20 as blocking agent. (A) Results including a specific stage for blocking. (B) Results by incorporating the blocking agent in the target solution. As observed in the graphs, even better results in terms of signal intensity were obtained when joining blocking (with polysorbate 20) and target recognition in the same stage.

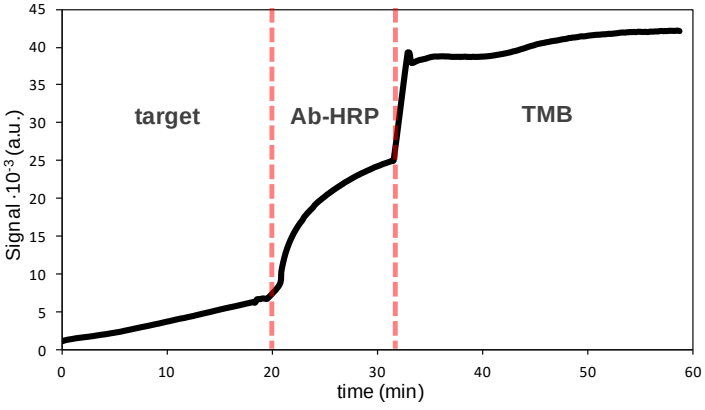

Fig. S12. Kinetic results of target recognition, secondary antibody labelled with horseradish peroxidase (Ab-HRP, 10 µg mL^{-1}) recognition, and signal development with TMB (3,3',5,5'-tetramethylbenzidine).

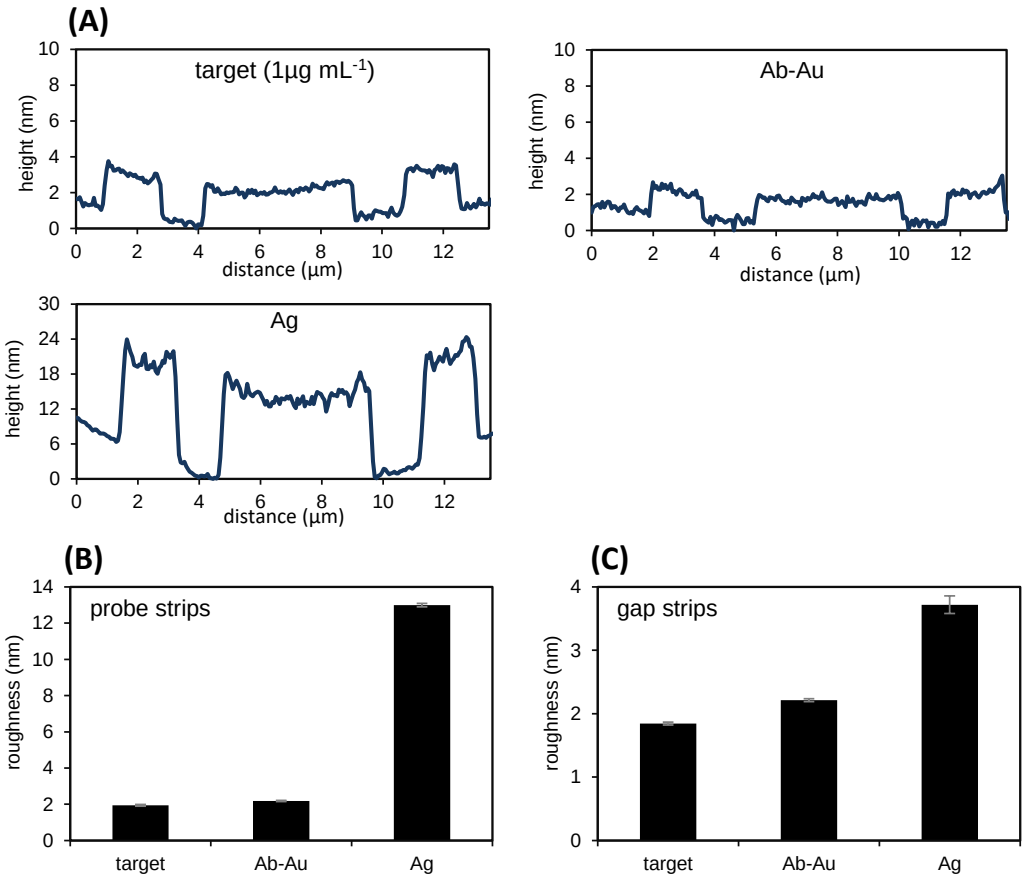

Fig. S13. AFM results of labelling and signal developing: (A) averaged cross sections, and roughness within (B) protein strips and (C) gaps (root mean squared roughness values).

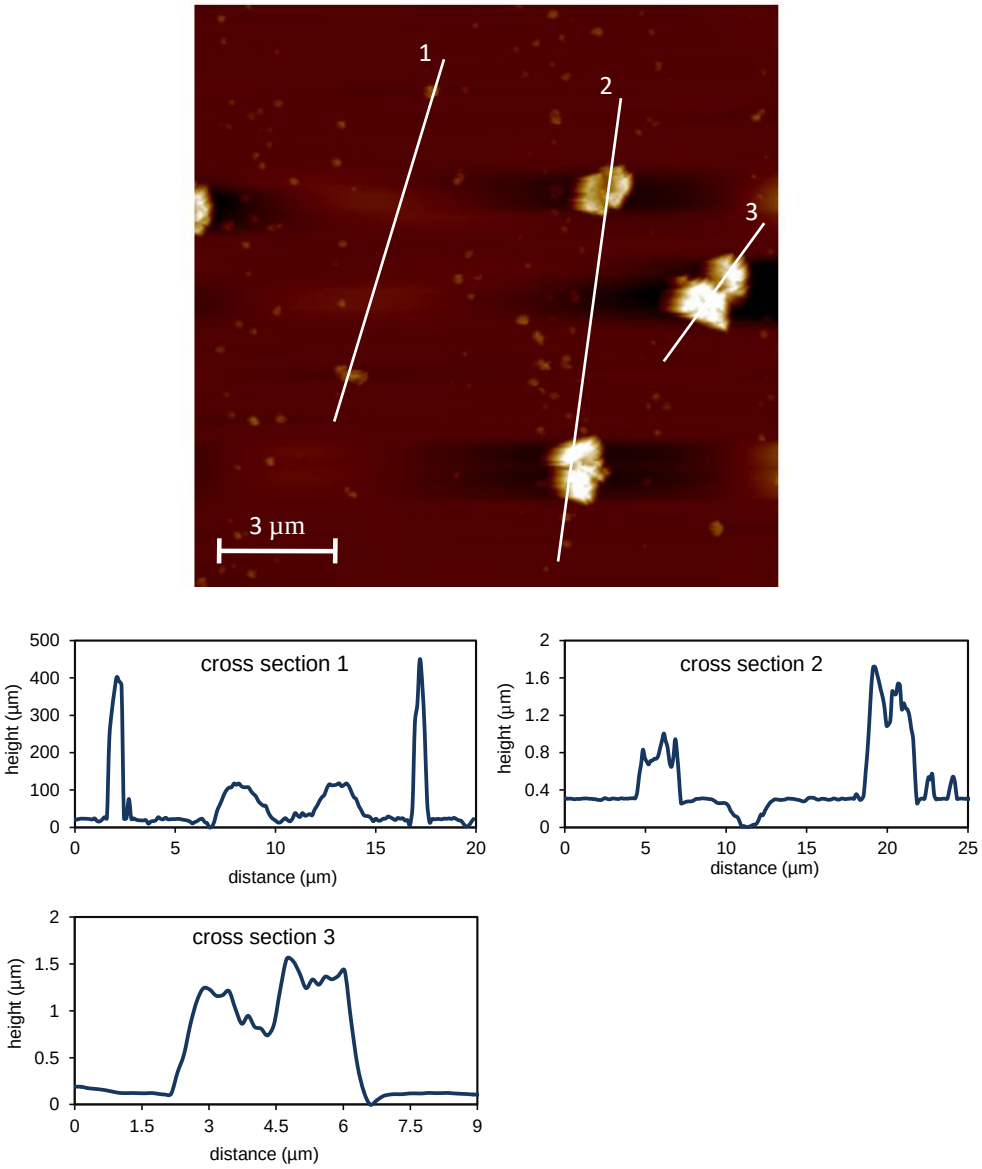

Fig. S14. AFM data of a biograting of the studied model system after Ab-Au recognition and a too long silver enhancement reaction. As shown, significant heterogeneities on the biograting were obtained after long silver precipitation times. Low adhesion of the precipitated silver on the glass substrate was also experimentally observed for strong silver precipitation conditions.

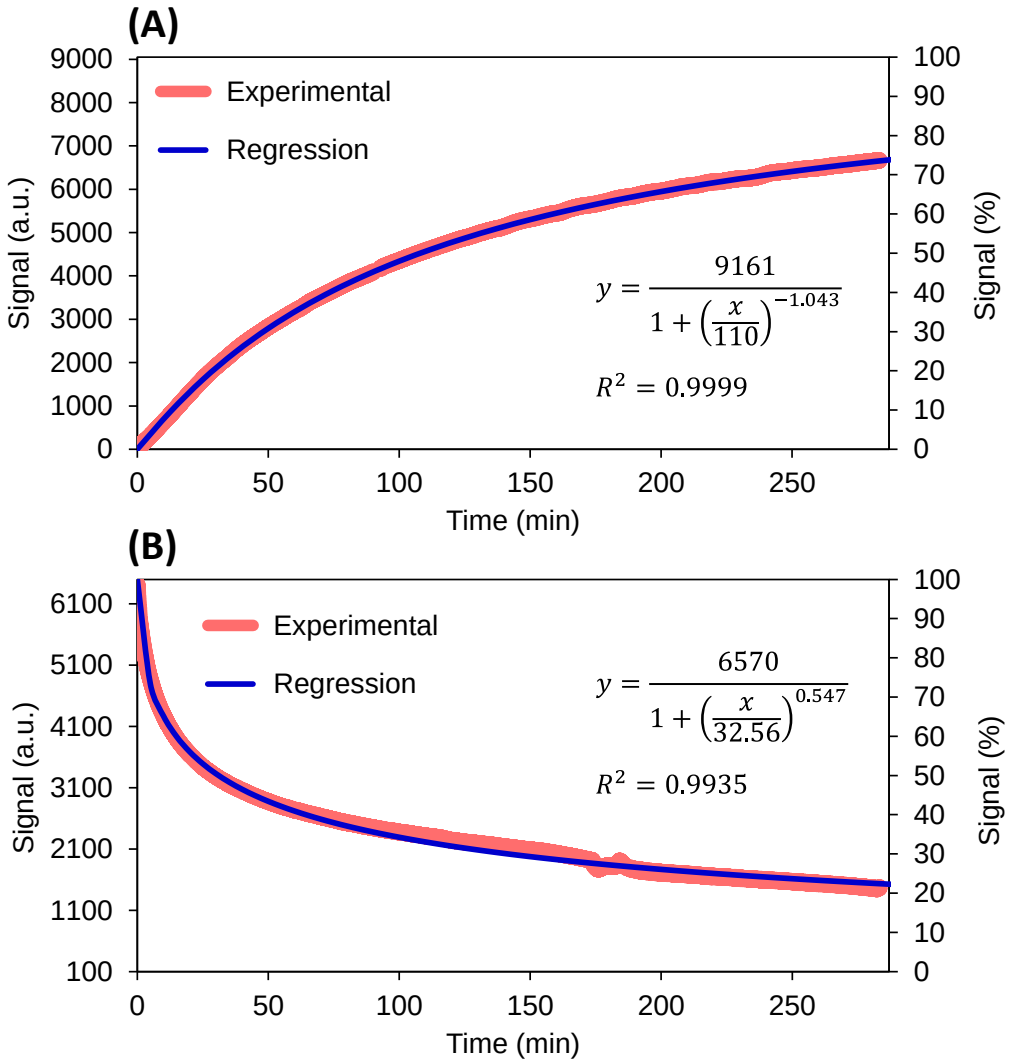

Fig. S15. Experimental and regression (sigmoidal, logistic 3 parameters) real-time curves for (A) recognition between the antibody KLH-2d (IV) and the immobilized BSA-2a conjugate, and (B) the following antibody displacement by free atrazine in solution.

Table S1. Screening study of bioreagents for displacement atrazine immunoassays.

		Ab (1/50 dilution)		Atz (0.1 mg mL^{-1})		Atz (1 µg mL^{-1})	
Hapten	**Ab**	**Slope[a]**	**Sig.[b]**	**Slope[a]**	**Sig.[b]**	**Slope[a]**	**Sig.[b]**
2a	KLH-2d (IV)	6.2 (0.971)	2948	-120.4 (0.983)	-8322	-68.8 (0.993)	-3407
	R10	13.5 (0.993)	5340	-16.0 (0.998)	-3381	-6.7 (0.999)	-975
	R11	23.6 (0.999)	15777	-38.2 (0.998)	-5365	-12.0 (0.999)	-2272
AMA[c]	KLH-2d (IV)	3.6 (0.997)	1760	-5.4 (0.999)	-1205	-	-
	R10	1.4 (0.982)	276	0	0	-	-
	R11	7.0 (0.969)	2766	-26.5 (0.967)	-7306	-	-
2b	KLH-2d (IV)	1.4 (0.991)	1410	-	-	-	-
	R10	0.9 (0.977)	41	-	-	-	-
	R11	0	0	-	-	-	-

[a] Slope (in signal/seconds units) and R^2 values (in brackets) of the linear regressions for particular time ranges (200-500 seconds for Ab and 50-150 seconds for Atz) after the addition of the corresponding bioreagent.
[b] Neat signal after 500 seconds for Ab additions and 200 seconds for Atz additions.
[c] Atrazine mercapturic acid.

Different antibodies (Ab) were incubated on biogratings constituted by BSA-hapten conjugates, and the corresponding binding events were analyzed by real-time in TIR-buffer. Specific time intervals of the recognition curves were fitted to a linear regression in order to determine the magnitude of their slope, and the signal variations after a given time were also measured. In this study, higher slopes and signal variations indicate greater Ab-hapten affinity.

The same strategy was used for the addition of atrazine (two concentration levels). Analogously to the previous approach, higher slopes and signal variations (in absolute value) correspond to greater antibody displacement by free atrazine.

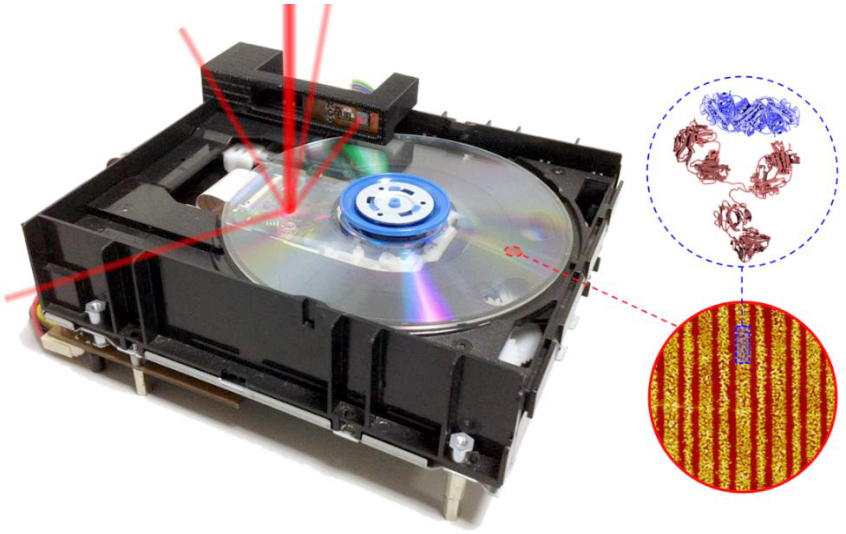

3.4.3 Diffractive protein gratings as optically active transducers for high-throughput label-free immunosensing

Anal. Chem., In revision (**2017**).

ABSTRACT

A novel label-free biosensor based on consumer electronics along with bioreceptor networks patterned as diffractive gratings (biogratings), has been developed. Regular compact disk surfaces were used as optically active scaffolds for producing arrays of functional BSA biogratings on low energy surfaces by a water-assisted variant of microcontact printing. An analytical compact disk scanner, comprising a LightScribe drive, was developed to measure the diffraction patterns of these biogratings, thus allowing biointeractions to be quantitatively sensed in multiplex and label-free fashion by means of diffraction efficiency changes. The approach was demonstrated by immunoassaying anti-BSA IgGs in solution, reaching well-correlated responses with quantification and detection limits of 1.3 and 5.2 nM, respectively. These results provide appealing insights into cost-effective, portable, and scalable alternatives for designing label-free biosensors.

Keywords: biograting, diffraction-based sensing, microcontact printing, compact disk, label-free, immunosensor.

1. Introduction

The raise of nanoscience has brought important advances for sensing biointeractions without conjugating specific signaling elements to the bioreagents. These label-free systems typically exploit nanoscale phenomena of different nature and enable more reliable results and simpler analytical protocols, among other important bioanalytical strengths.[1-3] Despite the great scientific activity involving label-free biosensing and the mature state reached in some instances, the development of label-free sensors to be disseminated beyond research environments (i.e., standard benchtop systems) is still challenging nowadays.

Diffractive gratings of bioreceptors (biogratings) are appealing optical transducers to design novel biosensors.[4,5] These biogratings are nanostructured networks constituted by biological probes themselves, patterned on non-structured solid substrates. As illustrated in Fig.1, binding events between immobilized bioreceptors and their targets increase the amount of matter constituting the biogratings. Consequently, their diffraction efficiency becomes enhanced and biointeractions can be sensed as increments in the light intensity of diffracted orders, according to the concept behind diffraction-based sensing (DBS). This technique enables background-free and label-free sensitive analysis, and its bioanalytical strengths have been demonstrated in previous studies and are supported by Axela Inc. and its dotLab benchtop system.[6-10]

Microcontact printing (μCP) is a practical method to create biogratings for DBS.[4,5,11] It basically lies in replicating the relief of a master nanostructure by polymerizing an elastomer on it, and

then using the resulting material as stamp to pattern biochemicals on solid surfaces.[12,13] µCP has proven to be a versatile nanofabrication approach, whereas its performance to pattern proteins on low energy surfaces is limited.[14] Also, this technique requires functional nanostructured masters, which are typically fabricated by complex and expensive nanofabrication methods.[15-17]

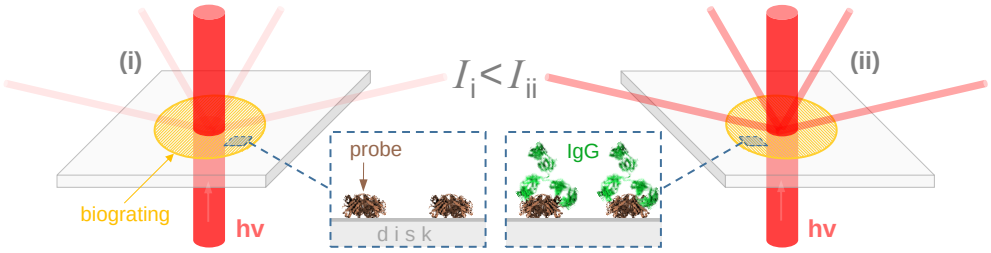

Fig. 1. Schematic illustration of diffraction-based sensing for protein biogratings (i) before and (ii) after interacting with specific IgGs. *I* refers to the light intensity of the diffracted orders.

Along these lines, to couple bioanalytical sciences with particular consumer electronics represents a smart way to conceive biosensors that face the inherent limitations of standard benchtop analytical systems.[18-21] Given their worldwide mass production, these electronics entail highly sophisticated and compact technologies at extremely low cost. Exploiting them for biosensing points towards portable, robust, inexpensive, and user-friendly analytical devices applicable in point-of-care settings.[22,23] The bioanalytical implementation of compact disk (CD) technologies is one of the most paradigmatic examples,[24,25] which has introduced important sensing and sample handling advances based on labeled strategies.[26,27] Regarding label-free, promising attempts have been reported,[28-30] but they are based on complex nanostructured materials as assay substrates and custom detection setups instead of standard disks and drives, respectively.

In this study, the strengths of biogratings for DBS, consumer electronics, µCP, and label-free detection are for the first time brought together in order to design effective CD-based biosensors. Our approach consists on fully exploiting these resources to develop a simple and scalable method to create arrays of functional protein biogratings on inexpensive analytical platforms, and to conceive a scanner to sense their transmitted diffraction patterns in a high-throughput and label-free fashion. As proof of concept, the bioanalytical performance of this biosensor was investigated using a representative immunoassay model system to determine specific IgGs.

2. Materials and methods

2.1 Materials

Sodium phosphate buffer (PBS, 8 mM, Na_2HPO_4, 2 mM KH_2PO_4, 137 mM NaCl, 2.7 mM KCl, pH 7.4), PBS-T (PBS containing Tween 20 0.05% v/v), and PBS-TT (PBS-T with taurine 0.1 M) were prepared with purified water (Milli-Q, Millipore Iberica, Madrid, Spain) and filtered through 0.22 μm pore size nitrocellulose membranes from Whatman GmbH (Dassel, Germany). Bovine serum albumin (BSA), Tween 20, taurine, and anti-BSA rabbit IgGs were supplied by Sigma-Aldrich (Madrid, Spain). Polydimethylsiloxane (PDMS) Sylgard 184 was from Dow Corning (Wiesbaden, Germany). Compact disks (CD-R LightScribe) were purchased from MediaRange (MPO Iberica, Madrid, Spain) and a commercial disk drive (GH24NS90) was from LG Electronics Inc. (Englewood Cliffs, USA). A 5.1 x 5.1 mm planar silicon photodiode (SLCD-6N2) from Silonex Inc. (Montreal, Canada) was used for the photosensor. The data acquisition board (DAQ, USB-2527) was from Measurement Computing (Norton, MA, USA).

Atomic force microscopy (AFM) were performed by non-contact mode in air using a Multimode 8 microscope (Bruker, Billerica, USA) and RFESPA probes (MPP-21120-10, Bruker). For field emission scanning electron microscopy (FESEM), gold were sputtered on the samples (20 seconds, 4.7 Å/sec) and a ZEISS Ultra 55 microscope (Oberkochen, Germany) was used.

2.2 Disks

Transparent disks that keep their central coordinate code (control feature zone, CFZ) were created from recordable LightScribe CDs by removing all the layers on the polycarbonate substrate (Fig. 2A), as the TED5 disks described elsewhere.[31] These disks comprise flat (unstructured) polycarbonate in one side, and a spiral-shaped grooved nanostructure (track) in the surface of the other one. In this study, the structured side of these disks was used as optically active master to create biogratings by microcontact printing (μCP). On the other hand, the same kind of disks were also employed as analytical platforms to hold (on their flat side) arrays of protein biogratings.

2.3 Biogratings fabrication

Custom motifs were designed and etched in the label side of LightScribe disks (Fig. S1) and used, together with standard compact disk cases (lids and base parts), as a simple alignment and positioning system to carry out the fabrication process in this study. To create the stamps for μCP, disks were introduced in the lid, positioned with the track side up, 70 mL of PDMS were pored on it, and the case was closed to align the disks (Fig. S2A). Next, the system was degassed in a vacuum chamber for 30 minutes and cured overnight at 60 ºC. Afterwards, PDMS blocks

(together with the master disks) were separated from the case (Fig. S2B) and aligned with a LightScribe template using the bottom part of a case (Fig. S2C). Finally, PDMS blocks were cut using a circular blade (8 mm diameter) according to the LightScribe template, peeled off from the master, and the resulting stamps were sonicated in ethanol (30% v/v in water, 5 minutes, 3 times) and dried under a stream of air (Fig. 2B-2C).

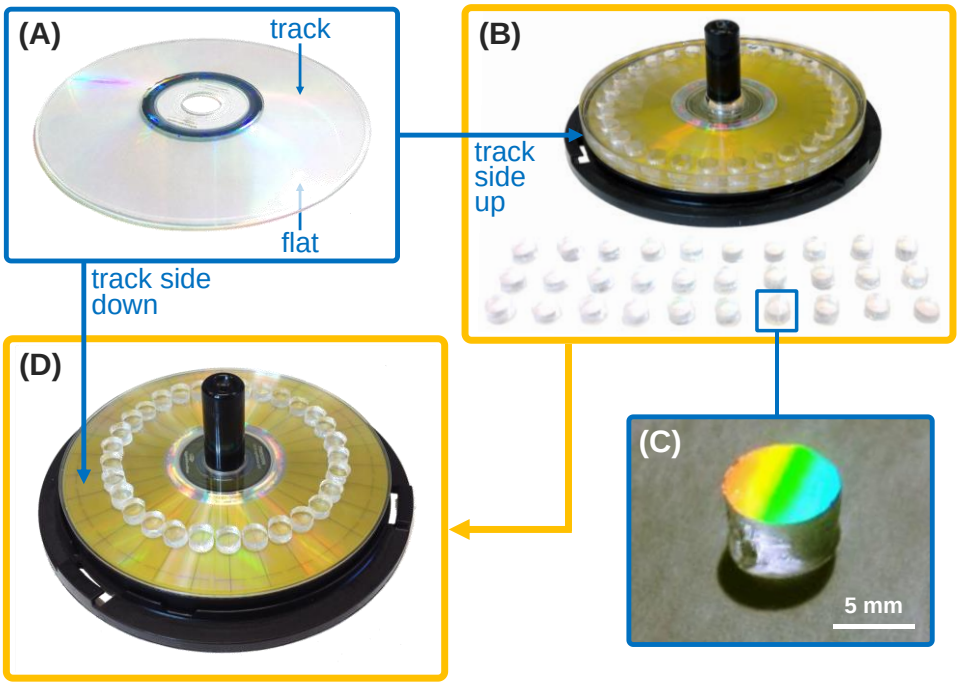

Fig. 2. Images of the biogratings fabrication process. (A) Transparent disk used as assay platforms and nanostructured masters. (B) PDMS-disk block aligned with the LightScribe template for cutting, and the resulting stamps. (C) Enlarged view of a single stamp diffracting white light. (D) Image of the stamps aligned on the disk-based platform.

To create the biogratings, 130 µL of probe protein solution in PBS were incubated on the structured side of the PDMS stamps. After an inking time, stamps were rinsed with water and dried under a stream of air. Then, the disks to be used as assay platforms (flat side up) and the corresponding LightScribe template were positioned using the bottom part of a case. Next, the grating side of the inked stamps were aligned using the template and put in contact with the disks surface (Fig. 2D). A slight pressure was applied with the tweezers to favor the contact, and the whole system was immersed in a lid containing water during the stamping time. Finally, stamps were removed, disks rinsed with PBS-T and water, and dried by centrifugation. Stamps were

sonicated in ethanol (30% v/v in water, 5 minutes, 3 times) and stored in this ethanolic solution to be reused.

2.4 Setup

An interconnection board (ICB) that acts as interface between the DAQ and the drive was created. As illustrated in Fig. S3, in the drive part this board was connected to the output port of the pickup unit, the actuator driver integrated in the main board of the disk drive, and the incorporated photosensor (comprising a photodiode), in order to manage the electronic signals for their control. The focusing system was disassembled and removed from the pickup unit (Fig. S4). In this study, a radial position of 42 mm (from the center) was selected for the pickup. Both the drive and the ICB were plugged to a single external power supply, and the DAQ was connected to a personal computer through a USB 2.0 port.

A LabVIEW application was implemented to monitor the signal from the photosensor, select the optical intensity of the laser (from 0 to 50 mW), and control the rotational velocity of the spindle motor (0 and from 500 to 10^4 rpm). An ALPC (automatic laser power control) algorithm, which uses the output signal from the laser power sensor incorporated in the pickup unit (front monitor, Fig. S4A), was also programmed in this application and used as feedback system to keep a constant laser intensity. Laser power was set to be maximal for the measurements in this study. A 3D-printed piece was created and used to fix the photosensor in the edge of the drive case in a tilted position (Fig. S3). Measurements were performed in darkness conditions using the 780 nm laser source of the drive. The analog signal acquired by the photosensor was digitalized by the DAQ and transferred to the computer to be quantified by the LabVIEW application.

2.5 Assay

The biointeraction between BSA and anti-BSA was used as model system in this study. BSA biogratings were created on polycarbonate disks as reported above, and 80 µL of specific IgG solutions in PBS-TT were incubated on them during 80 minutes. Then, disks were rinsed with water, dried by centrifugation, and analyzed using the developed disk drive analytical scanner.

2.6 Data processing

The maximal diffraction intensity registered along the longitudinal scan of each biograting was selected as analytical signal (Fig. S5). Four replicates of each condition were performed and considered to calculate averaged values and their standard deviations. For AFM analysis, Nanoscope software was employed, zeroth order flatten was applied to the scanned data, averaged cross sections were obtained by averaging single row profiles along the grating

direction within a given area, and roughness results were determined by root mean squared values. The structural dimensions were inferred from six replicates. FESEM data was analyzed by ImageJ software.[32]

3. Results and discussion

3.1 Biogratings fabrication and characterization

BSA is a water-soluble globular protein, mainly constituted by long α helices that conform prolate ellipsoid structures (14 x 4 x 4 nm) of 66.5 KDa. This is one of the most paradigmatic example of albumins, a group of proteins found at high concentrations in mammalians plasma, which are involved in multitude of biological functions.[33,34] For instance, serum albumins are osmotic pressure regulators into the circulatory system and act as carriers for many biochemicals in blood. Therefore, this immuno model system was selected to enhance the representativeness and the scope of this study.

Arrays of diffractive BSA gratings were created on the unstructured side of transparent LightScribe disks by μCP. For that, regular compact disks were investigated as optically active nanostructured materials from which immobilizing arrays of protein biogratings on polycarbonate surfaces by passive adsorption. This approach aims to introduce a cost-effective, homogeneous, and scalable alternative to other nanofabricated gratings typically used as masters for μCP.[15-17]

As observed in Fig. 3A and S6, the grating relief on the stamp corresponds to the opposite of the grooved structure on the master, as expected. The slight differences in the measured dimensions (Table S1) must be related with the deformability of PDMS. Most importantly, the structure on the PDMS stamp leads to favorable diffraction responses for DBS measurements. A single row of spots is obtained as diffraction pattern from this grating, which entails only two diffracted orders. Also, slightly lower roughness values were observed on the top of the stamp ridges (1.26 nm) than in the bottom of the master valleys (3.63 nm) (Fig. S7 and S8), which favors protein transfer during the subsequent stamping step.

The efficiency of regular μCP is rather moderate for patterning proteins on low energy surfaces, as described elsewhere.[14] The polycarbonate disks used in this study falls within this kind of surfaces (contact angle in water ≈ 88 degrees), and humidity plays an important role to improve protein transfer in these cases.[35] Herein we performed a screening study to assess different μCP experimental variables (Table S2), and the results showed that better performance is obtained if stamps and substrates are kept under water during the stamping time. Therefore, this water-assisted version of μCP was used to create BSA diffractive gratings in this development.

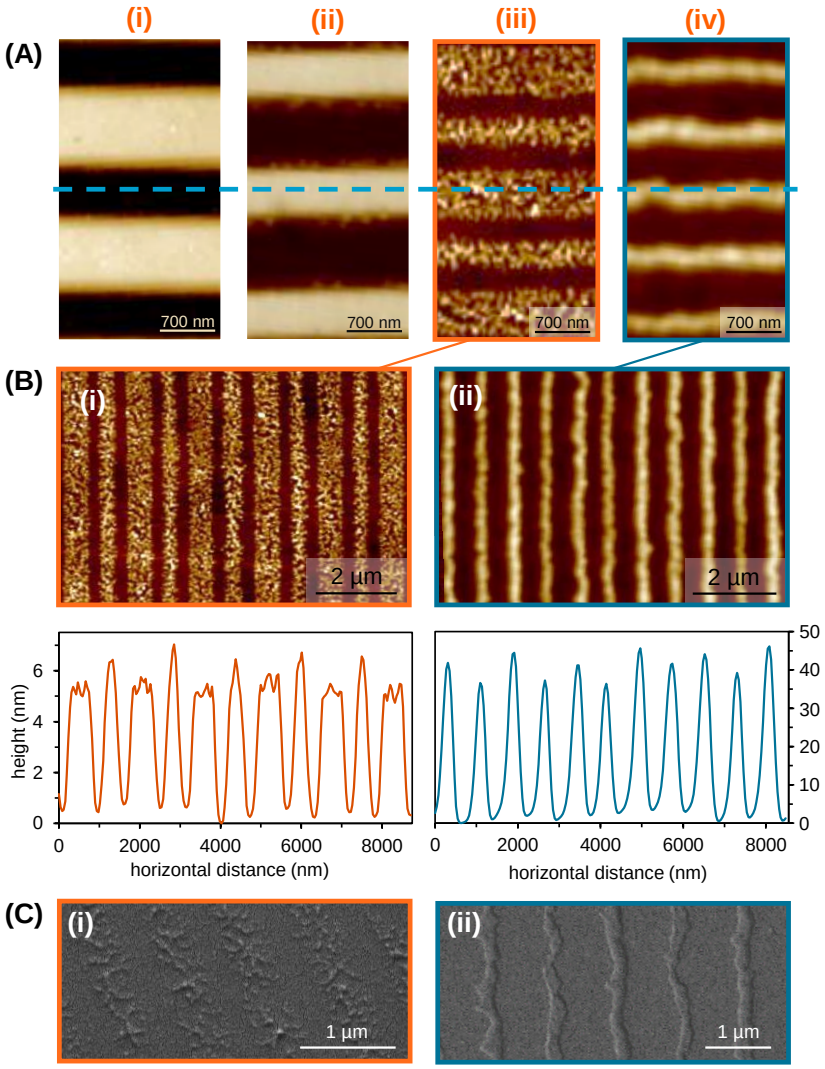

Fig. 3. Characterization results. (A) Aligned AFM data of gratings along the fabrication and assay stages: (i) polycarbonate master, (ii) PDMS stamp, and BSA biograting (iii) before and (iv) after IgGs incubation. (B) AFM scans of BSA biogratings (i) before and (ii) after IgGs incubation, and their corresponding averaged cross section profiles below. (C) FESEM images of BSA biogratings (i) before and (ii) after IgGs incubation. Biogratings were created by [BSA] = 7.5 mM, inking and stamping times of 40 min, and [IgG] = 670 nM.

Instead of reproducing the structure of the stamp, this fabrication process lead to biogratings constituted by alternated wider (660 ± 20 nm) and narrower (470 ± 60 nm) protein strips separated each other by gaps (210 ± 50 nm) within a 1550 ± 10 nm period (Fig. 3). This new

structure presents protein strips within the areas that correspond to deeper valleys of the stamp, as indicated in Fig. 3A. This pattern suggests a roof collapse deformation during the stamping process,[16] which could be either inherent to the stamp structure or motivated by excessive pressure initially applied to trigger the PDMS-polycarbonate contact. However, it must be highlighted that this structuration also lead to protein biogratings with good diffractive responses for DBS.

Well defined protein strips in the biogratings were observed by AFM. These strips comprise intercrossed networks of clusters and empty islands. Most of the clusters reach maximal heights of about 9 nm, whereas some scarce ones are up to around 15 nm tall (Fig. S9). These observations suggest protein strips constituted either by BSA monolayers immobilized in a range of orientations (4 and 14 nm for equatorial and polar axis, respectively) or by protein aggregates on the surface.

Specific IgG incubations led to a bell-shaped matter growth on the protein strips, as shown in Fig. 3A-3B, which mostly reaches maximal heights between 40 and 50 nm in the center of the strip (Fig. S10). Incubating only the surfactant used for blocking and stabilization purposes (Tween 20) does not lead to these topographies, but keep the original structure of BSA biogratings. Therefore, considering the dimensions of a single IgG molecule, these facts point out the formation of multilayers or aggregates when they recognize the patterned probes. This enhanced matter accumulation on the protein strips boosts the diffraction efficiency of the biogratings, and therefore improves the transduction of the biointeractions under study.

Protein biogratings, before and after specific IgG incubations, where also analyzed by FESEM. Though the gold coating slightly hinders the visualization of the grating features, these results match the characterization obtained by AFM (Fig. 3C and S11).

3.2 Disk drive-based bioanalytical scanner

A prototype drive to scan the diffracted patterns of protein biogratings arrayed on compact disk platforms have been developed in this study (illustrated in Fig. 4), in order to quantify biorecognition assays in label-free and high-throughput fashion. This setup controls the 780 nm laser integrated in the pickup unit and modulates its intensity by software. The implemented ALPC algorithm successfully stabilizes the laser intensity along time (Table S3), so the relative diffraction efficiency of biogratings on disks can be effectively determined by just measuring the intensity of a single diffracted order. As experimentally observed (Table S4), to normalize signals using the 0^{th} order intensity does not improve the results, so additional detectors can be avoided in this setup.

Fig. 4. Bioanalytical scanner. (A) Real image of the drive used as analyzer and the disk-based sensing platform. (B) Zoomed top view of the adapted drive. A disk was not included and a visible laser (650 nm) was switched on (instead of 780 nm) to better visualize the elements of the drive. See Fig. S3 for a general schematic illustration of the sensing setup.

The striped structure of the protein biogratings employed in this study generates suitable diffraction patterns (constituted by a row of spots) to be monitored by this disk drive. Thanks to its high divergence (77 degrees), the second order can be efficiently isolated from the other beams (and their backgrounds) with short distances without requiring specific optical elements. This fact enables to conceive simple and compact sensing devices that keep the dimensions of regular drives.

Biogratings were positioned on disks to have their strips oriented along the radial direction, i.e. perpendicular to the track embedded in the other side of the disk. This alignment avoid diffraction orders coming from both sides to overlap. Therefore, to collect the intensity of the second diffraction order from the biogratings, a photodiode-based photosensor was integrated in the edge of the drive case (Fig. 4). Since this photodiode achieves its maximal sensitivity when is perpendicularly irradiated, it was fixed to be tilted 77 degrees.

Standard pickup units integrate a lens within a focusing system designed to automatically focus the laser on the track (Fig. S4). The beam becomes highly focused when goes through this system, and therefore turns into extremely divergent beyond the plane of the track. This

configuration is not suitable for the diffractive measurements proposed in this study, because it makes all the diffracted beams (including the 0^{th}) to overlap. Therefore, the focusing system was disassembled and removed after demonstrating that it does not alter the functionality of the laser. This modification led to a circular (6 mm of diameter) collimated beam that enable well-defined diffraction patterns to be measured by transmission (Fig. S3).

The disk spinning was controlled and its velocity modulated with this drive, as described in section 2.4. This fact enables both, using the spindle motor to automatically scan along the longitudinal direction, and stopping rotation to perform static measurements in specific areas of the disk with good spatial resolution. The relative orientation between the laser and the striped structure of the gratings changes together with the disk rotation, and the system was tailored for the second diffraction order to hit the center of the photodiode when the laser irradiates the center of the biograting. As a result, the disk rotation leads to a bell-shaped scanned signal for every biograting (Fig. S5), where the maximum value corresponds to the analytical magnitude of interest.

This study was performed using the same laser than the one employed by LightScribe drives (780 nm), and the capability of this technology to perform the transmission measurements required for this sensing setup is supported by previous results of our group [31]. Moreover, the focusing system of the pickup unit does not involve feedback functions to manage the LightScribe irradiation. Therefore, arrays of biogratings on disks could be automatically scanned in regular LightScribe conditions. More than 115 biogratings per disk can be fabricated with the stamp dimensions employed in this study (8 mm diameter, 1 mm separation), whereas the multiplexing potential of this biosensor could be enhanced to more than 1000 gratings per disk by reducing to 2 mm the diameters of the stamps and the laser beam.

3.3 Biogratings optimization

The main variables in the fabrication of biogratings were studied in order to determine their relationships and to select the optimal conditions. Inking time (t_{ink}), stamping time (t_{stamp}), and protein concentration in the inking solution were assessed through a biparametric approach, since both t_{ink} and t_{stamp} were supposed to be correlated with protein concentration. First, biogratings were created in a range of inking times (from 0 to 160 min) and protein concentrations (from 0 to 15 mM), and then an analogous strategy was carried out to study the stamping time. Next, their diffraction response after incubating a constant concentration of IgGs (65 nM) was measured in label-free conditions using the developed scanner. In these experiments, higher surface density of probes and more favorable probe conformations to be recognized by the target, both increase the amount of matter constituting the biogratings and enhance their diffraction

efficiency. Therefore, conditions that lead to highest diffracted signals indicate optimal patterning for sensitive label-free immunosensing.

As shown in Fig. 5, both t_{ink} and t_{stamp} are indeed strongly correlated to protein concentration in the inking solution. The results reveal that every stamping and inking time entails a threshold probe concentration beyond which signal drops. This fact indicates that the surface density of probe proteins and/or their capability to be recognized by antibodies increases as expected until this maximal value. However, stronger µCP conditions (longer times and higher protein concentrations) could trigger probe desorption processes or more likely hinder the epitopes of the patterned proteins. Unspecific adsorptions on the gap strips of the biograting after these threshold conditions would also decrease the diffraction efficiency, so this phenomenon could be involved in this hooked response too. As a result, a BSA concentration of 7.5 mM, and inking and stamping times of 40 minutes, were selected as optimal values for the subsequent experiments.

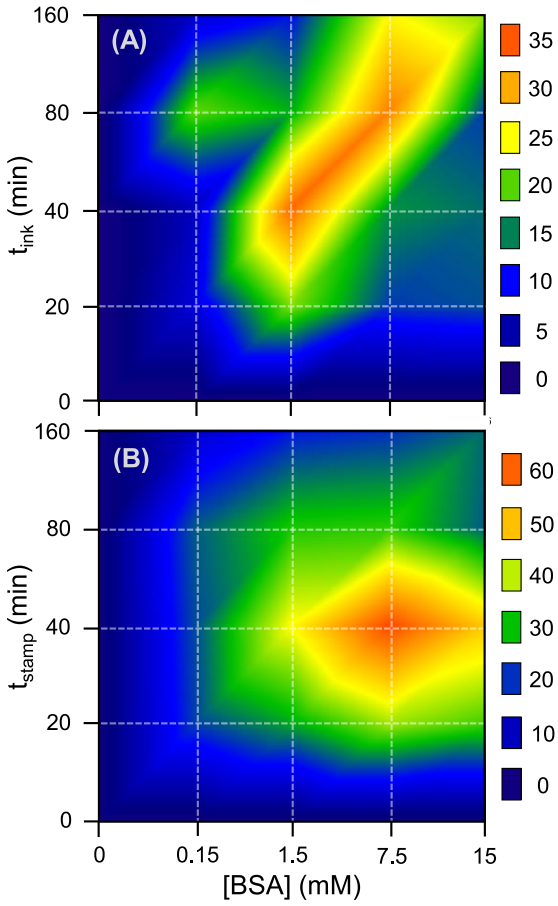

Fig. 5. Bi-parametric experimental assessment of µCP, comprising protein concentration versus (A) inking time and (B) stamping time. In the first experiment, t_{stamp} = 60 min was selected to be an intermediate value. In the second one, an optimal t_{ink} = 40 min was set. Color legends indicate the corresponding signal (a.u.) scale.

Rather large protein amounts are required to create these optimal biogratings, which must be mainly caused by the moderate protein-PDMS affinity during inking. BSA is a non-limiting probe in these regards, however this fact could be an important restricting factor when using expensive and/or scarce bioreceptors. The miniaturization of the stamps would provide important solutions in these cases. Also, biogratings of versatile binding biochemicals (protein A, lectins, avidin, etc.) could be patterned to mediate the attachment of costly probes, thus reducing their consumption. Moreover, it must be noted that the biosensor herein developed would also be compatible with other prospective biograting fabrication alternatives that address this issue.

3.4 Immunosensing

The label-free immunosensing response of this biosensor was studied in an immunoassay for determining specific anti-BSA IgGs in solution. Therefore, BSA biogratings were arrayed on compact disks by optimal μCP conditions and their diffractive response, after the incubation of IgG solutions (concentrations ranging from 0 to $6.6 \cdot 10^3$ nM), were analyzed in label-free fashion using the developed disk drive scanner.

Dose-response curves were experimentally obtained and their sensitivity was assessed by means of signal-to-noise ratios (SNR). Noise was calculated as the standard deviation obtained from the measurement of ten blank solutions (0 nM of IgGs). Although μCP usually involve moderate precision, whose solution is what many studies have focused on,[36-38] the intensities of the second diffracted order from these ten blank biogratings presented a favorable relative standard deviation of 0.6%.

As shown in Fig. 6, good results were obtained in the dose-response curve. Experimental data correlated well to an exponential trend ($R^2 = 0.9985$) that comprises a linear range from 5.2 to 243.3 nM of IgG ($R^2_{\text{linear}} = 0.9685$). Considering the signal-to-noise ratios, a detection limit (SNR = 3) of 1.3 nM and a quantification limit (SNR = 10) of 5.2 nM of IgGs were reached by this label-free immunoassay. Those are promising sensitivities that fall within the range of other optical label-free approaches currently found in the state-of-the-art.[39,40] Moreover, unlike theoretical and physical assessments, it must be noted that this experimental sensitivity is strongly affected by the properties of the employed bioreagents. Therefore, other binding systems and assay formats would provide different responses. For instance, engineering bioreceptors to display enhanced optical and biorecognition properties,[41,42] and using them to create biogratings, is an appealing prospective approach to boost the analytical performance of these label-free biosensor.

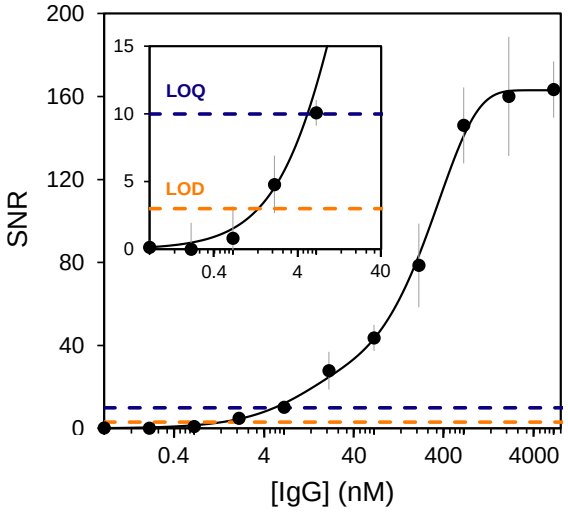

Fig. 6. Dose-response curve for label-free anti-BSA IgGs immunoassaying. Dots correspond to experimental measurements and continuous lines to the exponential (rise to maximum 4 parameters) adjustment. Inset graph zooms in the limit of detection (LOD) and limit of quantification (LOQ) zone.

4. Conclusions

The results presented in this study have demonstrated the performance of a novel biosensor designed to analyze label-free biorecognition assays in a huge number of biogratings created on disk-based assay platforms. The grooved nanostructures contained in regular recordable compact disks have proven to meet the compositional and structural requirements to act as large-scale and optically active masters for fabricating arrays of functional protein biogratings on polycarbonate surfaces, by a water-assisted variant of microcontact printing. We also demonstrated the capabilities of commercial disk drives tailored to scan transmitted diffraction patterns using non-focused laser irradiations at 780 nm. The implementation of this approach in consumer electronics is especially favored in LightScribe systems. All these advances together result in a sensitive immunosensor that introduces cost-effective alternatives to bring the strengths of label-free bioanalysis to non-specialized and resource-scarce settings. In addition to immunoassays, this biosensor could be easily implemented in a wide range of biorecognition assays for analyzing, in high-throughput and label-free fashion, biochemical targets of different nature (biomarkers, pathogens, allergens, etc.). For instance, the multiplexing potential of this system would be specially enhanced for nucleic acids hybridization assays. From these results, we also envision future advances marrying this diffractive biosensor with centrifugal microfluidics in order to conceive integrated lab-on-a-disk systems for point-of-care analysis.

Acknowledgements

This work was supported by the Spanish Ministry of Economy and Competitiveness (CTQ2013-45875-R), FEDER, and the Generalitat Valenciana (PROMETEO II/2014/040). M.A-O also

acknowledges the FPI program of the Spanish Ministry of Economy and Competitiveness for a PhD grant. Many thanks to Dr. Sergi Morais for sharing his expertise in the preparation of this manuscript.

References

(1) Kozma, P.; Kehl, F.; Ehrentreich-Förster, E.; Stamm, C.; Bier, F. F. *Biosens. Bioelectron.* **2014**, *58*, 287-307.
(2) Chauhan, R.; Singh, J.; Sachdev, T.; Basu, T.; Malhotra, B. D. *Biosens. Bioelectron.* **2016**, *81*, 532-545.
(3) Kussrow, A.; Enders, C. S.; Bornhop, D. J. *Anal. Chem.* **2012**, *84*, 779-792.
(4) Lee, J.; Icoz, K.; Roberts, A.; Ellington, A. D.; Savran, C. A. *Anal. Chem.* **2010**, *82*, 197-202.
(5) Goh, J. B.; Loo, R. W.; Goh, M. C. *Sens. Actuators B* **2005**, *106*, 243-248.
(6) Barrios, C. A.; Zhenhe, C.; Navarro-Villoslada, F.; López-Romero, D.; Moreno-Bondi, M. C. *Biosens. Bioelectron.* **2011**, *26*, 2801-2804.
(7) Goh, J. B.; Tam, P. L.; Loo, R. W.; Goh, M. C. *Anal. Biochem.* **2003**, *313*, 262-266.
(8) Wang, X.; Wang, X. *Chem. Commun.* **2013**, *49*, 5957-5959.
(9) Pak, B. J.; Vasquez-Camargo, F.; Kalinichenko, E.; Chiodini, P. L.; Nutman, T. B.; Tanowitz, H. B.; McAuliffe, I.; Wilkins, P.; Smith, P. T.; Ward, B. J.; Libman, M. D.; Ndao, M. *Plos Negl. Trop. Dis.* **2014**, *8*.
(10) Cleverley, S.; Chen, I.; Houle, J. F. *J. Chromatogr. B* **2010**, *878*, 264-270.
(11) Ye, G.; Wang, X. *Biosens. Bioelectron.* **2010**, *26*, 772-777.
(12) Romanov, V.; Davidoff, S. N.; Miles, A. R.; Grainger, D. W.; Gale, B. K.; Brooks, B. D. *Analyst* **2014**, *139*, 1303-1326.
(13) Wendeln, C.; Ravoo, B. J. *Langmuir* **2012**, *28*, 5527-5538.
(14) Kaufmann, T.; Ravoo, B. J. *Polym. Chem.* **2010**, *1*, 371-387.
(15) Wang, X.; Liu, X.; Wang, X. *Sens. Actuators B* **2015**, *220*, 873-879.
(16) Perl, A.; Reinhoudt, D. N.; Huskens, J. *Adv. Mater.* **2009**, *21*, 2257-2268.
(17) Guillon, S.; Salomon, S.; Seichepine, F.; Dezest, D.; Mathieu, F.; Bouchier, A.; Mazenq, L.; Thibault, C.; Vieu, C.; Leïchlé, T.; Nicu, L. *Sens. Actuators B* **2012**, *161*, 1135-1138.
(18) Zhang, D. M.; Liu, Q. J. *Biosens. Bioelectron.* **2016**, *75*, 273-284.
(19) Avella-Oliver, M.; Morais, S.; Puchades, R.; Maquieira, Á. *Trends Anal. Chem.* **2016**, *79*, 37-45.
(20) Grudpan, K.; Kolev, S. D.; Lapanantnopakhun, S.; McKelvie, I. D.; Wongwilai, W. *Talanta* **2015**, *136*, 84-94.
(21) Vashist, S. K.; Luppa, P. B.; Yeo, L. Y.; Ozcan, A.; Luong, J. H. T. *Trends Biotechnol.* **2015**, *33*, 692-705.
(22) Comina, G.; Suska, A.; Filippini, D. *Biosens. Bioelectron.* **2016**, *77*, 1153-1167.

(23) Petryayeva, E.; Algar, W. R. *RSC Adv.* **2015**, *5*, 22256-22282.
(24) Morais, S.; Puchades, R.; Maquieira, Á. *Anal. Bioanal. Chem.* **2016**, *408*, 4523-4534.
(25) Yu, H.-Z.; Li, Y.; Ou, L. M. L. *Acc. Chem. Res.* **2013**, *46*, 258-268.
(26) Burger, R.; Amato, L.; Boisen, A. *Biosens. Bioelectron.* **2016**, *76*, 54-67.
(27) Santiago-Felipe, S.; Tortajada-Genaro, L. A.; Carrascosa, J.; Puchades, R.; Maquieira, A. *Biosens. Bioelectron.* **2016**, *79*, 300-306.
(28) Barrios, C. A.; Canalejas-Tejero, V.; Herranz, S.; Moreno-Bondi, M. C.; Avella-Oliver, M.; Puchades, R.; Maquieira, A. *Plasmonics* **2014**, *9*, 645-649.
(29) Gopinath, S. C. S.; Awazu, K.; Fons, P.; Tominaga, J.; Kumar, P. K. R. *Anal. Chem.* **2009**, *81*, 4963-4970.
(30) Wang, X.; Zhao, M.; Nolte, D. D.; Ratliff, T. L. *Biosens. Bioelectron.* **2011**, *26*, 1871-1875.
(31) Avella-Oliver, M.; Morais, S.; Carrascosa, J.; Puchades, R.; Maquieira, Á. *Anal. Chem.* **2014**, *86*, 12037-12046.
(32) Schneider, C. A.; Rasband, W. S.; Eliceiri, K. W. *Nature Methods* **2012**, *9*, 671-675.
(33) Bern, M.; Sand, K. M. K.; Nilsen, J.; Sandlie, I.; Andersen, J. T. *J. Control. Release* **2015**, *211*, 144-162.
(34) Bujacz, A. *Acta Cryst.* **2012**, *68*, 1278-1289.
(35) Ricoult, S. G.; Nezhad, A. S.; Knapp-Mohammady, M.; Kennedy, T. E.; Juncker, D. *Langmuir* **2014**, *30*, 12002-12010.
(36) Volcke, C.; Gandhiraman, R. P.; Basabe-Desmonts, L.; Iacono, M.; Gubala, V.; Cecchet, F.; Cafolla, A. A.; Williams, D. E. *Biosens. Bioelectron.* **2010**, *25*, 1295-1300.
(37) Gunawan, C. A.; Ge, M. C.; Zhao, C. *Nat. Commun.* **2014**, *5*.
(38) McNulty, J. D.; Klann, T.; Sha, J.; Salick, M.; Knight, G. T.; Turng, L. S.; Ashton, R. S. *Lab Chip* **2014**, *14*, 1923-1930.
(39) Escorihuela, J.; González-Martínez, M. Á.; López-Paz, J. L.; Puchades, R.; Maquieira, Á.; Gimenez-Romero, D. *Chem. Rev.* **2015**, *115*, 265-294.
(40) Fenzl, C.; Hirsch, T.; Wolfbeis, O. S. *Angew. Chem. Int. Ed.* **2014**, *53*, 3318-3335.
(41) Hall, E. A. H.; Chen, S.; Chun, J.; Du, Y.; Zhao, Z. *Trends Anal. Chem.* **2016**, *79*, 247-256.
(42) Cui, Y. *Biosens. Bioelectron.* **2016**, *85*, 964-976.

SUPPORTING INFORMATION

Protein diffractive gratings as active optical substrates for high-throughput label-free immunosensing

Anal. Chem., In revision (**2017**).

Table S1. Dimensions of the structures on polycarbonate masters and PDMS stamps, calculated from AFM scans (numeric values in nanometers). Representative AFM data for these structures is presented in Fig. S6.

	Ridge height	Ridge width[a]	Valley width[a]	Slope width[b]	Period
Master	189 ± 1	540 ± 50	390 ± 30	314 ± 40	1580 ± 30
Stamp	175 ± 2	418 ± 40	523 ± 13	260 ± 30	1488 ± 11

[a] Note that, given the nature of µCP, the master ridges match the stamp valleys, and vice versa.
[b] Width of the horizontal projection of the slopes between valleys and ridges.

Table S2. Screening assessment for the µCP experimental conditions.

STAMPING CONDITIONS			RESULTS[b]	
Environment	**Temperature**	**Time**	**Signal Intensity**	**Homogeneity[c]**
Air	4 ºC	40 min	-	-
		Ovenight	-	+
	RT[a]	40 min	-	-
		Ovenight	-	-
Water	4 ºC	40 min	++	+
		Ovenight	++	++
	RT[a]	40 min	++	+
		Ovenight	++	++

[a] Room temperature (≈ 22 ºC).
[b] Poor (-), moderate (+), and good (++).
[c] Signal and shape homogeneity along the grating area.

For this assessment, BSA biogratings were fabricated on polycarbonate disks at different experimental conditions. Inking parameters were kept constant ([BSA] = 3.8 mM, t_{ink} = 80 min).Once stamped, successive incubations were applied on the gratings: (i) rabbit anti-BSA IgG in PBS-TT (33 nM, 20 min), (ii) goat anti-rabbit IgGs labelled with 5 nm colloidal gold nanoparticles in PBS-T (1/200, 15 min), and (iii) silver enhancer solution (6 min). Finally, the silvered gratings were qualitatively assessed. Equivalent results were obtained in biogratings fabricated with stamps of different diameters (6, 8, and 10 mm).

Table S3. Experimental results for the assessment of the laser stability. As observed, negligible relative standard deviations (RSD) were obtained in all the conditions.

Intensity (%)	Sampling time (seconds)[a]	Acquisition time (min)[b]	Averaged Intensity (a.u.)	SD	RSD (%)
100	1	210	1.156	0.003	0.2
100	10^{-2}	5	1.0071	0.0005	0.05
50	10^{-2}	5	0.847	0.001	0.07
10	10^{-2}	5	0.7488	0.0004	0.06

[a] Time ranges used to average output signals, for a DAQ sampling frequency of 10^6 samples/second.
[b] Duration of the monitored laser irradiations.

Table S4. Raw signal and normalized results of dose-response curves comprising a range of IgG concentrations (from 0 to 670 nM). As observed, the signal normalization led to slightly worst adjustments.

Approach	Adjustment (R^2)[a]
Raw (2^{nd} order intensity)	0.9983
Normalized ($2^{nd}/0^{th}$ orders intensity ratios)	0.9775

[a] Exponential rise to maximum 4 parameters.

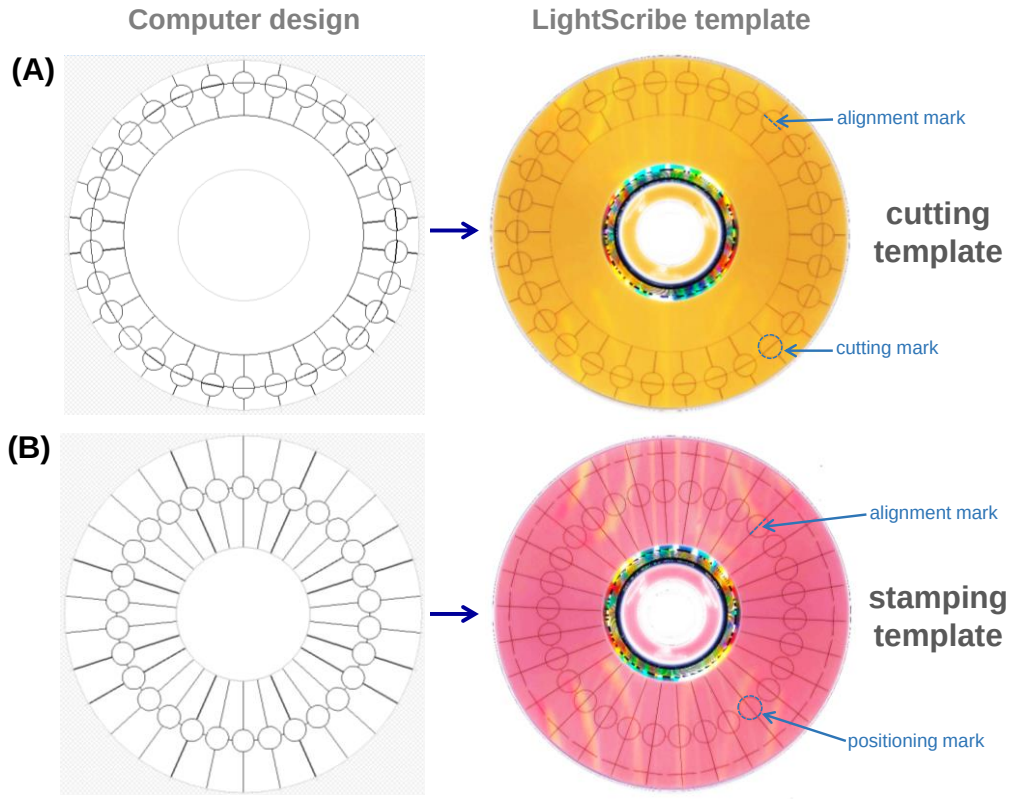

Fig. S1. Images of the computer designs and the resulting LightScribe template disks used for alignment and positioning purposes in this study. LightScribe disks are regular CDs or DVDs in one side (track side), and in the other one (label side) they comprise a photochromic/thermochromic material that becomes darker when irradiated by the drive (Trends Anal. Chem., 79, 2016, 37-45). Therefore, users can etch custom motifs on the label side of these disks. Nero CoverDesigner software was used to create the templates and to etch them. (A) Template for cutting the stamps from the polymerized PDMS. An external radius was selected in order to minimize the curvature of the track and to maximize the number of stamps per disk obtained with a constant curvature. The alignment marks in this template were used to create slight cuts (with a blade) on the PDMS in order to indicate the orientation of the grating. (B) Template for stamping on the assay platforms. In this case, this template was designed to array biogratings in a single radius (42 mm, from the center of the biograting). Note that the alignment marks in this template are rotated 90 degrees (with respect to the cutting template), thus orienting the biograting grooves perpendicular to the track.

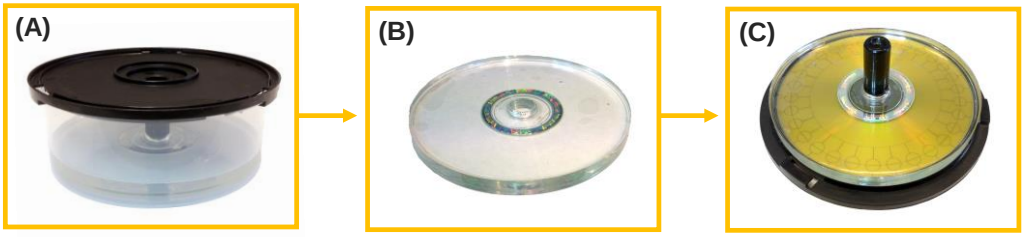

Fig. S2. (A) Setup to polymerize PDMS on the master disks. (B) Polymerized PDMS block (together with the master disk). (C) PDMS-master block aligned with the LightScribe template for cutting.

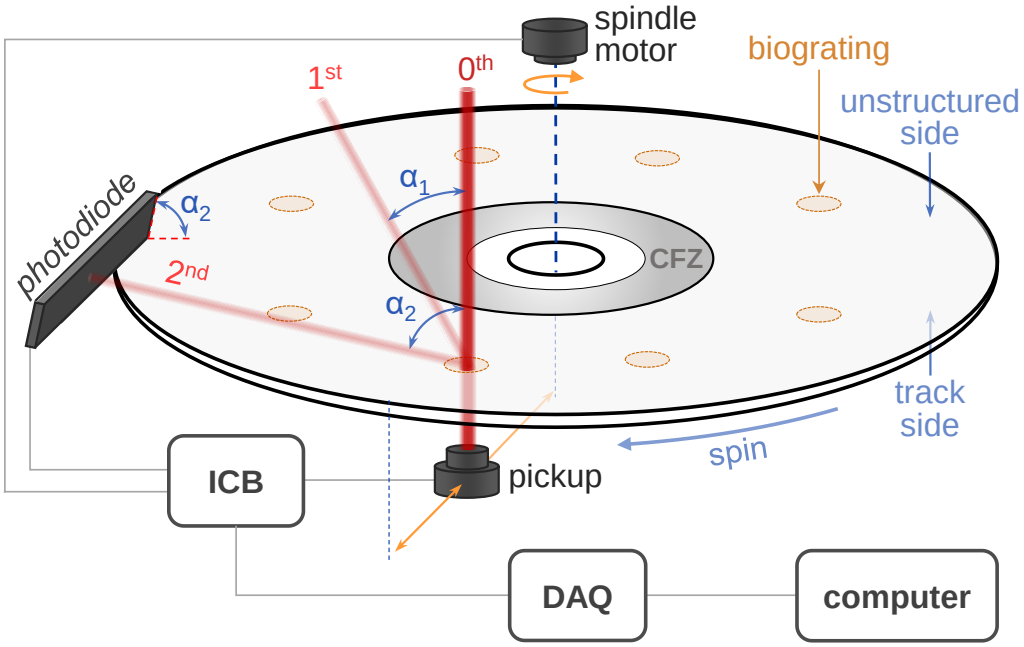

Fig. S3. Schematic illustration of the sensing configuration. Negative diffraction orders are omitted to simplify the plot.

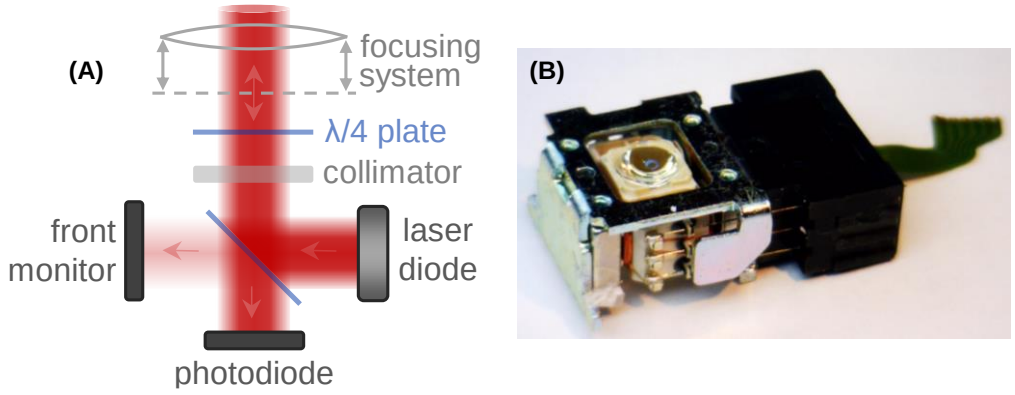

Fig. S4. (A) Schematic illustration of the pickup unit. (B) Image of the focusing system removed from the pickup.

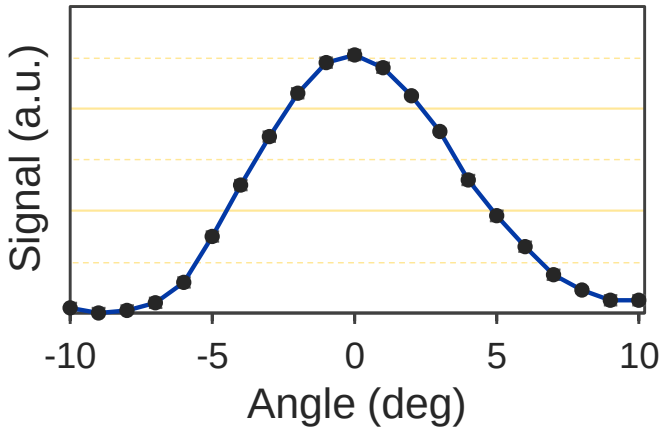

Fig. S5. Experimental scan of a single biograting for an array of rotation angles, where 0 degrees corresponds to the center of the grating.

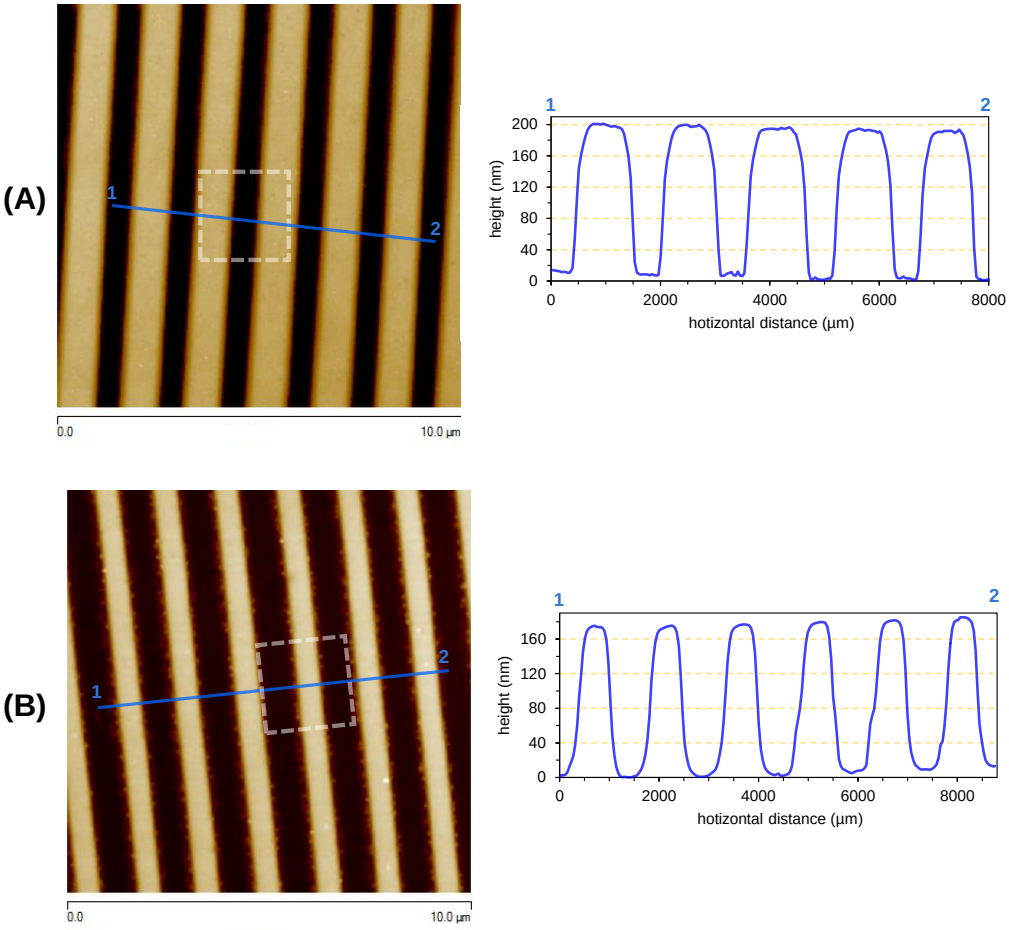

Fig. S6. AFM data and the corresponding averaged cross section profiles of the reliefs on (A) the polycarbonate master and (B) the PDMS stamp. Squared areas indicated with dashed white lines corresponds to the zoomed scans presented in Fig. S7 and S8.

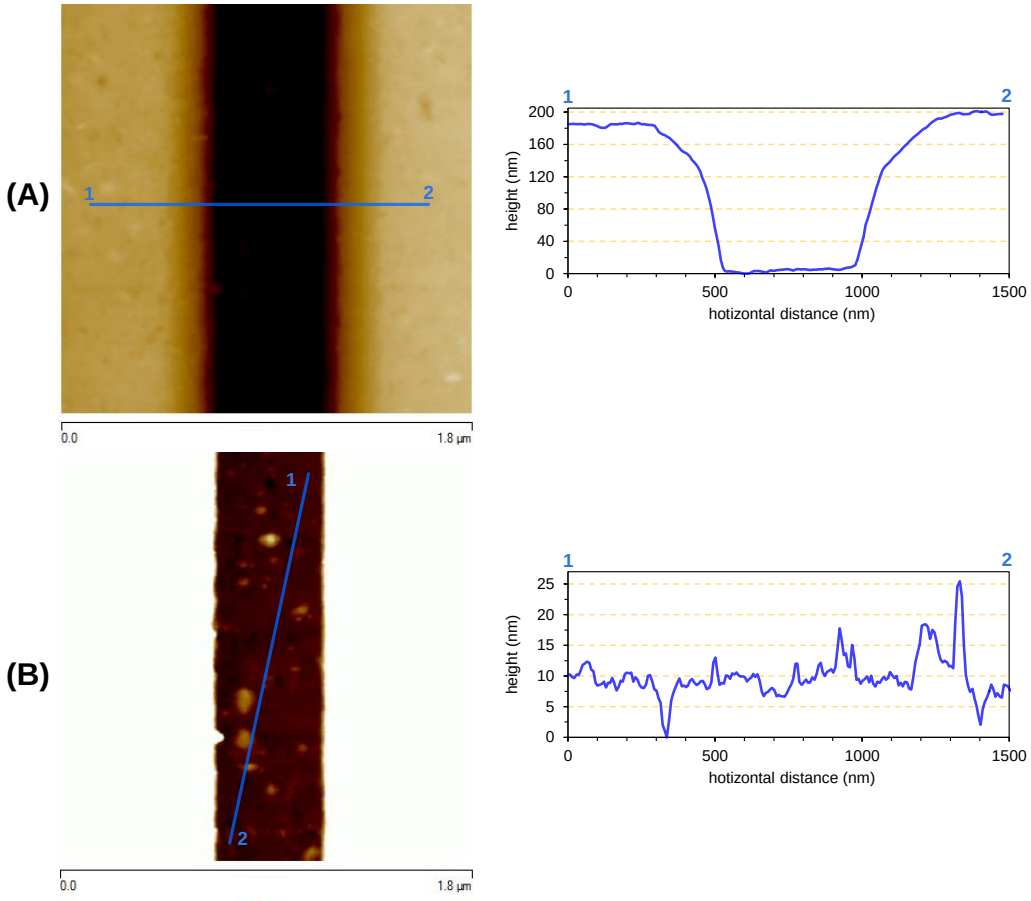

Fig. S7. AFM data of the master and the corresponding cross section profiles. The area scanned in this higher resolution measurement is indicated in Fig. S6A. Contrast values set for (A) the top of the rides and (B) the bottom of the valley. Calculated roughness in the bottom of the valley was 3.63 nm.

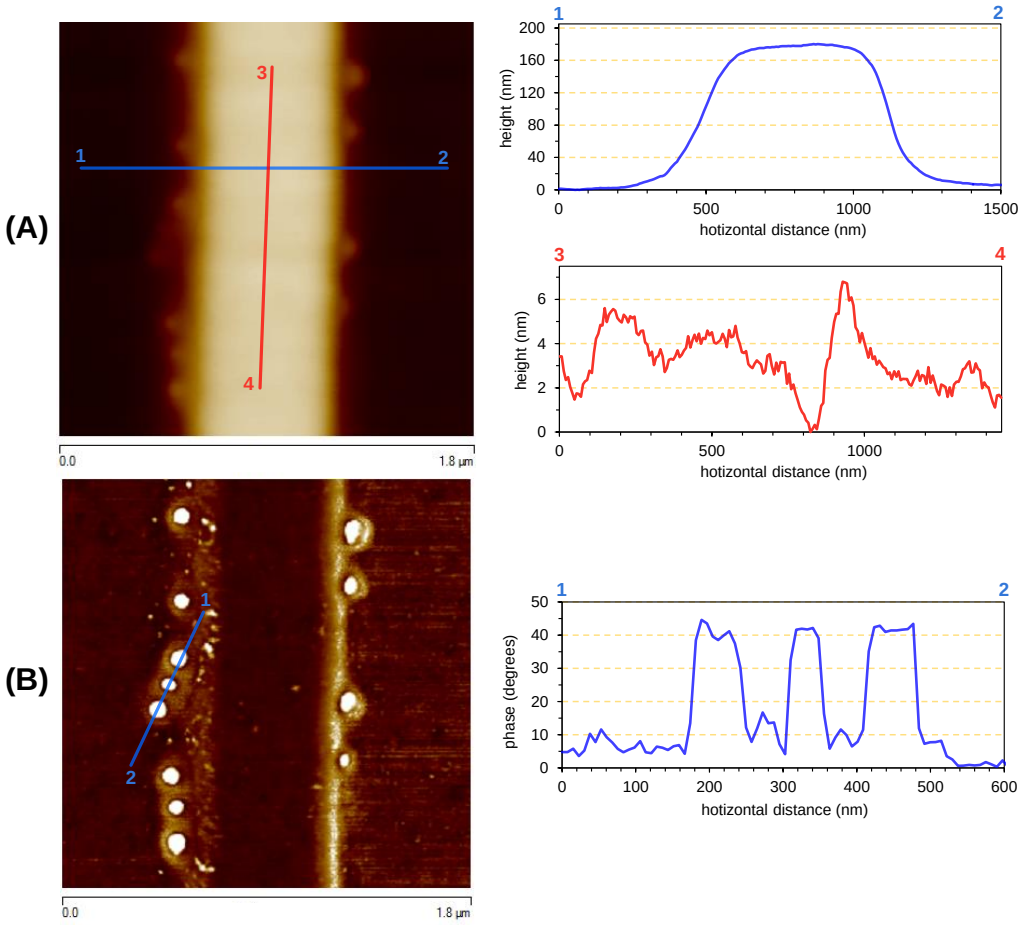

Fig. S8. AFM images of the stamp and the corresponding cross section profiles. The area scanned in this higher resolution measurement is indicated in Fig. S6B. (A) Height and (B) phase scans. Calculated roughness in the top of the ridge was 1.26 nm. Circular features with higher phase values (situated in the edge of the ridges) were revealed in the phase scans. This observation could indicate softer nanobubbles of encapsulated air within the PDMS. However, these features are not transferred to the subsequent protein gratings.

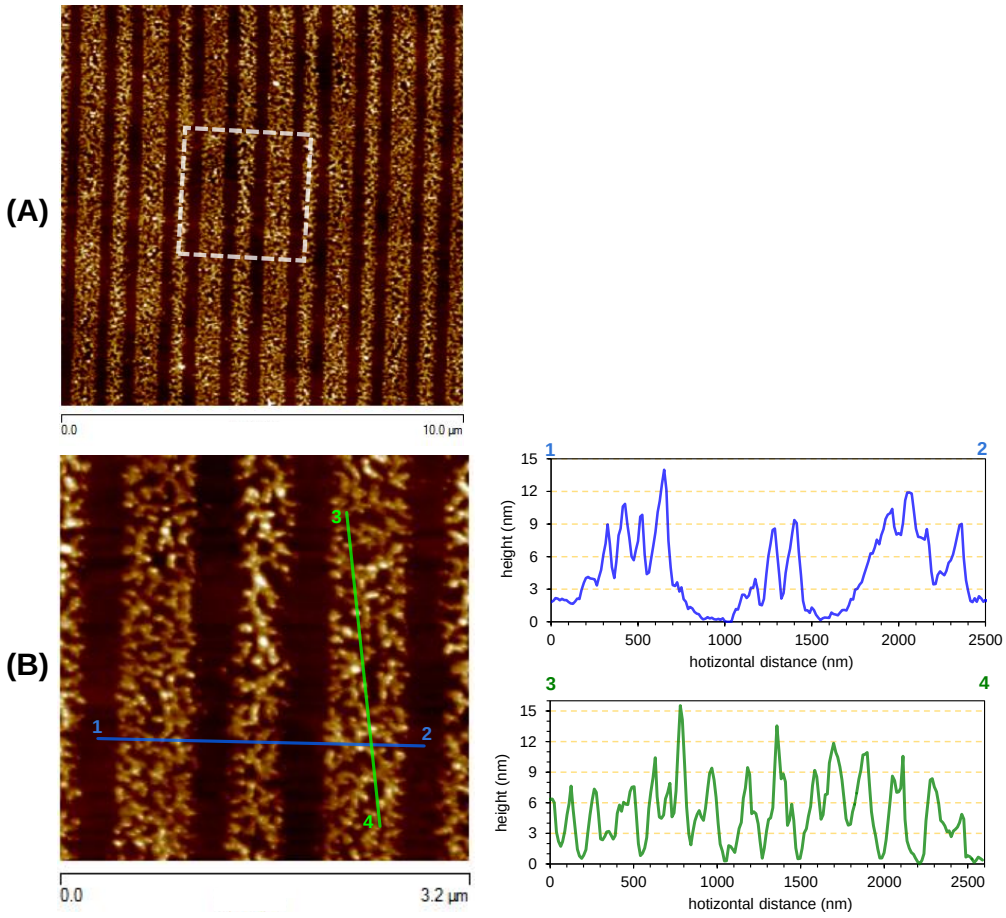

Fig. S9. AFM data of protein biogratings: (A) 10x10 µm scan and (B) higher resolution scan of the squared area indicated in the image above (and the corresponding cross section profiles). These biogratings were created by [BSA] = 7.5 mM and $t_{ink} = t_{stamp} = 40$ min.

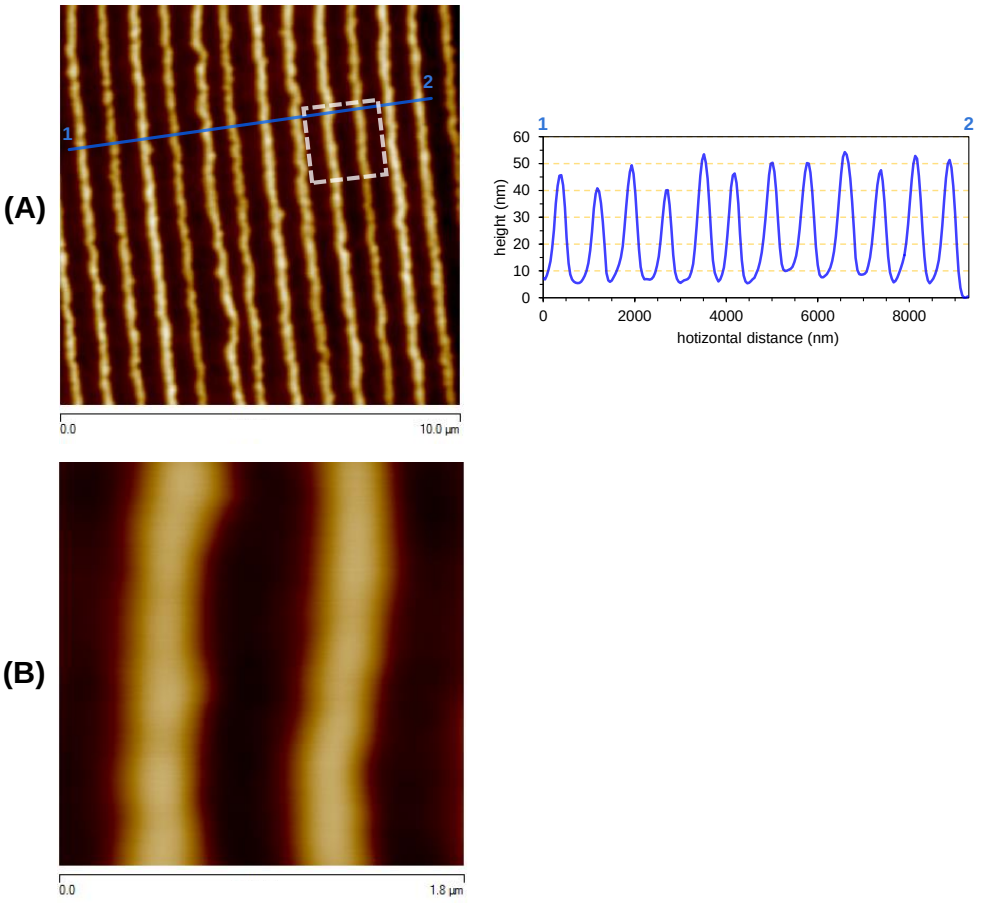

Fig. S10. AFM data of protein biogratings (obtained from [BSA] = 7.5 mM and $t_{ink} = t_{stamp} = 40$ min) after incubating selective IgGs (670 nM, in PBS-TT). (A) 10x10 µm scan and the corresponding cross section profile. Despite the moderate linearity of the top of the protein strips after reacting with IgGs, equivalent results were obtained by averaged cross sections (Fig. 3B, ii) and simple cross section profiles (Fig. S10A). (B) Higher resolution scan of the squared area indicated in the image above.

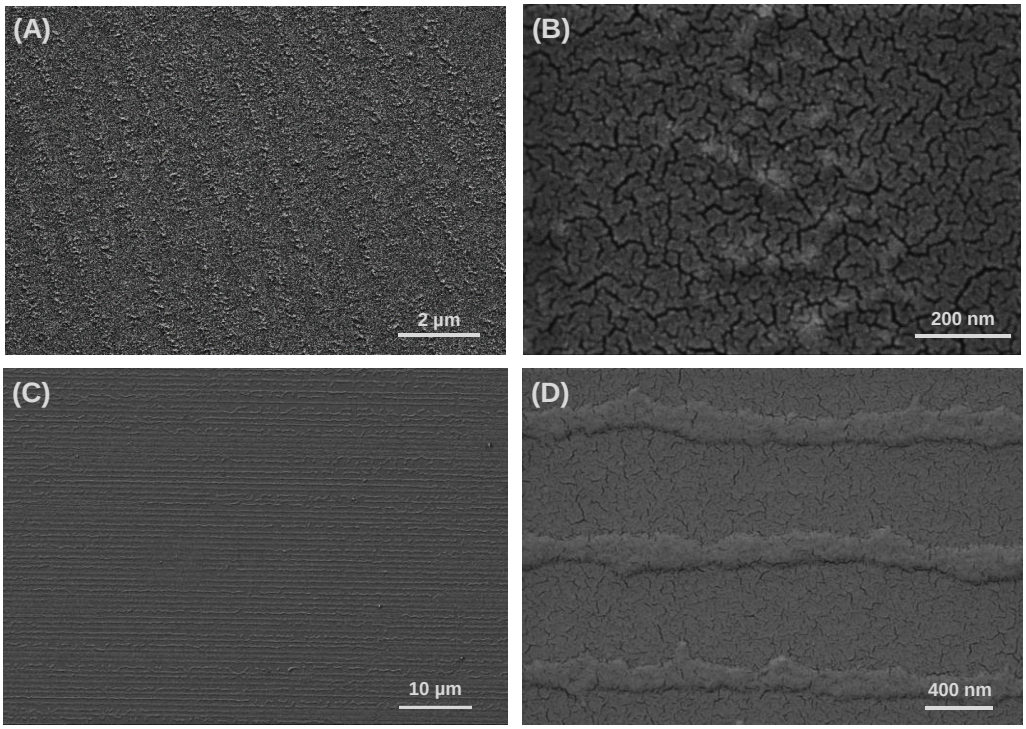

Fig. S11. FESEM images of (A and B) protein gratings (obtained from [BSA] = 7.5 mM and $t_{ink} = t_{stamp}$ = 40 min) and (C and D) the resulting biogratings after IgG incubation (670 nM, in PBS-TT).

3.4.4 Conclusions

Diffractive gratings of biological probes fabricated by microcontact printing on solid substrates enable biointeractions to be measured in label-free conditions by monitoring the intensity of diffracted orders. This strategy is compatible with endpoint and real-time analysis, multiple detection configurations, and substrate materials of different nature, whereas also permits to introduce labels and signal developers for improving sensitivity.

Implementing displacement immunoassays in DBS is a good option for the label-free determination of low molecular weight organic compounds in a sensitive manner. This study have also offered us the background knowledge to integrate DBS in compact disks. In particular, insights into the success of endpoint analysis by transmission measurements using protein gratings fabricated on unstructured polycarbonate surfaces (up side TED5), have been provided.

Standard TED5 platforms can be successfully used as a nanostructured master material to create optically active protein biogratings by a humidified variant of μCP. This strategy enables functional protein gratings to be arrayed on TED5 disks and then using adapted TED drives to analyze biorecognition assays in label-free and multiplexed fashion. In addition to immunoassays, as experimentally proved, this approach also opens a range of possibilities for introducing the arsenal of functional proteins that biotechnology offers in order to integrate other biorecognition strategies in this system. This development makes the most of consumer electronics to design a label-free biosensor based on cost-effective and industrially scalable materials, devices, and fabrication methods, whereas also reports for the first time a biosensor that enables label-free detection by only using assay platforms and scanners derived from standard disks and drives.

Future investigations to automatize the biogratings fabrication on the whole disk surface are suggested from these results. A transmission photodiode as long as the radial distance to be covered would just be required to scan gratings in multiple radius. Prospective studies should use the results herein reported to conceive disk drive analyzers capable of scanning in regular LightScribe conditions. Along these lines, the success of modified TED drives for analyzing TED5 disks by transmission measurements using additional photodiodes, was already herein proved in the second part of the first chapter (section 3.1.3). Furthermore, it must be noted that the focusing system included in the pickup unit of TED systems does not involve feedback functions to control the disk spinning. Consequently, its removal or absence is compatible with standard scanning conditions as long as the control feature zone (CFZ) is kept in the disk. Therefore, this approach involves consumer electronics and simple fabrication methods for bringing label-free detection of biorecognition assays to point-of-need scenarios.

4. General discussion

The development of biosensors based on consumer electronics is an attractive and powerful way to develop point-of-need systems, and to introduce new challenges in analytical sciences. Along these lines, compact disk technology has demonstrated appealing capabilities in sensing and sample handling terms. The results of this thesis introduce new alternatives that provide solutions in the current state of the art in biosensors, and extend the scope of disk-based systems. Within this framework, this research addresses the design of biosensors that focus on TED technology for label-free detection using sensing platforms and analyzers from standard compact disks and drives, respectively.

This research initially focused on exploring distinctive TED characteristics for bioanalysis. At first, a novel strategy to exploit photo- and thermochromic materials as substrates for biorecognition assays was introduced. Suitable protein immobilization features were shown by the photosensitive coatings of standard LightScribe disks, and the studied labels (organic dyes as antennas and polymeric microspheres as scattering labels) exhibited the expected interaction between substrates and the laser. This strategy is based on merely applying light to develop the analytical signal, and avoids additional steps that involve long incubations of expensive reagents. Thus it represents a simpler alternative to other signal developing methods used for bioanalysis. Rather than proving the concept for a specific application, the present work aims to present this approach to the scientific community. The results suggest that sensitivity is the main aspect to be addressed to fully develop this method, which could be improved by, for instance, conceiving more efficient antenna labels in energy transfer terms.

Besides, standard TED disks are powerful analytical platforms that can hold biorecognition assays on both sides of the disk to be scanned with TED drives by reflection and transmission measurements. The proposed signal processing procedure vastly improves the sensitivity of disk-based biosensors, and provides TED with a comparable performance to reference systems (CD and DVD) for colorimetric microarray immunoassays. The track independency of TED systems also permits sensing elements to be integrated that involve strong physicochemical modifications, an aspect that is neglected in biosensors when other disk technologies are used. For instance, a single platform can be tailored to analyze many biological assays of different natures; e.g., immunofiltration, cell culture, and turbidimetry, among others. The results position TED as a good candidate to open up new perspectives in compact disk biosensors, and to extend the scope of lab-on-a-disk systems based on regular disks and drives by, for example, introducing label-free detection.

Optimizing biorecognition assays and characterizing their behavior are key operations in the development of new biosensor systems. Along these lines, the theoretical-experimental method herein presented (INSEL), based on kinetics and mass transport phenomena, allows one to efficiently optimize and explore biorecognition systems. Good agreement between the

experimental and predicted kinetic curves demonstrates the success of this approach for both studied model systems: non competitive (sandwich) and competitive (coating conjugate-based) immunoassays. The results prove that the INSEL methodology permits to direct optimizations towards sophisticated objectives and to obtain better analytical performance than classical optimization approaches (e.g., checkerboard titration). Moreover, important parameters in biorecognition systems, like diffusion and bioreagent concentrations, can be explored by INSEL without additional experiments. These results also demonstrate the capabilities of disk-based microarrays as a routine technique to study biorecognition events. From a broader viewpoint, this work provides valuable knowledge on the biorecognition systems employed in other studies, and also suggests the prospective INSEL application to the biosensing advances presented in this thesis to achieve their maximal performance.

The microstructures of regular compact disks present appealing strengths to face the restrictions typically involved in label-free biosensing systems. Polycarbonate substrates from recordable CDs (TED5) and DVDs coated with silver exhibit tunable plasmonic responses and significant Raman enhancement. In addition to a Raman reporter (4-ATP), these structures can successfully analyze complex biological species, such as hemoglobin and exosomes from a lung cancer cell line. This study introduces a large-scale, inexpensive, and industrially scalable alternative to the typical SERS substrates produced by classical nanofabrication techniques. Moreover, these results, together with the previous knowledge on the analytical implementation of compact disk technology, suggest future developments towards cost-effective Raman scanners built from regular drives.

Finally, diffraction-based sensing (DBS) is a versatile and powerful technique to conceive compact disk-based label-free biosensors. Functional protein biogratings can be successfully fabricated by µCP on different substrates, and sensitively analyzed by DBS in a wide range of experimental configurations. This can provide real-time and endpoint information of both labeled and label-free biorecognition assays. Also, implementing displacement immunoassays with biogratings constituted by protein-hapten conjugates represents a good option to analyze low molecular weight organic compounds by DBS in label-free and sensitive fashion, as demonstrated for atrazine residues in water (detection limit of 1.1 ng/mL). This investigation has provided the knowledge to fully characterize this technique for its subsequent application in disk-based systems.

Along these lines, arrays of optically active protein biogratings can be fabricated on transparent polycarbonate disks by a humidified variant of µCP using the track side of TED5 disks as nanostructured masters. The multiplexed and label-free analysis of biorecognition assays is reached by scanning these disks with TED drives adapted to measure the transmitted diffraction pattern of biogratings. The performance of this system is demonstrated through well-correlated

dose-response curves and the label-free sensitive determination of antibodies in solution using an immunoassay model system. This study proves the concept to exploit compact disk technology to develop high-throughput, cost-effective, industrially scalable, sensitive, user-friendly, compact, and portable biosensors that combine the strengths of consumer electronics and label-free detection to offer new solutions for point-of-need analysis.

5. General conclusions

This thesis explores new concepts for the development of biosensors based on compact disk technologies. Rather than focusing on particular bioreagents and applications for specific targets, this research employs well-known robust biorecognition assays as representative model systems to explore novel bioanalytical techniques, tool, and methodologies beyond the current state of the art of biosensors. Different proteins and immunoassays were used as model systems: BSA/anti-BSA (sections 3.1.2, 3.4.2, and 3.4.3), direct immobilization of labeled IgGs (section 3.1.3), rabbit IgG/anti-rabbit IgG (section 3.2.2), competitive atrazine immunoassay (sections 3.2.2 and 3.4.2), hemoglobin and exosomes (section 3.3.2). Therefore, this research focused on proteins and aims to proof the concept from a broad applicability scope. Thus the resulting advances are suitable for any biorecognition system and assay format. Moreover, it is worth highlighting that this research keeps an eye on cost-effective materials and prototypes development in order to support the point-of-need potential of the reported advances.

The main facts concluded from this research and the corresponding future trends are listed below:

- The light-mediated signal developing system herein presented introduces new perspectives to exploit photo- and thermochromism for biosensing. Compared to other signaling systems, e.g., fluorophores, nanoparticles, and signal developers, this strategy offers a simpler, cheaper, and greener alternative, which is especially interesting for qualitative screening analysis and naked-eye detection. Our results suggest that future studies will have to improve the sensitivity of this signal developing system in order to fully implement it in real analytical scenarios. For instance, designing new labels that transfer energy more efficiently from the light source to the assay substrate will presumably provide appealing solutions to boost the sensitivity of this approach.

- Analytical TED implementation opens up a new range of opportunities to develop disk-based biosensors beyond the possibilities offered by other compact disk technologies. With TED biosensors, multiple biological assays of different natures and a wide range physicochemical surface modifications for biosensing can be introduced in regular disks, and sensitively analyzed using the drive as an analytical scanner. The integration of microfluidic elements into these systems suggests prospective lab-on-a-disk solutions with appealing point-of-need features. Moreover, this study has provided important insights into the design of novel disk-based bioanalytical tools that enable label-free analyses.

- INSEL permits biorecognition assays to be efficiently optimized and to predict their response in a rational fashion. Compared to the other typical strategies used in bioanalysis, such as checkerboard titration, INSEL minimizes the amount of experiments required to define the behavior of the binding events under study, and also

makes a kinetic and mass transport characterization of the system. To direct optimizations towards the custom objectives defined by users implies great versatility and a high potential to extend the scope of this tool to further scenarios. For instance, these results point towards prospective research to exploit INSEL in different biorecognition systems (nucleic acids, enzymes, etc.) and other applications (bioreagents selection, probes design, etc.).

- The disk-based SERS substrates herein presented are affordable materials that can be manufactured on an industrial scale, and that enable Raman analysis of complex biological samples under label-free conditions. Beyond hemoglobin and exosomes, these substrates may also be able to provide the Raman fingerprint of a wide range of biomacromolecular targets. Along these lines, their chemical functionalization to attach biological probes for performing biorecognition assays represents a prospective approach to develop extremely selective multiplexed biosensors. These results indicate potential Raman scanners based on TED drives to bring label-free SERS biosensing to non specialized settings.

- Biogratings are an interesting alternative to other nanostructured materials used to sense biorecognition events. These biomolecular networks present wide versatility in terms of substrate materials and detection setups, and enable label-free detection and real-time analyses, among other strengths. To analyze low-molecular-weight organic compounds, the biogratings of protein-hapten conjugates, together with displacement immunoassays, represent an appealing sensitive and label-free option. The results obtained in this research support the subsequent implementation of diffraction-based sensing into disk-based sensors for detecting unlabeled biorecognition events.

- The introduction of protein biogratings into polycarbonate platforms has enabled, for the first time, the development of a label-free biosensor ready to be implemented into standard disks and drives. This approach allows high-throughput and quantitative assays to be performed by non specialized personnel. These results introduce a set of new bioanalytical possibilities; e.g., the design of biogratings constituted by bioengineered probes with enhanced immobilization and biorecognition properties. The benefits of this biosensing principle would synergistically marry the implementation of microfluidics to conceive advanced label-free lab-on-a-disk systems for point-of-need analysis.

From a general viewpoint, this thesis explores and set ups novel bioanalytical solutions beyond the current state of the art. Representative biological assays prove the concept of the findings

obtained in this research and provide these developments with a broad scope for it to become the playground for prospective studies that focus on particular applications and biological targets. Besides, the practical performance of this research is supported by the development of robust, user-friendly, and effective assay substrates and prototypes. Beyond the results herein introduced, this thesis opens up a wide range of possibilities that stimulate promising advances to overcome the scientific and technological barrier for really distributing the benefits of bioanalytical sciences across societies.